Studies on glutathione conjugation reactions of some cyclic chalcone analogs to seek reactivity-biological activity relationships

Doctoral (Ph.D.) Dissertation

Dr. Fatemeh Kenari

Doctoral School of Pharmacological and Pharmaceutical Sciences

Head of the doctoral school: **Prof. Dr. Erika Pintér**

Program leader: **Prof. Dr. Pál Perjési**

Supervisor: **Prof. Dr. Pál Perjési**

Institute of Pharmaceutical Chemistry

Faculty of Pharmacy

University of Pécs

Pécs 2023

Table of Contents

1. Introduction

1.1. Chalcones

Chalcones (1,3-diphenyl-2-propen-1-ones), also known as benzalacetophenone or benzylidene acetophenone, are intermediary and precursor compounds found in flavonoid biosynthesis. Natural chalcones are mainly found in petals showing yellow and orange pigments, roots, leaves, and twigs of edible plants such as *Glycyrrhiza glabra* and *Piper methysticum* which have been traditionally used in medical practice owing to their wide-ranging biological and pharmacological activity. Natural chalcones are extremely diverse in structure. They are mainly found to be substituted by hydroxyl, methoxy, and methyl groups; nevertheless, uniform substitution of chalcones is rare. The diverse biological and pharmacological activity and high number of replaceable hydrogen substituents make them a perfect candidate for synthetic manipulations [1]. The interesting structure of chalcones attracted several researchers worldwide to investigate the chemical and biological properties of these compounds.

The basic structure of the parent compound consists of two aromatic rings attached by an enone moiety resulting in a planar structure (Figure 2). It exists in both (*Z*)- and (*E*)- isomeric forms; however, due to higher thermodynamic stability, the (*E*)- isomer is more accessible. Chalcones can be cyclized to form flavanones *via* an intramolecular Michael-addition reaction. The ease of structural modification and the wide variety of biological and pharmacological activities have led to high diversity in chalcone derivatives and, in turn to popularity in drug research and development.

Claisen–Schmidt condensation is the most common method of synthesis of chalcones, condensation of an aldehyde, and a proper ketone in a polar solvent using a base as a catalyst. Due to high interest in research and industry, many other methods were developed, which can be listed as aldol condensation, Suzuki reaction, Wittig reaction, Friedel-Crafts acylation with cinnamoyl chloride, Photo-Fries rearrangement of phenyl cinnamates, etc. [2,3].

Chalcones, among others, have been proven to have cytotoxic [4–6], anti-inflammatory [7,8], and anthelmintic [9] effects. Among them, some have been approved for clinical use. Metochalcone, isolated from *Pterocarpus marsupinum,* proved to have choleretic and diuretic effects, sofalcone [10] is a gastric mucosa protective agent, and hesperidin methylchalcone has improved the quality of life of those suffering from chronic venous disorder [11].

Gaining knowledge of chalcones' mechanism of action, their direct molecular targets, and their biotransformation is particularly important for the further development of chalcone-based medicinal agents.

1.1.1. Thiol-reactivity of chalcones

Interaction of chalcones with cellular macromolecules, as the molecular basis of their biological activities, is well documented. Such interactions may be broadly categorized into non-covalent versus covalent ones. It has been reported that chalcones could have non-covalent interactions with DNA, proteins, and specific lipids. The non-covalent nature of these interactions makes chalcones free from the possible genotoxicity and toxicities associated with the compounds that covalently bind to DNA [12]. Previously it was demonstrated that chalcones and their analogs show high intrinsic reactivity toward thiol groups. The polarized carbon-carbon double bond of the compounds acts as a soft electrophile. Thus this functionality shows much higher reactivity towards thiols than the harder nucleophilic amino and hydroxyl groups. Thiol groups are ubiquitously found in the structure of proteins and peptides. Among such reactions, GSH-GSSG ratio plays an important role in the cellular redox and antioxidant status of the cells. Accordingly, reactivity of chalcones with cellular thiols is argued to be responsible for various biological activities of chalcones and their analogs [13].

The Michael addition is a reaction in which a nucleophilic center (Michael-donor) is added to the electrophilic Michael acceptor, such as α,β-unsaturated carbonyls. The nucleophile that is added to the Michael acceptor can be categorized into two different classes: those which have a negative charge (e.g., OH^-, RS^-, CN^-) and those which are neutral (e.g., amines, thiols). Both kinds of nucleophiles can be added onto α,β-unsaturated enones regardless of their protonation state. In the case of the (*E*)-chalcone, the experimental pK_b value has been reported to be -5.00 [14]; therefore, in typical aqueous media (pH 4-8), only additions onto the non-protonated chalcones should be taken into consideration.

The general mechanisms of the addition of deprotonated (path A) and neutral (path B) nucleophiles onto non-protonated chalcones are shown in Figure 1 and Figure 2.

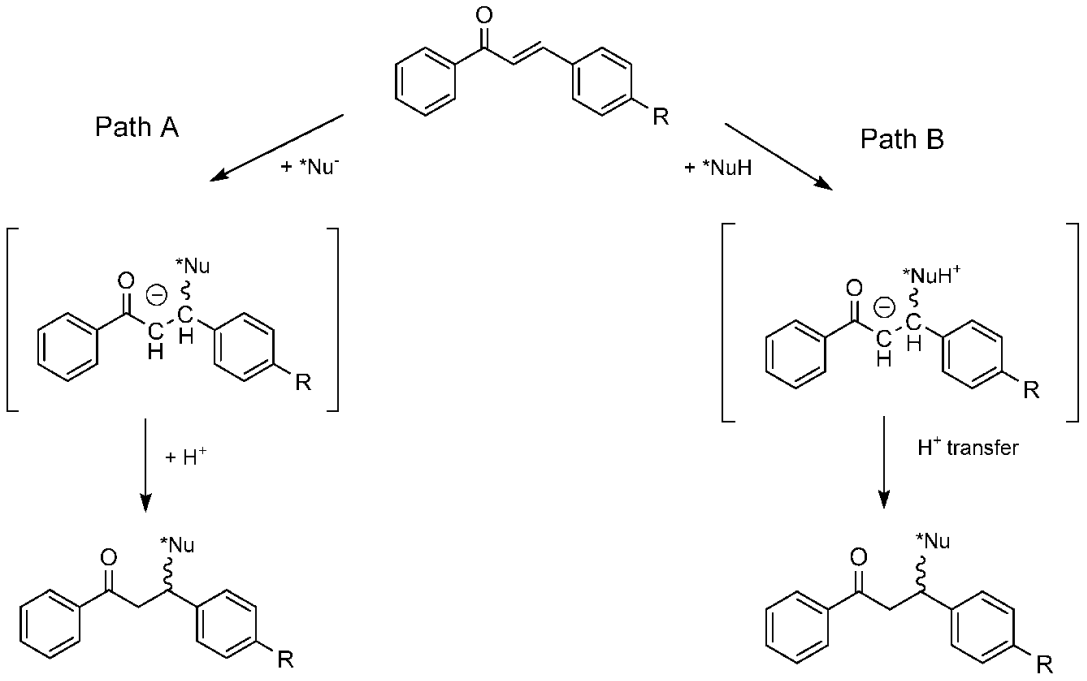

Figure 1. General mechanisms of the addition reaction of nucleophiles onto the activated double bonds of chalcones.

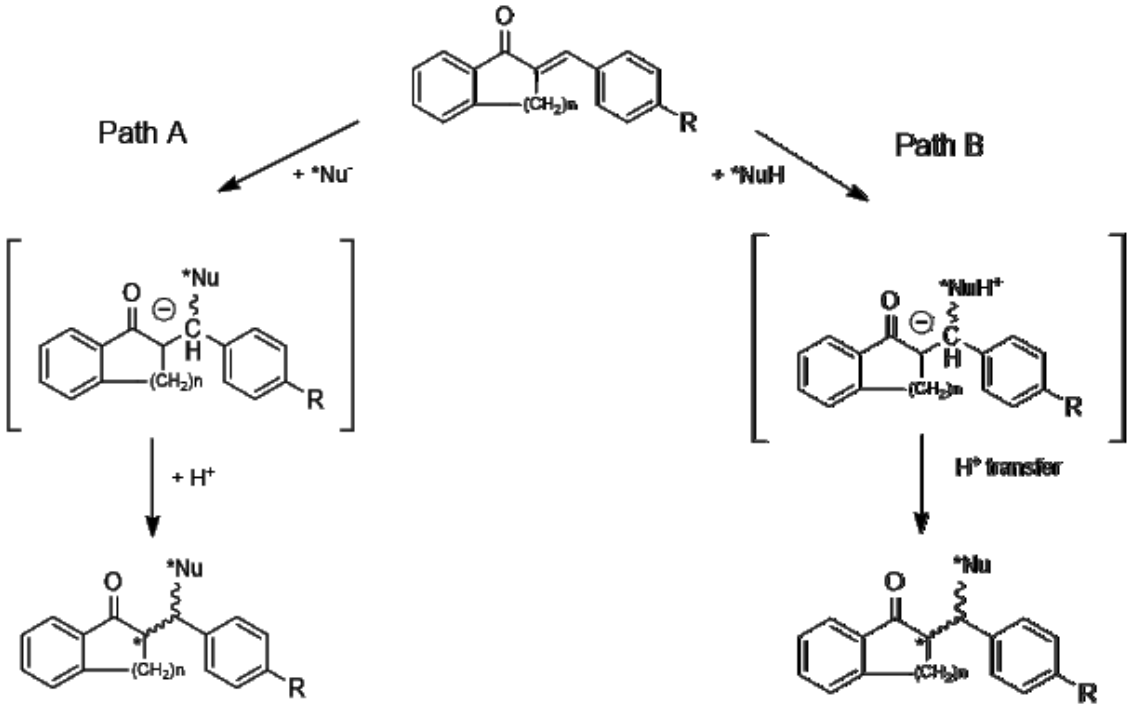

Figure 2. General mechanism of addition of a nucleophile onto the activated double bond of the cyclic chalcone analogs (*E*)-2-benzylideneindanone (n=1), (*E*)-2benzylidenetetralone (n=2), and (*E*)-2-benzylidinebenzosuberone (n=3).

1.1.2. The biological significance of chalcones

Several biological effects of chalcones and their synthetic analogs are associated with their spontaneous and enzyme-catalyzed reactivities. Different mechanisms of action were suggested for these activities, but the exact molecular target is not known in many cases. α,β-Unsaturated carbonyl systems have been shown to have antioxidant activity, sustaining the reduced environment of the cell by trapping and stabilizing reactive oxygen (ROS) and nitrogen species (RNS). In this section, we focus on those biological activities that are reported to be linked to these compounds' role as Michael acceptors. These Michael addition acceptor activities are generally associated with covalent addition of the chalcones to cellular thiol groups of reduced glutathione (GSH) or reactive cysteine residues of proteins [15].

1.1.3. IκB Kinases

Nuclear factor κB (NF-κB) is a family of transcription factors comprising five members, including p50, p52, p65 (RelA), c-Rel, and RelB. Under normal conditions, they are in an inactive state bound to the so-called inhibitor κB (IκB). Stimulating cells with factors such as inflammatory cytokines, e.g., TNF and IL-1, bacteria or viruses, the activation of IκB kinase (IKK complex) is triggered, which in turn phosphorylates IκB's two major serine residues. It activates the κB transcription factor and translocates it to the nucleus, inducing the transcription of enhansosome to increase transcription of various genes that regulate innate and adaptive immune functions and inflammatory responses [16].

Activation of the IKK complex requires activation of one of its catalytic substituents: IKKα or IKKß. Each is responsible for a different pathway of activation of NF-κB. Shortly, IKKß is accountable for the so-called classical pathway, in which the stimuli are mainly cell membrane receptors such as TNF and IL-1 and T- and B-cell receptors. The overall activation of classical results in the translocation of RelA-P50 dimer, and this pathway aims to contribute to the cell's survival in usual cases. The alternative pathway activates through lymphotoxin, CD40, receptor activator of NF-κB (RANK) and involves the IKKα and translocation of RelB-P52 dimer. It is particularly important in the development of the lymphoid organs, T- and B-cells, and antigen-presenting cells such as dendritic and medullary thymic epithelial cells. It generally regulates immune response and tolerance [17]. While normal activation of NF-κB is an inseparable component of survival and immunity, dysregulation of the pathway is linked to the expression of inflammatory and infection characteristics [18]. One way to manipulate the IKK complex is inhibition through covalent binding of its serine179 with a Michael-acceptor

that suppresses NF-κB activation and ultimately alleviates inflammatory responses and, in turn, inflammation-related cancer [7].

We can mention the following examples of chalcones interacting with the NF-κB pathway. Licochalcone A is reported to stop cell migration in addition to causing cell cycle arrest by inhibiting NF-κB [19]. Cardamonin, another chalcone with anti-inflammatory properties, showed to down-regulate NF-κB and protect development of colitis in a mice model [20]. Flavokavain A and B are inhibitors of IκB, resulting in ease in migration of P50 and P65 to the nucleus. They are proven to be potent inhibitors of TNFα-induced NF-κB [18]. Isoliquiritigenin has been reported to suppress IKK, ERK1/2, and p38 phosphorylation in murine macrophage cell line RAW 264.7, resulting in NF-κB inhibition and iNOS, COX-2, TNF-α, and IL-6 down-regulation [7,21].

1.1.4. Nrf2/ARE signaling pathway

Nuclear factor erythroid 2-related factor 2 (Nrf2) is a basic leucine-zipper-region transcription factor that plays a crucial role in induction and activation of genes responsible for cytoprotection and antioxidant activity, both in response to oxidative stress and constitutive activity [22]. It has been linked to cancer, diabetes, Alzheimer and other inflammatory diseases [23–26]. Under unstressed conditions, Nrf2 can be found in cytoplasm bonded to Keap1 (Kelch-like ECH-associated protein 1), which is degraded quickly through proteasomal mechanisms to keep its intracellular levels low. However, in the presence of ROS, other electrophilic species - or reduction in antioxidant capacity, i.e., decrease in reduced GSH or disruption of redox balance- the Nrf2/ARE pathway is activated by degradation of the Keap1-Nrf2 complex. It results from modifying the Keap1 cysteines, leading to a conformational change and assisting in the release of Nrf2. Nrf2 then translocates to the nucleus and binds to the antioxidant response element (ARE). Once Nrf2 is bounded to the ARE, the antioxidant genes are induced, including those coding phase II and phase III metabolic enzymes with the metabolizing, transportation, or excretion of endo- and xenobiotics. Among them, NADPH: quinone oxidoreductase 1 (NQO1) [27,28], sulfiredoxin I (Srxn1), Nrf2 dependent hem oxygenase-1 (HO1) [7], UDP-glucuronosyltransferase (UGT) as well as multidrug resistance-associated proteins (MRPs, MRP1-MRP9) [29] should be mentioned. Chalcones can take part in activating the Nrf2/ARE pathway regardless of the level of oxidative stress by either a) modification of Keap1 cysteine residue(s) and such promoting the dissociation of the Keap1-Nrf2 complex resulting in translocation of Nrf2 to the nucleus or b) supporting the translocation of Nrf2 to the nucleus by

interacting with kinases such as P38 mitogen-activated protein kinase (p38-MAPK), which mainly phosphorylate Nrf2, to accelerate separation from Keap1 [23,30].

There are more than 200 genes whose expression depends on the Nrf2 pathway in humans, which affect Phase I and Phase II metabolisms, inflammation, and inflammation-related cancer. In normal cells, Nrf2 activation results in acute detoxification, protecting DNA against common mutagens. In cancer cells, however, the all-time activation of Nrf2 supports cancer cells 'growth, metastasis, and negative outcomes. It has been reported that mutations in either Nrf2 or Keap1 may be responsible for sustained activation of Nrf2 and affect the regulation of cancer metabolism, microRNAs, and oncogenic signaling resulting in various cancer types [31]. The dual role of chalcones, acting as inductors of Nrf2 in normal cells [22,30] and suppressors of Nrf2 in cancerous cells [19], are important in drug development research.

For example, the anticolitic mechanism of action of sofalcone has been reported to be in connection with the Nrf2/ARE pathway. In this case, dissociation of the Keap1-Nrf2 complex occurs by biding the chalcone to Keap1 [10]. Another synthetic [32] and non-synthetic [33,34] chalcones showed to interact with this pathway. One example is the anti-arteritis effect of licochalcone A, which also resulted in drug-induced oxidative damage and, in turn, apoptosis.

1.2. Thiols

1.2.1. Glutathione

L-gamma-glutamyl-L-cysteinyl-glycine (glutathione, GSH) is a major tripeptide found and synthesized in significant (1-10 mM) concentrations in most mammalian cells [35]. The hepatic cells are the main sites of GSH production; however, all cells of the human body can synthesize glutathione to some degree except the epithelial tissue. Glutathione is made up of three amino acids, namely, L-glutamate, L-cysteine, and glycine, and is present in reduced (GSH) and oxidized (GSSG) form in the cells. Under physiological conditions, glutathione exists in a significantly higher concentration of GSH than GSSG (approximately 9:1). The exact ratio of the two forms, however, is organelle dependent. Biosynthesis of GSH (*de novo)* is completed through an enzyme-catalyzed two-step pathway consuming an ATP in each step. In step 1, L-glutamic acid is added to cysteine catalyzed by γ-glutamylcysteine synthetase (γGCS); in step 2, the glycine is added to glutamylcysteine catalyzed by glutathione synthetase (GS). Generally, the synthesis of GSH depends on the cysteine availability and the activity of the γGCS enzyme. Other ways through which GSH is made available to the body are (a) reduction of GSSG to two GSH molecules by glutathione-reductase (GR) using NADPH as well as (b)

gamma-glutamyltransferase(GGT)-catalyzed recycling of cysteine from glutathione conjugates to maintain the cysteine pool. GSH contributes to most of the intracellular thiol (SH) groups and participates in many important mechanisms in the body.

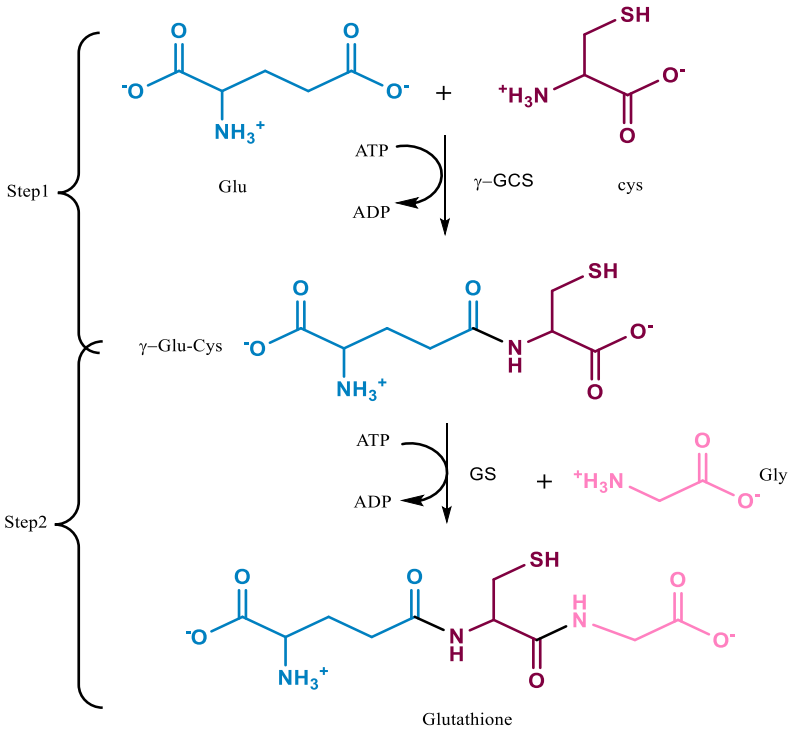

Figure 3. Biosynthetic pathway of glutathione (GSH).

Among the essential cellular functions of glutathione are (a) antioxidant activity, (b) metabolism and elimination of xenobiotics, (c) maintaining the cellular redox potential and playing an important role in (d) cell proliferation, (e) fatty acid biosynthesis and (f) signal transduction of gene expressions should be mentioned. Glutathione protects against endogenous oxidative stress produced due to oxygen consumption, immune cell activation, aging, and cancer and against exogenous oxidative stress resulting from drug intake, stress, and environmental pollution. Such factors produce oxidative species collectively named reactive oxygen species (ROS), reactive nitrogen species (RNS), and generally oxidants. Cells require a highly reduced environment to function properly. Accumulation of oxidative species such as superoxide anion radical (O_2^-), hydrogen peroxide (H_2O_2), and hydroxyl radical (·OH) result in changing the redox homeostasis of the cells. Superoxide anion is short-lived and is converted to hydrogen peroxide with the help of superoxide dismutase enzymes (SOD1 and SOD2). However, hydrogen peroxide has a longer half-life resulting in possibly irreversible damage to important cellular components. It can also further react with ferrous ions to generate hydroxyl radicals (Fenton reaction) [36].

GSH protects the reductive intracellular state by reducing reactive species, usually with the help of the glutathione peroxidase (GPx) enzymes. Moreover, it participates in glutathione S-transferase enzyme (GST)-catalyzed reactions in detoxifying xenobiotic metabolism and oxidative stress-related reactive products. GSH also plays a vital role in keeping essential antioxidants such as vitamin C and vitamin E in their reduced form resulting in maintaining redox balance [37]. Finally, GSH can reversibly bind to protein thiol residues (glutathionylation) to prevent their oxidative damage [36].

Nonenzymatic biotransformation is a significant component of the biotransformation of xenobiotics as the enzymatic ones due to spontaneous reactions of electrophilic species. Highly reactive electrophiles such as the endogenous 4-hydroxy-2-noneal or the exogenous NAPQI, the well-known metabolite of paracetamol, can react with GSH before their possible reaction with important cellular components such as DNA, RNA, and protein. These reactive electrophilic compounds are metabolized before exerting toxic effects in the cells, and less than expected attention has been given to non-enzymatic biotransformation. Sabzevari et al., for example, have concluded that GSH depletion is the responsible mechanism behind the cytotoxicity of hydroxychalcones by both conjugation-type and oxidation-type reactions [38].

1.2.2. N-acetylcysteine

N-acetylcysteine (NAC) is a non-toxic compound and precursor of glutathione biosynthesis. NAC is supplemented for the regulation of glutathione levels in the cells. Glutathione does not have good oral absorption, and to increase its concentration thus, NAC supplementation is advised. The most important use of NAC in medical practice is against acetaminophen poisoning. Moreover, chemically, it is a precursor of cysteine biosynthesis and, in turn, glutathione. It also involves a sulfhydryl functional group which can closely mimic the mechanism of glutathione in reaction with chalcones.

1.2.3. Glutathione S-Transferases

Glutathione transferases possess three main functions in living organisms: (a) catalytic activities, (b) binding of non-substrate ligands, and (c) involvement in protein-protein interactions [39] . The substrates of the GST-catalyzed reactions have three common properties: a) they are hydrophobic, b) they have an electrophilic (electron-deficient) atom (center), and c) they have spontaneous reactivity towards GSH.

One of the main catalytic functions of soluble GSTs is *participation in the cellular antioxidant system* [40]. They demonstrate activity toward several by-products of oxidative stress, including lipid- and DNA-hydroperoxides as well as the secondary peroxidation products such as acrolein, propenal, and 4-hydroxynonenal (HNE) [40–43].

Another well-known catalytic function of GSTs is the *isomerization of biologically important endogen molecules*. The enzymes can catalyze *cis-trans* isomerization reactions or the movement of a double bond within polycyclic molecules [41,44,45].

The third type of catalytic activity of glutathione transferases is the *conjugation of reduced glutathione (GSH)* with endogenous or exogenous electrophilic species involving the reactive thiol group of its cysteinyl moiety. Four groups of glutathione transferases can catalyze these characteristic reactions (a) canonical soluble (cytosolic) GSTs, (b) distantly related soluble (mitochondrial) Kappa-class GSTs, (c) hydrophobic (microsomal) MAPEG family GSTs, and (d) bacterial fosfomycin resistance proteins [46–50].

The cytosolic GST enzymes have two active sites per dimer, each consisting of at least two ligand binding regions: a particular binding site designated for GSH and a less specific binding site for the substrate. Glutathione (GSH) has three acidic (thiol, glycinyl carboxyl, glutamyl carboxyl) and one basic (amino) functional group. While only a small amount of the GSH thiol function is deprotonated at the physiological pH (pK_a of GSH(thiol) is around 9.2), the pK_a of GSH bound to most GSTs has been reported to be less than 7; meaning the enzyme-bound GSH is deprotonated at a higher degree at physiological pH – thus being activated for reaction with the electrophilic substrate [51].

Microsomes are fragments of endoplasmic reticulum and attached ribosomes that are isolated together when homogenized cells are centrifuged. Microsomal enzymes are typically found in the smooth endoplasmic reticulum, primarily in the liver, but also in the kidney, intestinal mucosa, and lungs. There are several microsomal enzymes, including flavin monooxygenases (FMO), cytochrome P450s (CYP), NADPH cytochrome c reductase, UDP glucoronyl transferases (UGT), glutathione-S-transferases (GST), epoxide hydrolases, among others. Hence, hepatic microsomes are commonly used to study the metabolic fate of drugs, as the liver is one of the major organs responsible for enzymatic drug elimination [52].

The MAPEG (Membrane Associated Proteins in Eicosanoid and Glutathione metabolism) family comprises six human proteins. Four of them (leukotriene C4 synthase, microsomal glutathione transferase (MGST) 1, 2, and 3) catalyze the reaction of GSH with

different electrophilic substrates. MGSTs also possess glutathione-dependent peroxidase activity [53–55]. MSGT1 was the first to be purified. It is a homotrimeric protein with a subunit size of 17 kDa. It is highly expressed in the liver but is also found in many other tissues such as the intestine, adrenal, renal, brain, lung, pancreas, and testis [56]. It is uniquely activated by sulfhydryl reagents such as N-ethylmaleimide (NEM), redox events, and proteolysis [54,55]. It was demonstrated that the Cys49 residue of the enzyme is the site of modification correlated to activation [57].

1.2.4. Glutathione and cancer

Reactive oxygen species (ROS) play an important role in tumor cell signaling, tumorigenesis, and cancer progression. Its production is considerably higher in cancerous cells due to higher growth and proliferation rate. Therefore, such cells commonly show higher expression of antioxidant systems such as Nrf2 and other enzymes related to GSH synthesis and utilization. Moreover, some tumors promote upregulation of GSH synthesis and turnover, such as ovarian, breast, and lung cancer.

Many chemotherapeutic agents bind to GSH through various reaction mechanisms. Cyclophosphamide, for example, an alkylating agent, binds through an S_N2 reaction, while N,N',N''-triethylenethiophosphoramide is a GST-substrate; cisplatin, a DNA cross-linking agent, has shown intrinsic thiol binding including GSH and NAC as well as being a GST substrate [58]. Some drugs are inactivated by transforming into GSH-conjugates, increasing their solubility [59]. On the other hand, enzymatic or nonenzymatic conjugation of some chemotherapeutic agents with GSH results in their bioactivation, through which the conjugates are as reactive or even more reactive than the parent compound. The mechanisms through which bioactivation occurs are the (a) cysteine S-conjugate β-lyase pathway, (b) non-enzymatically formed GSH S-conjugates, (c) activation through GSH-GSSG redox cycling, and (d) conjugates that transport and release the parent compound elsewhere [58]. In the case of bioactivation, those cells show higher expression of GSH, and the GST enzymes are more prone to be the target of the pharmacological effect of such activated agents.

Given the vital role of GSH in the survival and drug resistance of cancerous cells provides an exciting perspective on cancer treatment. While the elevation of GSH and GST was considered a sign of a bad prognosis until recently, exploring the dual nature of GSH reactivity can open new research pathways.

1.3. Structure-activity relationships of the chalcones

By modifying the chalcone structure, the electron density, steric effects, polarizability, and dipole moment, as well as physicochemical parameters such as log*P*, log*D*, and pK_a, may be affected. A conservative bioisosterism often affects steric parameters such as van der Waals radii. The effect of substituent results in considerable changes in a) bonding interactions, b) metabolic stabilities, c) physical features, and d) selective reactivity [3]. Additionally, the reactivity of Michael-acceptors is an important factor in drug development since too high reactivity can result in cellular damage and toxicity. Considering this importance, changing compounds' structure will help tailor their reactivity to the drug development needs; for this purpose, we will look at the significance of rings and the substituents on the structure of chalcones.

1.3.1. Significance of the rings

Dimmock et al. reported on the significance of the presence of the B ring in the structure of the chalcone; moreover, they discussed the importance of the distance between the A and B rings in the chalcone structure. As the number of carbons increases in the C ring of the analogs, it results in: a) a change in the distance of A and B rings, b) a change in the relative position of functional groups, c) a change in the spatial position of A and B ring in comparison to each other, as the A and B ring may be in the same or out of plane in relation to each other, and d) the relative angle between the aryl ring and its adjacent olefinic group. It was reported that the size of the C ring influences the distance between the A and B rings -measured from the middle of the rings- which is the lowest in the case of 5-membered ring analogs and increases in the case of 6 and 7-membered analogs, respectively [60].

Considering that the open chain chalcone structure is close to planar, the B ring was measured to be the most elevated in the **2**>**4**>**3** analogs compared to the A ring. The torsion angle follows the same pattern, and from the point of view of the proximity of the B ring to a double bond, analog **4** was reported to be the farthest, followed by **2** and **3** analogs [60]. Other significant distances in the molecule can be listed as a) the distance of carbon number 10 (C_{10}) measured from the center of A ring (*Ac*), b) the distance C_{10} to the axis 2 (*d1*), c) the distance of the *Ac* to the center of alkylene portion of cycloaliphatic ring, and d) the angle between C-C bonds connected to the carbonyl carbon (*Ψ2*) as well as e) the angle *Ψ4* shown in Figure 4, all of which reported to be inversely proportional to the potency of the compounds. On the contrary, increasing the distance of ring B in addition to that of axis 2 along with the distance

of ring A to the oxygen atom situated on the carbonyl group has shown to be directly proportional to the cytotoxicity and the bioactivity of the compounds [4]. Generally, it was emphasized that the ring's size correlates with the compounds' bioactivity and cytotoxicity against human tumor cell lines. Moreover, in the case of potency, **4**>**3**>**2** was reported in the case of cyclic compounds, while the open chain chalcones (**1**) is always slightly more potent than the indanone analog **2** [4,5,60].

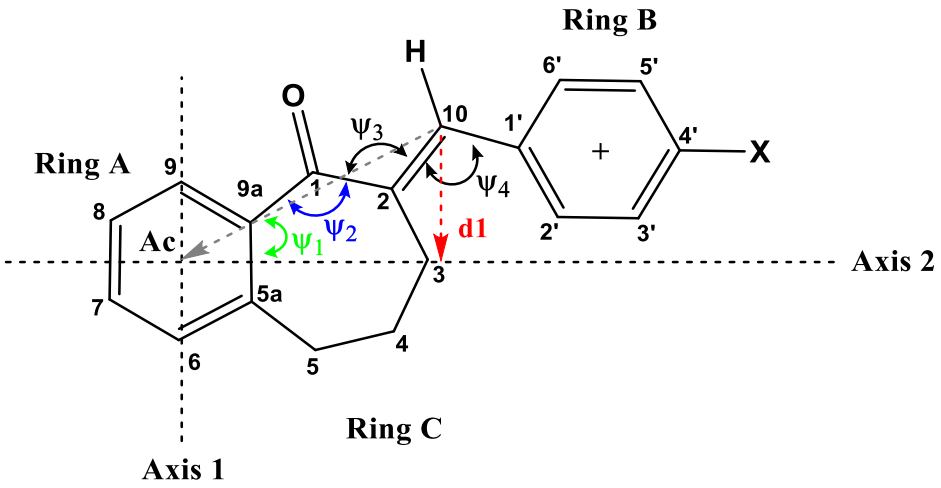

Figure 4.. Measurements ofΨ1-Ψ4 and d1 of compound **4b** [4].

1.3.2. Significance of substituents

By measuring the electronic properties of the different substituents (Hammett's σ), the electron donating groups - having negative sigma (σ) values- increase the electron density at the site of the B ring resulting in an enhanced van der Waals interaction at the site of binding. It was also shown that this property correlated with the cytotoxicity of these compounds. The hydrophobic (P_i constants) and steric (molar reactivity) properties were also plotted against the cytotoxicity, revealing that steric factors influenced cytotoxicity the most in comparison to the other properties [4]. In a QSAR study, Katsori et al. reported the clog*P* parameter to play an important part in the QSAR relationships [61].

Based on electron distribution and molecular electrostatic potential mapping, the most electrophile parts of chalcones were the C_1 and the C_{10} atoms. Substitution of an electron-withdrawing group on the A ring results in a higher electron deficiency on C_1. In contrast, the electrophilic characteristics of C_{10} increase as a more electron withdrawing group are found on the B ring, especially on the *para* position, therefore resulting in higher receptivity of a

nucleophilic attack. However, in the case of those chalcones that are conformationally restricted (cyclic ones), electron-donating substitution on ring B increased their cytotoxic effect in comparison to electron-withdrawing substitution [2,62].

Upon investigation of these compounds against murine cell lines and human tumor cell lines, in the case of P388 and L1210, it was proven that the highest activity attributes to compounds **4b** and **4c**. Furthermore, in the case of human T lymphocytes, more than 50% of the investigated substituted **3** and **4** analogs resulted in a higher activity than that of the reference substance melphalan. Hence concluding **4b** and **4c** analogs are the most active against murine P388 and L1210 cell lines. In comparison, **4b** was reported to have the greatest activity against the human T lymphocyte cell line and overall activity [4,60]. **4c** analog was reported to have more selective toxicity towards colon cancer and breast neoplasms, while the methoxy-substituted **4a** showed a higher selective toxicity to breast neoplasms [60].

Based on the previous results that **4b** and **4c** were the most cytotoxic and overall, the most active compound (**4b**) is the most out of plane, Dimmock et al. observed that an increase in deviation of coplanarity of A and B rings correlates in a higher activity [60].

Dimethylamino substituted chalcones proved to be one of the compounds with the lowest potency in the case of *in vitro* anti-inflammatory properties such as inhibiting NO production on RAW 264.7 cells and biosynthesis of interleukin-1. The observations was explained as a result of the movement of the lone pair of electrons of the nitrogen atom through the B ring to the carbon atom (C_{10}) bonded to the thiol group of GSH (and other endogenous thiols) resulting in weakening the C-S bond and in turn destabilizing of chalcone-thiol adducts. Chalcones substituted with low electron pair donating ability, and those with electron pair withdrawing capacity showed moderate and high potency, respectively [63].

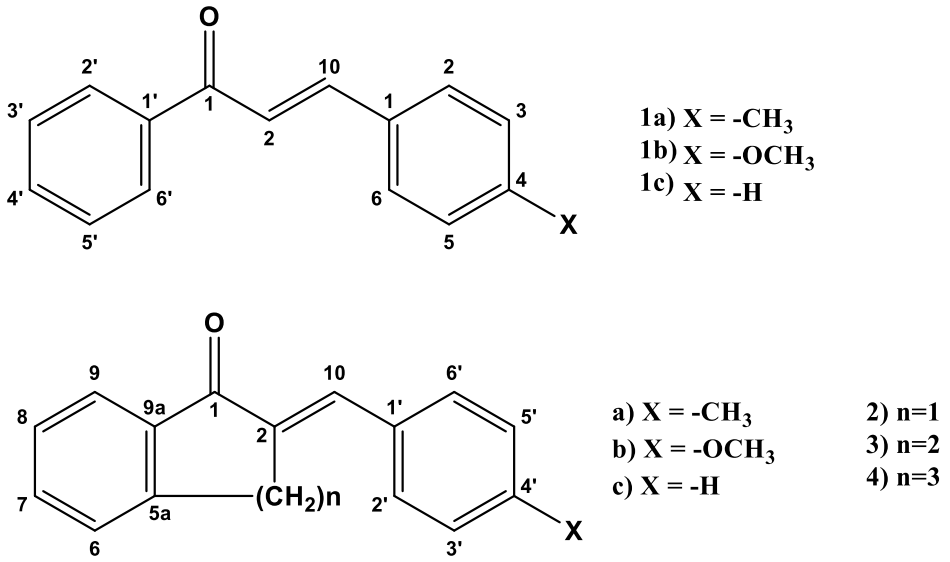

Figure 5. Structure of open chain and cyclic chalcone analogs.

1.4. (*E*)/(*Z*) isomerization of chalcones

Chalcones have the potential to exist in two different isomeric forms, namely (*E*) and (*Z*), based on the configuration of the C_2-C_{10} double bond of the enone moiety. The (*E*) isomers, also known as *trans* isomers, are thermodynamically more stable [1]. Theoretically, both of the isomers can be formed during synthesis of chalcones, however, due to the steric disadvantage, the (*Z*) isomer is unfavourable and the synthesis yields the pure (*E*) isomer [64]. There has been extensive research on the photoisomerisation and photodimerization of α,ß-unsaturated carbonyl systems [65–68]. Some cyclic compounds have been proven to undergo light initiated isomerization (day light and UV); the degree of isomerization has been reported to depend on the electronic characteristic of aromatic ring substituents and the size of C ring [64,66].

Previously Perjesi reported on isocratic HPLC separation of (*Z*)/(*E*) isomers of some cyclic chalcones (n=5-7). In each case but the indanone derivative (n=5) the (*Z*) isomer had a lower retention time in comparison to the respective (*E*) isomer. This finding is in agreement with the results of TLC investigation of log*P* of the same compounds, reporting that the respective Z isomers were less lipophilic [64,69].

2. Aims

The general aim of this Ph.D. work was to investigate the thiol (reduced glutathione (GSH) and N-acetylcysteine (NAC)) reactivity of 4/4'-substituted chalcones and seven-membered cyclic chalcone analogs *in vitro*. The specific aims are as follows

- Investigation of thiol-reactivity of chalcones (**1**) and seven-membered chalcone analogs (**4**) to study how
  (a) the 4(4')-aromatic substitution, and
  (b) incorporation of a seven-membered aliphatic ring into the chalcone moiety can affect the initial thiol reactivity of the derivatives.

- To study how the pH of the incubation medium affects the initial thiol-reactivity of the 4(4')-CH_3- and the 4(4')-OCH_3-substituted **1** and **4** derivatives,

- To study the stereochemical outcome of the thiol addition reactions onto the 4(4')-CH_3- and the 4(4')-OCH_3-substituted **1** and **4** derivatives at different pH,

- To study the metabolic stability of the **4c** derivative using rat liver microsomes, and

- To seek correlations between the observed thiol-reactivity and previously published cancer cell cytotoxic effects of some **1** and **4** derivatives.

3. Material and Methods

3.1.In vitro chalcone-GSH incubations

The starting (*E*) isomers of the chalcones were synthesized using a previously described method [5]. The purity was tested using TLC and HPLC-UV. The structure of both the (*E*) and (Z) isomers and those of the formed conjugates were verified using LC-MS measurements. Reduced glutathione (GSH) and *N*-acetylcysteine (NAC) were obtained from Sigma-Aldrich (Budapest, Hungary). The methanol (MeOH) CHROMASOLV gradient for HPLC was obtained from Honeywell (Hungary). Trifluoroacetic acid HiperSolve CHROMANORM was obtained from VWR (Budapest, Hungary), and formic acid from Fischer Chemicals. Deionized water was purified at the institute of pharmaceutical chemistry (University of Pécs) for use in HPLC and HPLC-MS measurements by Millipore Direct-Q^{TM}. Mobile phases used for HPLC measurements were degassed by an ultrasonic water bath for 5 minutes before use. Other chemicals used were of the analytical grade available.

To evaluate the reactivity of the investigated chalcones and their analogs with thiols, two solutions containing reduced glutathione (GSH) and *N*-acetylcysteine (NAC) were prepared as follows: Each solution was prepared at three different pH values (3.2, 6.3, and 8.0). The pH was set using freshly prepared 1M NaOH solution.

Solution (a) Solutions of GSH and NAC were prepared to a final volume of 1.5 cm^3 in deionized water with a concentration of 2.0×10^{-1} $mol \cdot L^{-1}$ (0.3 mmol thiol).

Solution (b) Chalcone solutions were freshly prepared before incubation to a 4.6 cm^3 volume of HPLC-grade methanol with a concentration of 6.5×10^{-3} $mol \cdot L^{-1}$ (0.03 mmol chalcone).

Solution (c) The GSH/NAC and chalcone solutions were pre-incubated in a 37 °C water bath for 15 minutes in the dark. Then, *solutions* (*a*) and (*b*) were mixed, resulting in a mixture of the thiol and the chalcone in a molar ratio of 10:1.

Solution (c) was kept in the dark in a temperature-controlled (37 °C) water bath for 315 min. To monitor the reaction by RP-HPLC and to qualitatively characterize the progress of the addition processes, the composition of the incubation mixtures was analyzed at the 15, 45, 75, 105, 135, 165, 195, 225, 255, 285, and 315 min time points by HPLC-UV.

To evaluate the initial (0 min) peak area of chalcones (**1a, 1b)**, and the cyclic analogs (**4a, 4b**), 4.6 cm^3 methanolic solution of each was prepared in the same way as above (solution

(b)), and the solutions were diluted with 1.5 mL of aqueous solution with the respective pH before analysis. Before mixing, the solutions were pre-incubated at 37 °C for 30 min.

To compare the products of the previously proven light-initiated (*E*)/(*Z*) isomerization of the parent compounds [64] with those of the non-light (retro-Michael reaction)-initiated isomerization, solutions of chalcone solutions (**1a-4b**) were prepared by method (b), and the solutions were subjected to unscattered laboratory light for 1 week. The solutions were analyzed by HPLC-UV and HPLC-MS.

3.2.Microsomal measurements

The starting (*E*) isomers of the chalcones were synthesized using a previously described method [5]. The purity was tested using TLC and HPLC-UV. The structure of both the (*E*) and (Z) isomers and those of the formed conjugates were verified using LC-MS measurements. Male rat pooled liver microsome 10 mg (M9066), magnesium chloride, 25mm syringe filters nylon membrane, pore size 0.45µm, and ß-nicotinamide adenine dinucleotide 2'-phosphate reduced tetrasodium salt hydrate (ß-NADPH) were purchased from Sigma Aldrich (Budapest, Hungary). Alamethicin, and reduced L-glutathione (GSH) BioChemica were obtained from Cayman Chemicals and ITW reagents. Methanol (MeOH) CHROMASOLV HPLC grade was obtained from Honeywell (Hungary). Millipore Direct-Q^{TM} at the Institute of Pharmaceutical Chemistry (University of Pécs) was used to provide deionized water for the measurements. Phosphate buffered Saline (PBS) pH 7.4 was prepared freshly on the day of incubation based on the 2014 Cold Spring Harbor Laboratory press method [70].

490µL PBS was mixed with 50µL of rat liver microsome (20 mg/mL protein) and 10 µL of alamethicin in methanol (50 µg/mg protein) and was left on ice for 15 minutes for microsomal activation. Then 100µL of NADPH solution (2.0 µmol/mL final concentration) was added, and the solution was vortexed to mix well. 25µL of a freshly prepared acetonitrile (ACN) solution of **4b** (final concentration 0.25 µmol/mL) and 100µL of $MgCl_2$ solution (final concentration of 5.0 µmol/mL) were added. After each addition, the solution was vortexed. The incubation volume was set to a total of 980 µL by the addition of 205 µL of PBS and left in a 37°C water bath for 3 minutes. Then 20 µL of GSH solution in PBS (final concentration of 5.0 µmol/mL) was added to bring the final volume to 1.0 mL. The mixture was vortex mixed for 10 seconds, taken to a shaking water bath, and kept in it for the incubation period (120 minutes). 150 µL samples were taken at 0, 30, 60, and 90-minute time points. (The 0-minute time points were considered the time of placement of the incubates into the water bath.) 150 µL ice-cold

methanol was used to stop the reaction at each time point. The 300 µL sample was centrifuged at 6000 rpm for 5 min; the supernatant was collected using a syringe and passed through a 0.45µm nylon membrane syringe filter. Control incubation containing all the constituents except the liver microsome was analyzed at 0, 30, 60, and 90-minute time points.

3.3.HPLC-UV measurements

The measurements were performed on an Agilent 1100 HPLC system coupled with a UV–VIS detector. The wavelength was set at 260 nm. The separation of the components was carried out in a reversed-phase chromatographic system. A Zorbax Eclipse XBD-C8 column (150 mm × 4.6 mm, particle size 5 µm; Agilent Technologies, Waldbronn, Germany) was used to separate the components. The injection volume was 10 µL. During the measurement, the column oven was set at room temperature (25 °C). Data were recorded and evaluated using Agilent ChemStation (B.03.01). Gradient elution was performed at a flow rate of 1.2 mL/min; the mobile phase consisted of (A) water and 0.1% trifluoroacetic acid and (B) methanol and 0.1% trifluoroacetic acid. The gradient profile was as follows: an isocratic period of 8 min of 40% mobile phase B, followed by a linear increase to 60% in 4 min, a second linear gradient to 90% in 3 min, and a 5 min isocratic period of 90%. The column was then equilibrated to the initial conditions with a 2 min linear gradient to 40%, followed by 3 min of the isocratic period.

3.4.HPLC-MS Measurements

HPLC HESI-MS analyses were performed on an Ultimate 3000 liquid chromatograph (Dionex, Sunnyvale, CA, USA) coupled with a Thermo Q Exactive Focus quadrupole-Orbitrap hybrid mass spectrometer (Thermo Fisher Scientific, Waltham, MA, USA). The scan monitored *m/z* values ranging from 100 to 1000 Da. Data was acquired using Q Exactive Focus 2.1 and Xcalibur 4.2 software (Thermo Fisher Scientific). Analysis of compounds and adducts was performed in HESI positive and negative ionization modes with the following parameters: spray voltage, 3500 V; vaporizer temperature, 300 °C; capillary temperature, 350 °C; spray and auxiliary gas flows, 30 and 10 arbitrary units, respectively; resolution, 35,000 at 200 *m/z*; and fragmentation, 20 eV.

HPLC separation was performed on an Accucore C18 column (150 mm × 2.1 mm, particle size 2.6 µm), and an Accucore C18 guard column (5 mm × 2.1 mm, particle size 2.6 µm) was also used. The injection volume was 5 µL; the flow rate was set to 0.4 mL/min. Data

analysis and evaluations were performed using Xcalibur 4.2 and FreeStyle 1.7 software. A binary gradient of eluents was used, consisting of mobile phases A and B.

The gradient parameters in chalcones were (A) water and 0.1% formic acid and (B) methanol and 0.1% formic acid. The gradient elution was as follows: isocratic elution for 1 min to 20% eluent B, continued by a linear gradient to 100% B in 9 min, followed by an isocratic plateau for 2 min. Then, the column was equilibrated to 20% B in 0.5 min and continued isocratically for 2.5 min. The sampler was at room temperature, and the column oven was at 40 °C.

The parameters of the gradient in the case of adducts were (A) water and 0.1% formic acid and (B) methanol and 0.1% formic acid. The gradient elution was as follows: isocratic elution for 1 min to 10% eluent B, continued by a linear gradient to 95% B in 13 min, followed by an isocratic plateau for 3 min. Finally, the column was equilibrated to 10% B in 0.1 min and continued isocratically for 2.9 min. The sampler was at room temperature, and the column oven was at 40 °C. The diode array detector was also set at 260 nm wavelength alongside MS analysis.

3.5. Molecular modeling

The structures **1c, 4c, CH_3SH,** and **CH_3S^-** were constructed using the Gaussview 6.0 software. Theoretical calculations were performed by DFT [71,72], implemented in the G16 [73] software package. The molecules were optimized using the hybrid exchange and correlation functional with long-range correction, M06-2X [74], combined with the basis set 6-311++G(d,p) in the gas phase. Frontier molecular orbitals (FMO) [75] were obtained. Molecular electrostatic potential maps contributed to the global electrophilicity analysis through their electronic isodensity surfaces. MEP [76] maps provide a visual representation of the electrostatic potential on the surface of a molecule, which can reveal regions of high and low electron density. The electrostatic potential V(**r**) [77] at point **r** is defined as.

$$V(\mathbf{r}) = \sum_{\alpha} \frac{Z_A}{|\mathbf{r}_\alpha - r_A|} - \int \frac{\rho(\mathbf{r})}{|\mathbf{r}_\alpha - \mathbf{r}|} d\mathbf{r} \quad (1)$$

4.

where Z_A is the charge of nuclei α at point $\boldsymbol{r}_\alpha$ and $\rho(\boldsymbol{r})$ is the charge density at point **r**. The local electrophilicity of the molecules was determined by the Fukui function [78,79], and then it was possible to predict the molecular site selectivity.

$$f(\mathbf{r}) = \left[\frac{\partial \rho(\mathbf{r})}{\partial N}\right]_v, \quad (2)$$

where N is the number of electrons in the system, and the constant term v in the partial derivative is external potential. Multiwfn 3.6 program [80] was used to calculate the Fukui. In addition, the *py*SiRC [81] – a machine-learning computational platform, was used to simulate oxidation reactions facilitated by free-radical compounds. To imitate the oxidation impact induced by a radical attack, the hydroxyl radical (·OH) was chosen as the archetype system of degradation reactions. The reaction rate constant of the oxidative attack caused by the hydroxyl radical on chalcones compounds was predicted using the XGBoost ML algorithm and the MACCS fingerprint was employed as a structural descriptor.

4. Results

4.1. Open chain Chalcones

4.1.1. Reactions performed under pH 8.0/7.4 conditions

This pH was chosen to mimic the GST-catalyzed reaction considering the pK_a values of reduced GSH and NAC, 8.83 and 9.52, respectively. In this pH, 3.6% of molecules in the case of GSH and 0.75% of NAC molecules exist in an ionized form which is the more reactive form of the thiols. Plotting the change of chromatographic peak areas of the parent compound **1a** and **1b** as a function of incubation time is indicating the composition of an equilibrium (Figures 6 and 7). By the end of the incubation period (315 min) with GSH, the initial area of the HPLC peak corresponding to the parent compounds **4a** and **4b** was reduced to 3.7% and 5.2%, respectively. In the case of the incubations with NAC, the initial areas of **1a** and **1b** was decreased to 5.2% and 9.8%, respectively (Table 1).

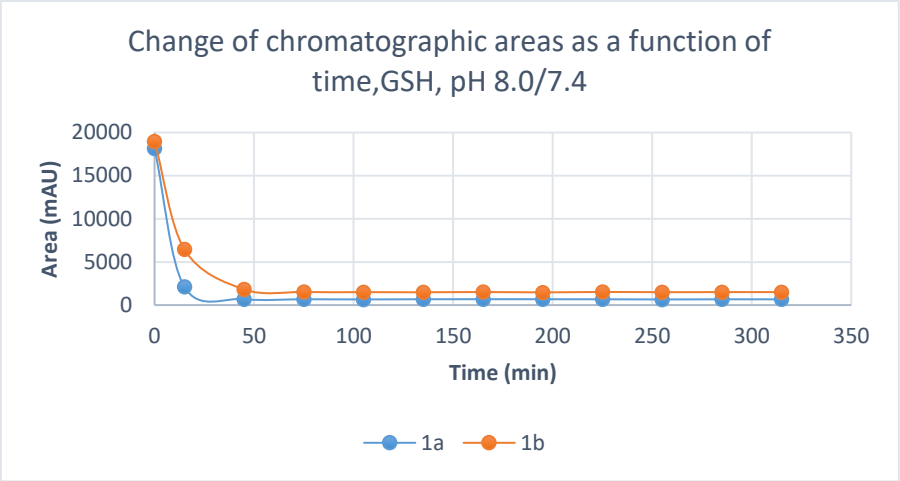

Figure 6. Change in the chromatographic peak area of chalcones **1a** and **1b** in the chalcone–GSH incubations at pH 8.0/7.4.

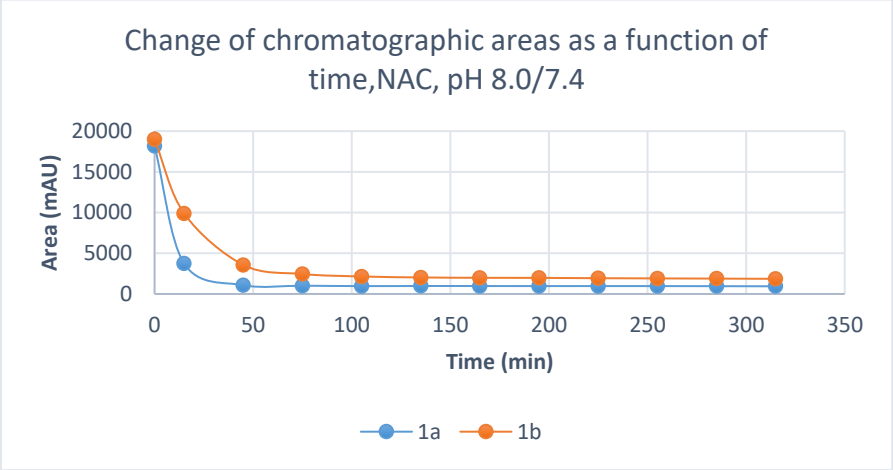

Figure 7. Change in the chromatographic peak area of chalcones **1a** and **1b** in the chalcone–NAC incubations at pH 8.0/7.4.

Based on the previously explained mechanism of the Michael addition reaction, a new chiral center is formed when the thiols are added to the chalcone counterpart. In the case of open-chain chalcone analogs, the addition reaction will result in one new chiral center; in the case of the cyclic ones, two new chiral centers will arise.

In the case of the open chain analogs and considering the inherent chirality of the two thiols, the formation of two diastereomeric adducts was expected. However, using our HPLC conditions, the **GSH-1** and **GSH-2** conjugates were not separated (Table 1).

Table 1. Retention times (t_R)[1] and integrated peak areas (A) of the investigated chalcones (**1a** and **1b**) and their GSH adducts (**GSH-1** and **GSH-2**)[2].

pH [3]	*Compound*	t_R *(E)-Chalcone*	*Area Ratio* [4] A_{315}/A_0	t_R *(Z)-Chalcone*	*Area (Z)-Chalcone*	t_R *GSH–1*	*Area GSH–1*	t_R *GSH–2*	*Area GSH–2*
3.2	**1a**	16.4	0.81	16.2	<100	13.8	4245	N/D [5]	-
3.2	**1b**	15.9	0.96	15.7	<100	11.9	3352	N/D [5]	-
6.3	**1a**	16.3	0.09	16.0	<100	13.2	16,571	N/D [5]	-
6.3	**1b**	15.8	0.21	15.5	<100	11.3	17,160	N/D [5]	-
8.0	**1a**	16.3	0.04	16.1 [6]	<100	13.3	17,419	N/D [5]	-
8.0	**1b**	15.7	0.08	15.5	<100	11.0	20,387	N/D [5]	-

[1]Retention times in minutes; [2]data refer to the average of two independent measurements at the 315 min time point; [3]pH value of the aqueous thiol solution; [4]ratios of peak areas measured at 0 and 315 min; [5]not detectable.

In the case of NAC incubations, the formed **NAC-1** and **NAC-2** adducts were present; however only partially separated. Based on the integration of the two overlapping peaks, the ratio of the two diastereomeric adducts was not equal and showed an (1.7–1.2 times) excess of the less polar diastereomers (Table 2).

Table 2. Retention times (t_R)[1] and integrated peak areas (A) of the investigated chalcones (**1a** and **1b**) and their NAC adducts (**NAC-1** and **NAC-2**)[2].

pH [3]	*Compound*	t_R *(E)-Chalcone*	*Area Ratio* [4] A_{315}/A_0	t_R *(Z)-Chalcone*	*Area (Z)-Chalcone*	t_R *NAC–1*	*Area NAC–1*	t_R *NAC–2*	*Area NAC–2*
3.2	**1a**	16.3	0.89	16.1	<100	15.2	1260	15.3	2173
3.2	**1b**	15.8	0.98	15.5	<100	14.1	1156	14.2	1507
6.3	**1a**	16.3	0.24	16.0	<100	15.1	4906	15.2	6457
6.3	**1b**	15.8	0.47	15.5	<100	14.1	4712	14.2	5422
8.0	**1a**	16.2	0.05	16.0	<100	15.1	6167	15.2	8875
8.0	**1b**	15.7	0.10	15.5	<100	14.1	7167	14.2	8975

[1]Retention times in minutes; [2] data refer to the average of two independent measurements at the 315 min time point; [3]pH value of the aqueous thiol solution; [4]ratios of peak areas measured at 0 and 315 min; [5]not detectable.

The structure of the parent chalcones (**1a** and **1b**), as well as their GSH and NAC conjugates, were verified by HPLC-MS (See Table 3 and Figures 8-13).

Table 3. Mass spectrometry data.

Type	*Value*	*1a*	*1b*
Chalcone	Formula	$C_{16}H_{14}O$	$C_{16}H_{14}O_2$
	$[M+H]^+_{th}$	223.1123	239.1072
	$[M+H]^+_{m}$	223.1117	239.1066
	ΔM	-2.69 ppm	-2.51 ppm
Chalcone-GSH adduct	Formula	$C_{26}H_{31}N_3O_7S$	$C_{26}H_{31}N_3O_8S$
	$[M+H]^+_{th}$	530.1961	546.1910
	$[M+H]^+_{m}$	530.1946	546.1892
	ΔM	-2.83 ppm	-3.30 ppm
	Number of isomers	1	1
Chalcone-NAC adduct	Formula	$C_{21}H_{23}NO_4S$	$C_{21}H_{23}NO_5S$
	$[M-H]^-_{th}$	384.1270	400.1219
	$[M-H]^-_{m}$	384.1246	400.1191
	ΔM	-6.25 ppm	-7.00 ppm
	Number of isomers	2	2

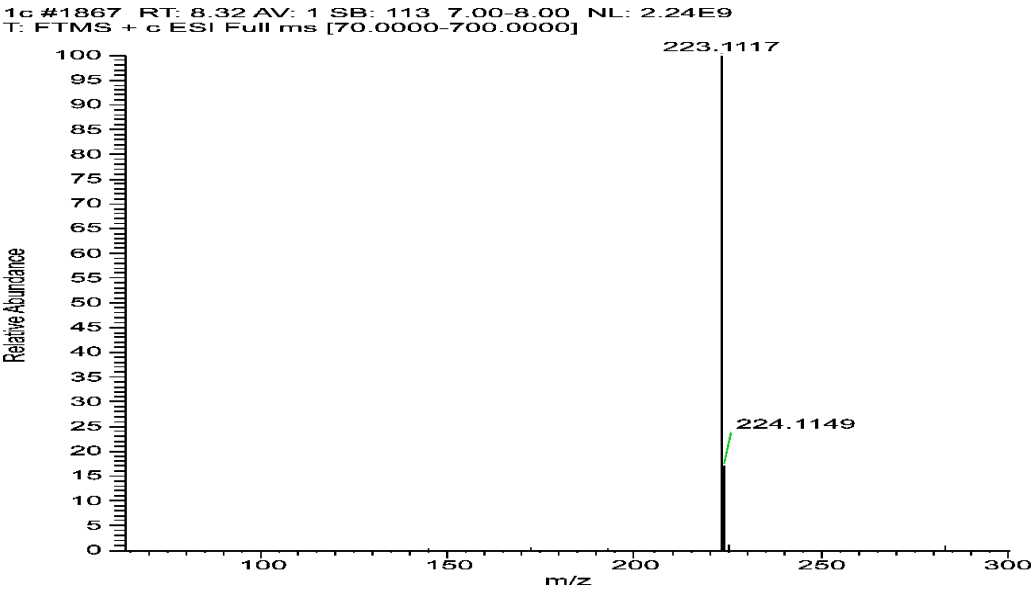

Figure 8. High resolution, positive mode HESI MS spectrum of chalcone **1a**

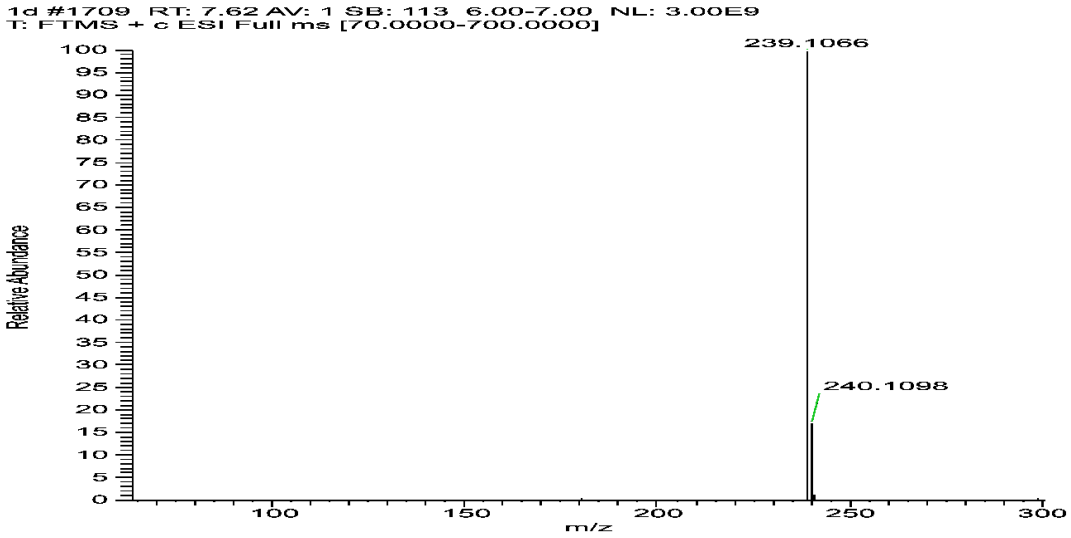

Figure 9. High resolution, positive mode HESI MS spectrum of chalcone **1b**.

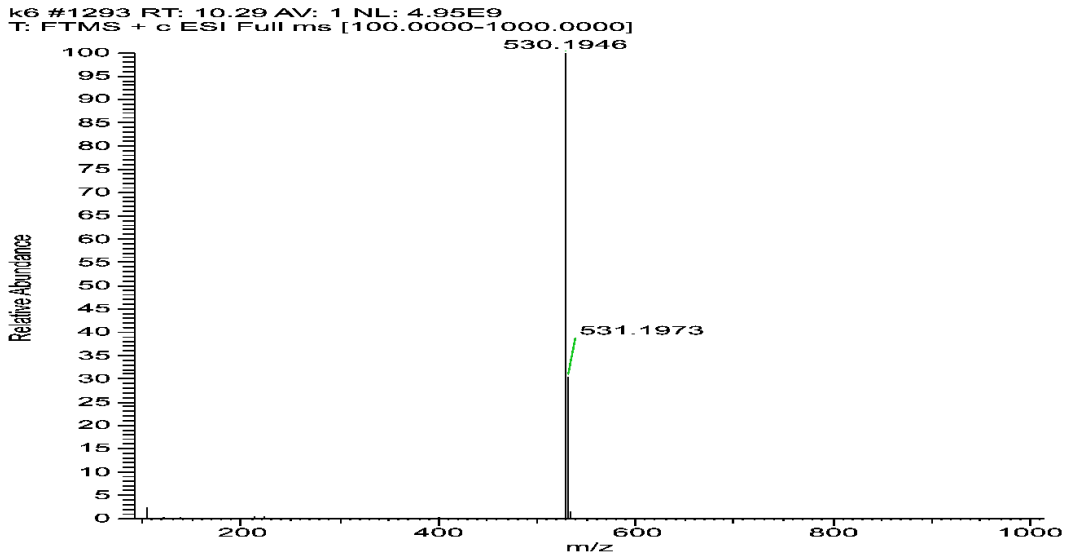

Figure 10. High resolution, positive mode HESI MS spectrum of chalcone **1a-GSH-1** conjugate.

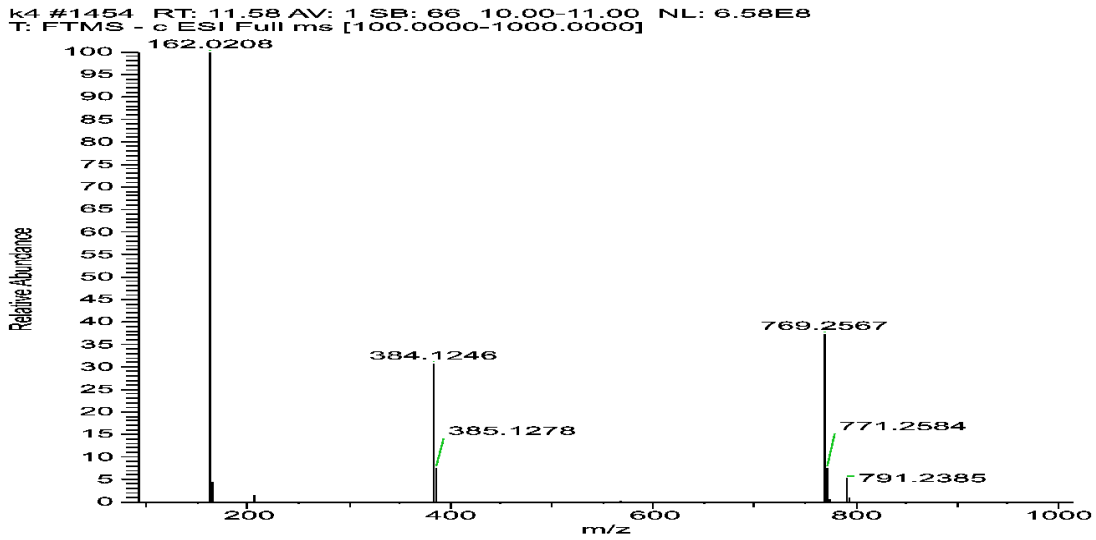

Figure 11. High resolution, negative mode HESI MS spectrum of chalcone **1a-NAC-1** conjugate.

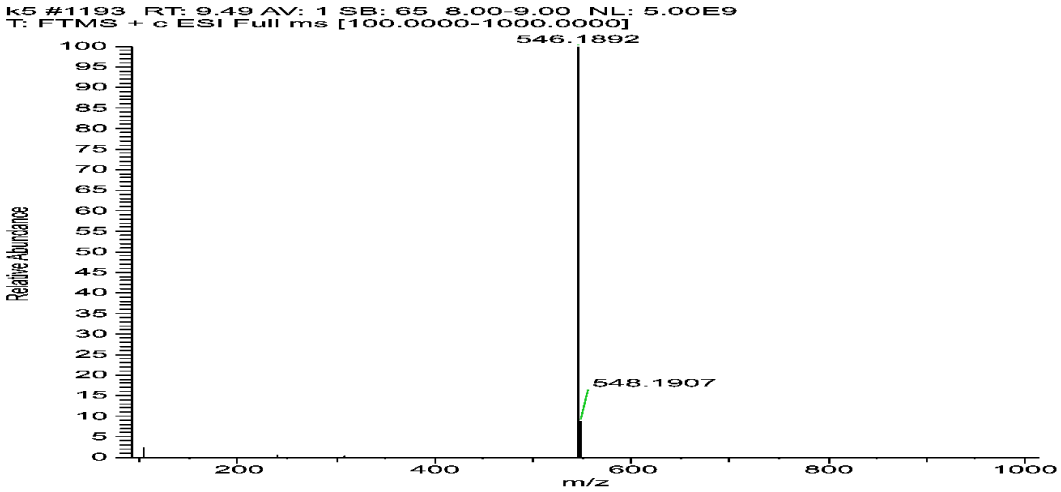

Figure 12. High resolution, positive mode HESI MS spectrum of chalcone **1b-GSH-1** conjugate.

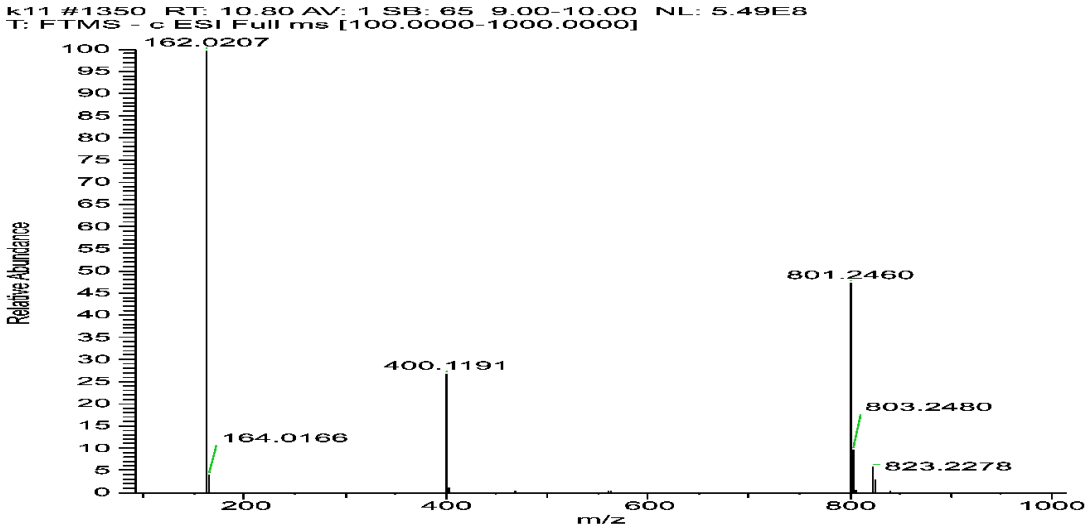

Figure 13. High resolution, negative mode HESI MS spectrum of chalcone **1b -NAC-1** conjugate.

The progress curve of peak-1 of GSH-conjugate (**GSH-1**) of compounds **1a** and **1b** plotted as a function of time shows a mild but constant increase in the AUC of the diastereomer (Figure 14).

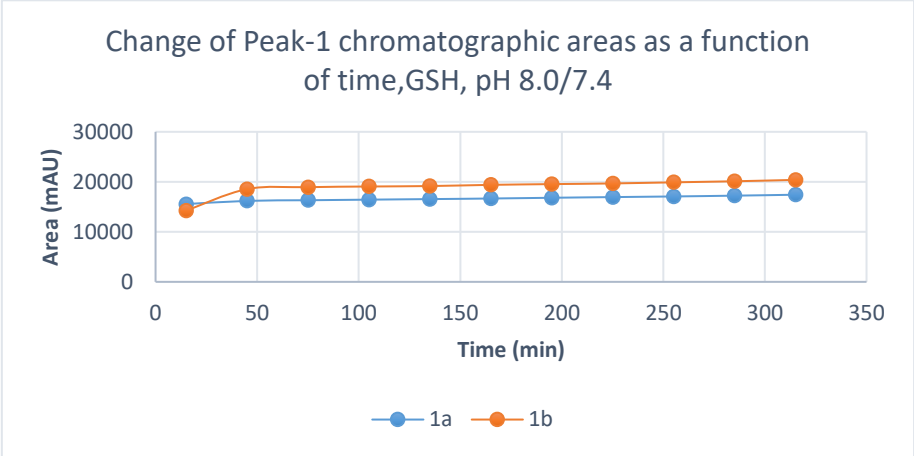

Figure 14. Change in the chromatographic peak area of **GSH-1** conjugate of chalcones **1a** and **1b** in the chalcone–GSH incubations at pH 8.0/7.4.

The progress curves of diastereomeric NAC adducts (**NAC-1** and **NAC-2**) formation as a function of the integrated HPLC peak areas (AUCs) are shown in Figures 15 and 16. As shown, the formation of the NAC-conjugates of **1a** increased in the first 45 min and remained the same over incubation. In the case of the NAC-conjugates of **1b**, the kinetic product (**NAC-1**) was rapidly formed in the first 15 min. After that, however, the **NAC-1** isomer of **1b** was

trans-isomerized to the thermodynamic product (**NAC-2**), reaching the equilibrium composition by the 105 min time point (Figures 15 and 16).

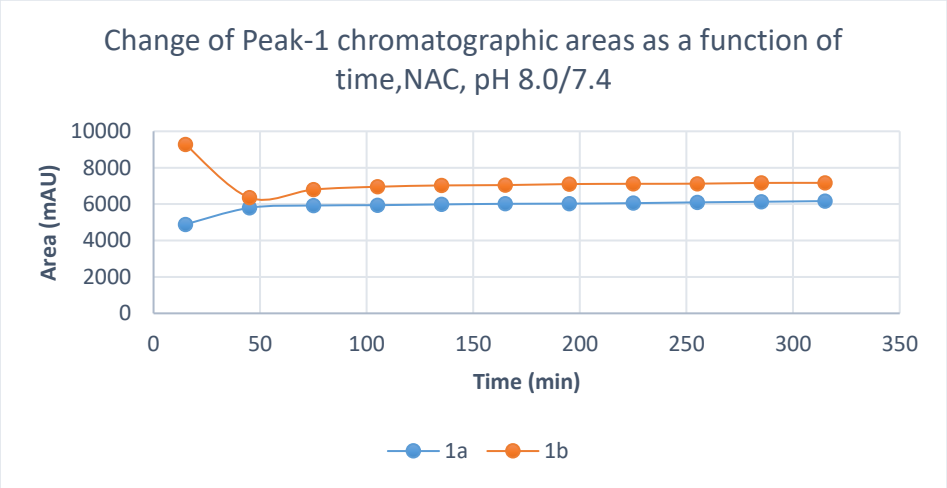

Figure 15. Change in the chromatographic peak area of conjugate adduct-1 (**NAC-1**) of chalcones **1a** and **1b** in the chalcone-NAC incubations at pH 8.0/7.4.

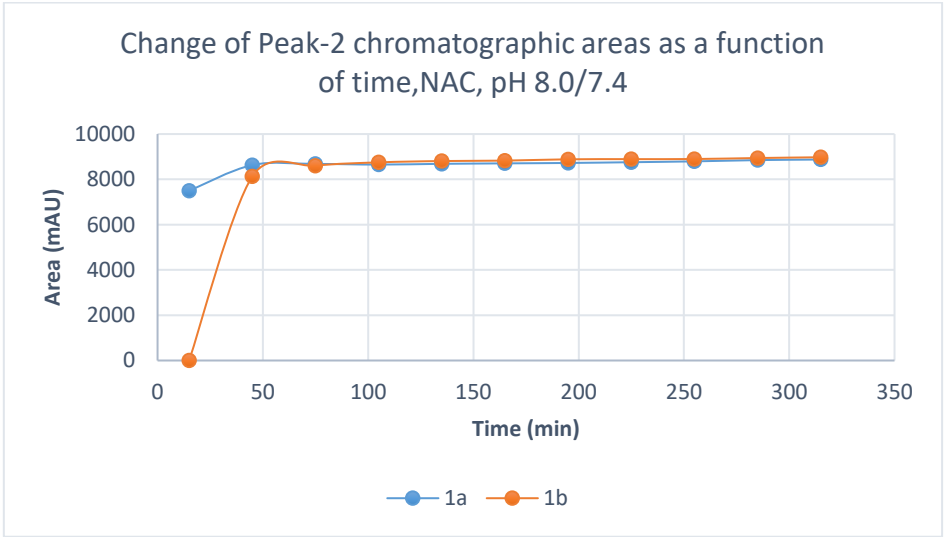

Figure 16. Change in the chromatographic peak area of conjugate adduct-2 (**NAC-2**) of chalcones **1a** and **1b** in the chalcone-NAC incubations at pH 8.0/7.4.

In addition to the data above, it is worth mentioning that during incubations with both NAC and GSH, some minor new peaks with a slightly lower retention time to the chalcone parent peak **1a** and **1b** (the unreacted ones) were formed. Our previous results suggest that these peaks are the (*Z*) diastereomers of the parent (*E*)-chalcones. Since these peaks do not arise in incubations performed without thiols, the formation of such peaks during the incubation can be

considered as a result of a retro-Michael addition reaction, a non-light-initiated isomerization of chalcones, and their analogs. To identify the structure of the expected (*Z*) diastereomers, light-initiated isomerization of **1a** and **1b** was performed. The results were compared with the non-light-initiated isomerization experiment. The formed compounds were identified as the respective (*Z*) isomers. Figures 17 and 18 demonstrate the chromatogram of light-initiated *E*/*Z* isomerization of compounds **1a** and **1b**.

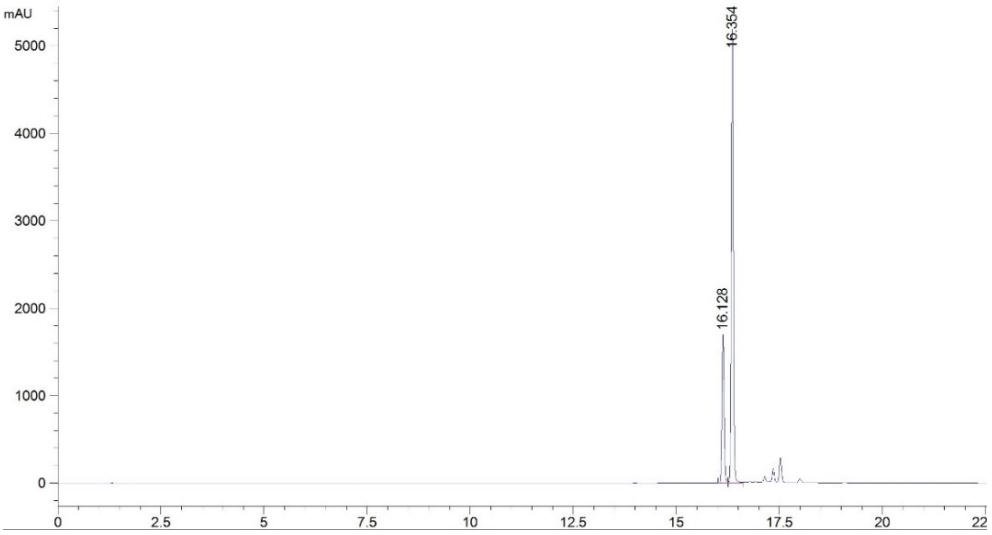

Figure 17. HPLC-UV-Vis spectrum of (*E*)(t_R 16.354 min) and (*Z*)(tr 16.128 min) isomeric mixture of chalcone **1a**.

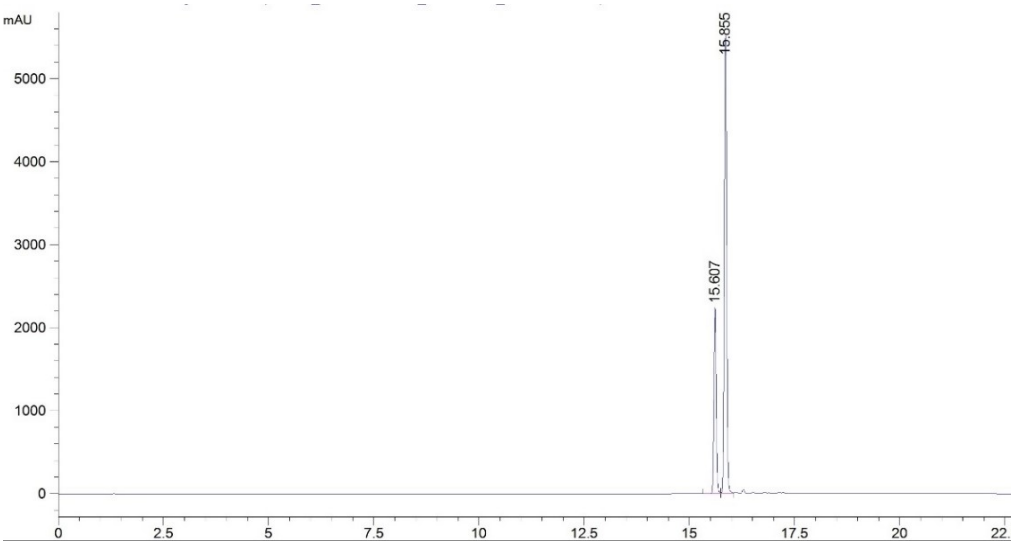

Figure 18. HPLC-UV-Vis spectrum of (*E*)(t_R 15.607 min) and (*Z*)(tr 15.855 min) isomeric mixture of chalcone **1b**.

4.1.2. Reactions performed under pH 6.3/6.8 condition

Reactions under slightly acidic conditions mimic the cellular milieu of cancer cells since their metabolism shifts to support their very costly rapid proliferation, migration, and survival [82]. Most of the glucose is converted into pyruvate and, in turn, lactic acid, even in the presence of oxygen, in contrast to the normal aerobic glucose metabolism, where pyruvate is further oxidized to carbon dioxide and water [83]. Accumulating lactic acid causes the pH of cancer cells to be slightly more acidic than normal cells [84]. Under these experimental conditions (pH 6.3/6.8), only about 0.9% of GSH and 0.2% of NAC molecules exist in the more reactive thiolate form. The progress of the reactions under such conditions was more restricted than that observed at pH 8.0/7.4. In the GSH incubations, the initial area of the parent compounds **1a** and **1b** was reduced to 9.4% and 21.4% by the end of the investigated period (Table 1). The respective figures for the NAC incubations were 24.4% and 46.8% (Table 2).

Progress curves of the reactions (Figures 19 and 20) indicated that the percentage figures represent compositions close to equilibrium. Similar to the results obtained under pH 8.0/7.4 conditions, the formation of a small amount of (*Z*) isomers was detected in the incubation mixtures.

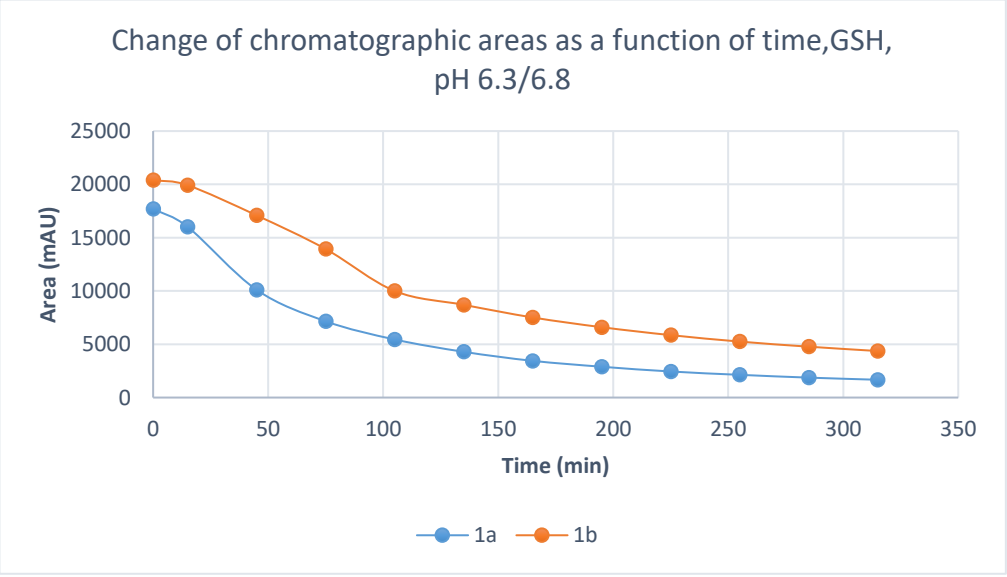

Figure 19. Change in the chromatographic peak area of chalcones **1a** and **1b** in the chalcone GSH incubations at pH 6.3/6.8.

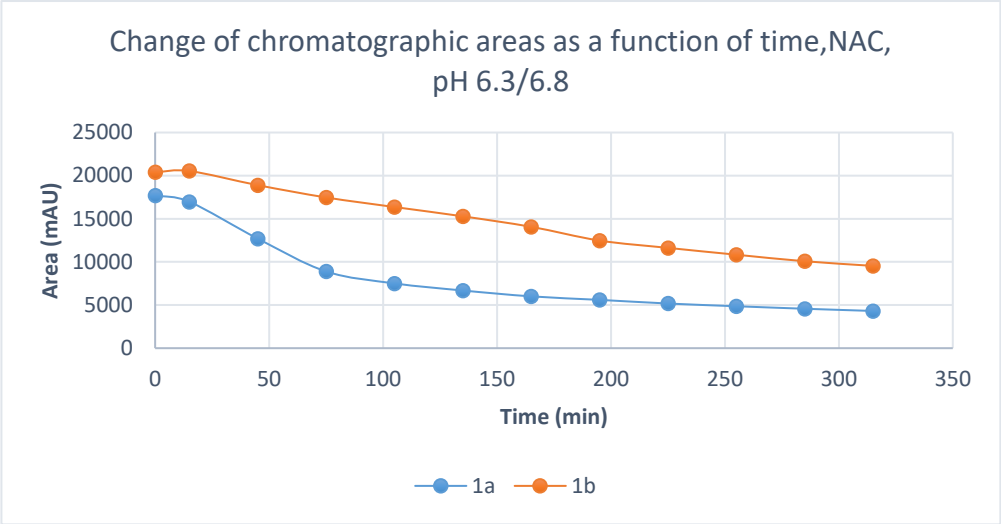

Figure 20. Change in the chromatographic peak area of chalcones **1a** and **1b** in the chalcone–NAC incubations at pH 6.3/6.8.

Progress curves of the formation of the chalcone-GSH and chalcone-NAC adducts showed two parallel concave curves with finite limits (Figures 21–23).

The progress curve of the diastereomeric peak-1 of compounds **1a** and **1b** in reaction with GSH shows a constant increase in the AUC (Figure 21). However, the AUC of the final time point is smaller in the case of this pH in comparison to pH 8.0/7.4 by 4.9% and 15.8% for compounds **1a** and **1b,** respectively.

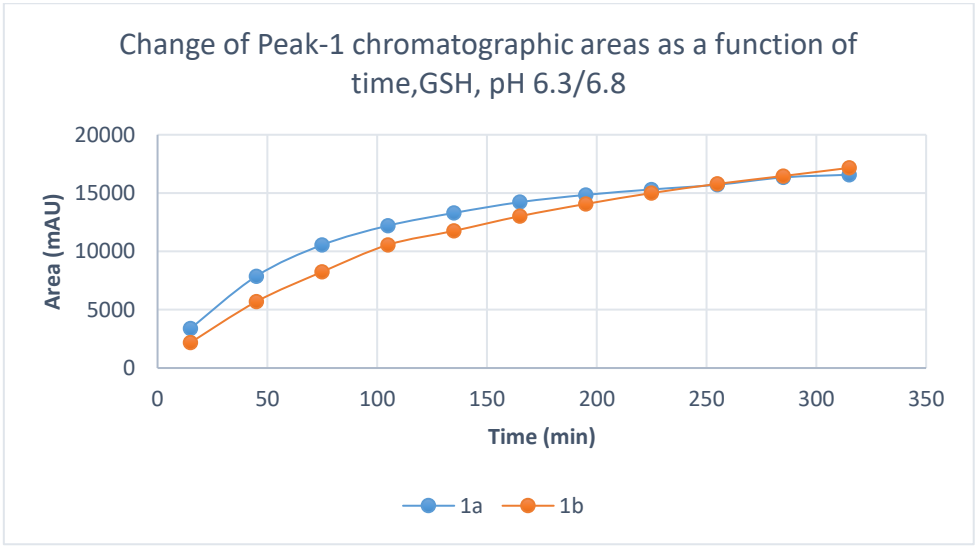

Figure 21. Change in the chromatographic peak area of conjugate adduct-1 of chalcones **1a** and **1b** in the chalcone–GSH incubations at pH 6.3/6.8.

The **NAC-1** and **NAC-2** show similar behavior to the **GSH-1** peak, where the AUC increases to the last time point, indicating that the equilibrium state has not been reached. The AUC of peaks-1 and 2 has been reduced by 20.4% and 27.2% in the case of **1a** and 34.2% and 39.6% in the case of **1b**. (Figures 22 and 23).

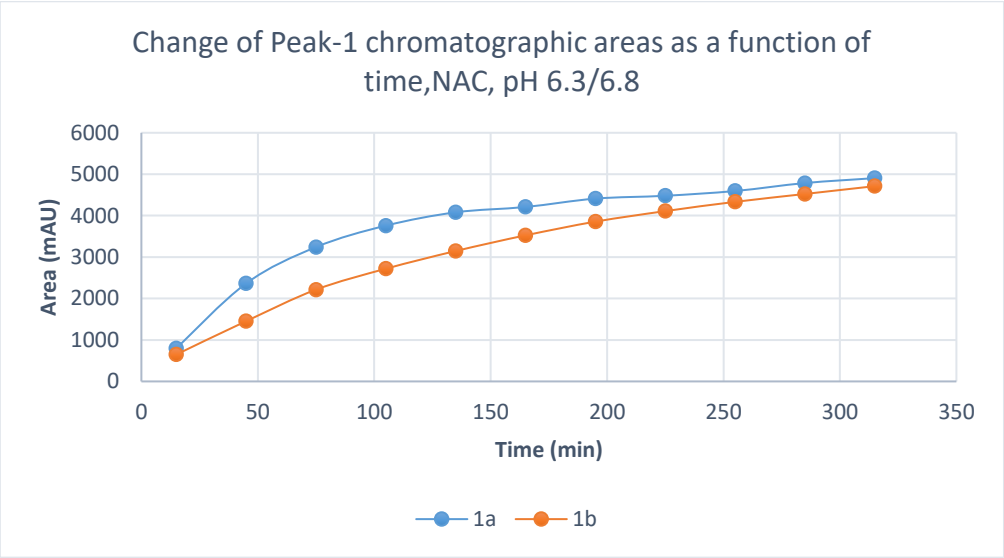

Figure 22. Change in the chromatographic peak area of conjugate adduct-1 of chalcones **1a** and **1b** in the chalcone-NAC incubations at pH 6.3/6.8.

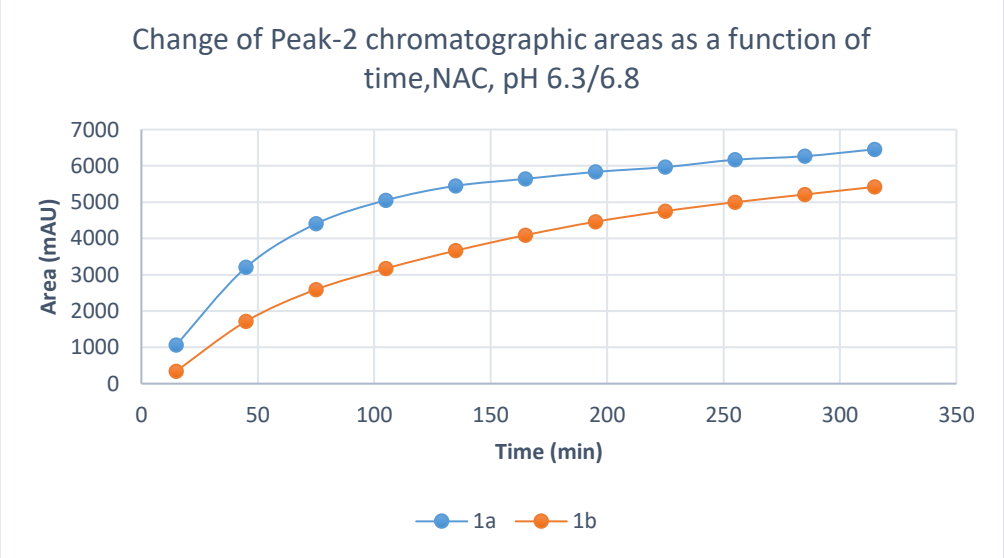

Figure 23. Change in the chromatographic peak area of conjugate adduct-2 of chalcones **1a** and **1b** in the chalcone–NAC incubations at pH 6.3/6.8.

4.1.3. Reactions performed under pH 3.2/3.7 condition

Reactions under stronger acidic conditions proceeded to a much lower extent than those under the above two conditions. It could be explained based on the stronger acidic conditions; the thiol function of both GSH and NAC exists exclusively in protonated (neutral) form. Although protonated thiols can act as nucleophilic reagents, their reactivity is much lower than their deprotonated (negatively charged) counterparts [28,85].

Only a small amount of adducts were detected in each chalcone–GSH/NAC incubates case. The chromatographic peak area values of the (*Z*) isomers were similar to those in the respective incubates at pH 8.0/7.4 and 6.3/6.8 (Tables 1 and 2).

Progress curves of the reaction of chalcones with GSH showed a linear downhill shape (Figure 24). A similar linear reduction in the chromatographic peak areas was also observed in the NAC incubations (Figure 25).

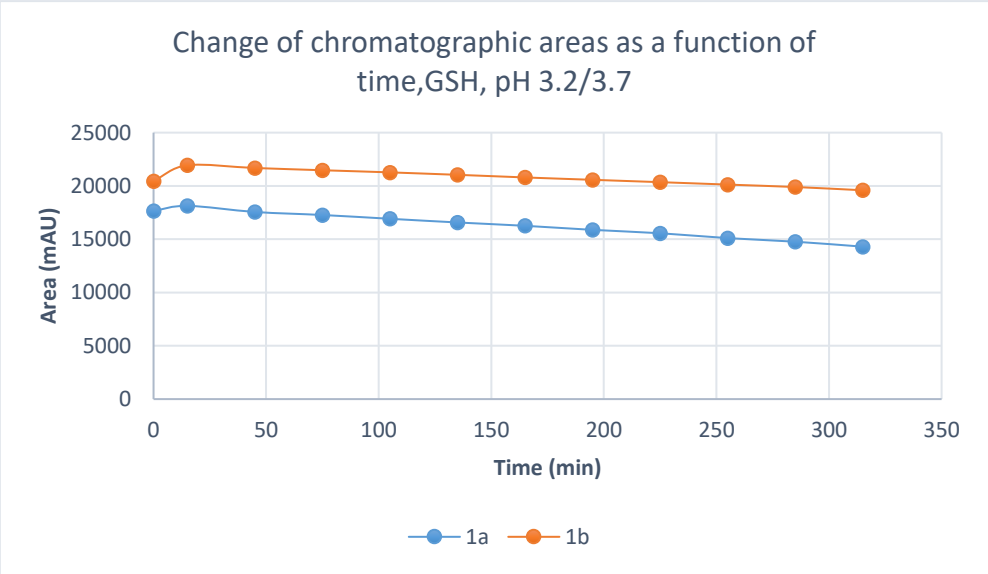

Figure 24 Change in the chromatographic peak area of chalcones **1a** and **1b** in the chalcone–GSH incubations at pH 3.2/3.7.

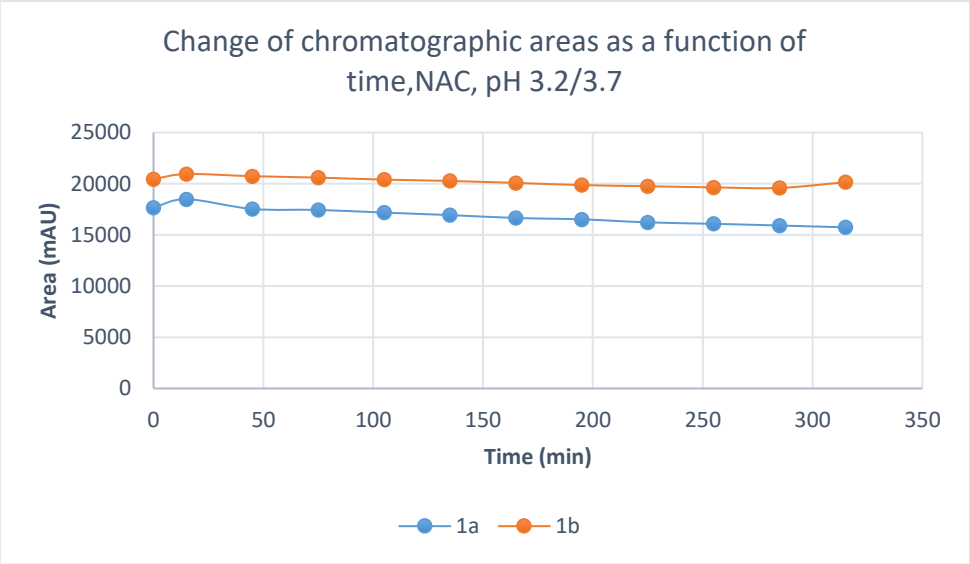

Figure 25. Change in the chromatographic peak area of chalcones **1a** and **1b** in the chalcone–NAC incubations at pH 3.2/3.7.

Over the incubation period, the chromatographic peak areas of the chalcone–GSH (Figure 26) and chalcone-NAC diastereomers (Figures 27 and 28) continuously increased.

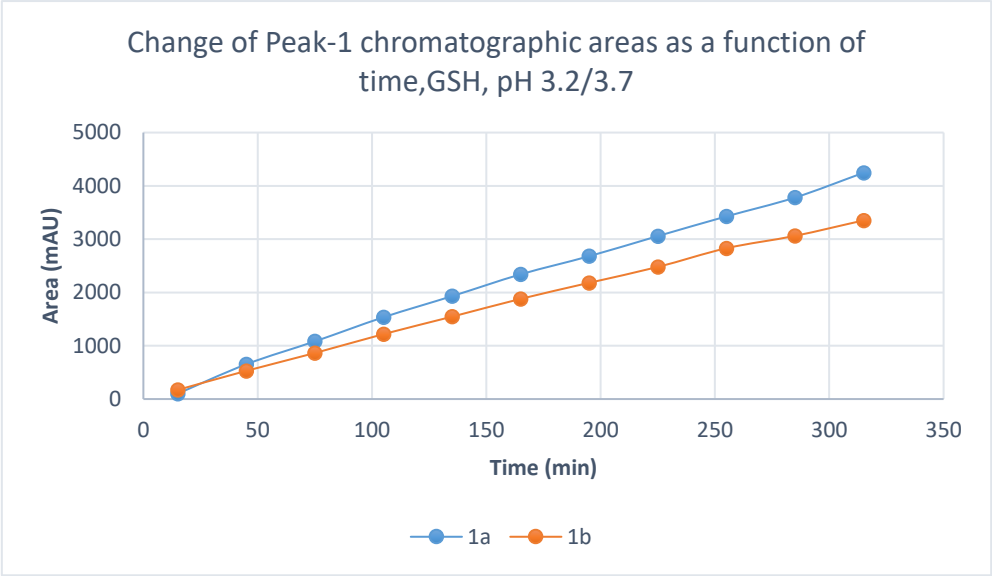

Figure 26 Change in the chromatographic peak area of conjugate adduct-1 of chalcones **1a** and **1b** in the chalcone–GSH incubations at pH 3.2/3.7

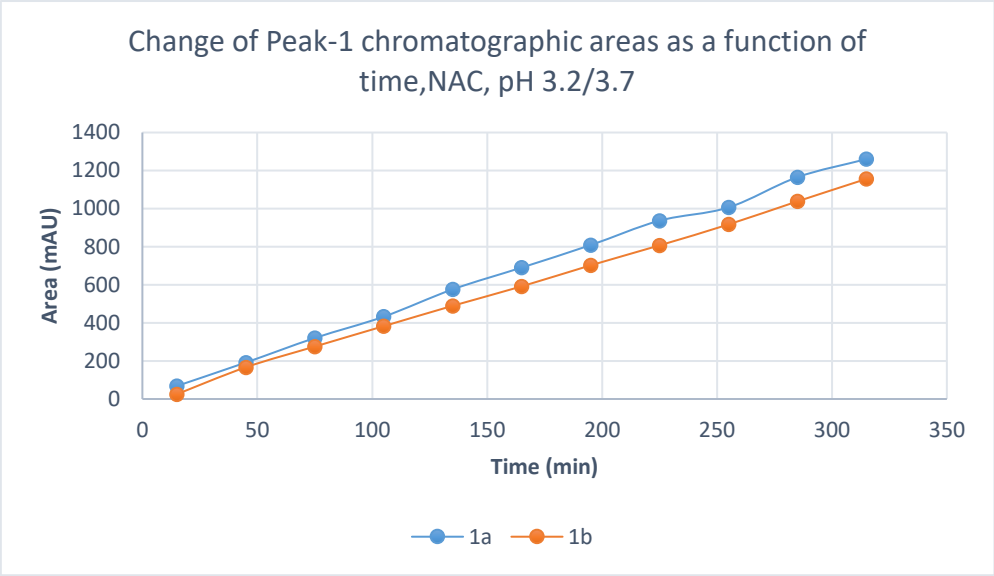

Figure 27. Change in the chromatographic peak area of conjugate adduct-1 of chalcones **1a** and **1b** in the chalcone–NAC incubations at pH 3.2/3.7.

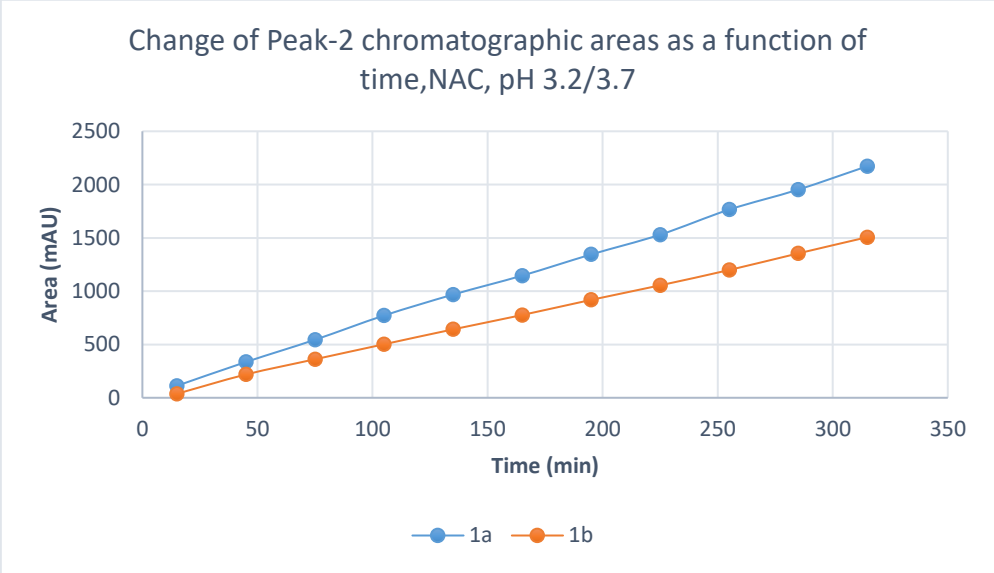

Figure 28. Change in the chromatographic peak area of conjugate adduct-2 of chalcones **1a** and **1b** in the chalcone–NAC incubations at pH 3.2/3.7.

4.2. (*E*)-2-benzylidinebenzosuberones

4.2.1. Reactions under Slightly Basic (pH 8.0/7.4) Conditions

Initially, we investigated the reactions of **4a** and **4b** under basic conditions. Considering the pK_a values of GSH (8.83) and NAC (9.52), about 3.6% of the GSH and 0.75% of the NAC molecules are under pH 7.4 conditions. The reaction with GSH (Figure 29) and NAC (Figure 30) showed that both cyclic chalcones have intrinsic reactivity with the investigated thiols. By the end of the incubation period (315 min) with GSH, the initial area of the HPLC peak corresponding to the parent compounds **4a** and **4b** was reduced by 43.5% and 26.3 %, respectively (Table 4). While the compounds were incubated with NAC, the respective figures were 7.9% and 7.6% (Table 5). Changes in the chromatographic peak areas of the starting chalcones as a function of the incubation time indicated that the compositions reflect the equilibrium only in the case of the NAC incubation (Figures 29 and 30).

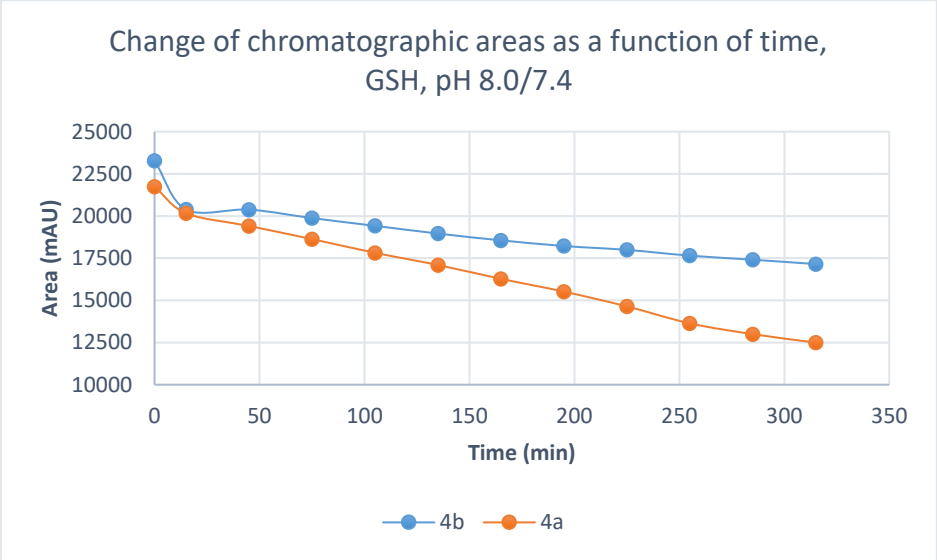

Figure 29. Change in the chromatographic peak area of chalcones **4a** and **4b** in the chalcone-GSH incubations at pH 8.0/7.4.

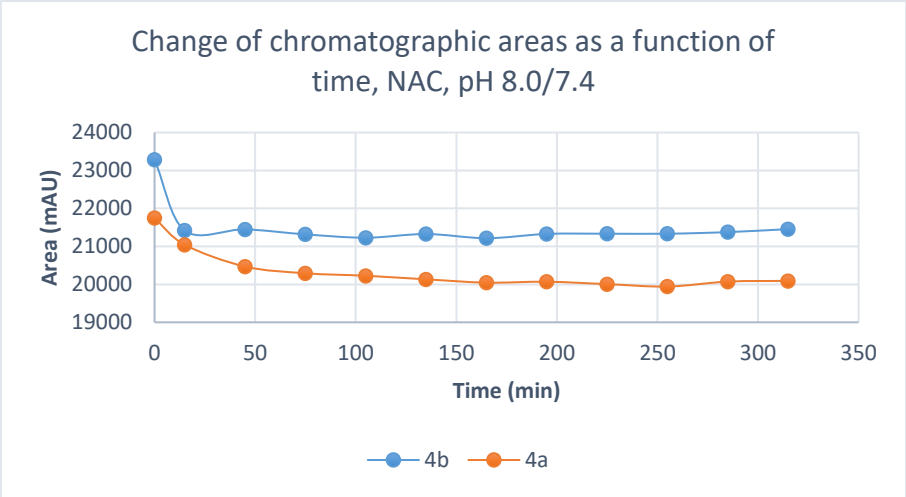

Figure 30. Change in the chromatographic peak area of chalcones **4a** and **4b** in the chalcone–NAC incubations at pH 8.0/7.4.

Table 4. Retention times (t_R)[1] and integrated peak areas (A) of the investigated cyclic chalcone analogs (**4a** and **4b**) and their GSH adducts[2].

pH [3]	*Compound*	*t_R (E)-Chalcone*	*Area Ratio* [4] *A_{315}/A_0*	*t_R (Z)-Chalcone*	*Area (Z)-Chalcone*	*t_R GSH–1*	*Area GSH–1*	*t_R GSH –2*	*Area GSH–2*
3.2	**4a**	17.1	0.89	16.8	55.1	14.8[5]	74.9	15.2[5]	111.5
3.2	**4b**	16.6	0.95	16.3	136.1	N/D[5]	-	N/D[5]	-
6.3	**4a**	17.0	0.84	16.7	446.6	14.6	297.2	15.1	331.8
6.3	**4b**	16.9	0.91	16.7	513.4	14.2	233.6	14.8	256.4
8.0	**4a**	17.4	0.57	17.1	302.8	15.0	2847.0	15.4	3216.3
8.0	**4b**	16.8	0.74	16.5	412.0	13.9	2584.9	14.6	2785.0

[1]Retention times in minutes; [2] data refer to the average of two independent measurements at the 315 min time point; [3] pH value of the aqueous thiol solution; [4] ratios of peak areas measured at 0 and 315 min; [5] not detectable.

Table 5. Retention times (t_R)[1] and integrated peak areas (A) of the investigated cyclic chalcone analogs (**4a** and **4b**) and their NAC adducts[2].

pH [3]	*Compound*	*t_R (E)-Chalcone*	*Area Ratio* [4] *A_{315}/A_0*	*t_R (Z)-Chalcone*	*Area (Z)-Chalcone*	*t_R NAC–1*	*Area NAC–1*	*t_R NAC–2*	*Area NAC–2*
3.2	**4a**	17.1	0.76	16.8	124.1	N/D[5]	-	N/D[5]	-
3.2	**4b**	16.6	0.88	16.3	126.9	N/D[5]	-	N/D[5]	-
6.3	**4a**	17.5	0.93	17.2	118.9	16.3	60.0	16.5	513.9
6.3	**4b**	16.7	0.91	16.4	184.5	15.3	61.8	15.6	392.1
8.0	**4a**	17.5	0.92	17.2	467.5	16.3	477.7	16.5	913.4
8.0	**4b**	17.0	0.92	16.8	541.9	15.7	347.5	15.9	624.2

[1]Retention times in minutes; [2] data refer to the average of two independent measurements at the 315 min time point; [3] pH value of the aqueous thiol solution; [4] ratios of peak areas measured at 0 and 315 min; [5] not detectable.

As a result of the addition reactions, two new chiral centers are formed. Considering the inherent chirality of the two thiols, the formation of four diastereomeric adducts was expected. However, only two separate peaks could be detected under the present chromatographic conditions. The analysis showed a slight excess of the less polar diastereomers in both cases. The structure of the parent chalcones (Figures 31 and 32) and their GSH and NAC conjugates were verified by HPLC-MS (Figures 33-36).

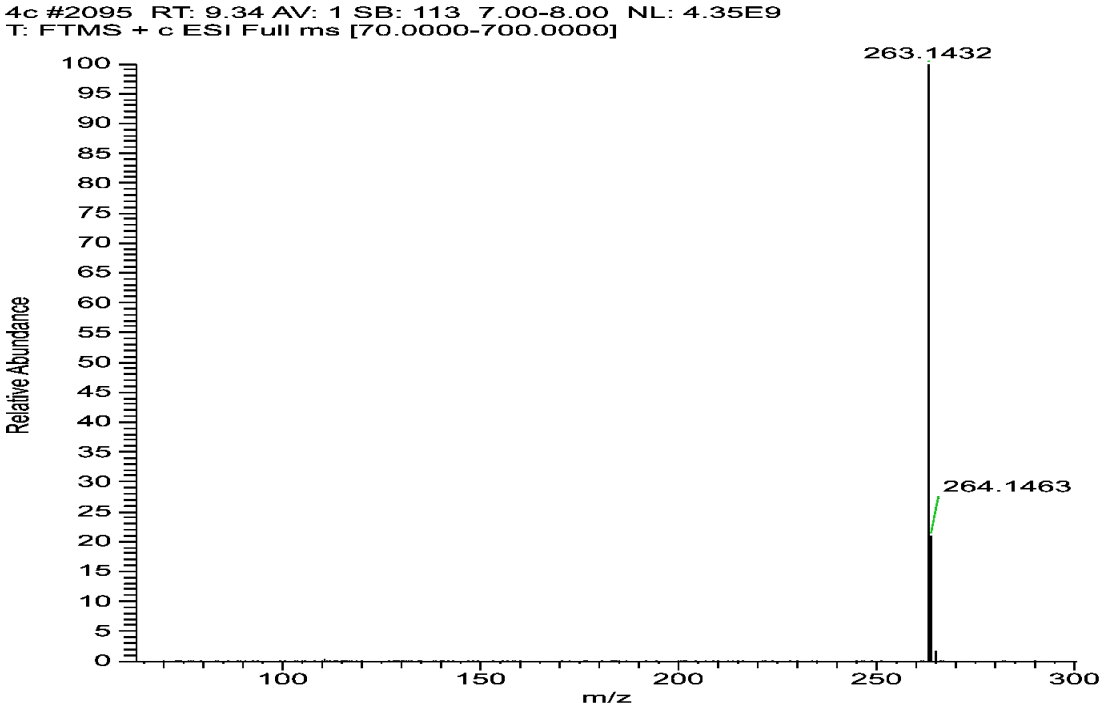

Figure 31. High-resolution, positive-mode HESI MS spectrum of chalcone **4a**.

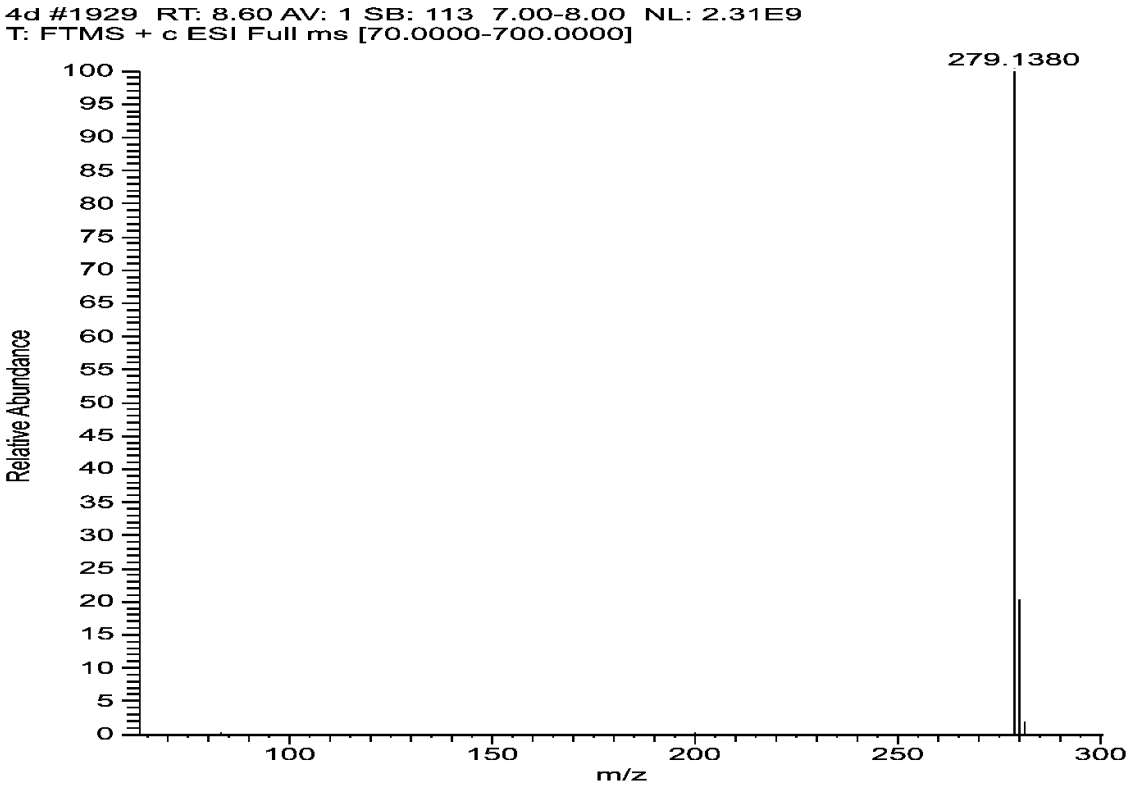

Figure 32. High-resolution, positive-mode HESI MS spectrum of chalcone **4b**.

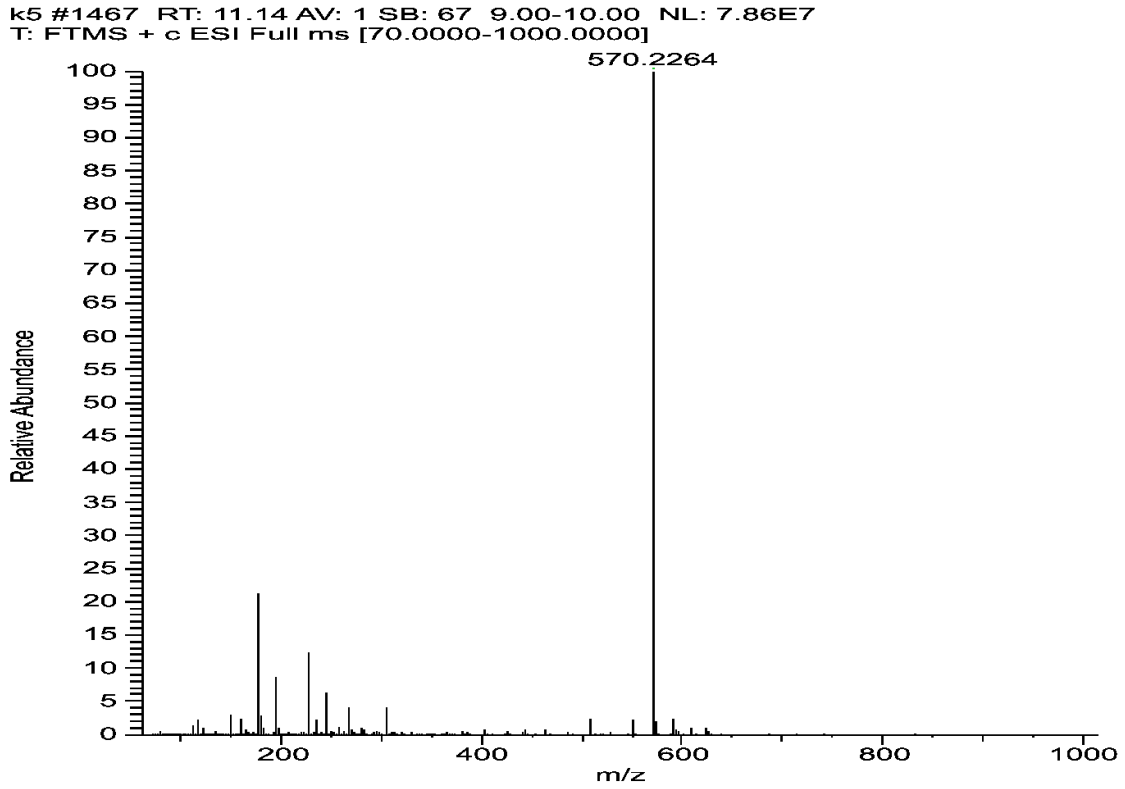

Figure 33. High-resolution, positive-mode HESI MS spectrum of chalcone **4a–GSH** conjugate.

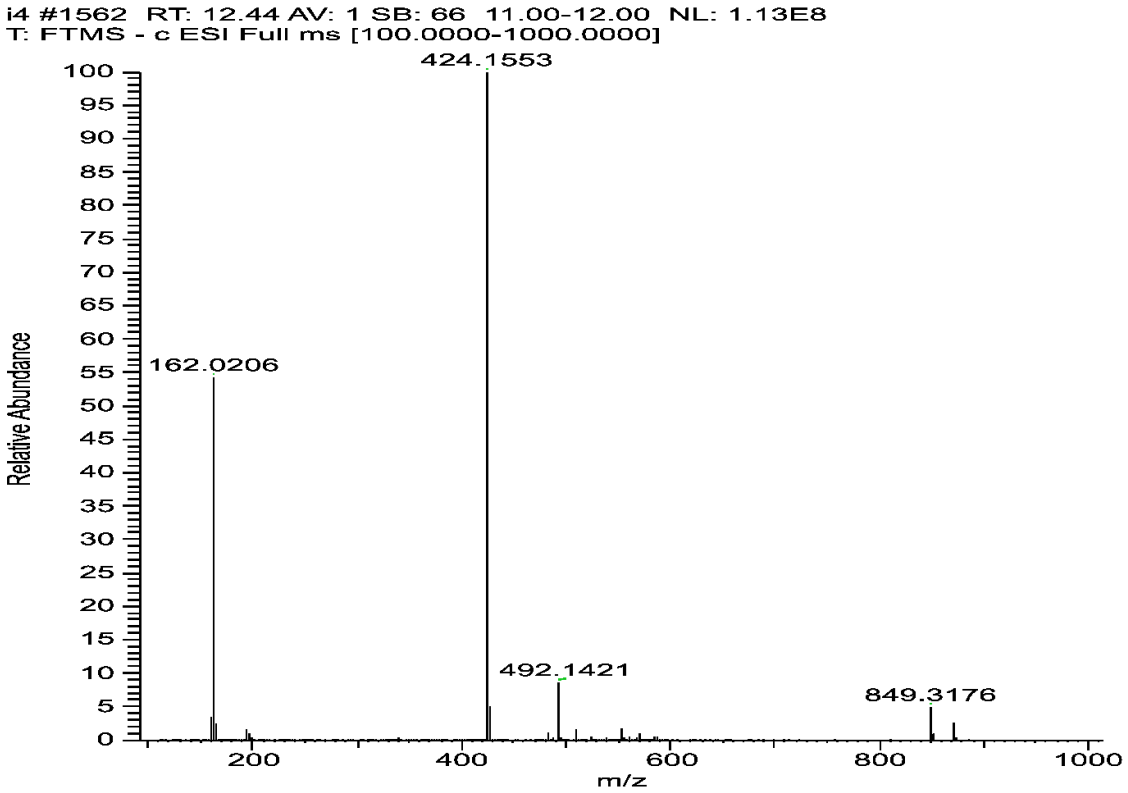

Figure 34. High-resolution, negative-mode HESI MS spectrum of chalcone **4a–NAC** conjugate.

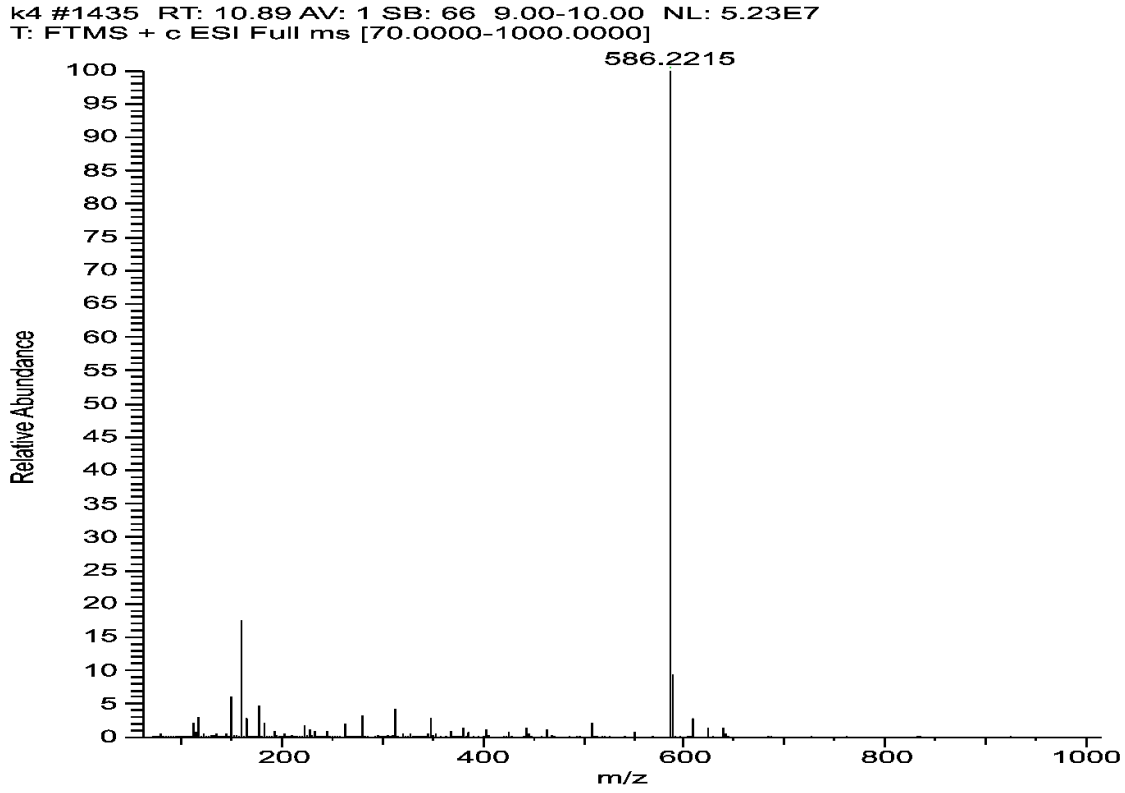

Figure 35. High-resolution, positive-mode HESI MS spectrum of chalcone **4b–GSH** conjugate.

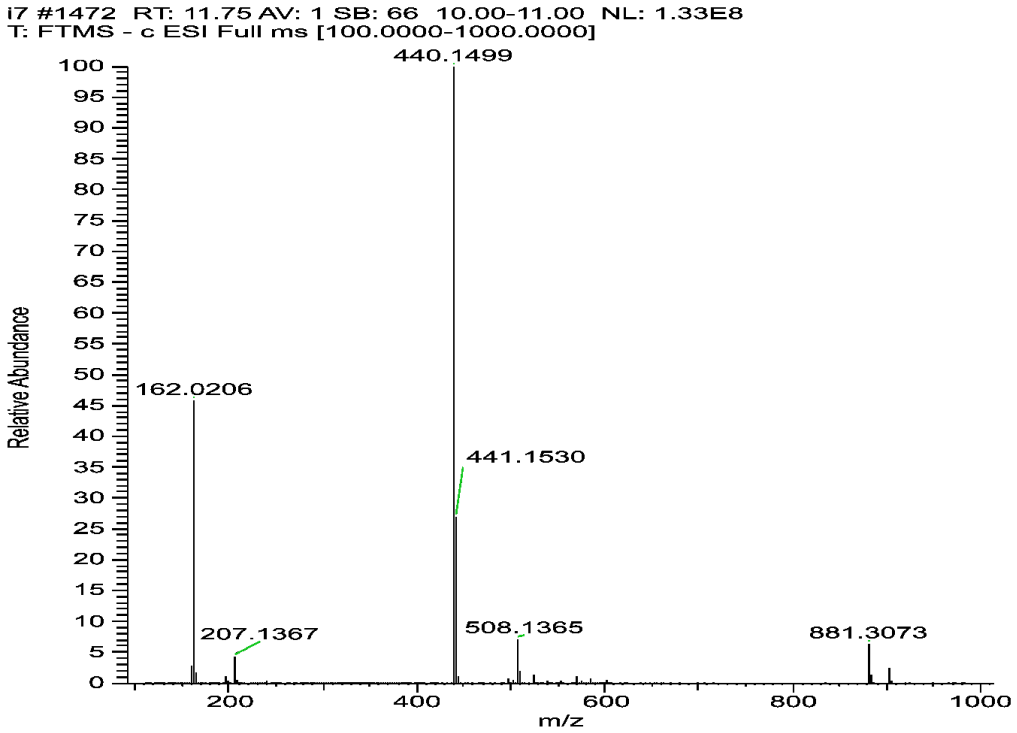

Figure 36. High-resolution, negative-mode HESI MS spectrum of chalcone **4b–NAC** conjugate.

The time course of increase of the two separated peaks, **GSH-1** and **GSH-2**, and **NAC-1** and **NAC-2** showed some characteristic differences. In the case of the GSH adducts of **4a** and **4b**, the peak areas almost linearly increased over time. The progress curves of formation of the adducts, however, showed somewhat different slopes, especially from the 105-minute time point (Figures 37 and 38). In the case of the NAC-adducts, the progress curves deviate from linearity. The curvatures of the concave curves differ from the 75-minute time point (Figures 39 and 40). By the end of the incubation period (315 min), the ratio of the two peaks of the GSH incubations remained close to unity (1.13 and 1.08 for **4a** and **4b**, respectively). In the case of the NAC incubations, the respective ratios were 1.91 and 1.80 (Tables 4 and 5). The formation of (*Z*)-chalcones could be detected in all four incubations. In the case of the NAC incubations, the area of the (*Z*)-peaks is comparable with those of the chalcone-NAC adducts (Tables 4 and 5).

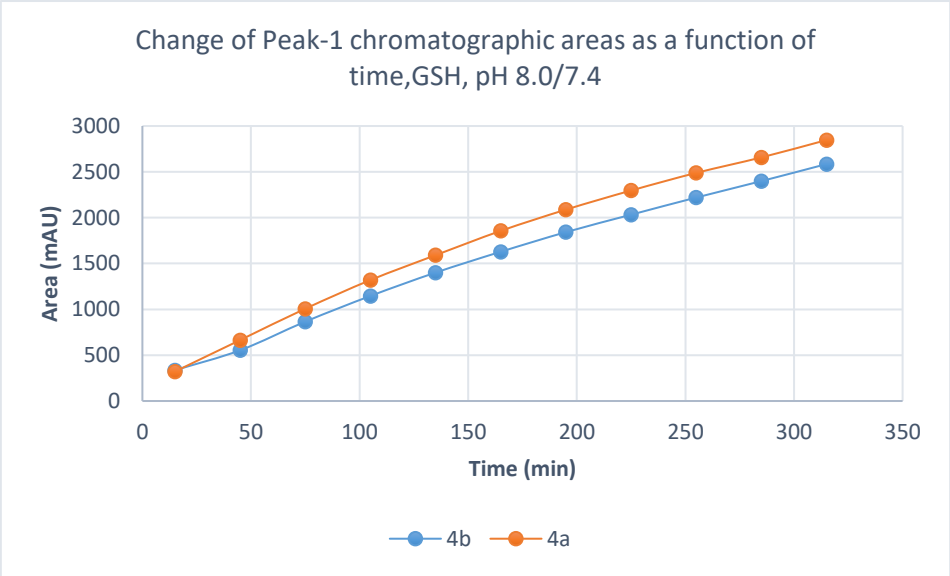

Figure 37. Change in the chromatographic peak area of conjugate adduct-1 of **4a** and **4b** in the chalcone-GSH incubations at pH 8.0/7.4.

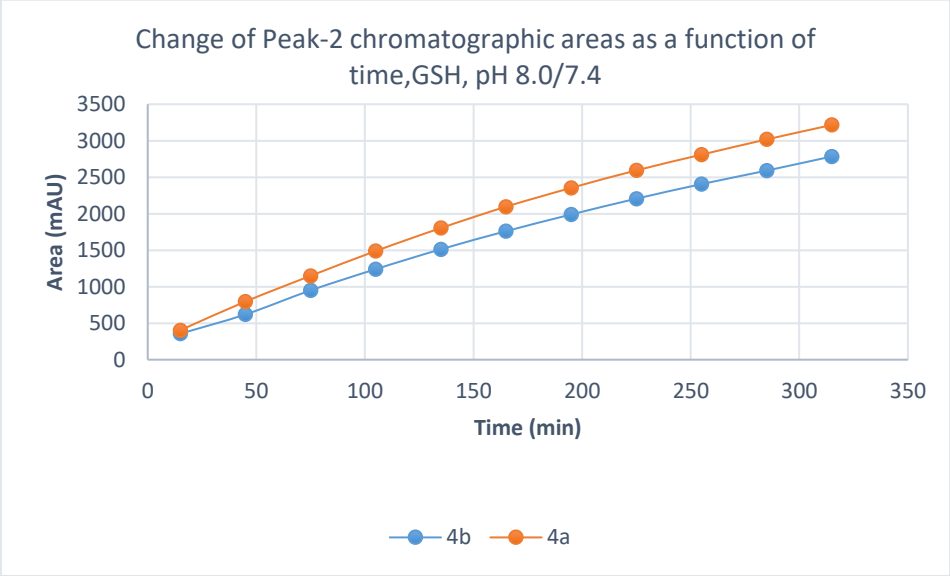

Figure 38. Change in the chromatographic peak area of conjugate adduct-2 of **4a** and **4b** in the chalcone-GSH incubations at pH 8.0/7.4.

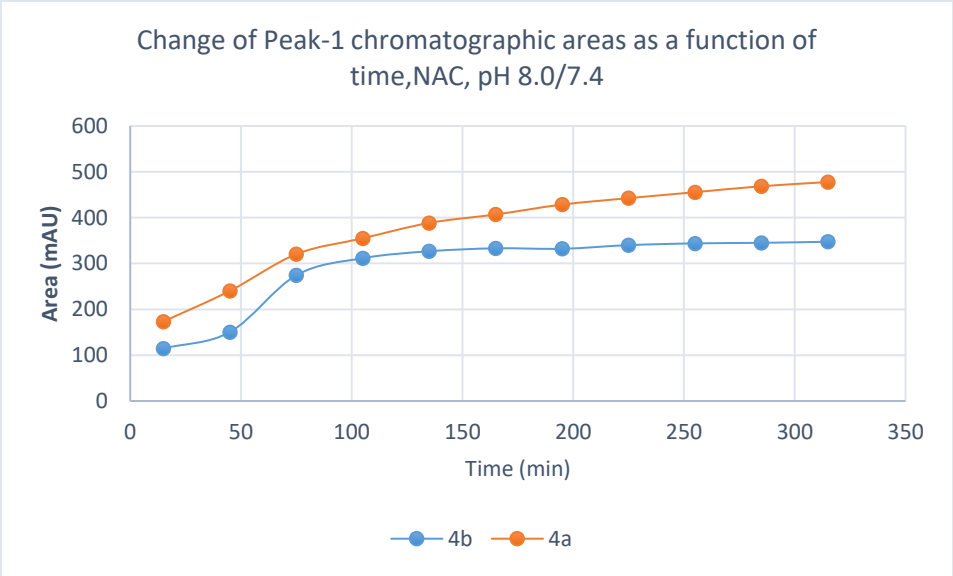

Figure 39. Change in the chromatographic peak area of conjugate adduct - of **4a** and **4b** in the chalcone-NAC incubations at pH 8.0/7.4.

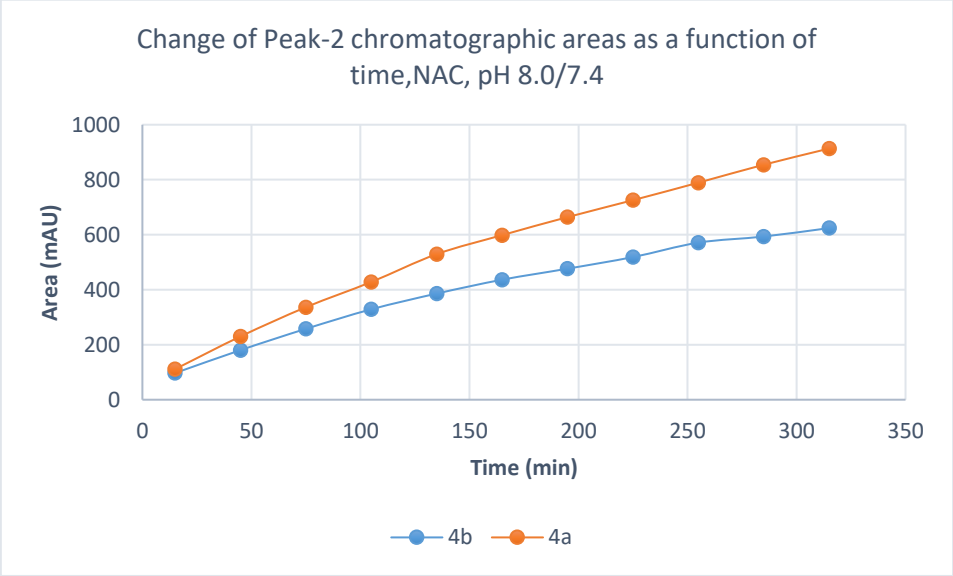

Figure 40. Change in the chromatographic peak area of conjugate adduct-2 of **4a** and **4b** in the chalcone-NAC incubations at pH 8.0/7.4.

4.2.2. Reaction under Slightly Acidic (pH 6.3/6.8) Conditions

As mentioned previously, the reaction of the cyclic chalcones with the two thiols under slightly acidic conditions (virtual pH 6.8) mimics the cellular milieu of the cancer cell [84]. Under such conditions, about 0.9% of the GSH molecules and 0.2% of the NAC molecules exist in the more reactive thiolate form. The change in the concentration (chromatographic peak areas) of the starting chalcones **4a** and **4b** show parallelism in both reactions (Figures 41 and

42). By the end of the incubation period (315 min) with GSH, the initial area of the HPLC peak of **4a** and **4b** was reduced by 16.1% and 9.1%, respectively. While the compounds were incubated with NAC, the respective figures were 8.9% and 7.1%. These latter figures are very close to those obtained under slightly basic conditions (Tables 4 and 5).

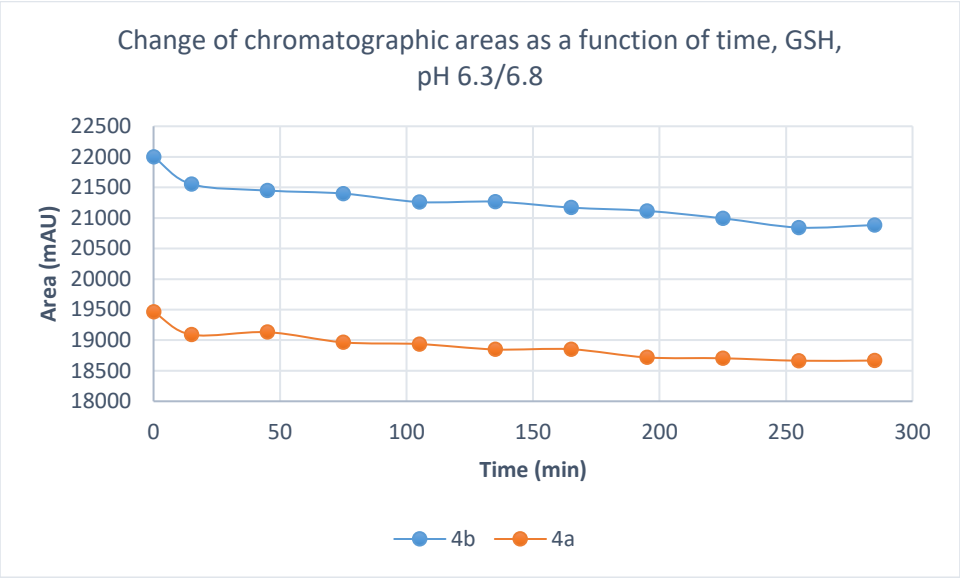

Figure 41. Change in the chromatographic peak area of chalcones **4a** and **4b** in the chalcone–GSH incubations at pH 6.3/6.8.

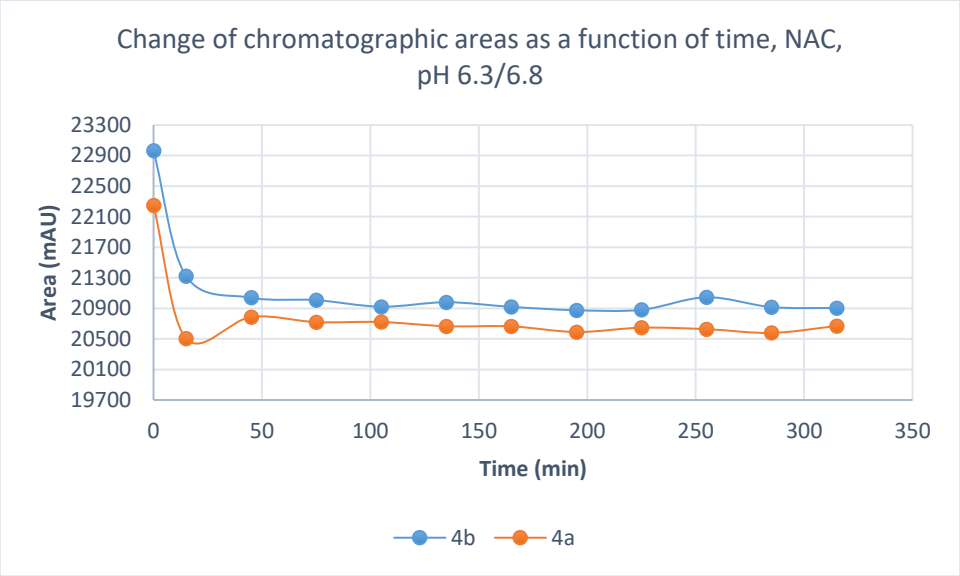

Figure 42. Change in the chromatographic peak area of chalcones **4a** and **4b** in the chalcone–NAC incubations at pH 6.3/6.8.

In the GSH incubations, the separated HPLC peak areas of the **4a-GSH** and **4b-GSH** diastereomers increased closely parallel over time (Figures 43 and 44).

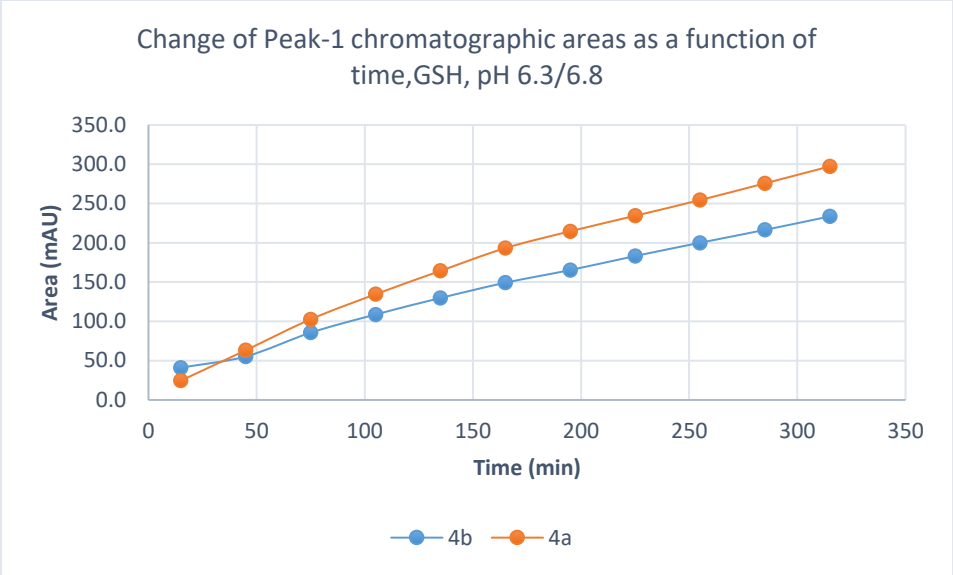

Figure 43. Change in the chromatographic peak area of conjugate adduct-1 of chalcones **4a** and **4b** in the chalcone–GSH incubations at pH 6.3/6.8.

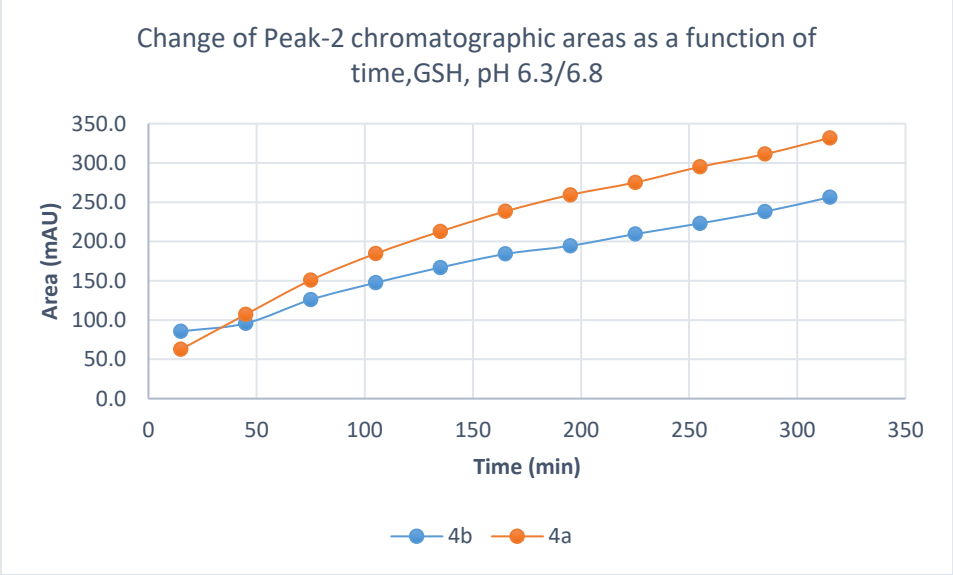

Figure 44. Change in the chromatographic peak area of conjugate adduct-2 of chalcones **4a** and **4b** in the chalcone–GSH incubations at pH 6.3/6.8.

At the end of the incubation period, the ratio of the area of two separated peaks of the chalcone-GSH adducts is close to unity (1.12 and 1.10 for **4a** and **4b**, respectively) (Table 4).

A similar tendency could be observed for the **NAC-2** peak (peak with the higher retention time) area of **4a** and **4b** (Figure 46). At the same time, the chromatographic peak area of the **NAC-1** peak of **4b** remained practically unchanged, but that of **4a** slightly increased (Figure 45).

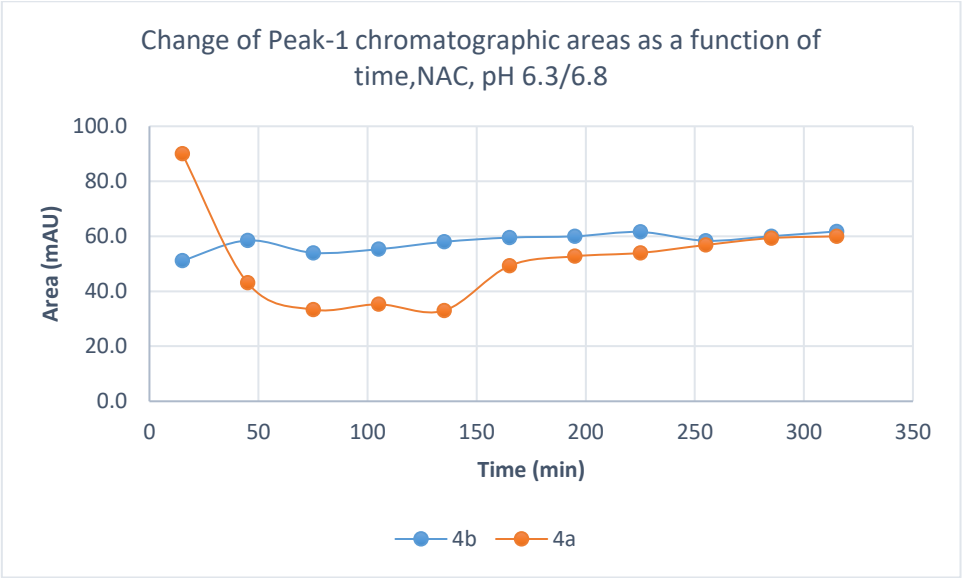

Figure 45. Change in the chromatographic peak area of conjugate adduct-1 of chalcones **4a** and **4b** in the chalcone–NAC incubations at pH 6.3/6.8.

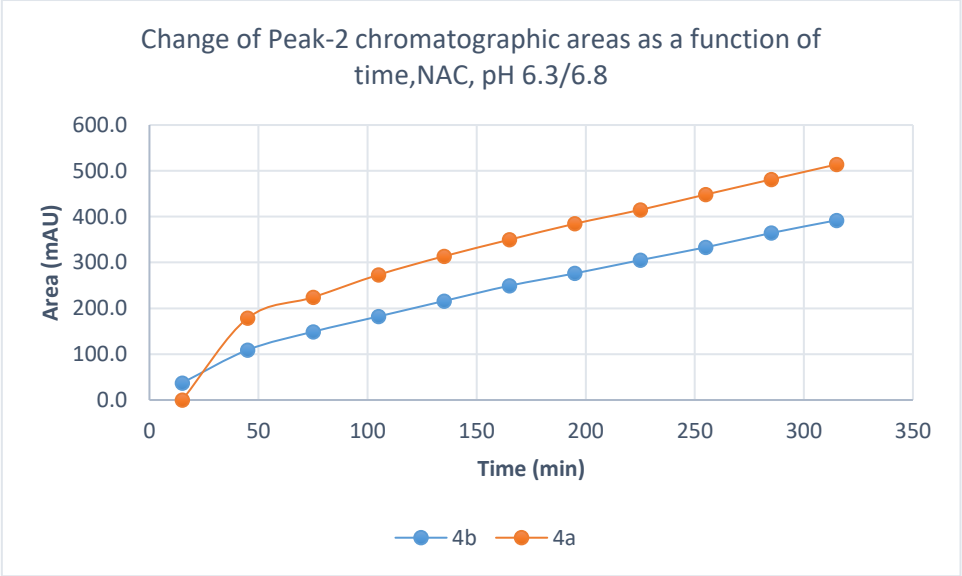

Figure 46. Change in the chromatographic peak area of conjugate adduct-2 of chalcones **4a** and **4b** in the chalcone–NAC incubations at pH 6.3/6.8.

As a result, the ratio of the **NAC-2**/**NAC-1** areas at the 315 min time point was 8.57 and 6.34 for **4a** and **4b**, respectively (Table 6). In all four incubations, the peak areas of the (*Z*)-chalcones are comparable to those of the formed adducts (Table 6). Since the only source of the (*Z*) isomers under the experimental conditions is the retro-Michael reactions, it is reasonable to presume that the observed diastereomeric distributions do not reflect the results of the kinetics-controlled reactions.

Table 6. HPLC-UV areas of the (Z) isomers and the diastereomeric **NAC-1** and **NAC-2** peaks in the NAC-incubation of **4a** and **4b** under slightly acidic (pH 6.3/6.7) conditions.

Compound	*Time (minute)*	*Area Z-Chalcone*	*Area NAC-1*	*Area NAC-2*	*Ratio Area NAC-2/NAC-1*
4a	75	91.8	35.3	224.1	6.3
	165	107.2	52.7	349.7	6.6
	255	114.9	56.8	448.3	7.9
	315	118.9	60.0	513.9	8.6
4b	75	136.5	54.0	148.9	2.8
	165	159.4	59.5	249.3	4.2
	255	175.3	58.4	333.2	5.7
	315	184.5	61.8	392.1	6.3

4.2.3. Reaction under Acidic (pH 3.2/3.8) Conditions

Under stronger acidic conditions, the thiol function of both GSH and NAC exists exclusively in protonated (neutral) form. Although the protonated thiols can act as nucleophilic reagents, their reactivity is much lower than their deprotonated (negatively charged) counterparts [28,85].

In the chalcone-GSH incubations, progress curves of the reactions (reduction of the initial area of the chalcones) showed a very slight downhill linear shape (Figure 47). At the end of the incubations, the initial values of the peak areas of **4a** and **4b** were reduced by 10.6% and 5.3%, respectively. At the same time, a linear increase in the peak area of the **4a-GSH** adducts (peaks 1 and 2) could be observed in parallel (Figures 48 and 49). The peaks corresponding to the respective **4b-GSH** adducts could not be detected. The ratio of the **4a-GSH** isomeric peaks (315 min time point) was 1.48. The areas of the respective (*Z*) isomers were much lower than in the pH 8.0 and pH 6.3 incubations (Table 6).

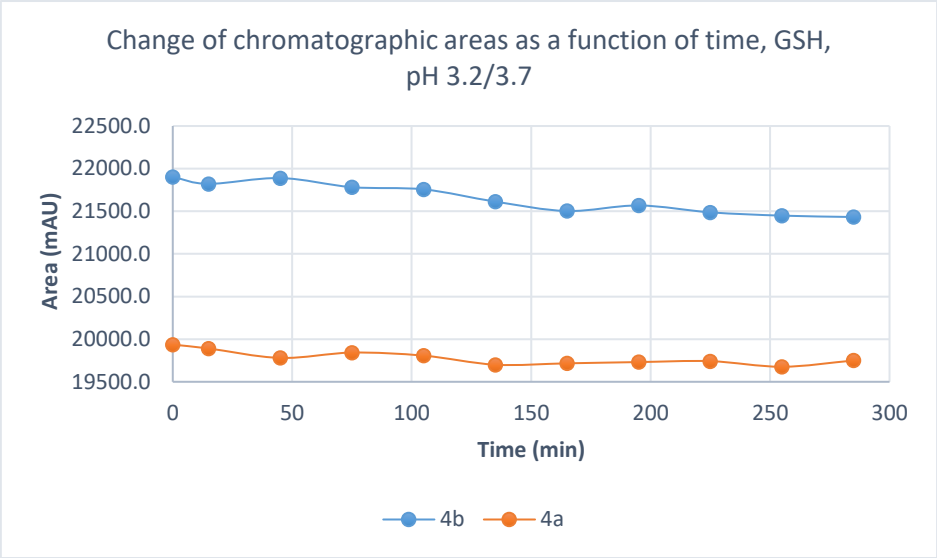

Figure 47. Change in the chromatographic peak area of chalcones **4a** and **4b** in the chalcone–GSH incubations at pH 3.2/3.7.

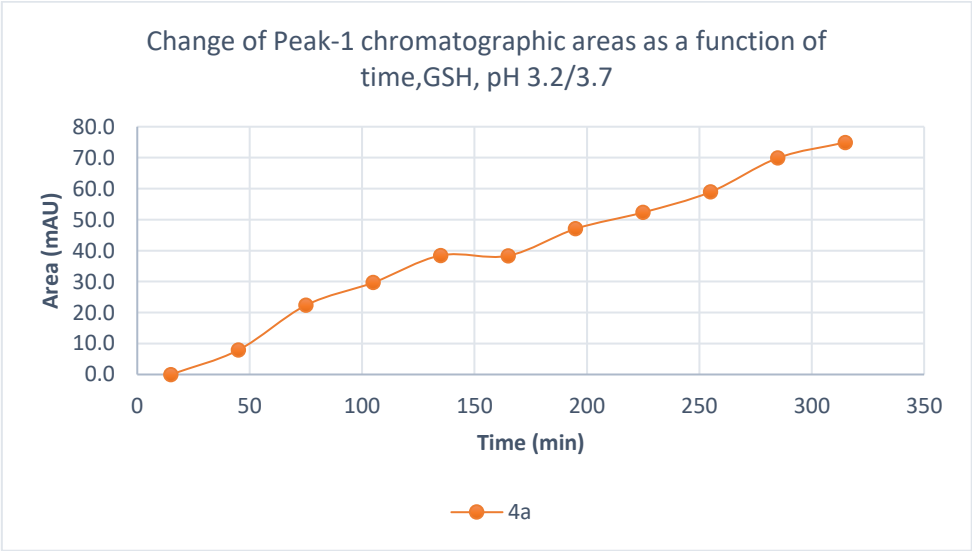

Figure 48. Change in the chromatographic peak area of conjugate adduct-1 of chalcones **4a** in the chalcone–GSH incubations at pH 3.2/3.7.

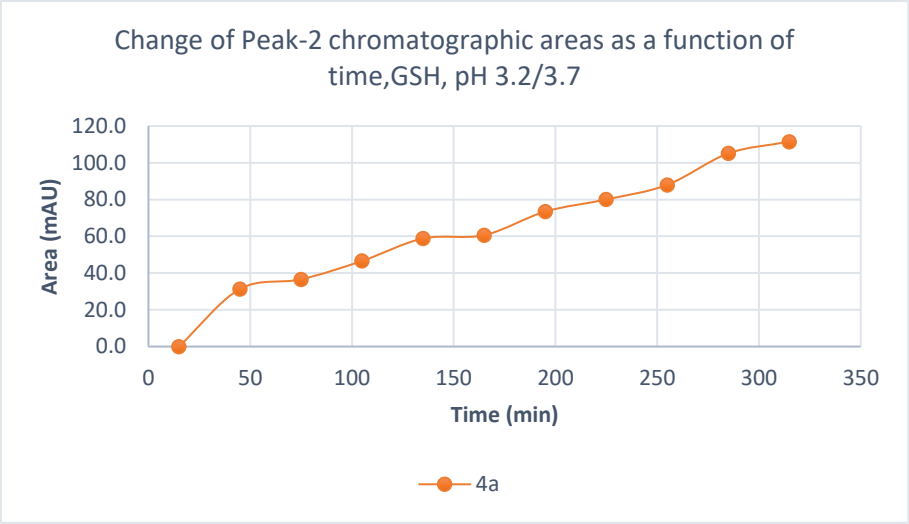

Figure 49. Change in the chromatographic peak area of conjugate adduct-2 of chalcones **4a** in the chalcone–GSH incubations at pH 3.2/3.7.

In the chalcone-NAC incubations, the reduction of the initial area of the chalcones showed a very slight downhill linear shape with somewhat different slopes (Figure 50). The initial peak area of **4a** and **4b** was reduced by 23.7% and 12.1% by the 315 min time point (Table 6). However, no **4-NAC** peaks could be identified. HPLV-UV analysis of the incubates showed the formation of several small peaks, more polar than the parent **4a** and **4b**. HPLC-MS investigations indicated the expected adduct formation, but it was impossible to identify them in the HPLC-UV chromatograms (Figures 51 and 52). In both incubations, the formation of the (*Z*) isomers could be seen (Table 6).

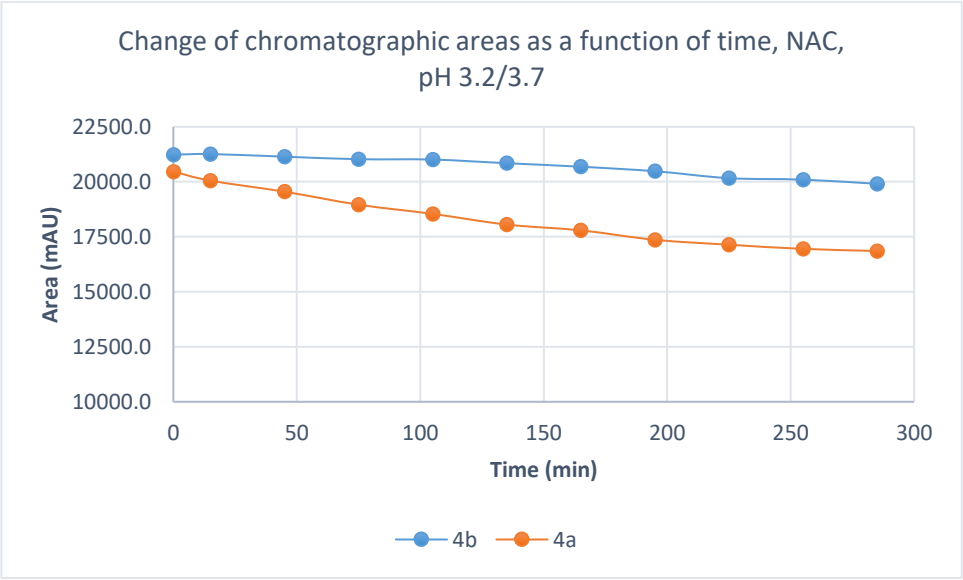

Figure 50. Change in the chromatographic peak area of chalcones **4a** and **4b** in the chalcone–NAC incubations at pH 3.2/3.7.

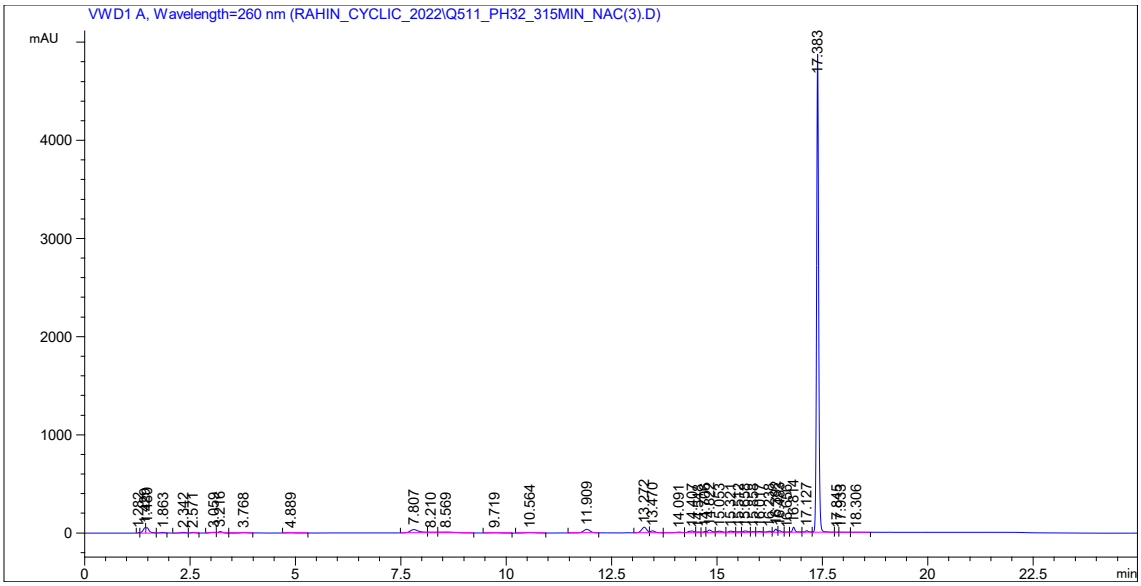

Figure 51. HPLC-UV chromatogram of pH 3.2/3.7 incubation (315 min time point) of chalcone **4a** and NAC.

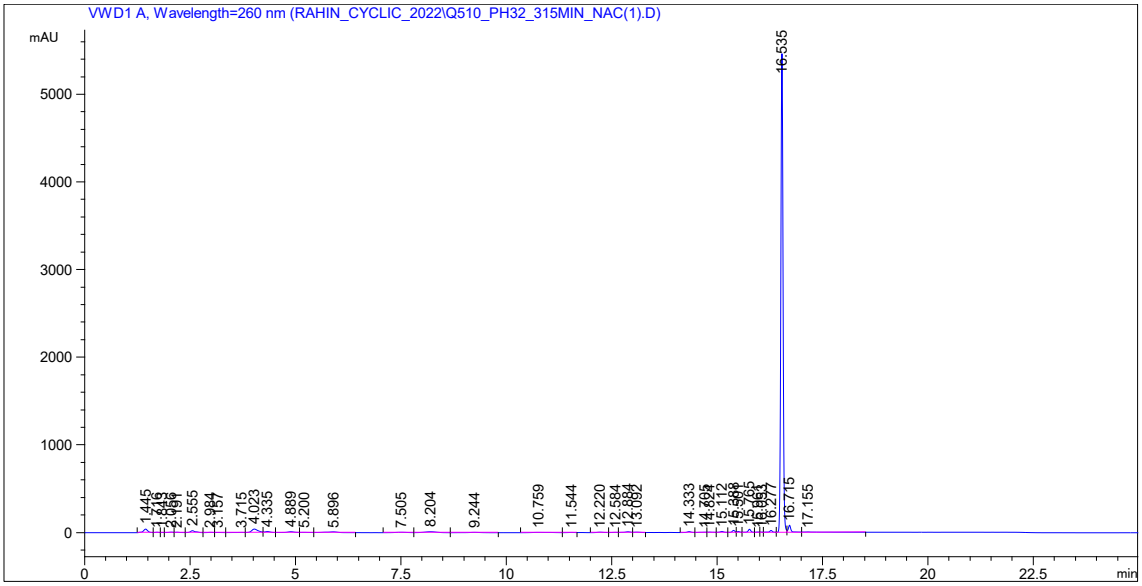

Figure 52 HPLC-UV chromatogram of pH 3.2/3.7 incubation (315 min time point) of chalcone **4b** and NAC.

4.2.4. Molecular modeling analysis

Table 7 shows the calculated values for molecular properties of **4a**, **4b,** methanethiol (**CH_3SH**), and deprotonated methanethiol [**CH_3S^-**]. The highest occupied molecular orbital energy (E_{HOMO}) reflects the ability of a molecule to donate electrons, the lowest unoccupied

molecular orbital energy (E_{LUMO}) demonstrates the ability to accept electrons (see Figure 53), and the gap energies ($\Delta E_{LUMO\text{-}HOMO}$) are related with the chemical stability of molecules.

Table 7. Reactivity indices were obtained for **1c**, **4c**, **CH_3SH**, and **CH_3S^-** at the M06-2X/6-311++G(d,p) level of theory.

Descriptors	**1c** kcal.mol^{-1}	kcal.mol^{-1}	**CH_3SH** kcal.mol^{-1}	**CH_3S^-** kcal.mol^{-1}
E_{HOMO}	-183.24	-180.38	-183.240	-173.453
E_{LUMO}	-35.98	-28.44	-2.979	77.998
$\Delta E_{HOMO\text{-}LUMO}$	147.27	151.94	180.261	251.451
Chemical potential (μ)	-109.608	-104.405	-93.109	-47.728
Chemical hardness (η)	147.264	151.930	180.261	251.451
Electrophilicity index (ω)	40.791	35.873	24.047	4.530

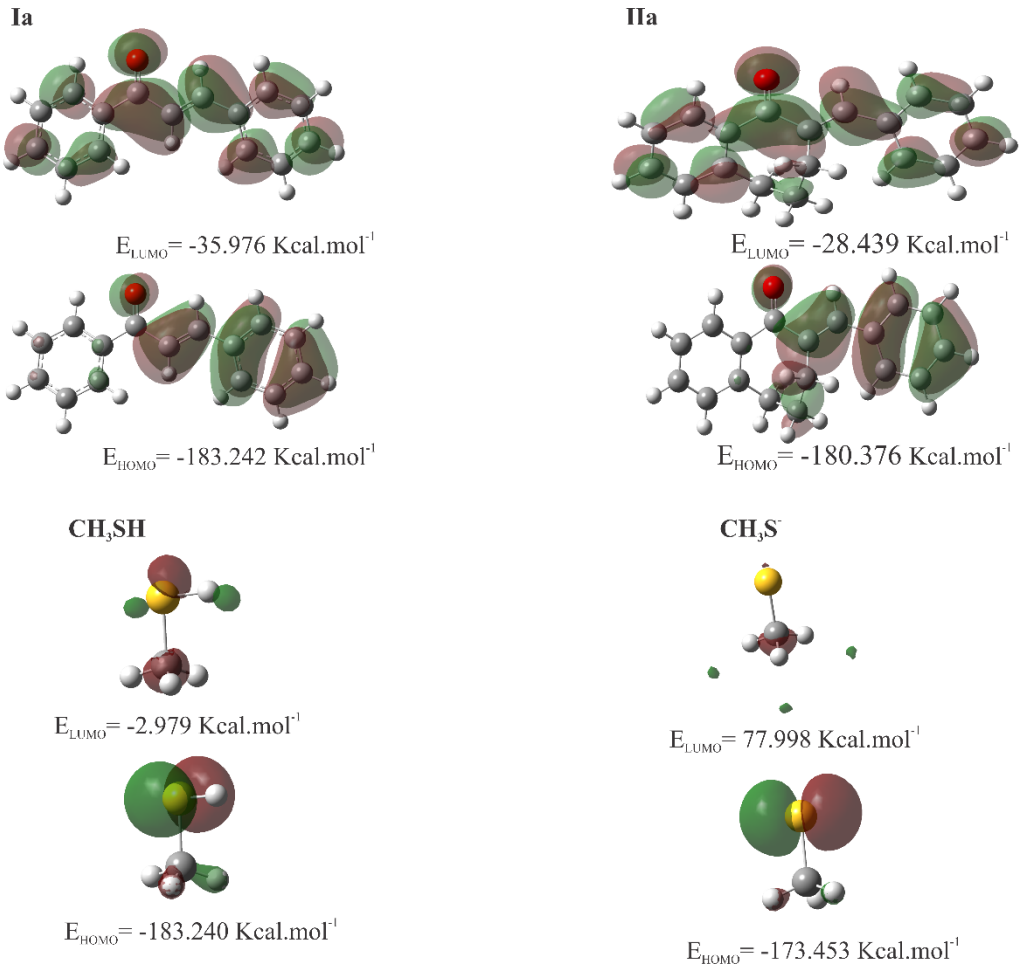

Figure 53 HOMO and LUMO plots for **1c**, **4c**, **CH3SH**, and **CH3S$^-$** calculated at the M06-2X/6-311++G(d,p) level of theory.

The chemical potential, chemical hardness, and electrophilicity are defined as ($\boldsymbol{\mu} = \left(\frac{\partial E}{\partial N}\right)_{\upsilon}$), ($\boldsymbol{\eta} = \frac{1}{2}\left(\frac{\partial^2 E}{\partial N^2}\right)_{\upsilon}$), and ($\boldsymbol{\omega} = \frac{\mu^2}{2\eta}$), respectively. $\boldsymbol{\eta}$ indicates the resistance of the molecule to alter its electronic density distribution and is higher for **4c**. On the other hand, $\boldsymbol{\mu}$ indicates the change in free energy when electrons are added or removed from the molecule. At the same time, $\boldsymbol{\omega}$ is a measure of a molecule's tendency to act as an electrophile. The value of $\boldsymbol{\omega}$ increased for **1c,** and $\boldsymbol{\mu}$ decreased when compared to **4c**.

Figure 54 shows the isosurfaces of the Fukui function (obtained from electron density) for the molecules **1c**, **4c,** and **CH_3SH**, with focus on atoms that can undergo nucleophilic attack ($\boldsymbol{f^+} = [\boldsymbol{\partial \rho(r)/\partial N}]^{+}_{\upsilon(r)}$,). The positive and negative regions of the Fukui function are represented by the green and blue isosurfaces, respectively.

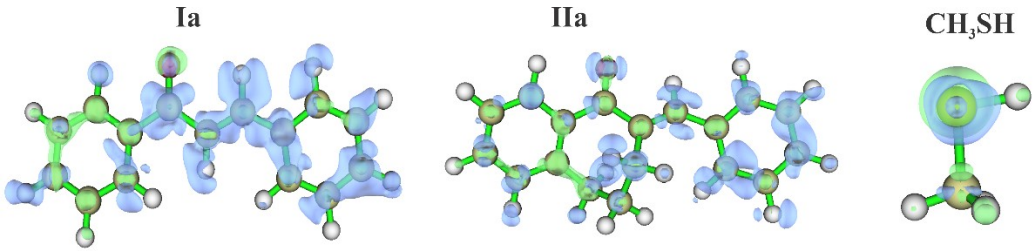

Figure 54 Isosurfaces of the Fukui f^+Function, calculated at a proper value of 0.08 for the molecules **1c**, 4c, **CH_3SH**, and **CH_3S^-**.

In order to depict the distribution of electric charge on the molecular surface, a molecular electrostatic potential (MEP) map was generated (Figure 55). The red spots on the MEP surface represent the electron-rich sites and are susceptible to electrophilic attack. In contrast, the blue spots represent the electron-depleted regions and are sites susceptible to nucleophilic attack. For **CH_3S^-**, the MEP is reddish due to the −1 negative charge resulting from deprotonation.

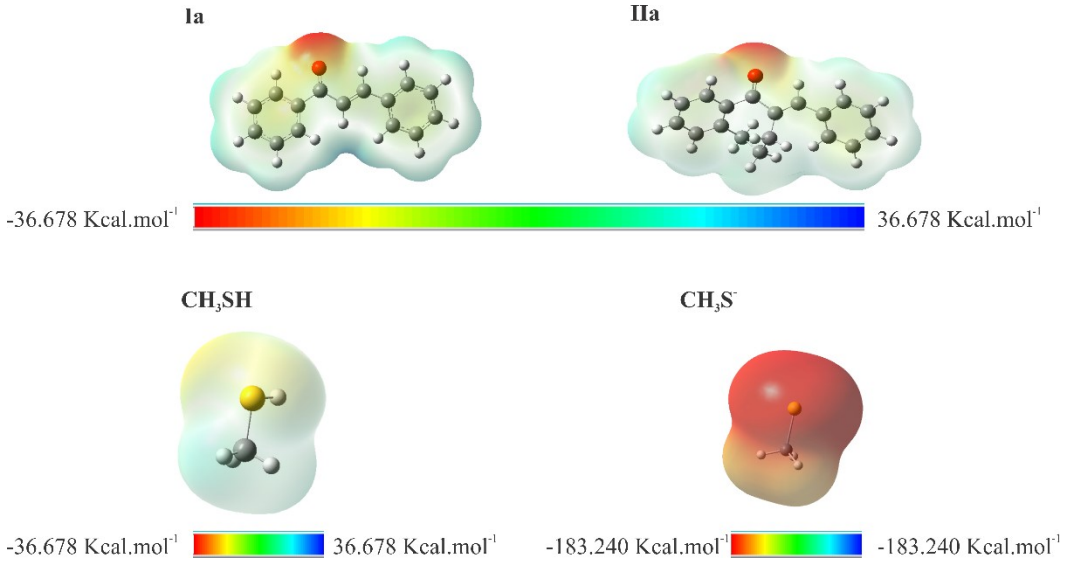

Figure 55 MEP surface contour of the total SCF electronic density for molecules **1c**, **4c**, **CH_3SH**, and **CH_3S^-** at the M06-2X/6-311++G(d,p) level of theory.

The k_{OH} rate constants were calculated for chalcone compounds, and the results indicate that the compounds with the highest k_{OH} values point to greater reactivity. The order of reactivity potential was observed as **CH_3SH** (9.15×10^9 M^{-1} s^{-1}) **1c** (9.01×10^9 M^{-1} s^{-1}) > **4c** (7.85×109 M−1 s−1) > **CH_3S^-** (5.48×10^9 M^{-1} s^{-1}).

4.2.5. Microsomal incubation

Microsomal incubation of **4b** was performed using alamethicin-activated rat liver microsomes. Alamethicin is a peptide antibiotic that forms voltage-dependent channels in the lipid bilayers by oligomerizing various alamethicin molecules [86] . In the first three minutes of the experiments, **4b** were incubated with rat liver microsomes in the presence of alamethicin. Since the parent compound has no hydroxyl substituent, only the oxidation and reduction reactions were expected over this period. Then, GSH was added to the mixtures. From then on, reaction with GSH of the parent compound and its possible oxidative metabolites could also occur. These latter derivatives could be formed in spontaneous or GST-catalyzed reactions.

HPLC-MS investigation of the control incubates (without adding microsomes) indicated the formation of the expected **4b-GSH** adducts (Table 8). Under the present chromatographic conditions, similar to the previous results, two separated chalcone-GSH peaks appeared in the chromatograms (Figure 56 lower panel). The structure of the **4b-GSH**-adducts (**4b-GSH-1** and **4b-GSH-2**) was verified by positive mode HR-MS

Besides the GSH conjugates, formation of the respected (*Z*)-isomer of the parent **(*E*)-4b** was observed (Figure 56 upper panel). Since the reaction mixtures were kept in the dark, the formation of the **(*Z*)-4b** can only be explained due to the retro-Michael reaction of the formed adducts [85]. The structure of the **(*E*)-4b** and **(*Z*)-4b** was verified based on the positive mode HR-MS of the isomeric mixture obtained by light isomerization of the pure **(*E*)-4b**.

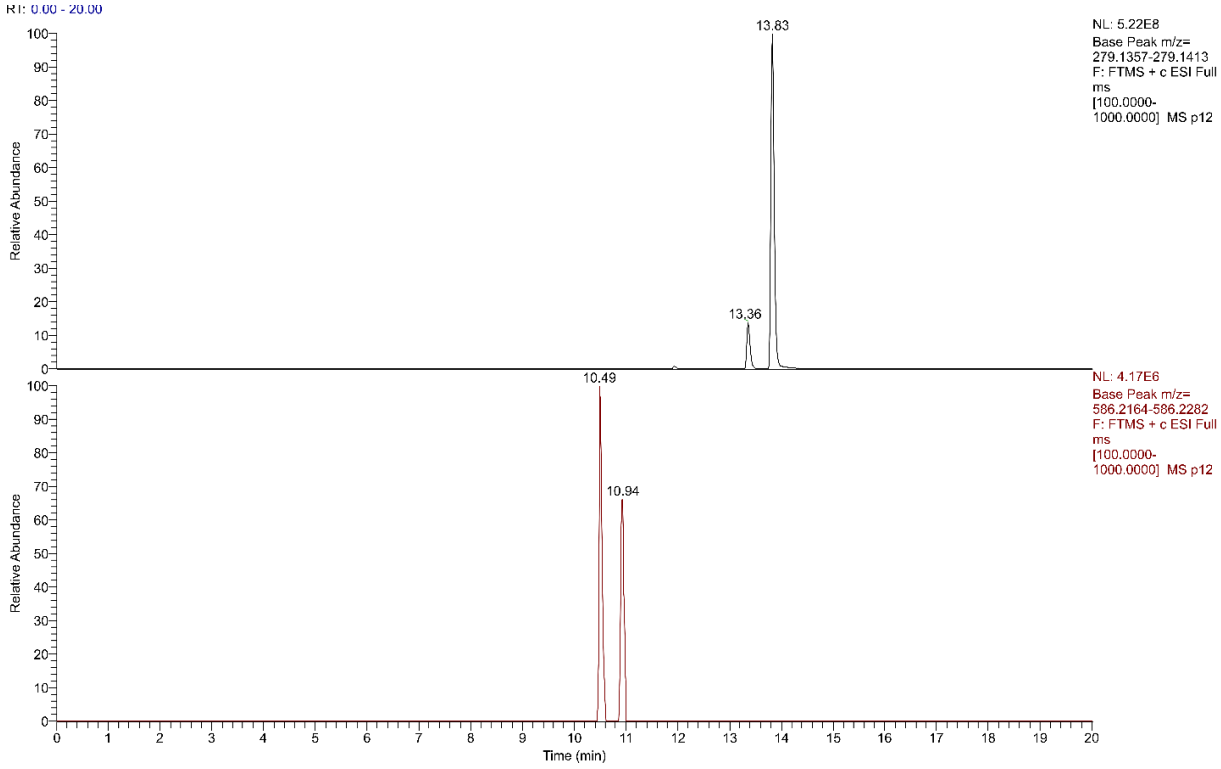

Figure 56. High resolution, positive mode HESI MS chromatogram of (*E*)-2-[(4-methoxyphenyl)methylene]-1-benzosuberone (**4b**) control incubate (90-minute sample). Upper panel: t_r 13.36 min: (*Z*)-2-[(4-methoxyphenyl)methylene]-1-benzosuberone; t_r 13.83 min: (*E*)-2-[(4-methoxyphenyl)methylene]-1-benzosuberone. Lower panel: **4b-GSH-1**: t_r 10.49 min.; **4b-GSH-2**: t_r 10.94 min.

The sum of the AUC of the two diastereomeric **4b-GSH** peaks was higher at each time point than in the respective control incubate. Although the ionization response factors of the four diastereomers are not known, the significant differences between the AUCs measured in the control and the microsomal incubates strongly support that the alamethicin-activated microsomes accelerate the chalcone-GSH conjugation reaction (Table 8).

Table 8. HPLC-MS peak areas (AUCs) of the **4b**, the **4b-GSH** isomeric peaks, and that of the oxidative metabolites of **4b** as a function of incubation time.

Compound	t_R *(min)*	***Control 0 min***	***Control 90 min***	***Microsome 0 min***	***Microsome 90 min***
(E)-4b	13.8	4,093,677,464	2,215,039,743	8,297,984,438	3,815,982,269
(Z)-4b	13.32	495,826,994	299,494,818	856,426,548	550,348,953
4b-GSH-1	10.47	1,466,946	18,724,489	2,210,842	50,714,479
4b-GSH-2	10.86	2,493,046	12,017,553	4,293,434	61,264,226
Nor-4b	12.25	N/D	N/D	7,206,428	81,441,916
4b+O	11.93	N/D	N/D	11,740,789	44,057,081

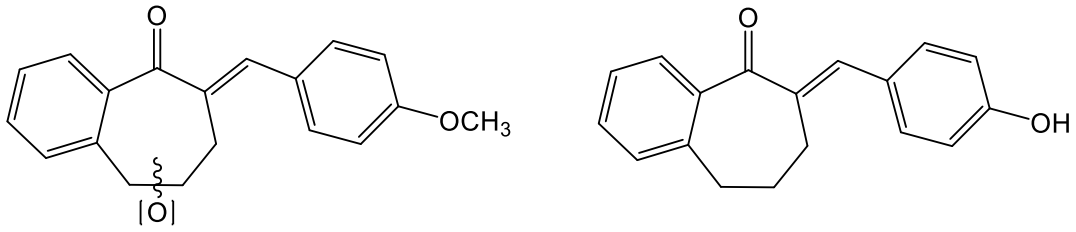

4b+O **nor-4b**

Figure 57 Structures of the products formed in the microsomal oxidation of **4b**.

In the analysis of the total ion MS spectrum of microsomal incubates, two products were found whose formation can be explained by CYP-catalyzed reactions: an oxygenated **4b (4b+O)** and the demethylated derivative (**nor-4b**). The AUC of both peaks increased over the incubation time (Table 8). The exact structure of the formed oxygenated metabolite needs further investigation. Lack of formation of a GSH-adduct of the possible epoxide metabolite; however, it is reasonable to suppose that the formed oxygenated metabolite is a hydroxyl derivative of **4b**. The demethylation reaction of **4b** resulted in the respective 4'-OH derivative (Figure 57). HPLC-MS analysis did not indicate the presence of a signal of the corresponding alcohol.

5. Discussion

Michael-type thiol reactivity of chalcones and related compounds is frequently associated with biological activities [7,22,28,85,87–90]. In contrast, several examples demonstrate that non-covalent interactions of chalcones with cellular macromolecules can play an important role in the biological effects of the compounds [11]. In a QSAR study, Katsori et al. found the clog*P* parameter to play an important part in the QSAR relationships. The authors found that the electronic effects are comparatively unimportant in the anticancer effect of the investigated chalcones [61]. However, the open-chain **1a** and **1b** possess weaker cytotoxicity than the cyclic **4a** and **4b** analogs. Furthermore, cytotoxicity and cell cycle modulating effects of **4a** and **4b** showed characteristic differences.

Investigation of the spontaneous reactivity of chalcones **1a**, **1b** and their seven-membered cyclic analogs **4a**, **4b** demonstrated that both GSH and NAC react with the investigated chalcones under acidic (pH 3.2/3.7, pH 6.3/6.8) and basic (pH 8.0/7.4) conditions. However, the rate of the initial reactions and the composition of the equilibriums was affected by the nature of the reactants and the pH of the incubation mixtures.

Analysis of the effect of the 4-substituents under basic (pH 8.0/7.4) or slightly acidic (pH 6.3/6.8) conditions showed the 4-methyl substituted **1a** and **4a** to display the higher initial reactivity. ^{13}C NMR shifts – indicating the electron density around the particular nuclei – of the C_{10} atom of **1a** (144.9 ppm), **1b** (144.6 ppm), **4a** (138.0 ppm), and **4b** (137.7 ppm) were reported to be very similar [91]. The observed difference in the reactivity of the chalcones with different substituents can be explained by the stability of the thiol-adducts. An early work of Humphlett et al. demonstrated that the activity of the α-hydrogen atom of the chalcone adduct, the resonance stabilization of the enone formed by cleavage, and the anionic stability of the thiolate ion are the determining factors of the reverse process. The authors found the α-keto and the β-phenyl substitutions as determining factors in the effective reverse reactions [92]. Since the 4-methoxy substitution can more effectively increase the electron density on the carbon-carbon double bond, and the formed chalcone is resonance-stabilized, the elimination process is more effective in the case of **1b (4b)** than **1a (4a)**. The observation further strengthens the previously suggested view that the different reactivities can be (at least partly) the result of the different stability of the thiol adducts [93,94]. Similar conclusions were withdrawn by d'Oliveira et al. while investigating a few chalcones and their rigid quinolone analogs [93].

The results obtained in the pH 6.3/6.7 incubations are similar to those of the pH 8.0/7.4 (Tables 4 and 5). Under such conditions, the composition of both incubations represents equilibrium mixtures. Under both conditions, the conversion of **4a** is somewhat higher in the case of both thiols.

The ratio of the area of the two separated peaks in the GSH incubates (315 min time point) was close to the unity for **4a** and **4b** under both pH (pH 8.0/7.4 and 6.3/6.8) conditions (Table 4). On the contrary, HPLC analysis of the reactions of **1a** and **1b** with NAC showed different (1.8-8.57 times) excess of the least polar diastereomer (Table 5). The observed diastereoselectivity was affected by the nature of the 4-substituents and the pH. Thus, the methyl–substituted **4a** showed higher diastereoselectivity at both pH values. Diastereoselectivity was increased as the pH was reduced (Table 5). It is worth mentioning, however, that the observed diastereoselectivities do not reflect the diastereoselectivity of the addition reactions (retro-Michael reactions).

Under the acid conditions (pH 3.2/3.8), the formation of the respective conjugates is exclusively due to the nucleophilic addition of the protonated thiol forms onto the polarized carbon-carbon double bounds. A comparison of the respective compositions of the GSH incubates showed that the derivatives with the same substituent possess similar GSH reactivities (Table 4). However, different results were obtained in the case of the reactions with NAC. The 315-minute percent conversion was found to be higher for **4a** (23.7%) and **4b** (12.1%) than those of the corresponding open-chain chalcones **1a** and **1b** (10.9% and 1.5%, respectively) (Table 8). However, no **4-NAC** adducts could be identified in the HPLC-UV chromatograms. Instead, several small, unidentified peaks appeared (Figures 49 and 50). HPLC-MS analysis could identify the expected conjugates.

Concerning the effect of the cyclic structure, incorporation of the seven-membered ring into the chalcone moiety reduced the spontaneous thiol-reactivity (Table 9). Since the nature of thiols and the aromatic substituents are the same, the ring structure can explain the observed differences in reactivities of the two series. Amslinger et al. investigated the thiol reactivity of chalcones with various substituents in their α-position. The kinetics of thiol reactivities of the derivatives were correlated with some of their biological effects directly connected to their Michael acceptor ability [15,87]. For example, α-methyl substitution of 2',3,4,4'-tetramethoxychalcone (TMC) decreased, the α-cyano substitution substantially increased the thiol reactivity of the nonsubstituted TMC [88]. Based on these earlier observations, it is

reasonable to suppose that the reduced reactivity of the benzosuberone derivatives **4a** and **4b** is the consequence of added effects of the α-alkyl substitution and the conformational strain caused by the cyclic structure of the starting enone and the reaction intermediate. Further research is needed to characterize the electronic and stereochemical effects of ring numerically.

Table 9. Percent reduction of initial chalcone HPLC-UV peaks in the 315-minute GSH and NAC incubation mixtures of the series **1** and **4**. *Calculated based on data published in [77].

Compound	*pH*	*Reagent thiol*	*Reduction of initial peak area (t=315 min) (%)*	*Reagent thiol*	*Reduction of initial peak area (t=315 min) (%)*
1a	8.0/7.4	GSH	96.3*	NAC	94.8*
4a	8.0/7.4	GSH	43.5	NAC	7.6
1b	8.0/7.4	GSH	92.1*	NAC	90.2*
4b	8.0/7.4	GSH	26.3	NAC	7.9
1a	6.3/6.7	GSH	90.6*	NAC	75.6*
4a	6.3/6.7	GSH	16.1	NAC	7.1
1b	6.3/6.7	GSH	78.3*	NAC	53.3*
4b	6.3/6.7	GSH	9.1	NAC	9.0
1a	3.2/3.7	GSH	19.3*	NAC	10.9*
4a	3.2/3.7	GSH	10.6	NAC	23.7
1b	3.2/3.7	GSH	4.2*	NAC	1.5*
4b	3.2/3.7	GSH	5.3	NAC	12.1

As a result of the addition reaction of the open-chain compound **1a** and **1b**, formation of two diastereomeric adducts are possible. While the chromatographic conditions could not separate the GSH-adducts, both diastereomers were detected during the NAC reaction. In these reactions, diastereoselectivity was observed; the less polar diastereomer was 1.7-1.2 times more favored than the other adduct (Table 2). The selectivity was inversely proportional to the pH and varied with the substituents.

The above findings provide further evidence to support the formation of a six-membered cyclic intermediate stabilized by hydrogen bonds as an intermediate compound during the reaction of chalcones with protonated thiols. This notion was previously proposed in the reaction of GSH with 4'-hydroxychalcone bis-Mannich derivatives [95]. As per our earlier explanation, the *Re*-side of the planar enone group is attacked by the protonated thiol, forming

a six-membered intermediate where the bulky aryl ring occupies a pseudoequatorial position. (Figure 55).

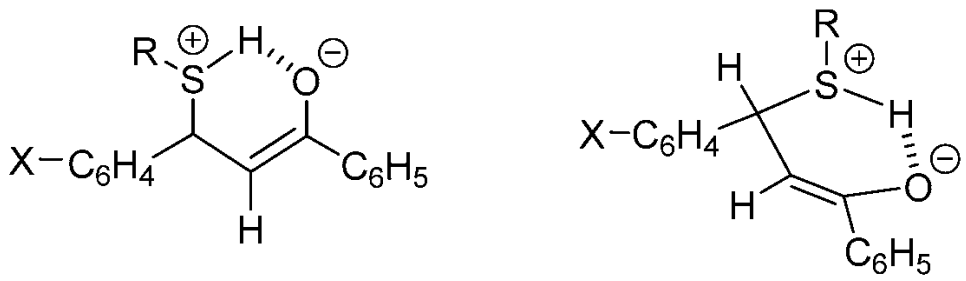

Figure 58 Possible enolate intermediate of the addition of protonated thiols onto chalcones[94].

As a result of the addition reactions to the cyclic chalcones **4a** and **4b**, formation of four diastereomeric adducts is possible. Because of the inherent chirality of GSH and NAC, two *cis* adducts and two *trans* adducts are expected to be formed (Figure 56).

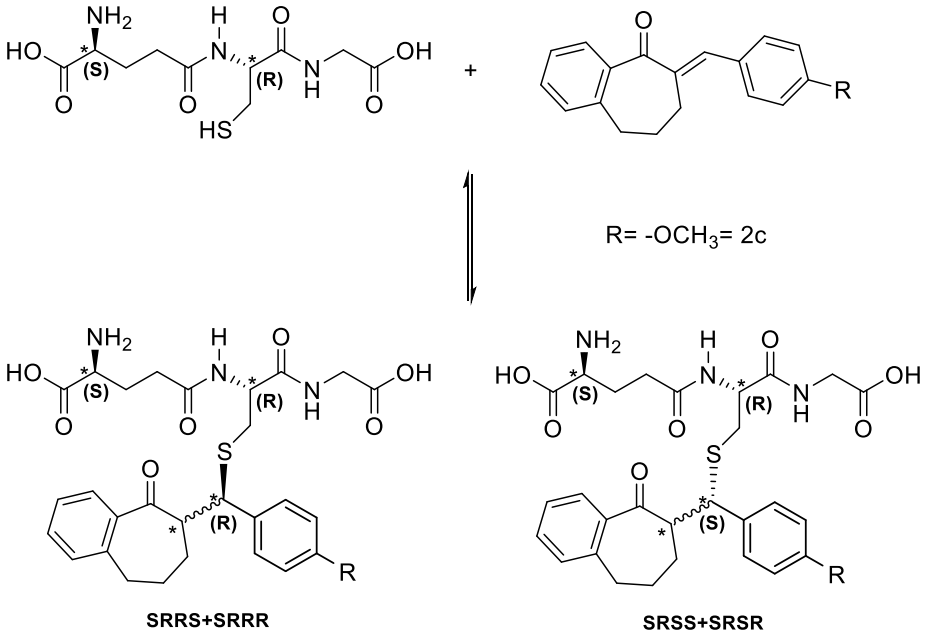

Figure 59 Structure and stereochemistry of the **4b-GSH** adducts.

Earlier, Armstrong et al. reported on the stereochemistry of the GSTM 4-4-catalyzed reaction of GSH and the open-chain chalcone analog (*E*)-(4'-X-phenyl)-3-butene-2-ones (PBO). In the reactions, a higher amount of the more polar adducts were formed [46]. Based on the results of HPLC separation of the diastereomeric pairs of the PBO-GSH [96] and the **4-**

GSH [94] adducts, we can presume that the two separated peaks formed in the present reactions correspond to the diastereomeric *cis* and *trans* adducts.

The retro-thia-Michael reactions can result in formation of the respective (*Z*)-isomers as well. Therefore, to obtain authentic reference (*Z*) isomers, the stereochemically homogeneous (*E*) isomers of **1** and **2** were submitted to light-initiated isomerization, as it was published before [64]. As a result, HPLC-MS data agreed with the respective (*Z*) isomers. Since all experiments were performed in the dark, the retro thia-Michael reaction could be the only source of the (*E*)/(*Z*) isomerization.

In the case of **4a** and **4b** reactions with both thiols relatively high amount of (*Z*)-isomer was detected, and the disappearance of starting compounds was witnessed in the progression curve of the incubations due to the net change of reversible reaction under both slightly basic and slightly acidic conditions. However, detected HPLC peak areas of the (*Z*)-isomer in the case of **1a** and **1b** were significantly small (<100mAU at 315 min) [94].

To obtain physicochemical properties insights into different reactivities of chalcones (**1**) [94] and their seven-membered cyclic analogs (**4**), HOMO and LUMO molecular orbital energy and some electrophilic reactivity parameters of **1c**, **4c**, - and as model thiols – **CH_3SH** and **CH_3S^-** were calculated (Table 6). According to the Hard and Soft, Acids and Bases (HSAB) theory [97], nucleophilic-electrophilic reactions occur preferably between electrophiles and nucleophiles of similar hardness or softness. In the case of the α,ß-unsaturated ketones, the carbonyl oxygen atom withdraws electrons from the C_2=C_{10} bond – generating an electron deficiency at C_{10} – the most likely site to receive nucleophilic attacks. In methanethiol, the nucleophilic attacks can occur at the sulfur atom. In compounds **1c** and **4c**, the carbonyl O has a high negative charge density, indicating its Lewis base behavior. On the other hand, regions of lower charge density, which appear in blue, indicate the Lewis acid behavior of the molecules.

The LUMO energy showed that **1c** (-35.98 kcal/mol) is more acidic than **4c** (-28.44 kcal/mol. The LUMO energy of **CH_3SH** is (-2.979 kcal/mol), which increases to (77.99 kcal/mol) in its deprotonated form (**CH_3S^-**). These characters are also reflected by all the other determined parameters (Table 7). Therefore, molecular orbital calculations provided data to support the experimental findings. The equilibrium (close-to-equilibrium) compositions of **1a** and **1b** show a higher product ratio than the cyclic chalcone analog **4a** and **4b**.

During the microsomal incubations, the **4b-GSH** proceeded to form in confirmation of our *in vitro* incubations. Furthermore, the analysis of the microsomal incubates confirmed the presence of **4b-GSH** adducts. The sum of the conjugates at each sampling time point was significantly larger than those of the control incubate; one may conclude that the alamethicin-activated microsome accelerated the chalcone-GSH conjugation as previously concluded regarding other microsomal enzymes [98,99]. Since compound **4b** is relatively lipophilic [100], it could be the substrate of both the microsomal glutathione transferases (MGSTs) [53–56] and the so-called microsome-associated GST enzymes. These latter GST forms are associated with the outer microsomal membranes, and their characteristics resemble those of the cytosolic GSTs [101].

In the analysis of the total ion MS spectrum of microsomal incubates, two products were found whose formation can be explained by CYP-catalyzed reactions: an oxygenated **4b** (**4b+O**) and the demethylated derivative (**nor-4b**) (Figure 57). The AUC of both peaks increased over the incubation time (Table 8). The exact structure of the formed oxygenated metabolite needs further investigation. Lack of formation of a GSH-adduct of the possible epoxide metabolite; however, it is reasonable to suppose that the formed oxygenated metabolite is a hydroxyl derivative of **4b**. The demethylation reaction of **4b** resulted in the respective 4'-OH derivative (Figure 57).

Earlier studies on the 4'-OH-metabolite (**nor-4b**) showed the compound to have a pronounced effect on the modulation of mitochondrial respiratory functions. Phosphorylation inhibitory effect and/or partial uncoupling of the compound resulted in stimulation of mitochondrial activity and increased formation of ROS [102]. Formation of a high amount of (*Z*)-isomer in the microsomal incubation might be a contributing molecular event in the observed biological effects of the compound. Furthermore, the GSH-reactivity of **4b** can also take part in the previously reported apoptotic effect of the compound.

6. Conclusion

Both chalcones **1a**, **1b** and their seven-membered cyclic analogs (**4a**, **4b**) showed intrinsic reactivity towards GSH and NAC under physiological (pH 7.4) conditions. The reactivity of the open-chain chalcones was higher than that of the cyclic ones. Furthermore, the reactivity of the compounds is also affected by the aromatic substituent found in position 4 of the benzylidene moiety. These observations serve as a basis for planning and synthesizing other chalcone/cyclic chalcone derivatives with optimized thiol-reactivity.

Microsomal biotransformation of **4b** showed the compound to be metabolized by the CYP and the GST enzymes. As a result of CYP-catalyzed transformations, one monooxygenated (**4b+O**) and the demethylated (**nor-4b**) metabolites were identified. In addition, a noticeable amount of **(*Z*)-4b** was also identified in the incubates. Since the (*Z*)-isomer of the parent compound has a different three-dimensional structure, degree of conjugation, and lipophilicity [64], the formation of this isomer might be a molecular event that plays a role in the observed biological effects of the compound.

Furthermore, the GSH-reactivity of **4b** can affect the compound's bioavailability. Such reactions also take part in the previously reported apoptotic effect of this class of compounds. It should be mentioned, however, that while the thiol reactivity of **4a** and **4b** is comparable, there is a two-order of magnitude difference in the cytotoxicity against most of the investigated cancer cell lines.

The anticancer potential of chalcones is correlated with their ability to act on various molecular targets such as ABCG2, tubulin, activated nuclear B cell growth (NF-κB), vascular endothelial growth factor (VEGF), tyrosine kinase receptor (EGFR), mesenchymal-epithelial transition factor (MET), 5-α reductase, ACP-reductase, histone deacetylase, p53, CDC25B (protein tyrosine phosphatase), retinoic acid receptors, estrogenic topoisomerase receptors and MDM2 [89]. Considering the present and our previous results [4,5,60], it is reasonable to suppose that the molecular basis of the different biological effects of **4a** and **4b** is related to the non-covalent interactions of the compounds [12].

7. List of publications and presentations

Publications

1. Perjési, P.; Caridad, N.P.; Aline, B.; Giulio, D. d'Oliveira; Kenari, F. The Chemistry of GST-Catalyzed Reactions. In *Glutathione: Biosynthesis, Functions and Biological Implications*; Perjési, P., Ed.; Nova Science Publishers: Hauppauge, New York, **2019**; pp. 373–403. ISBN 978-1-5361-4740-7.

2. Kenari, F.; Molnár, S.; Perjési, P. Reaction of Chalcones with Cellular Thiols. The Effect of the 4-Substitution of Chalcones and Protonation State of the Thiols on the Addition Process. Diastereoselective Thiol Addition. *Molecules* **2021**, 26, 4332. doi:10.3390/molecules26144332.

3. Kenari, F.; Molnár, S.; Pintér, Z.; Bitaraf, S.; Perjési, P. (*E*)-2-Benzylidenecyclanones: Part XVII. An LC-MS Study of Microsomal Transformation Reactions of (*E*)-2-[(4'-Methoxyphenyl) Methylene]-Benzosuberon-1-One: A Cyclic Chalcone Analog. *J. Pharm. Biopharm. Res*. **2023**, 4, 326–339, doi:10.25082/JPBR.2022.02.004.

4. Kenari, F.; Molnár, S.; Borges, I.D.; Napolitano, H.B.; Perjési, P. (*E*)-2-Benzylidenecyclanones: Part XVIII Study the Possible Link between Glutathione Reactivity and Cancer Cell Cytotoxic Effects of Some Cyclic Chalcone Analogs A Comparison of the Reactivity of the Open-Chain and the Seven-Membered Homologs. *Int. J. Mol. Sci.* **2023**, *24*, 8557. https://doi.org/10.3390/ijms24108557.

Other publications

1. Sadighpour, T.; Mubarak, M.; Sabaeifard, P.; Saeifar, S.; Kenari, F. COVID-19 and Renal Involvement; Evolving Role of Thromboinflammation, Vascular and Glomerular Disease in the Pathogenesis. *J. Nephropathol*. **2021**, 10. doi:10.34172/jnp.2021.23.

2. Rozmer, Z.; Kenari, F.; Tyukodi, L.; Kulcsár, G.; Huber, I.; Perjési, P. A PTE GYTK Gyógyszerészi Kémiai Intézetben folyó kutatásokról I. Szerkezet-reaktivitás és szerkezet-hatás vizsgálatok. *Magy. Kém. Foly. Kém. Közl*. **2022**, 128, 53–59. doi:10.24100/MKF.2022.02.53.

List of conference posters and presentations

1. Kenari, F.; Perjési, P. Study on Interaction of Reduced Glutathione (GSH) with Cyclic Chalcone Analogs.; [s.n.], Ed.; Pécsi Tudományegyetem Általános Orvostudományi Kar: Pécs, **2018**; p. [36]-[36].

2. Kenari, F.; Perjési, P. Study of Interaction of Reduced Glutathione (GSH) with Chalcone and Some Cyclic Chalcone Analogues. *Acta Pharm. Hung*. **2017**, 87, 156–157.

3. Perjési, P.; Almási, A.; Kenari, F.; Kuzma, M.; Fliszár-Nyúl, E. Non-Enzyme Catalyzed Metabolic Transformations of Xenobiotics. *Acta Pharm. Hung*. **2017**, 87, 113.

4. Kenari, F.; Molnár, S.; Kulcsár, G.; Perjési, P. Study of Interaction of Reduced Glutathione (GSH) with Some Chalcone Analogues. In VIII. Interdiszciplináris Doktorandusz

Konferencia 2019: Absztrakt kötet. 8th Interdisciplinary Doctoral Conference 2019: Book of Abstracts; Bódog, F., Csiszár, B., Eds.; Pécsi Tudományegyetem Doktorandusz Önkormányzat, Pécs, **2019**; pp. 122–122. ISBN 978-963-429-374-3.

5. Kenari, F.; Bernardes, A.; Noda, PC.; Molnár, S.; Kulcsár, G.; Perjési, P. Study of Interaction of Reduced Glutathione (GSH) with Some Chalcone Analogs in Vitro and in Vivo. *Acta Pharm. Hung*. **2020**, 90, 123–124.

6. Kenari, F.; Perjési, P. Study on Interaction of Reduced Glutathione (GSH) with Cyclic Chalcone Anaglogues.; Magyar Gyógyszerésztudományi Társaság (MGYT): Budapest, **2018**; p. abstract.

8. References

1. Rozmer, Z.; Perjési, P. Naturally Occurring Chalcones and Their Biological Activities. *Phytochem. Rev.* **2016**, *15*, 87–120, doi:10.1007/s11101-014-9387-8.
2. Go, M.; Wu, X.; Liu, X. Chalcones: An Update on Cytotoxic and Chemoprotective Properties. *Curr. Med. Chem.* **2005**, *12*, 483–499, doi:10.2174/0929867053363153.
3. Gomes, M.N.; Muratov, E.N.; Pereira, M.; Peixoto, J.C.; Rosseto, L.P.; Cravo, P.V.L.; Andrade, C.H.; Neves, B.J. Chalcone Derivatives: Promising Starting Points for Drug Design. *Mol. Basel Switz.* **2017**, *22*, 1210, doi:10.3390/molecules22081210.
4. Dimmock, J.R.; Zello, G.A.; Oloo, E.O.; Quail, J.W.; Kraatz, H.-B.; Perjési, P.; Aradi, F.; Takács-Novák, K.; Allen, T.M.; Santos, C.L.; et al. Correlations between Cytotoxicity and Topography of Some 2-Arylidenebenzocycloalkanones Determined by X-Ray Crystallography. *J. Med. Chem.* **2002**, *45*, 3103–3111, doi:10.1021/jm010559p.
5. Perjési, P.; Das, U.; De Clercq, E.; Balzarini, J.; Kawase, M.; Sakagami, H.; Stables, J.P.; Lorand, T.; Rozmer, Z.; Dimmock, J.R. Design, Synthesis and Antiproliferative Activity of Some 3-Benzylidene-2,3-Dihydro-1-Benzopyran-4-Ones Which Display Selective Toxicity for Malignant Cells. *Eur. J. Med. Chem.* **2008**, *43*, 839–845, doi:10.1016/j.ejmech.2007.06.017.
6. Ouyang, Y.; Li, J.; Chen, X.; Fu, X.; Sun, S.; Wu, Q. Chalcone Derivatives: Role in Anticancer Therapy. *Biomolecules* **2021**, *11*, doi:10.3390/biom11060894.
7. Nasir Abbas Bukhari, S.; Jantan, I.; Jasamai, M. Anti-Inflammatory Trends of 1, 3-Diphenyl-2-Propen-1-One Derivatives. *Mini-Rev. Med. Chem.* **2013**, *13*, 87–94, doi:10.2174/1389557511307010087.
8. Mahapatra, K.D.; Bharti, K.S.; Asati, V. Chalcone Derivatives: Anti-Inflammatory Potential and Molecular Targets Perspectives. *Curr. Top. Med. Chem.* **2017**, *17*, 3146–3169, doi:10.2174/1568026617666170914160446.
9. Rudrapal, M.; Khan, J.; Dukhyil, A.A.; Alarousy, R.M.; Attah, E.I.; Sharma, T.; Khairnar, S.J.; Bendale, A.R. Chalcone Scaffolds, Bioprecursors of Flavonoids: Chemistry, Bioactivities, and Pharmacokinetics. *Molecules* **2021**, *26*, doi:10.3390/molecules26237177.
10. Kim, W.; Lee, H.; Kim, S.; Joo, S.; Jeong, S.; Yoo, J.-W.; Jung, Y. Sofalcone, a Gastroprotective Drug, Covalently Binds to KEAP1 to Activate Nrf2 Resulting in Anti-Colitic Activity. *Eur. J. Pharmacol.* **2019**, *865*, 172722, doi:10.1016/j.ejphar.2019.172722.
11. Guex, J.J.; Enriquez Vega, D.M.E.; Avril, L.; Boussetta, S.; Taïeb, C. Assessment of Quality of Life in Mexican Patients Suffering from Chronic Venous Disorder – Impact of Oral Ruscus Aculeatus-Hesperidin–Methyl-Chalcone–Ascorbic Acid Treatment – 'QUALITY Study.' *Phlebology* **2009**, *24*, 157–165, doi:10.1258/phleb.2009.008066.
12. Kozurkova, M.; Tomeckova, V. Interaction of Chalcone Derivatives with Important Biomacromolecules. In *Chalcones and Their Synthetic Analogs*; Nova Science Publishers, Inc, 2020; p. 95 ISBN 978-1-5361-8709-0.
13. Zhou, B. Diverse Molecular Targets for Chalcones with Varied Bioactivities. *Med. Chem.* **2015**, doi:10.4172/2161-0444.1000291.
14. Noyce, D.S.; Jorgenson, M.J. Carbonyl Reactions. XIX. The Basicities of Substituted Chalcones. *J. Am. Chem. Soc.* **1962**, *84*, 4312–4319.
15. Amslinger, S. The Tunable Functionality of α,β-Unsaturated Carbonyl Compounds Enables Their Differential Application in Biological Systems. *ChemMedChem* **2010**, *5*, 351–356, doi:10.1002/cmdc.200900499.
16. Liu, T.; Zhang, L.; Joo, D.; Sun, S.-C. NF-KB Signaling in Inflammation. *Signal Transduct. Target. Ther.* **2017**, *2*, 17023, doi:10.1038/sigtrans.2017.23.

17. Brown, K.D.; Claudio, E.; Siebenlist, U. The Roles of the Classical and Alternative Nuclear Factor-KappaB Pathways: Potential Implications for Autoimmunity and Rheumatoid Arthritis. *Arthritis Res. Ther.* **2008**, *10*, 212, doi:10.1186/ar2457.
18. Folmer, F.; Blasius, R.; Morceau, F.; Tabudravu, J.; Dicato, M.; Jaspars, M.; Diederich, M. Inhibition of TNFα-Induced Activation of Nuclear Factor KB by Kava (Piper Methysticum) Derivatives. *Biochem. Pharmacol.* **2006**, *71*, 1206–1218, doi:10.1016/j.bcp.2005.12.032.
19. Laphanuwat, P.; Kongpetch, S.; Senggunprai, L.; Prawan, A.; Kukongviriyapan, V. Licochalcone A Induces Cholangiocarcinoma Cell Death Via Suppression of Nrf2 and NF-KB Signaling Pathways. *Asian Pac. J. Cancer Prev.* **2022**, *23*, 115–123, doi:10.31557/APJCP.2022.23.1.115.
20. James, S.; Aparna, J.S.; Babu, A.; Paul, A.M.; Lankadasari, M.B.; Athira, S.R.; Kumar, S.S.; Vijayan, Y.; Namitha, N.N.; Mohammed, S.; et al. Cardamonin Attenuates Experimental Colitis and Associated Colorectal Cancer. *Biomolecules* **2021**, *11*, doi:10.3390/biom11050661.
21. Kim, J.-Y.; Park, S.J.; Yun, K.-J.; Cho, Y.-W.; Park, H.-J.; Lee, K.-T. Isoliquiritigenin Isolated from the Roots of Glycyrrhiza Uralensis Inhibits LPS-Induced INOS and COX-2 Expression via the Attenuation of NF-KB in RAW 264.7 Macrophages. *Eur. J. Pharmacol.* **2008**, *584*, 175–184, doi:10.1016/j.ejphar.2008.01.032.
22. de Freitas Silva, M.; Pruccoli, L.; Morroni, F.; Sita, G.; Seghetti, F.; Viegas, C.; Tarozzi, A. The Keap1/Nrf2-ARE Pathway as a Pharmacological Target for Chalcones. *Mol. Basel Switz.* **2018**, *23*, 1803, doi:10.3390/molecules23071803.
23. Qin, J.-J.; Cheng, X.-D.; Zhang, J.; Zhang, W.-D. Dual Roles and Therapeutic Potential of Keap1-Nrf2 Pathway in Pancreatic Cancer: A Systematic Review. *Cell Commun. Signal.* **2019**, *17*, 121, doi:10.1186/s12964-019-0435-2.
24. Almeida, M.; Soares, M.; Ramalhinho, A.C.; Moutinho, J.F.; Breitenfeld, L.; Pereira, L. The Prognostic Value of NRF2 in Breast Cancer Patients: A Systematic Review with Meta-Analysis. *Breast Cancer Res. Treat.* **2020**, *179*, 523–532, doi:10.1007/s10549-019-05494-4.
25. Sandberg, M.; Patil, J.; D'Angelo, B.; Weber, S.G.; Mallard, C. NRF2-Regulation in Brain Health and Disease: Implication of Cerebral Inflammation. *Neuropharmacology* **2014**, *79*, 298–306, doi:10.1016/j.neuropharm.2013.11.004.
26. Bhakkiyalakshmi, E.; Sireesh, D.; Rajaguru, P.; Paulmurugan, R.; Ramkumar, K.M. The Emerging Role of Redox-Sensitive Nrf2–Keap1 Pathway in Diabetes. *Pharmacol. Res.* **2015**, *91*, 104–114, doi:10.1016/j.phrs.2014.10.004.
27. den Braver-Sewradj, S.P.; den Braver, M.W.; Toorneman, R.M.; van Leeuwen, S.; Zhang, Y.; Dekker, S.J.; Vermeulen, N.P.E.; Commandeur, J.N.M.; Vos, J.C. Reduction and Scavenging of Chemically Reactive Drug Metabolites by NAD(P)H:Quinone Oxidoreductase 1 and NRH:Quinone Oxidoreductase 2 and Variability in Hepatic Concentrations. *Chem. Res. Toxicol.* **2018**, *31*, 116–126, doi:10.1021/acs.chemrestox.7b00289.
28. Dinkova-Kostova, A.T.; Holtzclaw, W.D.; Cole, R.N.; Itoh, K.; Wakabayashi, N.; Katoh, Y.; Yamamoto, M.; Talalay, P. Direct Evidence That Sulfhydryl Groups of Keap1 Are the Sensors Regulating Induction of Phase 2 Enzymes That Protect against Carcinogens and Oxidants. *Proc. Natl. Acad. Sci.* **2002**, *99*, 11908–11913.
29. Zhang, M.; An, C.; Gao, Y.; Leak, R.K.; Chen, J.; Zhang, F. Emerging Roles of Nrf2 and Phase II Antioxidant Enzymes in Neuroprotection. *Prog. Neurobiol.* **2013**, *100*, 30–47, doi:10.1016/j.pneurobio.2012.09.003.
30. Egbujor, M.C.; Saha, S.; Buttari, B.; Profumo, E.; Saso, L. Activation of Nrf2 Signaling Pathway by Natural and Synthetic Chalcones: A Therapeutic Road Map for Oxidative

Stress. *Expert Rev. Clin. Pharmacol.* **2021**, *14*, 465–480, doi:10.1080/17512433.2021.1901578.
31. Smolková, K.; Mikó, E.; Kovács, T.; Leguina-Ruzzi, A.; Sipos, A.; Bai, P. Nuclear Factor Erythroid 2-Related Factor 2 in Regulating Cancer Metabolism. *Antioxid. Redox Signal.* **2020**, *33*, 966–997, doi:10.1089/ars.2020.8024.
32. Kao, Y.-T.; Chen, Y.-S.; Tang, K.-W.; Lee, J.-C.; Tseng, C.-H.; Tzeng, C.-C.; Yen, C.-H.; Chen, Y.-L. Discovery of 4-Anilinoquinolinylchalcone Derivatives as Potential NRF2 Activators. *Mol. Basel Switz.* **2020**, *25*, 3133, doi:10.3390/molecules25143133.
33. Su, X.; Li, T.; Liu, Z.; Huang, Q.; Liao, K.; Ren, R.; Lu, L.; Qi, X.; Wang, M.; Chen, J.; et al. Licochalcone A Activates Keap1-Nrf2 Signaling to Suppress Arthritis via Phosphorylation of P62 at Serine 349. *Free Radic. Biol. Med.* **2018**, *115*, 471–483, doi:10.1016/j.freeradbiomed.2017.12.004.
34. Lv, H.; Ren, H.; Wang, L.; Chen, W.; Ci, X. Lico A Enhances Nrf2-Mediated Defense Mechanisms against t-BHP-Induced Oxidative Stress and Cell Death via Akt and ERK Activation in RAW 264.7 Cells. *Oxid. Med. Cell. Longev.* **2015**, *2015*, 709845, doi:10.1155/2015/709845.
35. Forman, H.J.; Zhang, H.; Rinna, A. Glutathione: Overview of Its Protective Roles, Measurement, and Biosynthesis. *Glutathione Health Dis.* **2009**, *30*, 1–12, doi:10.1016/j.mam.2008.08.006.
36. Kennedy, L.; Sandhu, J.K.; Harper, M.-E.; Cuperlovic-Culf, M. Role of Glutathione in Cancer: From Mechanisms to Therapies. *Biomolecules* **2020**, *10*, doi:10.3390/biom10101429.
37. Scirè, A.; Cianfruglia, L.; Minnelli, C.; Bartolini, D.; Torquato, P.; Principato, G.; Galli, F.; Armeni, T. Glutathione Compartmentalization and Its Role in Glutathionylation and Other Regulatory Processes of Cellular Pathways. *BioFactors* **2019**, *45*, 152–168, doi:10.1002/biof.1476.
38. Sabzevari, O.; Galati, G.; Moridani, M.Y.; Siraki, A.; O'Brien, P.J. Molecular Cytotoxic Mechanisms of Anticancer Hydroxychalcones. *Chem. Biol. Interact.* **2004**, *148*, 57–67, doi:10.1016/j.cbi.2004.04.004.
39. Sherratt, P.J.; Hayes, J.D. Glutathione S-transferases. *Enzyme Syst. Metab. Drugs Xenobiotics* **2001**, 319–352.
40. Sharma, R.; Ansari, G.S.; Awasthi, Y.C. Physiological Substrates of Glutathione S-Transferases. *Toxicol. Glutation Transferases CRC Press N. Y.* **2006**, 179–203.
41. Wu, B.; Dong, D. Human Cytosolic Glutathione Transferases: Structure, Function, and Drug Discovery. *Trends Pharmacol. Sci.* **2012**, *33*, 656–668.
42. Zimniak, P. Substrates and Reaction Mechanisms of Glutathione Transferases. *Toxicol. Glutathione Transferases* **2007**, 24–46.
43. Hubatsch, I.; Ridderstrom, M.; Mannervik, B. Human Glutathione Transferase A4-4: An Alpha Class Enzyme with High Catalytic Efficiency in the Conjugation of 4-Hydroxynonenal and Other Genotoxic Products of Lipid Peroxidation. *Biochem. J.* **1998**, *330*, 175–179.
44. Johansson, A.-S.; Mannervik, B. Human Glutathione Transferase A3-3, a Highly Efficient Catalyst of Double-Bond Isomerization in the Biosynthetic Pathway of Steroid Hormones. *J. Biol. Chem.* **2001**, *276*, 33061–33065.
45. Gu, Y.; Guo, J.; Pal, A.; Pan, S.-S.; Zimniak, P.; Singh, S.V.; Ji, X. Crystal Structure of Human Glutathione S-Transferase A3-3 and Mechanistic Implications for Its High Steroid Isomerase Activity. *Biochemistry* **2004**, *43*, 15673–15679.
46. Armstrong, R.N. Structure, Catalytic Mechanism, and Evolution of the Glutathione Transferases. *Chem. Res. Toxicol.* **1997**, *10*, 2–18.

47. Ladner, J.E.; Parsons, J.F.; Rife, C.L.; Gilliland, G.L.; Armstrong, R.N. Parallel Evolutionary Pathways for Glutathione Transferases: Structure and Mechanism of the Mitochondrial Class Kappa Enzyme RGSTK1-1. *Biochemistry* **2004**, *43*, 352–361.
48. Jowsey, I.R.; Thomson, R.E.; Orton, T.C.; Elcombe, C.R.; Hayes, J.D. Biochemical and Genetic Characterization of a Murine Class Kappa Glutathione S-Transferase. *Biochem. J.* **2003**, *373*, 559–569.
49. Morgenstern, R.; Guthenberg, C.; Depierre, J.W. Microsomal Glutathione S-transferase: Purification, Initial Characterization and Demonstration That It Is Not Identical to the Cytosolic Glutathione S-transferases A, B and C. *Eur. J. Biochem.* **1982**, *128*, 243–248.
50. Bernat, B.A.; Laughlin, L.T.; Armstrong, R.N. Fosfomycin Resistance Protein (FosA) Is a Manganese Metalloglutathione Transferase Related to Glyoxalase I and the Extradiol Dioxygenases. *Biochemistry* **1997**, *36*, 3050–3055.
51. Perjési, P.; Caridad, N.P.; Aline, B.; Giulio, D. d'Oliveira; Kenari, F. The Chemistry of GST-Catalyzed Reactions. In *Glutathione: Biosynthesis, Functions and Biological Implications*; Perjési, P., Ed.; Pharmacology-Research, Safety Testing and Regulation; Nova Science Publishers: Hauppauge, New York, 2019; pp. 373–403 ISBN 978-1-5361-4740-7.
52. Hill, J.R. In Vitro Drug Metabolism Using Liver Microsomes. *Curr. Protoc. Pharmacol.* **2003**, *23*, doi:10.1002/0471141755.ph0708s23.
53. Lundqvist, G.; Yücel-Lindberg, T.; Morgenstern, R. The Oligomeric Structure of Rat Liver Microsomal Glutathione Transferase Studied by Chemical Cross-Linking. *Biochim. Biophys. Acta BBA-Protein Struct. Mol. Enzymol.* **1992**, *1159*, 103–108.
54. Jakobsson, P.-J.; Mancini, J.A.; Riendeau, D.; Ford-Hutchinson, A.W. Identification and Characterization of a Novel Microsomal Enzyme with Glutathione-Dependent Transferase and Peroxidase Activities. *J. Biol. Chem.* **1997**, *272*, 22934–22939.
55. Jakobsson, P.-J.; Morgenstern, R.; Mancini, J.; Ford-Hutchinson, A.; Persson, B. Common Structural Features of MAPEG—a Widespread Superfamily of Membrane Associated Proteins with Highly Divergent Functions in Eicosanoid and Glutathione Metabolism. *Protein Sci.* **1999**, *8*, 689–692.
56. Surapureddi, S.; Svartz, J.; Magnusson, K.-E.; Hammarström, S.; Söderström, M. Colocalization of Leukotriene C Synthase and Microsomal Glutathione S-transferase Elucidated by Indirect Immunofluorescence Analysis. *FEBS Lett.* **2000**, *480*, 239–243.
57. Weinander, R.; Ekström, L.; Andersson, C.; Raza, H.; Bergman, T.; Morgenstern, R. Structural and Functional Aspects of Rat Microsomal Glutathione Transferase. *J. Biol. Chem.* **1997**, *272*, 8871–8877, doi:10.1074/jbc.272.14.8871.
58. Potęga, A. Glutathione-Mediated Conjugation of Anticancer Drugs: An Overview of Reaction Mechanisms and Biological Significance for Drug Detoxification and Bioactivation. *Molecules* **2022**, *27*, doi:10.3390/molecules27165252.
59. Cooper, A.J.L.; Hanigan, M.H. 10.17 - Metabolism of Glutathione S-Conjugates: Multiple Pathways. In *Comprehensive Toxicology (Third Edition)*; McQueen, C.A., Ed.; Elsevier: Oxford, 2018; pp. 363–406 ISBN 978-0-08-100601-6.
60. Dimmock, J.R.; Kandepu, N.M.; Nazarali, A.J.; Kowalchuk, T.P.; Motaganahalli, N.; Quail, J.W.; Mykytiuk, P.A.; Audette, G.F.; Prasad, L.; Perjési, P.; et al. Conformational and Quantitative Structure−Activity Relationship Study of Cytotoxic 2-Arylidenebenzocycloalkanones. *J. Med. Chem.* **1999**, *42*, 1358–1366, doi:10.1021/jm9806695.
61. Katsori, A.-M.; Hadjipavlou-Litina, D. Chalcones in Cancer: Understanding Their Role in Terms of QSAR. *Curr. Med. Chem.* **2009**, *16*, 1062–1081, doi:10.2174/092986709787581798.

62. López, S.N.; Castelli, M.V.; Zacchino, S.A.; Domínguez, J.N.; Lobo, G.; Charris-Charris, J.; Cortés, J.C.G.; Ribas, J.C.; Devia, C.; Rodríguez, A.M.; et al. In Vitro Antifungal Evaluation and Structure–Activity Relationships of a New Series of Chalcone Derivatives and Synthetic Analogues, with Inhibitory Properties against Polymers of the Fungal Cell Wall. *Bioorg. Med. Chem.* **2001**, *9*, 1999–2013, doi:10.1016/S0968-0896(01)00116-X.
63. Jin, Y.L.; Jin, X.Y.; Jin, F.; Sohn, D.H.; Kim, H.S. Structure Activity Relationship Studies of Anti-Inflammatory TMMC Derivatives: 4-Dimethylamino Group on the B Ring Responsible for Lowering the Potency. *Arch. Pharm. Res.* **2009**, *31*, 1145, doi:10.1007/s12272-001-1281-7.
64. Perjési, P. (E)-2-Benzylidenebenzocyclanones: Part XIII—(E)/(Z)-Isomerization of Some Cyclic Chalcone Analogues. Effect of Ring Size on Lipophilicity of Geometric Isomers. *Monatshefte Für Chem.-Chem. Mon.* **2015**, *146*, 1275–1281.
65. Schleuder, M.; Am Ali, F.; Otto, H. Spektroskopische Und Chromatographische Untersuchungen Zur Photochemischen Isomerisierung von α, β-Diungesattigten Ketonen. *Pharm.* **2003**, *58*, 308–311.
66. IWATA, S.; NISHINO, T.; INOUE, H.; NAGATA, N.; SATOMI, Y.; NISHINO, H.; SHIBATA, S. Antitumorigenic Activities of Chalcones (II). Photo-Isomerization of Chalcones and the Correlation with Their Biological Activities. *Biol. Pharm. Bull.* **1997**, *20*, 1266–1270, doi:10.1248/bpb.20.1266.
67. Imbach, J.-L.; Pohland, A.E.; Weiler, E.D.; Cromwell, N.H. Nuclear Magnetic Resonance Spectra of Derivatives of Various Substituted Indanones and Tetralones. *Tetrahedron* **1967**, *23*, 3931–3941, doi:10.1016/S0040-4020(01)97903-7.
68. Kevill, D.N.; Weiler, E.D.; Cromwell, N.H. Cis-Trans Isomerism of Exocyclic α, β-Unsaturated Indanones and Tetralones. *J. Org. Chem.* **1964**, *29*, 1276–1278.
69. Perjesi, P.; Takacs, M.; Osz, E.; Pinter, Z.; Vamos, J.; Takacs-Novak, K. In-Solution and On-Plate Light-Catalyzed E/Z Isomerization of Cyclic Chalcone Analogues. Lipophilicity of E- and Z-2-(X-Benzylidene)-1-Benzosuberones. *J. Chromatogr. Sci.* **2005**, *43*, 289–295, doi:10.1093/chromsci/43.6.289.
70. Phosphate-Buffered Saline (PBS; 0.1 m, PH 7.4). *Cold Spring Harb. Protoc.* **2014**, *2014*, pdb.rec085126, doi:10.1101/pdb.rec085126.
71. Hohenberg, P.; Kohn, W. Inhomogeneous Electron Gas. *Phys. Rev.* **1964**, *136*, B864.
72. Kohn, W.; Sham, L.J. Self-Consistent Equations Including Exchange and Correlation Effects. *Phys. Rev.* **1965**, *140*, A1133.
73. Frisch, M.; Trucks, G.; Schlegel, H.; Scuseria, G.; Robb, M.; Cheeseman, J.; Scalmani, G.; Barone, V.; Petersson, G.; Nakatsuji, H. Gaussian 16 Revision C. 01. 2016; Gaussian Inc. *Wallingford CT* **2016**, *421*.
74. Zhao, Y.; Truhlar, D.G. The M06 Suite of Density Functionals for Main Group Thermochemistry, Thermochemical Kinetics, Noncovalent Interactions, Excited States, and Transition Elements: Two New Functionals and Systematic Testing of Four M06-Class Functionals and 12 Other Functionals. *Theor. Chem. Acc.* **2008**, *120*, 215–241.
75. Zhang, G.; Musgrave, C.B. Comparison of DFT Methods for Molecular Orbital Eigenvalue Calculations. *J. Phys. Chem. A* **2007**, *111*, 1554–1561.
76. Weiner, P.K.; Langridge, R.; Blaney, J.M.; Schaefer, R.; Kollman, P.A. Electrostatic Potential Molecular Surfaces. *Proc. Natl. Acad. Sci.* **1982**, *79*, 3754–3758.
77. Naray-Szabo, G.; Ferenczy, G.G. Molecular Electrostatics. *Chem. Rev.* **1995**, *95*, 829–847.
78. Fukui, K. The Role of Frontier Orbitals in Chemical Reactions (Nobel Lecture). *Angew. Chem. Int. Ed. Engl.* **1982**, *21*, 801–809.
79. Fukui, K. Role of Frontier Orbitals in Chemical Reactions. *science* **1982**, *218*, 747–754.

80. Lu, T. Multiwfn. Software Manual 2014.
81. Sanches-Neto, F.O.; Dias-Silva, J.R.; Keng Queiroz Junior, L.H.; Carvalho-Silva, V.H. "Py SiRC": Machine Learning Combined with Molecular Fingerprints to Predict the Reaction Rate Constant of the Radical-Based Oxidation Processes of Aqueous Organic Contaminants. *Environ. Sci. Technol.* **2021**, *55*, 12437–12448.
82. Rohani, N.; Hao, L.; Alexis, M.S.; Joughin, B.A.; Krismer, K.; Moufarrej, M.N.; Soltis, A.R.; Lauffenburger, D.A.; Yaffe, M.B.; Burge, C.B. Acidification of Tumor at Stromal Boundaries Drives Transcriptome Alterations Associated with Aggressive Phenotypes. *Cancer Res.* **2019**, *79*, 1952–1966.
83. Jiang, B. Aerobic Glycolysis and High Level of Lactate in Cancer Metabolism and Microenvironment. *Genes Dis.* **2017**, *4*, 25–27, doi:10.1016/j.gendis.2017.02.003.
84. Deberardinis, R.J. Is Cancer a Disease of Abnormal Cellular Metabolism? New Angles on an Old Idea. *Genet. Med.* **2008**, *10*, 767–777, doi:10.1097/GIM.0b013e31818b0d9b.
85. Berne, D.; Ladmiral, V.; Leclerc, E.; Caillol, S. Thia-Michael Reaction: The Route to Promising Covalent Adaptable Networks. *Polymers* **2022**, *14*, 4457.
86. Leitgeb, B.; Szekeres, A.; Manczinger, L.; Vágvölgyi, C.; Kredics, L. The History of Alamethicin: A Review of the Most Extensively Studied Peptaibol. *Chem. Biodivers.* **2007**, *4*, 1027–1051.
87. Amslinger, S.; Al-Rifai, N.; Winter, K.; Wörmann, K.; Scholz, R.; Baumeister, P.; Wild, M. Reactivity Assessment of Chalcones by a Kinetic Thiol Assay. *Org. Biomol. Chem.* **2013**, *11*, 549–554.
88. Al-Rifai, N.; Rücker, H.; Amslinger, S. Opening or Closing the Lock? When Reactivity Is the Key to Biological Activity. *Chem. Eur. J.* **2013**, *19*, 15384–15395.
89. Zhuang, C.; Zhang, W.; Sheng, C.; Zhang, W.; Xing, C.; Miao, Z. Chalcone: A Privileged Structure in Medicinal Chemistry. *Chem. Rev.* **2017**, *117*, 7762–7810.
90. Wang, J.; Wang, S.; Song, D.; Zhao, D.; Sha, Y.; Jiang, Y.; Jing, Y.; Cheng, M. Chalcone Derivatives Inhibit Glutathione S-Transferase P1-1 Activity: Insights into the Interaction Mode of α, B-Unsaturated Carbonyl Compounds. *Chem. Biol. Drug Des.* **2009**, *73*, 511–514.
91. Perjési, P.; Linnanto, J.; Kolehmainen, E.; Ősz, E.; Virtanen, E. E-2-Benzylidenebenzocycloalkanones. IV. Studies on Transmission of Substituent Effects on 13C NMR Chemical Shifts of E-2-(X-Benzylidene)-1-Tetralones, and-Benzosuberones. Comparison with the 13C NMR Data of Chalcones and E-2-(X-Benzylidene)-1-Indanones. *J. Mol. Struct.* **2005**, *740*, 81–89.
92. Allen, C.; Humphlett, W. The Thermal Reversibility of the Michael Reaction: V. The Effect of the Structure of Certain Thiol Adducts on Cleavage. *Can. J. Chem.* **1966**, *44*, 2315–2321.
93. d'Oliveira, G.D.; Custodio, J.M.; Moura, A.F.; Napolitano, H.B.; Pérez, C.N.; Moraes, M.O.; Prókai, L.; Perjési, P. Different Reactivity to Glutathione but Similar Tumor Cell Toxicity of Chalcones and Their Quinolinone Analogues. *Med. Chem. Res.* **2019**, *28*, 1448–1460.
94. Kenari, F.; Perjési, P. Study on Interaction of Reduced Glutathione (GSH) with Cyclic Chalcone Anaglogues.; [s.n.], Ed.; Pécsi Tudományegyetem Általános Orvostudományi Kar: Pécs, 2018; p. [36]-[36].
95. Bernardes, A.; D'Oliveira, G.D.; Silezin, A.; Kuzma, M.; Molnár, S.; Noda Pérez, C.; Perjési, P. Reagent-induced Asymmetric Induction in Addition Reaction of Reduced Glutathione onto Bis-Mannich Chalcones. *Arch. Pharm. (Weinheim)* **2018**, *351*, 1700386.
96. Armstrong, R.N. Glutathione S-Transferases: Reaction Mechanism, Structure, and Function. *Chem. Res. Toxicol.* **1991**, *4*, 131–140, doi:10.1021/tx00020a001.

97. LoPachin, R.M.; Gavin, T.; DeCaprio, A.; Barber, D.S. Application of the Hard and Soft, Acids and Bases (HSAB) Theory to Toxicant–Target Interactions. *Chem. Res. Toxicol.* **2012**, *25*, 239–251, doi:10.1021/tx2003257.
98. Boase, S.; Miners, J.O. In Vitro–in Vivo Correlations for Drugs Eliminated by Glucuronidation: Investigations with the Model Substrate Zidovudine. *Br. J. Clin. Pharmacol.* **2002**, *54*, 493–503.
99. Yan, Z.; Caldwell, G.W. Metabolic Assessment in Liver Microsomes by Co-Activating Cytochrome P450s and UDP-Glycosyltransferases. *Eur. J. Drug Metab. Pharmacokinet.* **2003**, *28*, 223–232, doi:10.1007/BF03190489.
100. Rozmer, Z.; Perjési, P.; Takács-Novák, K. Use of RP-TLC for Determination of Log *P* of Isomeric Chalcones and Cyclic Chalcone Analogues. *J. Planar Chromatogr. – Mod. TLC* **2006**, *19*, 124–128, doi:10.1556/JPC.19.2006.2.7.
101. Morgenstern, R.; Guthenberg, C.; Mannervik, B.; DePierre, J.W. The Amount and Nature of Glutathione Transferases in Rat Liver Microsomes Determined by Immunochemical Methods. *FEBS Lett.* **1983**, *160*, 264–268.
102. Guzy, J.; Vašková-Kubálková, J.; Rozmer, Z.; Fodor, K.; Mareková, M.; Poškrobová, M.; Perjési, P. Activation of Oxidative Stress Response by Hydroxyl Substituted Chalcones and Cyclic Chalcone Analogues in Mitochondria. *FEBS Lett.* **2010**, *584*, 567–570, doi:10.1016/j.febslet.2009.11.098.

9. Acknowledgements

First and and foremost, I am immensely grateful to my supervisor Prof. Dr. Pál Perjési for his exceptional mentorship and support. His insightful feedback was instrumental in shaping this thesis and enriching my understanding of the subject matter.

I would like to extend my appreciation to Dr. Zsuzsanna Rozmer head of the institute of Pharmaceutical Chemistry and my colleagues who have accompanied me on this academic journey.

To Patrick , my beloved husband, for his understanding, patience, and unconditional support.

To my parents, Dr. Leyla Fallahkohan and Alireza Kenari, your unwavering belief in my abilities has motivated me to push beyond my limits and strive for the best.

COPIES OF PUBLICATIONS

1. Perjési, P.; Caridad, N.P.; Aline, B.; Giulio, D. d'Oliveira; Kenari, F. The Chemistry of GST-Catalyzed Reactions. In *Glutathione: Biosynthesis, Functions and Biological Implications*; Perjési, P., Ed.; Nova Science Publishers: Hauppauge, New York, **2019**; pp. 373–403. ISBN 978-1-5361-4740-7.

2. Kenari, F.; Molnár, S.; Perjési, P. Reaction of Chalcones with Cellular Thiols. The Effect of the 4-Substitution of Chalcones and Protonation State of the Thiols on the Addition Process. Diastereoselective Thiol Addition. *Molecules* **2021**, 26, 4332. doi:10.3390/molecules26144332.

3. Kenari, F.; Molnár, S.; Pintér, Z.; Bitaraf, S.; Perjési, P. (*E*)-2-Benzylidenecyclanones: Part XVII. An LC-MS Study of Microsomal Transformation Reactions of (*E*)-2-[(4'-Methoxyphenyl) Methylene]-Benzosuberon-1-One: A Cyclic Chalcone Analog. *J. Pharm. Biopharm. Res*. **2023**, 4, 326–339, doi:10.25082/JPBR.2022.02.004.

4. Kenari, F.; Molnár, S.; Borges, I.D.; Napolitano, H.B.; Perjési, P. (*E*)-2-Benzylidenecyclanones: Part XVIII Study the Possible Link between Glutathione Reactivity and Cancer Cell Cytotoxic Effects of Some Cyclic Chalcone Analogs A Comparison of the Reactivity of the Open-Chain and the Seven-Membered Homologs. *Int. J. Mol. Sci.* **2023**, *24*, 8557. https://doi.org/10.3390/ijms24108557.

Chapter 12

THE CHEMISTRY OF GST-CATALYZED REACTIONS

***Pál Perjési*[*1], *Caridad Noda Perez*[1,2], *Aline Bernardes*[1,2], *Giulio D. d'Oliveira*[1,2], *Fatemeh Kenari*[1]**

[1]Institute of Pharmaceutical Chemistry, University of Pécs, Pécs, Hungary,
[2]Instituto de Química, Universidade Federal de Goiás, Goiânia, Goiás, Brasil.

ABSTRACT

Non-endogenous substances (xenobiotics) that enter living organisms can undergo chemical transformations (biotransformation). As a result, new chemical entities are formed in different organs, tissues and cell compartments of the bodies. The reactions are principally divided into Phase I and Phase II transformations. In Phase I reactions, the parent compounds are structurally modified mainly by oxidation, reduction and hydrolysis. Phase II reactions include conjugation of the parent compounds or their transformed derivatives with glucuronic acid, sulfate, glycine or glutathione, among others. This chapter summarizes the catalytic functions of the soluble glutathione transferase (GST) enzymes and gives examples for the mechanism and stereochemistry of the GST-catalyzed transformations of the most frequently occurring types of endogenous and exogenous substrates (alkyl-aryl-halides, epoxides, α,β-unsaturated carbonyls and quinones). The selected examples play important role either in determination of GST activities or biological action of the substrates.

Keywords: Glutathione, Glutathione transferase (GST), Phase II biotransformation, Glutathione conjugation, acrolein (ACR), ethacrynic acid (ETK), 4-hydroxynonenal (HNE), chalcone

* Corresponding Author address
Email: pal.perjesi@gytk.pte.hu

INTRODUCTION

Non-endogenous substances (xenobiotics) that enter living organisms can undergo chemical transformations (biotransformation). As a result, new chemical entities are formed in different organs, tissues and cell compartments of the bodies. The history of such research is dated back to 1841, when Alexander Ure reported on conversion of benzoic acid to hippuric acid in the body [1]. The chemistry of the transformation was later confirmed by Wilheim Keller [2]. Since then several different biotransformation pathways of xenobiotics have been identified. They are principally divided into Phase I and Phase II transformations, after Richard Tecwyn Williams [3,4]. In Phase I reactions, the parent compounds are structurally modified mainly by oxidation, reduction and hydrolysis. The most common functional groups exposed or introduced in the Phase I reactions are the hydroxyl (-OH), amino (-NH-), and the carboxyl (-COOH) groups. Phase II reactions include conjugation of the parent compounds or their transformed derivatives with glucuronic acid, sulfate, glycine or glutathione, among others. Acetylation and methylation are also examples of Phase II transformations [5].

Formation of N-acetylcysteine conjugates of halogen-substituted benzene derivatives was discovered in 1879 [6-8]. However, the complete metabolic sequence leading to formation of N-acetylcysteine conjugates (mercapturic acids) remained unknown for over 80 years. The first publication demonstrating link between reaction of halogen substituted benzenes with glutathione and mercapturic acid formation of the studied aromatics was described by a team lead by Sibyl James and H. G. Bray [9-11]. In 1961, Booth *et al*. described the direct enzymatic formation of glutathione conjugates in the cytosol of liver and other organs [12]. This observation lead to the work of Chasseaud and Boyland demonstrating the existence of distinct classes of glutathione transferases [13].

Glutathione transferases (GSTs) (EC 2.5.1.18) are represented by a superfamily of isoenzymes catalyzing conjugation of glutathione (GSH; γ-Glu-Cys-Gly) with a wide range of nonpolar compounds of exogenous and endogenous origin containing electrophilic atoms of carbon, sulfur, nitrogen, or phosphorous, which assists in defense of the cell against possible toxic action of these compounds. In addition to conjugation reactions, a number of GST isoforms can catalyze GSH-dependent reduction of organic hydroperoxides and isomerization of various unsaturated compounds [13]. These enzymes also have some non-catalytic functions that relate to the sequestering of carcinogens, intracellular transport of a

wide spectrum of hydrophobic ligands, and modulation of signal transduction pathways [14]

GSTs are found in all major eukaryotic taxa including fungi, plant and animals. In any given organism multiple GST isoforms are expressed. In mammals, GST is present in virtually all organs and tissues, but the highest enzyme activity is found in the liver. Mammalian GST superfamily includes three subfamilies of isoenzymes: the cytosolic GST, the mitochondrial GST, and the microsomal MAPEG [15].

The cytosolic GSTs are the most numerous and most extensively studied. Historically, these enzymes have been first identified in mammalian tissues [13]. Mammalian cytosolic GSTs are dimeric proteins, which -based on the amino acid sequence homology- are grouped into seven classes, designated Alpha (α), Mu (μ), Pi (π), Sigma (σ) Theta (θ), Zeta (ζ), and Omega (ω), and comprise 17 isoenzymes [15-17]. The mitochondrial (Kappa-class) GSTs, reported to be also present in peroxisomes, are soluble enzymes integrated into the mitochondrial matrix [18,19]. The soluble GSTs appeared to be involved primarily in the metabolism of electrophilic foreign chemicals (xenobiotics) as well as in detoxication of endogenously derived electrophilic metabolites [20]. Microsomal GSTs are trimeric integral membrane proteins that are now called membrane-associated proteins in eicosanoid and glutathione metabolism (MAPEG) [21]. Likewise, the cytosolic and mitochondrial (soluble) GST isoenzymes, the microsomal isoenzymes can also catalyze conjugation of GSH with electrophilic compounds, but they principally participate in isomerization of unsaturated compounds and biosynthesis of leukotrienes and prostaglandins [20].

The soluble GSTs exist as dimeric proteins, with an approximate molecular weight of 25 000 dalton for each. Each of the subunits possesses a GSH binding site (G-site) and an adjacent relatively hydrophobic binding site (H-site) for the substrate. In addition, in various isoenzymes (particularly in the Alfa-, Mu- and the Pi-class) a non-substrate binding site has been recognized. This has been described as a transport site for large hydrophobic molecules. Among the non-catalytic ligands of GSTs are steroids, bile acids, heme, bilirubin, and a variety of organic dyes, drugs and other xenobiotics. [22].

Usually the dimers are made from identical chains but heterodimers made of two different chains from the same class are also found.[23]. The standardized GST nomenclature identifies the species with a lower-case initial (hGSTP1-2, for human), the class by a capital following GST (hGSTP1-2, for Pi), followed by an Arabic numeral representing the subfamily of both subunits (hGSTP1-2, for a heterodimer in the Pi-class subfamily 1 and 2) [24].

This chapter summarizes the catalytic functions of the soluble GST enzymes and gives examples for the mechanism and stereochemistry of the GST-catalyzed transformations of the most frequently occurring types of substrates (alkyl-aryl-halides, epoxides, α,β-unsaturated carbonyls and quinones). The selected examples play important role either in determination of GST activities, or biological action of the substrates.

FUNCTIONS OF GLUTATHIONE TRANSFERASES

Glutathione transferases possess three main functions in the living organisms: (a) catalytic activities, (b) binding of non-substrate ligands, and (c) involvement in protein-protein interactions [25]. In this chapter only the catalytic functions of the GST enzymes are discussed.

One of the main catalytic functions of soluble GSTs is *participation in the cellular antioxidant system* [26]. They demonstrate activity toward a number of by-products of oxidative stress, including lipid- and DNA-hydroperoxides as well as the secondary peroxidation products such as acrolein (propenal) and 4-hydroxynonenal (HNE) [17,22,27]. The reactive peroxidation products (e.g., hydroperoxides of unsaturated fatty acids) are converted to less toxic alcohols *via* their GST-catalyzed reactions with reduced glutathione (GSH). The reduction is a two-step reaction. The first step (1) is an enzymic reduction of the peroxide to the corresponding alcohol, with the concomitant formation of sulfenic acid derivative of glutathione (GSOH). The second step (2) is a spontaneous process in which the formed GSOH reacts with a molecule of GSH to form oxidized glutathione (GSSG) and water [28].

$$\text{R-OOH} + \text{GSH} = \text{R-OH} + \text{GSOH} \quad (1)$$

$$\text{GSOH} + \text{GSH} = \text{GSSG} + \text{H}_2\text{O} \quad (2)$$

The reactive α,β-unsaturated aldehydes react with GSH in a Michael-type addition reaction to result in formation of the respective GSH-conjugates [15]. Furthermore, oxidation of catecholamines results in formation of quinoidal compounds that are substrates of GST isoforms [29].

Another well-known function of GSTs is *isomerization of biologically important endogen molecules*. The enzymes can catalyze *cis-trans* isomerization reactions or *movement of a double bond* within a polycyclic molecule [22,30].

Most notable in this regard is conversion of GSH-dependent conversion of Δ^5-3-ketosteroids (e.g., androst-5-en-3,17-dione) to a Δ^4-3-ketosteroid (androst-4-ene-3,17-dione) catalyzed by hGSTA3-3, which is involved in biosynthesis of steroid hormones such as testosterone and progesterone. Figure 1. shows the mechanism of the reaction, in which proton (H_β) transfer from carbon-4 of the steroid to the enzyme (Tyr-9) bound, deprotonated GSH (GS^-) represents the initial step. It is followed by relocation of the negative charge on carbon-6 and protonation of the rearranged anion by the GSH-bound Tyr-9 of the enzyme. These latter two steps might either occur concerted or sequential [30-33].

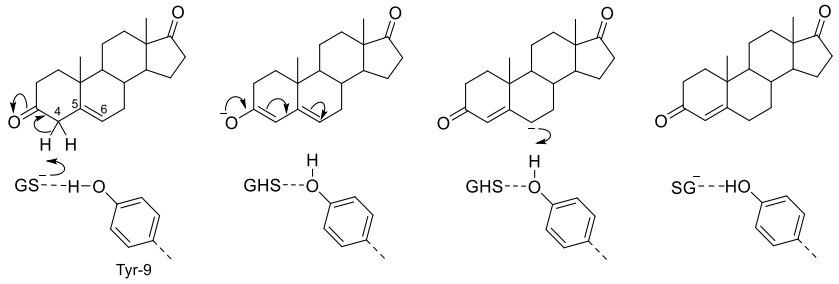

Figure 1. Mechanism of hGSTA3-3-catalyzed isomerization of Δ^5-3-ketosteroids. Based on reference [31].

A further example of the GST-catalyzed physiological isomerization reactions is the conversion of 13-*cis*-retinoic acid to all-*trans* retinoic acid, a reaction that increase the affinity of the retinoid to its receptor [34]. Another distinct, physiologically important isomerization is the conversion of maleylacetoacetate to fumarylacetoacetate catalyzed by GSTZ1-1 which is part of catabolism of phenylalanine and tyrosine [35]. The reaction mechanism is proposed to involve transient addition of GSH to the substrate followed by rotation around the formed single bond and elimination of GSH (Figure 2) [36].

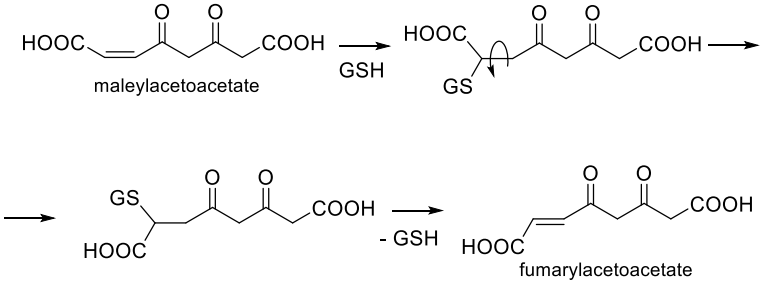

Figure 2. Proposed mechanism of GSH-dependent isomerization of maleylacetoacetate to fumarylacetoacetate. Based on reference [36].

GST-catalyzed isomerization is also involved in biosynthesis of prostaglandins and leukotrienes. The first step of the biosynthesis is the prostaglandin endoperoxide synthase (PGHS)-catalyzed conversion of arachidonic acid to the common prostaglandin precursor prostaglandin H_2 (PGH_2). Prostaglandin endoperoxide synthase has two isoforms, PGHS-1 and PGHS-2. The enzymes have two catalytic activities: cyclooxygenase and hydroperoxidase. The two isoforms are frequently referred to as COX-1 and COX-2 [37]. PGH_2 can be converted to a number of products, among them to PGE_2 or to PGD_2 by intramolecular redox reactions (Figure 3).

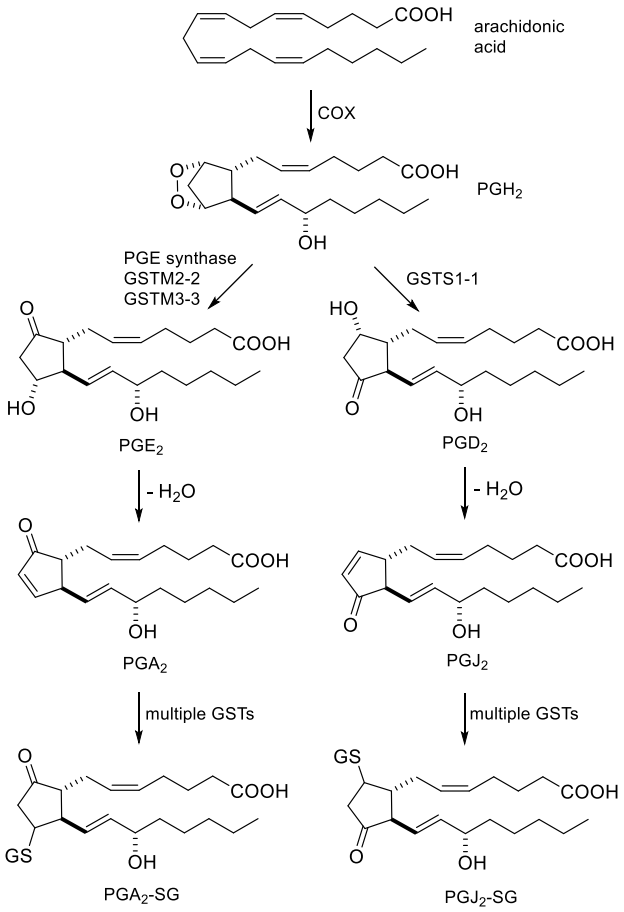

Figure 3. Conversion of PGH_2 to PGE_2, PGD_2, PGA_2 and PGJ_2 by GST enzymes.

Conversion of PGH_2 to PGD_2 is catalyzed by a Sigma class GST (GSTS1-1), which is a versatile repertoire of species-specific conjugase and reductase activities [38]. The H-site of GSTS1-1 is extended, resulting in a unique deep cleft where the prostaglandin was suggested to bind with its peroxide group pointing at the thiolate of GSH [39]. Several mechanisms of the reaction are taking into considerations [28]. The reaction of PGH_2 yielding PGE_2 is catalyzed by the by the MPEG enzyme PGE synthase (PTGES1) [40] or the soluble GSTM-2-2 and GSTM3-3 [41].

The third type of catalytic activities of glutathione transferases is *conjugation of reduced glutathione (GSH) with endogenous or exogenous electrophilic species* involving the reactive thiol group of its cysteinyl moiety. Four groups of proteins are able to catalyze this characteristic reaction of glutathione transferases: (a) canonical soluble (cytosolic) GSTs, (b) distantly related soluble (mitochondrial) Kappa-class GSTs, (c) hydrophobic (microsomal) MAPEG family GSTs and (d) bacterial fosfomycin resistance proteins [42-46]. The sequence similarities of the six mammalian MAPEG classes are quite low [47]. Nevertheless, all MAPEG show a similar trimeric structure with four transmembrane helices for each subunit [28]. Mammalian MAPEG can be roughly subdivided into the MGST1/PTGES1 group and the MGST2/MGST3/LTC4/FLAP group [48,49]. Among all families of GSH-dependent enzymes, GST and MAPEG are the most versatile catalysts converting a wide range of sulfur-, oxygen-, or carbon-containing electrophilic substances.

The catalytic events of GST's can be divided into two processes: (1) binding and activation of GSH, and (2) binding the electrophilic reaction partner. The first process is common in all soluble GSTs, while the second depends on the chemical nature and structure of the electrophile. It is worth mentioning that the former name "glutathione S-transferase" is misleading because the glutathionyl moiety (not a sulfur atom) is transferred [50].

BINDING AND ACTIVATION OF GSH

Cytosolic GSTs have been most extensively studied in human, rat and mouse tissues where they are the most abundant. The Pi-class enzyme is the most widely distributed isoenzyme and usually the most abundant [51]. The cytosolic enzymes have two active sites per dimer which behave independently of one another [52]. Each active site consists of at least two ligand binding regions: the GSH binding site, which is very specific for GSH, and the substrate binding site, which is less specific. The consequence of this latter characteristics is the ability of GSTs to react with a wide variety of agents.

The detailed understanding of the enzymatic mechanism needs a knowledge of the three-dimensional structure of each GST isoenzyme. There have been several comprehensive reviews on three-dimensional structure investigations of which results are not discussed here in details. Interested readers are directed towards these reviews which cover the structural, biochemical and genetic aspects of the field [53-55].

Glutathione (GSH) has three acidic (thiol, glycinyl carboxyl, glutamyl carboxyl) and one basic (amino) functional groups (Figure 4). The macroscopic protonation constants (K_1-K_4) were determined by several authors Each publication reported the pK_a of the sulfhydryl group of GSH in aqueous solution to be around pK_a 9.2. [56-59]. Accordingly, it is only a rather small percent of the GSH molecules exist in S-deprotonated form at physiological pH. It has been proved, however, that the pK_a of GSH bound to most GSTs is less than 7 [60]. Therefore, the enzyme-bound GSH is largely deprotonated at physiological pH – thus being activated for reaction with electrophilic substrates.

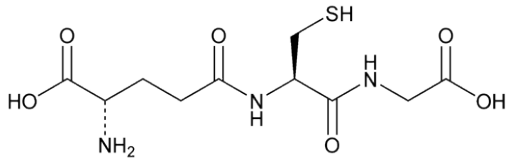

Figure 4. Structure of reduced glutathione (GSH).

The enzyme-bound thiolate of glutathione (GS^-) is stabilized by a hydrogen bond between the proton of a hydroxyl group in the protein and the sulfur atom of the thiolate [61,62]. In most GSTs the hydrogen-bond donor is the hydroxyl group of a tyrosine residue close to the N-terminal of the protein: Tyr-7 in the Pi-class GST [63], Tyr-6 in the Mu-class GST [64] and Tyr-9 in the Alfa-class GST [65]. In Alfa-class GSTs, a secondary interaction of the ε-nitrogen atom of Arg-15 with the sulfur of GSH additionally helps to stabilize the thiolate [66]. Figure 5. shows schematic drawing of residues that interact with glutathione in the GSH binding site of Alfa-class GST.

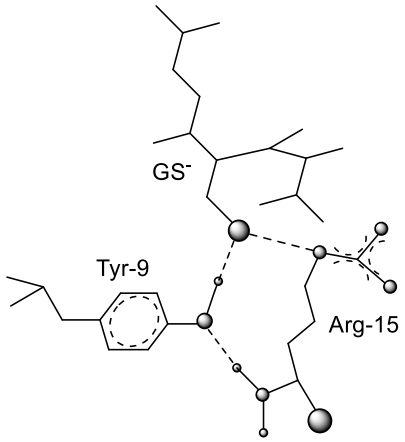

Figure 5. Schematic drawing of residues that interact with glutathione in the GSH binding site of Alfa-class GST. Based on reference [66].

In contrast to binding and activation of GSH (at the G-site), which are not identical but show high degree of similarity [63-66], a variety of chemical and structurally diverse electrophilic substrates can bind to the electrophile binding site (H-site) of the GST enzymes. The H-site cavities of the Mu- and Alfa-class GSTs are generally hydrophobic, while those of the Pi-class enzymes are lined with both hydrophobic and hydrophilic surfaces [67].

CONJUGATION OF GSH WITH ENDOGENOUS ELECTROPHILES

GST-catalyzed reactions involve reactions of electrophilic oxidized products of endogenous substances (e.g., lipids, nucleic acids, neurotransmitters) with GSH. These reactive electrophiles can chemically modify the primary structure of cellular macromolecules (e.g., lipids, nucleic acid), being potentially toxic metabolites. One of the most investigated toxic lipid peroxidation products is 4-hydroxynonenal (HNE) (Figure 6). It is a reactive α,β-unsaturated aldehyde formed during oxidative degradation of unsaturated fatty acids [68,69,70]. Reactive α,β-unsaturated carbonyl compounds are suspected to play role in mutagenesis and carcinogenesis [71]. HNE can modulate a number of signaling processes mainly through forming covalent adducts with nucleophilic functional groups in proteins, nucleic acids, and membrane lipids. These properties have been extensively summarized in some excellent reviews [72-78].

There are three major detoxification pathways to convert HNE to less reactive chemical species and control their steady-state intracellular concentrations. Firstly, the main catabolic reactions are the formation of adducts with glutathione (GSH), which occurs spontaneously or can be catalyzed by glutathione-S-transferases (GSTs). Secondly, HNE can be reduced to 1,4-dihydroxy-2-nonene (DHN) by aldo-keto reductases (AKRs) or alcohol dehydrogenases (ADH). Thirdly, HNE can be oxidized to 4-hydroxy-2-nonenoic acid (HNA) by aldehyde dehydrogenase (ALDH) [79].

trans-4-Hydroxynon-2-enal (HNE), as an α,β-carbonyl compound, possesses electrophilic beta-carbon atom due to the polar carbonyl group conjugated with the carbon-carbon double bond (Figure 6). Considering this type of electron polarizability, HNE is considered to be a soft electrophile which preferentially forms 1,4-Michael type adduct with soft nucleophiles. Cysteine sulfhydryl groups are the primary soft nucleophilic targets of HNE while lysine and histidine residues are harder biological nucleophiles [79]. Figure 6. shows reaction of HNE with GSH.

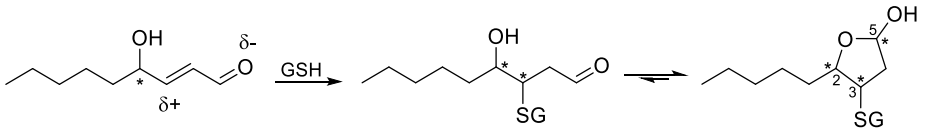

Figure 6. GST-catalyzed conjugate addition of GSH onto 4-HNE followed by cyclic hemiacetal formation.

HNE has a chirality at carbon-4. Although HNE is formed in tissues as racemate, enantiospecific HNE effects have not been widely investigated. Wakita *et al* [80] investigated the stereochemistry of cysteine adduct of HNE. Because HNE generated in lipid peroxidation is a racemic mixture of 4*R*- and 4*S*-enantiomers, the HNE Michael adducts, possessing three chiral centers at C-2, C-3, and C-5 in the tetrahydrofuran moiety (Figure 6), are composed of at least eight isomers. It was found that the open-chain adduct form an equilibrium mixture of the anomeric cyclic hemiacetal diastereomers [80].

The reaction is catalyzed by specialized isoforms of GSTs exemplified by the murine mGSTA4-4 [81,82] and the human hGSTA4-4 [83]. These enzymes are catalyzing the conjugation of HE with very high catalytic efficiency, exceeding 106 $M^{-1}s^{-1}$, which is among the highest catalytic efficiencies of any GST with any substrate. The possible reasons of the significantly high catalytic efficiencies are discussed in detail [22].

Another type of endogenous oxidized metabolites with electrophilic character are 1,2- and 1,4-benzoquinone derivatives, which can be formed by oxidation of *o*- and *p*-dihydroxybenzenes and their substituted derivatives. Quinones represent a class of biotransformation products which can create a variety of hazardous effects *in vivo*, including acute cytotoxicity, immunotoxicity, and carcinogenesis. The mechanisms by which quinones cause these effects can be quite complex [84]. Quinones are Michael acceptors, and cellular damage can occur through alkylation by quinones of crucial cellular proteins and/or DNA. Alternatively, quinones are highly redox active molecules which can redox cycle with their semiquinone radicals, leading to formation of reactive oxygen species (ROS) [84,85].

One of the well-known examples of formation of endogenous quinones is dopamine-*o*-quinone, which is suspected to be involved in development of oxidative stress-initiated neurodegenerative diseases, such as Parkinson-disease [86].

Dopamine oxidation seems to be a complex pathway in which dopamine *o*-quinone, aminochrome and 5,6-indolequinone are formed. Dopamine oxidation to dopamine *o*-quinone, aminochrome and 5,6-indolequinone seems to play an important role in the neurodegenerative processes of Parkinson's disease as aminochrome induces: (i) mitochondria dysfunction, (ii) formation and stabilization of neurotoxic protofibrils of alpha synuclein, (iii) protein degradation dysfunction of both proteasomal and lysosomal systems and (iv) oxidative stress [87].

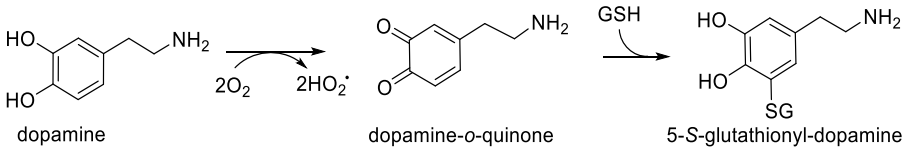

Figure 7. GST-catalyzed reaction of dopamine-*o*-quinone with GSH.

Dopamine-*o*-quinone is the precursor of formation of aminochrome and 5,6-indolequinone [83,87]. Quinones, similar to α,β-unsaturated aldehydes and ketones, are soft nucleophiles, having preference to react with the soft nucleophilic thiol compounds. One of the possible protective mechanisms of preventing dopamine-induced neurotoxicity is reaction of the unstable (reactive) dopamine-*o*-quinone with GSH. Dopamine-*o*-quinone can react with GSH catalyzed by GSTM2-2 (Figure 7) [87]. Conjugation reactions of GSH with quinones are additional examples of Michael additions. In these reactions glutathionyl

hydroquinone derivatives are formed, which may be regarded as a reduced quinone. GSH conjugation of *o*-quinones prevents redox cycling as well and can be considered as important cytoprotective mechanism [88,89].

Apart from conjugation reactions with electrophilic metabolites of xenobiotics to protect the cells, there are some GSH-conjugates that are formed in different tissues and play important role in biosynthesis of regulatory biomolecules or have such a function themselves. In this respect, role of GSTs in metabolism of eicosanoids is remarkable [89].

As shown on Figure 3, the common precursor PGH_2 can be isomerized to PGE_2 and PGD_2. The isomerizations are GST-catalyzed processes which are catalyzed by different soluble GST isoforms. PGE_2 and PGD_2 can be transformed to the dehydration product prostaglandin A_2 (PGA_2) and prostaglandin J_2 (PGJ_2), respectively. Both PGA_2 and PGJ_2 – being α,β-unsaturated ketones - form GSH-conjugate, which reaction plays important roles in their biological activities [90,91].

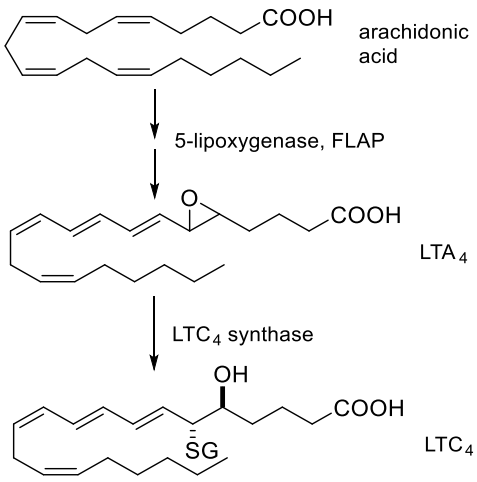

Figure 8. Formation of LTA_4 from arachidonic acid and conversion of LTA_4 to LTC4.

GST enzymes are also involved in biosynthesis of leukotrienes. Leukotrienes are also derived from arachidonic acid, abundant in biological membranes (Figure 8). The releases arachidonic acid can be converted to the unstable epoxide leukotriene A_4 (LTA_4) by 5-lipoxygenase and the 5-lipoxygenase-activating protein (FLAP). One of the possible transformations of LTA_4 is stereoselective conjugation with GSH catalyzed by the membrane-bound enzyme LTC_4 synthase (Figure 8). LTC_4 synthase differs from conventional glutathione *S*-transferase (GST) by its

selectivity for LTA_4 and its analogs, microsomal localization, and failure to conjugate xenobiotics [92,93].

Hepoxilins are biologically active epoxy alcohols formed from arachidonic acid by 12-lipoxygenase-catalyzed hydroperoxidation and subsequent molecular rearrangement (Figure 9). The rearrangement is catalyzed by the ferric ion protoporphyrin subunit, which is present in hematin, hemoglobin and other hemeproteins. There are two positional isomeric hepoxilins, Hepoxilin A_3 (8-hydroxy-11,12-epoxyeicosa-(5*Z*,9*E*,14*Z*)-trienoic acid) and Hepoxilin B_3 (hydroxyl at C10) [94,95]. The epoxide function of hepoxilins is subject to reaction with epoxide hydrolase or GST. It is worth mentioning that the GSH-conjugation occurred at C-11 rather than the allylic C-9 position [96].

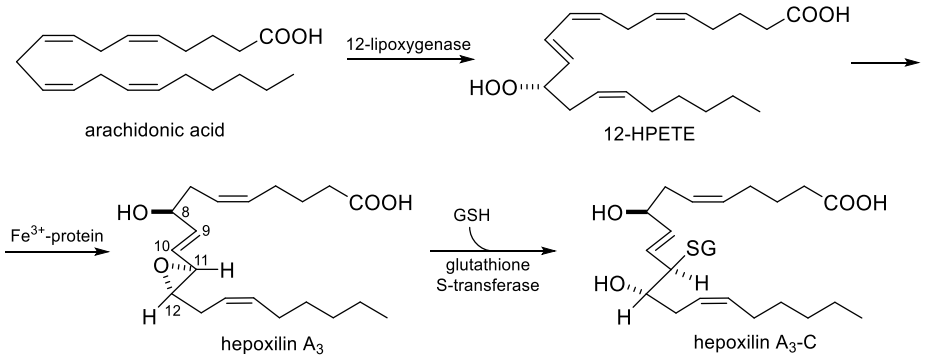

Figure 9. Formation of Hepoxilin A3 from arachidonic acid and conjugation of Hepoxilin A3 with GSH to form Hepoxilin A3-C.

CONJUGATION OF GSH WITH EXOGENEOUS ELECTROPHILES

Reaction with GSH of electrophilic species of exogeneous origin (xenobiotics) is referred to as an example of Phase II biotransformations. In these reactions the electrophilic substrates (typically metabolites of the parent compound) react with GSH in a spontaneous or GST-catalyzed reaction to form GSH-conjugates in nucleophilic substitution or addition reactions. The products undergo further metabolic transformations to form either N-acetylcysteine (mercapturate) or thioalcohol (SH) derivatives [97]. It is the mercapturic acid (mercapturate) derivative that is typically the final metabolite, which is eliminated from the body in the urine. In general, glutathione conjugation is regarded as detoxication reaction.

However, depending of the chemical nature of the substrate, the pathways can generate reactive intermediates [98,99].

From mechanistic aspects, conjugation reactions of GSH with xenobiotics can be classified into two major categories: (a) substitution, and (b) addition reactions. The most important structures involved in nucleophilic substitution reactions are (a) aromatic electrophiles, (b) aliphatic electrophiles, and (c) oxidative electrophiles Those involved in addition reactions are (a) epoxides, (b) alkenes, (c) quinones and (d) organic isothiocyanates [[97].

Nucleophilic substitution reactions

Aromatic substitution

Nucleophilic substitution is the reaction of an electron pair donor (the nucleophile, :Nu) with an electron pair acceptor (the electrophile). There are four principal mechanisms of nucleophilic aromatic substitution reactions: (a) S_NAr mechanism; (b) S_N1 mechanism, (c) benzyne mechanism, and (d) $S_{RN}1$ mechanism [100,101]. In the case of GST catalyzed reactions, only the S_NAr mechanism can operate. In these reactions, an electron withdrawing group on the aromatic nucleus makes the system susceptible to nucleophilic attack. The mechanism is similar to that of the electrophilic aromatic substitution except that an anion rather than a cation intermediate is involved. The nucleophile adds to the aromatic ring to afford a delocalized anion from which the leaving group is eliminated.

Physiologically relevant substrates which can undergo S_NAr reaction is rather limited, however, the reaction plays an important role in mechanistic studies of GSTs. A well-investigated example is the reaction between 1-chloro-2,4-dinitrobenzene (CDNB) and GSH (Figure 10).

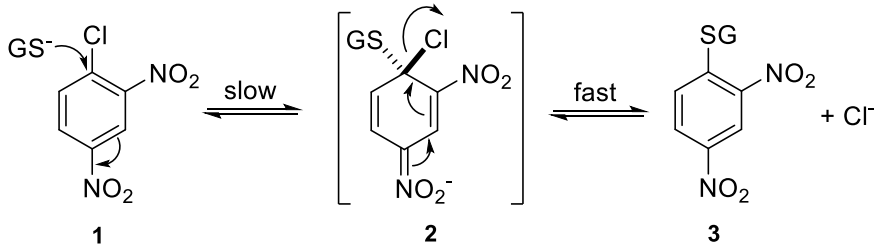

Figure 10. Aromatic substitution (S_NAr) reaction of 1-chloro-2,4-dinitrobenzene (CDNB) and GSH.

CDNB (**1**) reacts readily with deprotonated GSH (GS^-) even in a spontaneous, non-catalyzed reaction [102]. Furthermore, the size of CDNB is small compared with the H-site of most GSTs. For these reasons, CDNB is conjugated by most GSTs and is used in the laboratory as a universal substrate for assaying GSTs [103]. In the first step, reaction of CDNB with GSH results in formation of a Meisenheimer-complex type carbanion intermediate (**2**). In the second step, the leaving group (chloride ion) gets detached leading to regeneration of the aromatic ring (**3**) [22].

Reactions with sp^3-hybridized electrophilic centers

Reactions with non-aromatic substrates with sp^3 hybridized electrophilic centers include, for example, haloalkanes, hydroperoxides and disulfides. [28]. The reactions can, in principle, proceed *via* S_N2 mechanism with a carbon, oxygen or sulfur atom as the electrophilic center. The sp^3-hybridized electrophile must have a leaving group (:X) in order for the reaction to take place. In the case of the S_N2 reactions, the reaction proceeds through a transition state in which the negative charge of the sulfur atom is relocated to the leaving group. For example, when a tetrahedral carbon of an alkyl halide (X=halogen) is attacked, it is forced to adopt a bipyramidal configuration with the approaching sulfur in one apical position and the leaving group in the other (Figure 11). In the case of chiral carbon center, inversion of the configuration (Walden inversion) occurs [104].

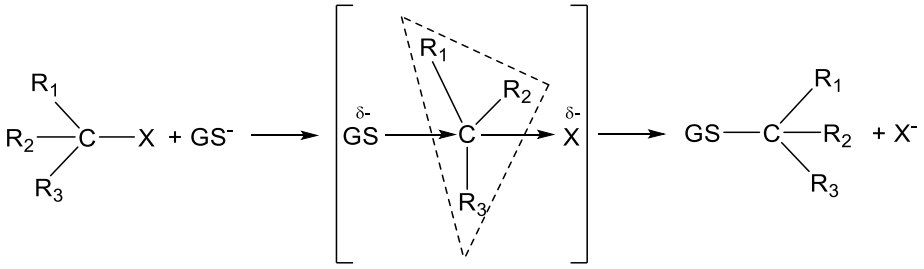

Figure 11. Walden inversion of the sp^3-hyridized carbon atom of an alkyl halide. Based on reference [104].

Haloalkanes and haloalkenes are important industrial chemicals and environmental contaminants. Many of them are toxic and suspected carcinogen. The toxicity of these chemicals is associated with their bioactivation to reactive intermediates by the cytochrome P450s or the GSTs [105]. GSTs, particularly the Theta-class GSTT1-1 catalyze the biotransformation of a range of haloalkanes.

Dichloromethane (**4**) (an important industrial solvent), for example, undergoes GST-dependent biotransformation to formaldehyde [106]. The reaction mechanism involves the GSTT1-catalyzed displacement of chloride from dichloromethane to give S-(chloromethyl)glutathione (**5**). Hydrolysis of the formed conjugate gives S-(hydroxymethyl)glutathione (**6**), which is the hemithioacetal of formaldehyde and glutathione, which is in equilibrium with formaldehyde (**7**) and GSH (Figure 12).

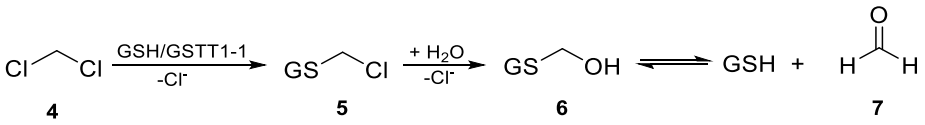

Figure 12. Glutathione transferase-dependent biotransformation of dichloromethane.

1,2-Dihaloalkanes (**8**) are also important group of chemicals. Many of them have been proved to be mutagenic and some of them are rodent carcinogenic. The mutagenic and, perhaps, the carcinogenic effect of these chemicals are associated with their biotransformation to reactive intermediates. Dihaloalkanes (**8**) undergo GST-catalyzed biotransformation to S-(2-haloethyl)glutathione (**9**), which undergo intramolecular cyclization to form thiiranium (episulfonium) ions (**10**). The reactive thiiranium ions thus formed may react with nucleophilic sites in DNA to give the adduct S-[2-N^7-guanyl)ethyl]glutathione (**11**) (Figure 13) [107].

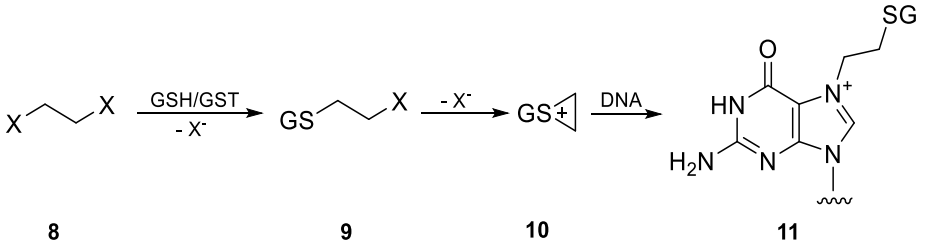

Figure 13. Glutathione-dependent biotransformation of 1,2-dihaloethanes. Reaction of the episulfonium ion metabolite with guanine.

GST-catalyzed reaction of epoxide metabolites of polycyclic aromatic hydrocarbons [108] and aflatoxins [109] represent one of the main detoxification pathways of these reactive Phase I metabolites. Benzo[a]pyrene (BaP) is strongly carcinogenic in certain extrahepatic tissues of rodents such as skin, lung,

forstomach or mammary gland, but only weakly carcinogenic in liver. BaP has to be activated by CYP enzymes in order to become cytotoxic and genotoxic. There is strong evidence that diol-epoxides, primarily the (+)-*anti*-7,8-dihydroxy-9,10-oxy-7,8,9,10-tetrahydrobenzo[a]pyrene (BaPDE) (**12**) (Figure 14) is the ultimate carcinogenic metabolite [108]. Human Alfa-class hGSTP1-1, hGSTA1-1 and hGSTA2-2 are able to conjugate (+)-*anti*-BaPDE with GSH resulting in formation of adduct (**13**) *via* stereoselective *trans* addition (Figure 14). The glutathionyl moiety is selectively linked to the benzyl (C-10) carbon atom. The stereochemistry of the reaction is in accordance with the S_N2 mechanism [110]. The transformation plays a protective role against the carcinogenicity of BaP and other polycyclic hydrocarbons [111].

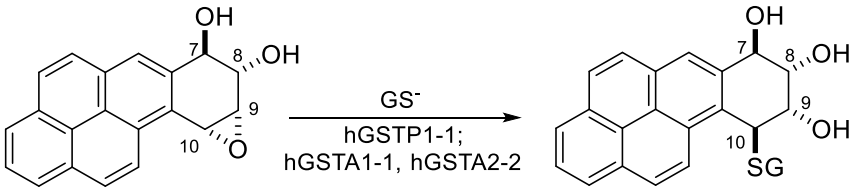

12 **13**

Figure 14. GSTA1-1-catalyzed epoxide ring opening and GSH addition on (+)-*anti*-BaPDE.

Nucleophilic addition reactions

Reaction with N-acetyl-p-benzoquinone-imine (NAPQI)

The title compound, N-acetyl-p-benzoquinone-imine (NAPQI), is a CYP450-catalyzed oxidation product of acetaminophen, the extensively used analgesic (Figure 15). The hepatotoxicity of the compound is a clinically important problem and an exemplary instance how acquired factors (e.g., diet, drugs, diabetes, obesity) can enhance hepatotoxicity [112]. The first cases reporting the association between acetaminophen (paracetamol) overdose and acute liver injury and fatal hepatotoxicity were reported in the 1960s. Acute paracetamol overdose is now the most common cause of acute liver injury and acute liver failure in the UK, US, Canada, Australia, and Scandinavia [113]. Covalent binding of NAPQI to hepatic proteins is a widely accepted mechanism for the hepatotoxicity of this drug [112].

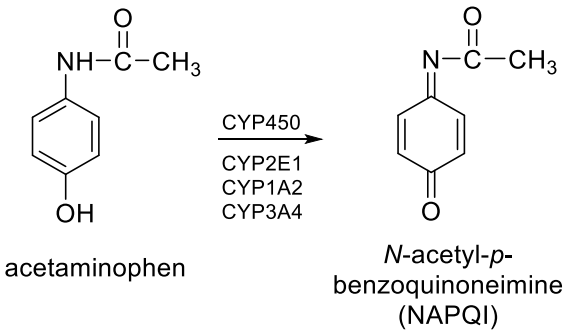

Figure. 15. CYP450-dependent oxidation of acetaminophen (paracetamol).

Once formed within hepatocytes, NAPQI preferentially binds to the cysteine residue of glutathione in a reaction catalyzed by Pi-class glutathione S-transferases [114], resulting in NAPQI-GSH conjugate. The reaction between GSH and NAPQI is a formal addition process in which the oxidized acetaminophen (NAPQI) is reduced to the aromatic GSH-substituted acetaminophen derivative (Figure 16). This conjugate is then metabolized stepwise by γ-glutamyl transpeptidase, dipeptidase, and N-acetylase, cleaving off the γ-glutamyl and glycine residues to ultimately form inert cysteine and mercapturate conjugates that are renally excreted [97].

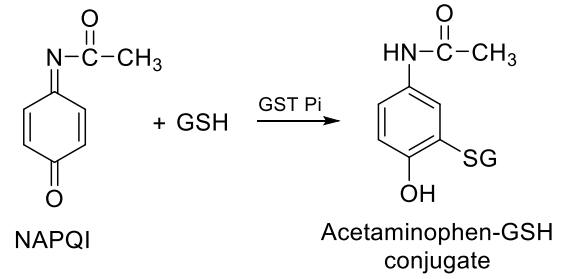

Figure 16. Conjugation of N-acetyl-*p*-benzoquinone-imine (NAPQI) with GSH.

Reaction with acrolein

Acrolein (ACR; propenal) is a ubiquitous environmental pollutant, highly abundant in tobacco smoke, cooking, and automobile exhaust fumes. It is also

generated endogenously by cellular metabolism and lipid peroxidation [115]. Moreover, ACR is also a metabolite of the anticancer drug cyclophosphamide and is believed to be the main cause of its toxicity [116]. ACR is the most reactive electrophile among α, β-unsaturated aldehydes. Its cellular toxicity relies mainly on its ability to deplete glutathione and to form DNA and protein adducts [117]. Formation of ACR-protein covalent adducts is principally due to a Michael addition where the β-carbon of acrolein reacts with nucleophilic sites [117].

The main pathway for elimination of acrolein is conjugation with glutathione (GSH) in the liver, followed by enzymatic cleavage of the γ-glutamic acid and glycine residues, respectively, in the liver and in the kidney [115]. It has been pointed out by Esterbauer and others [118] that acrolein reacts 110-150 times faster with GSH than HNE. While GSH conjugation of acrolein can proceed without catalyst, it is the same enzyme (GSTA-4-4) that mediates formation of the HNE-SG conjugate (Figure 17). Such reactivity was found to be a common metabolic pathway for several different propenal derivatives [119]. Overexpression of GSTA-4-4 in mouse pancreatic islet endothelial cells resulted in increase of cell viability. In addition, the GSTA4-4-transfected cells showed a significantly greater growth rate than the wild-type cells, indicating that acrolein is detoxified by GSTA4-4-mediated conjugation with GSH [120]. Acrolein is also a substrate for GSTA1-1, GSTM1-1, GSTP1-1, and GSTT1 [115].

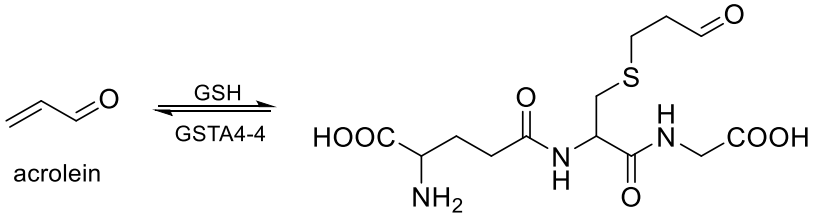

Figure 17. Reaction of acrolein with GSH.

Reaction with ethacrynic acid

Ethacrynic acid (EA) is a widely used diuretic drug, structurally characterized by a presence of an α,β-unsaturated carbonyl moiety reactive towards sulphydryl groups (Figure 18). EA is known to be conjugated to GSH in spontaneous and GST-catalyzed reactions [121]. Both the parent compound (EA) and its GSH-conjugate (EA-SG) are potent inhibitors of GST enzymes. It was shown that EA-SG was an inhibitor of the GSTs due to its greater affinity for the enzymes than that of the

parent molecule [122], whereas EA itself inhibits GSTP through reversible covalent interactions [123]. Because of these properties and because of the ability of EA to deplete cellular GSH, EA is potentially clinically useful as a modulator of drug resistance linked with the GSH/GST system [124].

The conjugation kinetics of glutathione (GSH) and ethacrynic acid (EA) were studied in rat liver perfusion studies. It was found that GSH conjugation of EA occurred spontaneously but at a rate considerably less than that for enzyme-catalyzed GSH conjugation. GSH conjugation of EA accounted almost completely for the total removal of EA because unchanged EA was found minimally in bile [125].

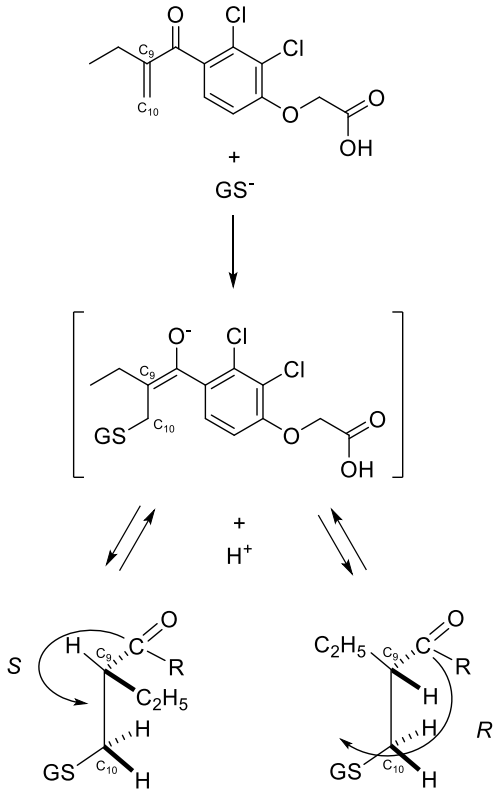

Figure 18. Reaction of ethacrynic acid with GSH.

The stereochemistry of GSH addition to EA catalyzed by GSTA1-1, GSTA1-2 and GSTP1-1 isoformes was studied by van Iersel *et al* [126]. When GSH is added onto the C9-C10 double bond of EA, C-9 becomes an asymmetric carbon atom (Figure 18). Due to the chiral centers, inherent in GSH, formation of the enantiomeric forms of the new chiral center results in formation of two diastereomeric adducts. The authors found that the addition reaction catalyzed by the GSTP1-1 isoform resulted in stereoselective formation of one of the adducts. The observed stereoselectivity was rationalized by enzyme-catalyzed protonation of the enolate intermedier [126].

Reaction with chalcones and chalcone analogues

Hydroxy- and methoxy-substituted chalcones (**14**) are intermediary compounds of biosynthetic pathway of a very large and widespread group of plant constituents known collectively as flavonoids [127]. Among the naturally occurring chalcones and their synthetic analogs, several compounds displayed cytotoxic (cell growth inhibitor) activity towards cultured tumor cells. Chalcones are also effective *in vivo* as cell proliferating inhibitors, anti-tumor promoting, anti-inflammatory and chemopreventive agents [127-130].

Nucleophilic addition of cellular thiols onto the polarized carbon-carbon double bond (Michael-reaction) is frequently associated with the biologic effects of chalcones and related α,β-unsaturated carbonyl compounds [127-130]. Such a reaction can alter intracellular redox status (redox signaling), which can modulate events such as DNA synthesis, enzyme activation, selective gene expression, and regulation of the cell cycle [131]. Several biological effects (e.g., NQO1 inducer [132], anti-inflammatory [133], GST P1-1 inhibitory [134]) of chalcones have been associated with their Michael-type reactivity towards reduced glutathione (Figure 19).

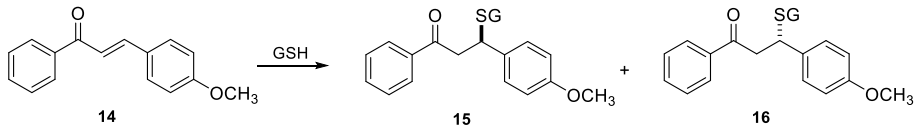

Figure 19. Reaction of 4-methoxychalcone (**14**) with GSH.

Earlier, formation of diastereomeric adducts was observed in the GSTM4-4-catalyzed reactions of GSH and the open-chain chalcone analogue (*E*)-(4'-X-

phenyl)-3-butene-2-ones (Figure 20). In the reactions the more polar adducts were formed in the case of each investigated open-chain chalcone analogues. The observed (diastereo)selectivity (9:1) was presumed to be the result of selective enzyme-catalyzed protonation of the enolate intermediate of the more polar adducts with more extended dispersion of charge in the transition state [135].

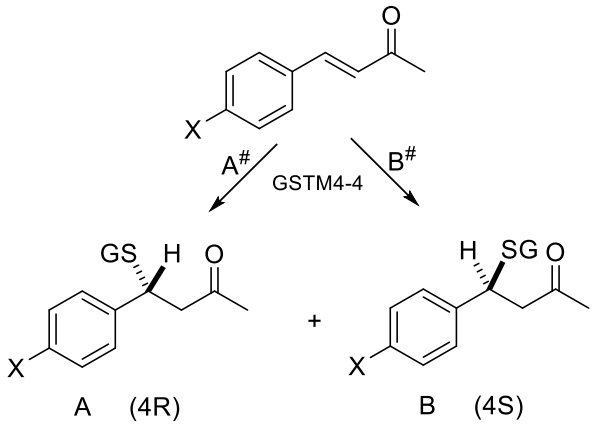

Figure 20. Stereochemistry of GSTM4-catalyzed addition of GSH onto (*E*)-(4'-X-phenyl)-3-butene-2-ones. Based on reference [135].

In our previous work, stereochemistry of non-enzyme-catalyzed addition reaction of the hydroxychalcone (**17**) and its *bis*-Mannich derivative (**18**) was compared at different pH (Figure 21). In the case of (Y) a remarkable diastereoslectivity was observed when the reaction was conducted under acidic conditions. The observed stereoselectivity can be rationalized by ion-pair formation between the protonated Mannich-nitrogens and the deprotonated GSH(glutamate)-carboxylate [136]. Similar selectivity could not be observed when non-Mannich chalcone derivatives have been investigated. The results support importance of non-covalent interactions in developing of the transition states of these addition reactions onto the investigated enones.

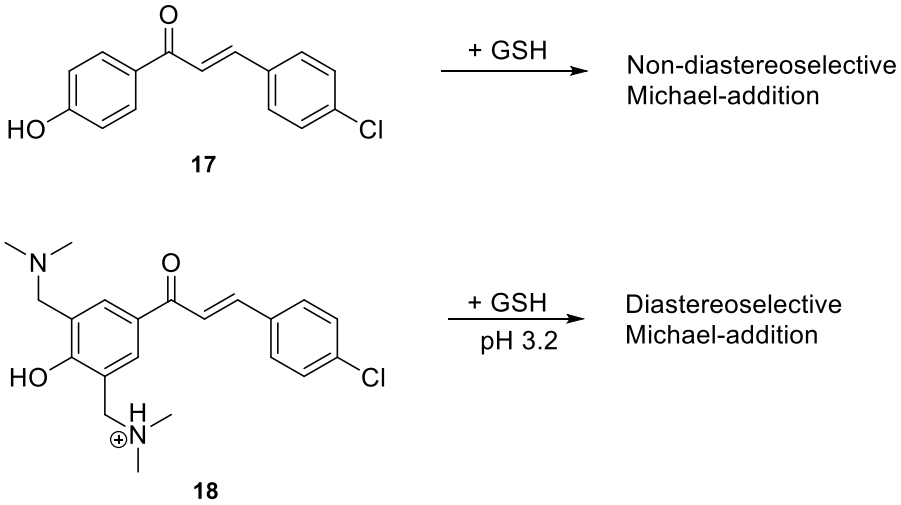

Figure 21. Reaction 4-hydroxychalcone (**17**) and its bis-Mannich derivative (**18**) with GSH. Based on reference [136].

Acknowledgement

The present contribution is dedicated to the 650th anniversary of the foundation of the University of Pécs, Hungary. The authors express their special thanks to Zsuzsanna Erdős-Moravecz for her skilled assistance in preparation of the manuscript.

REFERENCES

[1] Ure, A. On gouty concentrations; with a new method of treatment. Med. Chir. Trans. 1841, 24, 30–35.
[2] Keller, W. Ueber verwandlung der benzoesaure in hippursaure. Ann. 1842, 43, 108-111.
[3] Williams, R. T. Detoxication mechanisms. The metabolism of drugs and allied organic compounds. Chapman and Hall: London, UK, 1947.
[4] Williams, R. T. Detoxication mechanisms. The metabolism and detoxication of drugs, toxic substances, and other organic compounds, 2nd ed. Chapman and Hall: London, UK 1959.
[5] Conti, A.; Bickel, M. H. History of drug metabolism: discovery of the major pathways in the 19th century. Drug Metab. Rev. 1977, 6, 1-50.
[6] Baumann, E.; Preuss, C. Ueber bromophenylmercaptursaure. Ber. Deut. Chem. Ges. 1879, 12, 806-810.
[7] Jaffe, M. Ueber die nach einfuhrung von brombenzol und chlorbenzol im organismus entstehenden schwefelhaltigen sauren. Ber. Deut. Chem. Ges. 1879, 12, 1092-1098.
[8] Baumann, E. Ueber cystin and cysteine. Z. Physiol. Chem. 1884, 8, 299-305.
[9] Barnes, M. M.; James, S. P.; Wood, P. B. The formation of mercapturic acids. 1. Formation of mercapturic acid and the levels of glutathione tissues. Biochem. J. 1959, 71, 680-690.
[10] Bray, H. G.; Franklin, T. J.; James, S. P. The formation of mercapturic acids. 2. The possible role of glutathionase. Biochem. J. 1959, 71, 690-696.
[11] Bray, H. G.; Franklin, T. J.; James, S. P. The formation of mercapturic acids. 3. N-Acetylation of S-substituted cysteines in the rabbit, rat and guinea pig. Biochem. J. 1959, 73, 465-473.
[12] Booth, J.; Boyland, E.; Sims, P. An enzyme from rat liver catalysing conjugations with glutathione. Biochem. J. 1961, 79, 516-524.
[13] Boyland, E.; Chasseaud, L. F. The role of glutathione and glutathione S-transferases in mercapturic acid biosynthesis. Adv. Enzymol. Relat. Areas Mol. Biol. 1969, 32, 173-219.
[14] Listovsky, I.; Arias, I. M. Ligandin and glutathione S-transferases: Historical milestones. In Toxicology of glutathione transferases; Awasthi, Y. C., Ed.; CRC Press: Boca Raton, FL, 2007; pp. 1-9.
[15] Hayes, J. D.; Flanagan, J. U.; Jowsey, J. R. Glutathione transferases. Annu. Rev. Pharmacol. Toxicol. 2005, 45, 51-58.

[16] Testa, B.; Kraemer, S. D. The biochemistry of drug metabolism. – An introduction Part 1. Principles and overview. Chem. Biodivers. 2006, 3, 1053-1101.
[17] Wu, B.; Dong, D. Human cytosolic glutathione transferases: Structure, function, and drug discovery. Trends Pharmacol. Sci. 2012, 33, 656-668.
[18] Gallagher, E. P.; Gardner, J. L.; Barber, D. S. Several glutathione S-transferase isozymes that protect against oxidative injury are expressed in human liver mitochondria. Biochem. Pharmacol. 2006, 71, 1619-1628.
[19] Morel, F.; Aninat, C. The glutathione transferase kappa family. Drug Metab. Rev. 2011, 43, 281-291.
[20] Zimniak, P.; Singh, S. P. Families of glutathione transferases. In Toxicology of glutathione transferases; Awasthi, Y. C., Ed.; CRC Press: Boca Raton, FL, 2007; pp 11-26.
[21] Morgenstern, R.; Zhang, J.; Johansson, K. Microsomal glutathione transferase 1: Mechanism and functional roles. Drug Metab. Rev. 2011, 43, 300-306.
[22] Zimniak, P. Substrates and reaction mechanisms of glutathione transferases. In Toxicology of glutathione transferases; Awasthi, Y. C., Ed.; CRC Press: Boca Raton, FL, 2007; pp. 71-101.
[23] Oakley, A. Glutathione transferases: a structural perspective. Drug. Metab. Rev. 2011, 43, 138-151.
[24] Mannervik, B.; Board, P. G.; Hayes, J. D.; Listowsky, I.; Pearson, W. R. Nomenclature for mammalian soluble glutathione transferases. Methods Enzymol. 2005, 401, 1-8.
[25] Sherratt, P. J.; Hayes, J. D. Glutathion S-transferases. In Enzyme systems that metabolize drugs and other xenobiotics; Ioannides, C., Ed.; Wiley and Sons: Chichester, UK, 2002.
[26] Sharma, R.; Ansari, G. A. S.; Awasthi Y. C. Physiological substrates of glutathione S.transferases. In Toxicology of glutathione transferases; Awasthi, Y. C., Ed.; CRC Press: Boca Raton, FL, 2007; pp. 179-203.
[27] Hubatsch, L.; Ridderstrom, M.; Mannervik B. Human glutathione S-transferase A4-4. An alfa-class enzyme with high catalytic efficiency in the conjugation of 4-hydroxynonenal and other genotoxic products of lipid peroxidation. Biochem. J. 1998, 330, 175-179.
[28] Deponte, M. Glutathione catalysis and the reaction mechanism of glutathione-dependent enzymes. Biochim. Biophys. Acta. 2013, 1830, 3217-3266.
[29] Segura-Aguilar, J.; Bae, S.; Widersten, M.; Welch, C. J.; Mannervik, B. Human class Mu glutathione transferases, in particular isoenzyme M2-2, catalyze detoxication of the dopamine metabolite aminochrome, J. Biol. Chem. 1997, 272, 5727–5731.

[30] Johansson, A. S.; Mannervik, B. Human glutathione transferase A3-3, a highly efficient catalyst of double-bond isomerization in the biosynthetic pathway of steroid hormones. J. Biol. Chem. 2001, 276, 33061-33065.
[31] Gu, Y.; Guo, J.; Pal, A.; Pan, S. S.; Zimniak, P.; Singh, S. V.; Ji, X. Crystal structure of human glutathione S-transferase A3-3 and mechanistic implications for its high steroid isomerase activity. Biochem. 2004, 43, 15673-15679.
[32] Taes, K.; Olin, B.; Mannervik, B. Structural basis for featuring of steroid isomerase activity in alfa class glutathione transferases. J. Mol. Biol. 2010, 397, 332-340.
[33] Calvaresi, M.; Stenta, M.; Garavelli, M.; Altoe, P.; Bottoni, A. Computational evidence for the catalytic mechanism of human glutathione S-transferase A3-3: A QM/MM investigation. ACS Catal. 2012, 2, 280-286.
[34] Chen, H.; Juchau, M. R. Biotransformation of 13-*cis*- and 9-*cis*-retinoic acid to all-*trans*-retinoic acid in rat conceptal homogenates. Drug Metabol. Dispos. 1998, 26, 222-228.
[35] Fernandez-Canon, J. M.; Penalva M. A. Characterization of a fungal maleylacetoacetate isomerase gene and identification of its human homologue. J. Biol. Chem. 1998, 273, 329-337.
[36] Seltzer, S.; Lin, M. Maleylacetone cis-trans isomerase. Mechanism of the interaction of coenzyme glutathione and substrate malylacetone in the presence and absence of enzyme. J. Am. Chem. Soc. 1979, 101, 3091-3097.
[37] Williams, C. S., DuBois, R. N. Prostaglandin endoperoxide synthase: why two isoforms? Am. J. Physiol. 1996, 270, G393-400.
[38] Jowsey, J. R.; Thomson, A. M.; Flanagan, J. U.; Murdock, P. R.; Moore, G. B. T.; Meyer, D. J.; Murphy, G. J.; Smith, S. A.; Hayes, J. D. Mammalian class Sigma glutathione S-transferases: Catalytic properties and tissue-specific expression of human and rat GSH-dependent prostaglandin D2 synthases. Biochem. J. 2001, 359, 507–516.
[39] Kanaoka, Y.; Ago, H.; Inagaki, E.; Nanayama, T.; Miyano, M.; Kikuno, R.; Fujii, Y.; Eguchi, N.; Toth, H.; Urade, Y.; Hayaishi, O. Cloning and crystal structure of hematopoietic prostaglandin D synthase. Cell. 1997, 90, 1085-1095.
[40] Jakobsson, P. J.; Thorén, S.; Morgenstern, R.; Samuelsson, B. Identification of human prostaglandin E synthase: a microsomal, glutathione-dependent, inducible enzyme, constituting a potential novel drug target. Proc. Natl. Acad. Sci. USA. 1999, 96, 7220-7225.
[41] Beuckmann, C. T.; Fujimori, K.; Urade, Y.; Hayaishi, O. Identification of mu-class glutathione transferases M2-2 and M3-3 as cytosolic prostaglandin E synthases in the human brain. Neurochem. Res. 2000, 25, 733-738.

[42] Armstrong, R. N. Structure, catalytic mechanism, and evolution of the glutathione transferases. Chem. Res. Toxicol. 1997, 10, 2-18.
[43] Ladner, J. E.; Parsons, J. F.; Rife, C. L.; Gilliland, G. L.; Armstrong, R. N. Parallel evolutionary pathways for glutathione transferases: structure and mechanism of the mitochondrial class kappa enzyme rGSTK1-1. Biochemistry. 2004, 43, 352-361.
[44] Jowsey, I. R.; Thomson, R.E.; Orton, T. C.; Elcombe, C. R.; Hayes, J. D. Biochemical and genetic characterization of a murine-class Kappa glutathione S-transferase. Biochem. J. 2003, 373, 559-569.
[45] Morgenstern, R.; Guthenberg, C.; DePierre, J. W. Microsomal glutathione S-transferase. Purification, initial characterization and demonstration that it is not identical to the cytosolic glutathione S-transferases A, B and C. Eur. J. Biochem. 1982, 128, 243-248.
[46] Bernat, B. A.; Laughlin, L. T.; Armstrong, R. N. Fosfomycin resistance protein (FosA) is a manganese metalloglutathione transferase related to glyoxalase I and the extradiol dioxygenases. Biochemistry, 1997, 36, 3050-3055.
[47] Pearson, W. R. Phylogenies of glutathione transferase families. Methods Enzymol. 2005, 401, 186-204.
[48] Bresell, A.; Weinander, R.; Lundqvist, G.; Raza, H.; Shimoji, M.; Sun, T. H.; Balk, L.; Wiklund, R.; Eriksson, J.; Jansson, C.; Persson, B.; Jakobsson, P. J.; Morgenstern, R. Bioinformatic and enzymatic characterization of the MAPEG superfamily. FEBS J. 2005, 272, 1688-1703.
[49] Martinez Molina, D.; Eshaghi, S.; Nordlund, P. Vatalysis within the lipid bilayer-structure and mechanism of the MAPEG family of integral membrane proteins. Curr. Opin. Struct. Biol. 2008, 18, 442-449.
[50] Mannervik, B.; Board, P. G.; Hayes, J. D.; Listowsky, I.; Pearson, W. R. Nomenclature for mammalian soluble glutathione transferases. Methods Enzymol. 2005, 401, 1-8.
[51] Suzuki, T.; Coggan, M.; Show, D. C.; Board, P. G. Electrophoretic and immunological analysis of human glutathione S-transferase isozymes. Ann. Hum. Genet. 1987, 51, 95-106.
[52] Danielson, U. H.; Mannervik, B. Kinetic independence of the subunits of cytosolic glutathione transferase from the rat. Biochem. J. 1985, 231, 263-267.
[53] (a) Hayes, J. D.; Pulford, D. J. The Glutathione S-Transferase supergene family: Regulation of GST and the contribution of the isoenzymes to cancer chemoprotection and drug resistance Part I. Crit. Rev. Biochem. Mol. Biol. 1995, 30, 445-520. (b) Hayes, J. D.; Pulford, D. J. The Glutathione S-Transferase supergene family: Regulation of GST and the contribution of the isoenzymes to

cancer chemoprotection and drug resistance Part II. Crit. Rev. Biochem. Mol. Biol. 1995, 30, 521-600.
[54] Higgins, L. G.; Hayes, J. D. Mechanisms of induction of cytosolic and microsomal glutathione transferase (GST) genes by xenobiotics and pro-inflammatory agents. Drug Metabol. Rev. 2011, 43, 92-137.
[55] Mohana, K.; Achary, A. Human cytosolic glutathione-S-transferases: quantitative analysis of expression, comparative analysis of structures and inhibition strategies of isozymes involved in drug resistance. Drug Metabol. Rev. 2017, 49, 318-337.
[56] Pirie, N. W.; Pinhey, K. G. The titration curve of glutathione. J. Biol. Chem. 1929, 84, 321-333.
[57] Li, N. C.; Gawron, O.; Bascuas, G. Stability of zinc complexes with glutathione and oxidized glutathione. J. Am. Chem. Soc. 1954, 76, 225-229.
[58] Martin, R. B.; Edsall, J. T. Glutathione: ionization in basic solutions and molecular rearrangement in strongly acid solution. Bull. Soc. Chim. Biol. 1958, 40, 1763-1771.
[59] Mirzahosseini, A.; Somlyay, M.; Noszál, B. The comprehensive acid–base characterization of glutathione. Chem. Phys. Lett. 2015, 622: 50–56.
[60] Chen, W. J.; Graminski, G. F.; Armstrong, R. N. Dissection of the catalytic mechanism of isoenzyme 4-4 of glutathione S-transferase with alternative substrates. Biochem. 1988, 27, 647-654.
[61] Parsons, J. F.; Armstrong, R. N. Proton configuration in the ground state and transition state of a glutathione transferase-catalyzed reaction inferred from the properites of tetradeca(3-fluorotyrosyl)glutathione transferase. J. Am. Chem. Soc. 1996, 118, 2295-2296.
[62] Thorson, J. S.; Shin, I.; Chapman, E.; Stenberg, G.; Mannervik, B.; Schultz, P. G. Analysis of the role of the active site tyrosine in human glutathione transferase A1-1 by unnatural amino acid mutagenesis. J. Am. Chem. Soc. 1998, 120, 451-452.
[63] Reinemer, P.; Dirr, H. W.; Ladenstein, R.; Huber, R.; Lo Bello, M.; Federici, G.; Parker, M. W. Three-dimensional structure of class π glutathione S-transferase from human placenta in complex with S-hexylglutathione at 2.8 Å resolution. J. Mol. Biol. 1992, 227, 214-226.
[64] Ji, X.; Zhang, P.; Armstrong, R. N.; Gilliland, G. L. The three-dimensional structure of a glutathione S-transferase from the Mu gene class. Structural analysis of the binary complex of isoenzyme 3-3 and glutathione at 2.2-.ANG. resolution. Biochem. 1992, 31, 10169-10184.
[65] Sinning, I.; Kleywegt, G. J.; Cowan, S. W.; Reinemer, P.; Dirr, H. W.; Huber, R.; Gilliland, G. L.; Armstrong, R. N.; Ji, X.; Board, P. G.; Olin, B.; Mannervik,

B.; Jones, T. A. Structure determination and refinement of human alpha class glutathione transferase A1-1, and a comparison with the Mu and Pi class enzymes. J. Mol. Biol. 1993, 232, 192-212.
[66] Bjornestedt, R.; Stenberg, G.; Widersten, M.; Board, P. G.; Sinning, I.; Jones, T. A.; Mannervik, B. Functional significance of arginine 15 in the active site of human alpha glutathione transferase A1-1. J. Mol. Biol. 1995, 247, 765-773.
[67] Ji, X.; Tordova, M.; O'Donnell, R.; Parsons, J. F.; Hayden, J. B.; Gilliland, G. L.; Zimniak, P. Structure and function of the xenobiotic substrate-binding site and location of a potential non-substrate-binding site in a class π glutathione S-transferase. Biochem. 1997, 36, 9690-9702.
[68] Witz, G. Biological interactions of α,β-unsaturated aldehydes. Free Rad. Biol. Med. 1989, 7, 333-349.
[69] Spickett, C. M. The lipid peroxidation product 4-hydroxy-2-nonenal: Advances in chemistry and analysis. Redox. Biol. 2013, 1, 145-152.
[70] Sousa, B. C.; Pitt, A., R.; Spickett, C. M. Chemistry and analysis of HNE and other prominent carbonyl-containing lipid oxidation compounds. Free Rad. Biol. Med. 2017, 111, 294-308.
[71] Eder, E.; Scheckenbach, S.; Deininger, C.; Huffman, C. The possible role of α,β-unsaturated carbonyl compounds in mutagenesis and carcinogenesis. Toxicol. Letters. 1993, 67, 87-103.
[72] Shoeb, M.; Ansari, N. H.; Srivastava, S. K.; Ramana, K. V. 4-hydroxynonenal in the pathogenesis and progression of human diseases. Curr. Med. Chem. 2014, 21, 230–237.
[73] West, J. D.; Marnett, L. J. Endogenous reactive intermediates as modulators of cell signaling and cell death. Chem. Res. Toxicol. 2006, 19, 173–194.
[74] Barrera, G.; Pizzimenti, S.; Ciamporcero, E. S.; Daga, M.; Ullio, C.; Arcaro, A.; Cetrangolo, G. P.; Ferretti, C.; Dianzani, C.; Lepore, A.; Gentile, F. Role of 4-hydroxynonenal-protein adducts in human diseases. Antiox. Redox Signal. 2015, 22, 1681-1702.
[75] Roede, J. R.; Jones, D. P. Reactive species and mitochondrial dysfunction: mechanistic significance of 4-hydroxynonenal. Environmental and Molecular Mutagenesis. 2010, 51, 380–390.
[76] Guéraud, F.; Atalay, M.; Bresgen, N.; Cipak, A.; Eckl, P. M.; Huc, L.; Jouanin, I.; Siems, W.; Uchida, K. Chemistry and biochemistry of lipid peroxidation products. Free Rad. Res. 2010, 44, 1098–1124.
[77] Chen, Z. H.; Niki, E. 4-hydroxynonenal (4-HNE) has been widely accepted as an inducer of oxidative stress. Is this the whole truth about it or can 4-HNE also exert protective effects? IUBMB Life. 2006, 58, 372–373.

[78] Aldini, G.; Carini, M.; Yeum, K.-J.; Vistoli, G. Novel molecular approaches for improving enzymatic and nonenzymatic detoxification of 4-hydroxynonenal: toward the discovery of a novel class of bioactive compounds. Free Rad. Biol. Med. 2014, 69, 145–156.
[79] Schaur, R. J.; Siems, W.; Bresgen, N.; Eckl, P. M. 4-Hydroxy-nonenal – A bioactive lipid peroxidation product. Biomol. 2015, 5, 2247-2337.
[80] Wakita, C.; Maeshima, T.; Yamazaki, A.; Shibata, T.; Ito, S.; Akagawa, M.; Ojika, M.; Yodoi, J.; Uchida, K. Stereochemical configuration of 4-hydroxy-2-nonenal-cysteine adducts and their stereoselective formation in a redox-regulated protein. Biol. Chem. 2009, 284, 28810-28822.
[81] Zimniak, P.; Eckles, M. A.; Saxena, M.; Awasthi, Y. C. A subgroup of class alpha glutathione S-transferases: cloning of cDNA for mouse lung glutathione S-transferase GST 5.7. FEBS Lett. 1992, 313, 173-176.
[82] Zimniak, P.; Shinghal, S. S.; Srivastava, S. K.; Awashti, S.; Sharma, R.; Hayden, J. B.; Awashti, Y. C. Estimation of genomic complexity, heterologous expression, and enzymatic characterization of mouse glutathione S-transferase mGSTA4-4 (GST 5.7). J. Biol. Chem. 1994, 269, 992-1000.
[83] Hubatsch, I.; Ridderstrom, M.; Mannervik, B. Human glutathione transferase A4-4: an alpha class enzyme with high catalytic efficiency in the conjugation of 4-hydroxynonenal and other genotoxic products of lipid peroxidation. Biochem. J. 1998, 330, 175-179.
[84] Bolton, J. L.; Trush, M. A.; Penning, T. M.; Dryhurst, G.; Monks, T. J. Role of quinones in toxicology. Chem. Res. Toxicol. 2000, 13, 135-160.
[85] Bolton, J. L.; Dunlap, T. Formation and biological targets of quinones: cytotoxic versus cytoprotective effects. Chem. Res. Toxicol. 2017, 30, 13–37.
[86] Bisaglia, M.; Soriano, M. E.; Arduini, I.; Mammi, S.; Bubacco, L. Molecular characterization of dopamine-derived quinones reactivity toward NADH and glutathione: implications for mitochondrial dysfunction in Parkinson disease. Biochim. Biophys. Acta. 2010, 1802, 699-706.
[87] Segura-Aguilar, J.; Paris, I.; Muñoz, P.; Ferrari, E.; Zecca, L.; Zucca, F. A. Protective and toxic roles of dopamine in Parkinson's disease. J. Neurochem. 2014, 129, 898-915.
[88] Dagnino-Subiabre, A.; Cassels, B. K.; Baez, S.; Johansson, A.-S.; Mannervik, B.; Segura-Aguilar, J. Glutathione transferase M2-2 catalyzes conjugation of dopamine and dopa *o*-quinones. Biochem. Biophys. Res. Commun. 2000, 274, 32–36.
[89] Blair, I. A. Endogeneous glutathione adducts. Curr. Drug Metrabol. 2006, 7, 853-872.

[90] Bogaards, J. J. P.; Venekamp, J. C.; van Bladeren, P. J. Stereoselective conjugation of prostaglandin A2 and prostaglandin J2 with glutathione, catalysed by the human glutathione S-transferases A1-1, A2-2, M1a-1a, and P1-1. Chem. Res. Toxicol. 1997, 10, 310-317.
[91] Bowers-Gentry, R. C.; Deems, R. A.; Harkewicz, R.; Dennis, E. A. Eicosanoid lipidomics. In Functional lipidomics; Feng, L.; Prestwich, G. D., Eds.; CRC Press: Boca Raton, FL, 2006; pp 79-100.
[92] Nicholson, D. W.; Ali, A.; Klemba, M. W.; Munday, N. A.; Zamboni, R. J.; Ford-Hutchinson, A. W. Human leukotriene C_4 synthase expression in dimethyl sulfoxide-differentiated U937 cells. J. Biol. Chem. 1992, 267, 17849-17857.
[93] Welsch, D. J.; Creely, D. P.; Hauser, S. D.; Mathis, K. J.; Krivi, G. G.; Isakson, P. C. Molecular cloning and expression of human leukotriene C_4 synthase. Proc. Natl. Acad. Sci. USA. 1994, 91, 9745-9749.
[94] Pace-Asciak, C. R. Hepoxilins: a review on their cellular actions. Biochim. Biophys. Acta. 1994, 1215, 1-8.
[95] Pace-Asciak, C. R. Arachidonic acid epoxides: Demonstartion throught [18O]oxygen studies of an intramolecular transfer of the terminal hydroxyl group of (12S)-hydroperoxyeicosa-5,8,10,14-tetraenoic acid to form hydroxyepoxides. J. Biol. Chem. 1984, 259, 8332-8337.
[96] Pace-Asciak, C. R.; Laneuville, O.; Su, W. G.; Corey, E. J.; Gurevich, N.; Wu, P.; Carlen, P. L. A glutathione conjugate of hepoxilin A3: formation and action in the rat central nervous system. Proc. Natl. Acad. Sci. 1990, 87, 3037-3041.
[97] Parkinson, A. Biotransformation of xenobiotics. In Casarett and Doull's Toxicology. The basic science of poisons, 6th. Ed.; Klaassen, C. D. (Ed.); Mc Graw-Hill: New York, NY, 2001, pp. 133-224.
[98] Davis, C. D.; Hanumegowda, U. M. The role of drug metabolism in toxicity. In Drug metabolism handbook. Concepts and applications. Nassar, A. F.; Hollenberg, P. F.; Scatina, J. (Eds); Wiley: Hoboken, NJ, 2009, pp. 561-628.
[99] Park, B. K.; Boobis, A.; Clarke, S.; Goldring, C. E. P.; Jones, D.; Kenna, J. G.; Lambert, C.; Laverty, H. G.; Naisbitt, D. J.; Nelson, S.; Nicoll-Griffith, D. A.; Obach, R. S.; Routledge, P.; Smith, D. A.; Tweedie, D. J.; Vermeulen, N.; Williams, D. P.; Wilson, I. D.; Baillie, T. A. Managing the challenge of chemically reactive metabolites in drug development Nat. Rev. Drug Discov. 2011, 10, 292–306.
[100] Pietra, F. Mechanisms for nucleophilic and photonucleophilic aromatic substitution reactions. Q. Rev. Chem. Soc. 1969, 23, 504-521.
[101] Makosza, M. Nucleophilic aromatic substitution, general corrected mechanism and versatile synthetic tool. Org. Med. Chem. I. J. 2017, 2, 555-576.
[102] Abdelaal, Y. A. I.; Roe, M. Conjugation of chlorodinitrobenzene with reduced glutathione in the absence and presence of glutathione transferase from

larvae of the southern armyworm, *Spodoptera eridania*. Pest. Biochem. Physiol. 1990, 36, 248-258.
[103] Jakoby, W. B. The glutathione S-transferases: a group of multifunctional detoxification proteins. Adv. Enzymol. Rel. Areas Mol. Biol. 1978, 46, 383-414.
[104] Ivarrson, Y.; Mannervick, B. Combinatorial protein chemistry in three dimensions: A paradigm fort he evolution of glutathione transferases with novel activities. In Toxicology of glutathione transferases; Awasthi, Y. C., Ed.; CRC Press: Boca Raton, FL, 2007; pp. 47-69.
[105] Anders, M. W. Glutathione-dependent bioactivation of haloalkanes and haloalkenes. Drug. Metab. Rev. 2004, 36, 583-594.
[106] Hashmi, M.; Dechert, S.; Dekant, W.; Anders, M. W. Bioactivation of [13C] dichloromethane in mouse, rat, and human liver cytosol. 13C Nuclear magnetic resonance spectroscopic studies. Chem. Res. Toxicol. 1994, 7, 291-296.
[107] Ozawa, N.; Guengerich, F. P. Evidence for formation of an S-[2-(N7-guanyl)ethyl]glutathione adduct in glutathione mediated binding of the carcinogen 1,2-dibromoethane to DNA. Proc. Natl. Acad. Sci. USA. 1983, 80, 5266-5270.
[108] Hesse, S.; Krupski-Brennstuhl, G.; Cumpelik, O.; Mezger, M.; Wiebel, F. J. Glutathione depletion suppresses conjugation of benzo[a]pyrene metabolites and (±)-trans-7,8-dihydroxy-7,8-dihydrobenzo[a]pyrene metabolites with glutathione but does not affect their binding to DNA in C3H/10T1/2 mouse fibroblasts. Carcinogen. 1987, 8, 1051-1058.
[109] Ziglari, T.; Allameh, A. The significance of glutathione conjugation in aflatoxin metabolism. In Aflatoxins. Recent advances and future prospects, Razzaghi-Abayaneh, M. (Ed.); IntechOpen; London, UK, 2013, pp 267-286.
[110] Jernström, B.; Funk, M.; Frank, H.; Mannervik, B.; Seidel, A. Glutathione S-transferase A1-1-catalysed conjugation of bay and fjord region diol epoxides of polycyclic aromatic hydrocarbons with glutathione. Carcinogen. 1996, 17, 1491-1498.
[111] Sundberg, K.; Widersten, M.; Seidel, A.; Mannervik, B.; Jernström, B. Glutathione conjugation of bay- and fjord-region diol epoxides of polycyclic aromatic hydrocarbons by glutathione transferases M1-1 and P1-1. Chem. Res. Toxicol. 1997, 10, 1221-1227.
[112] Kalsi, S. S.; Dargan, P. I.; Waring, W. S.; Wood, D. M. A review of the evidence concerning hepatic glutathione depletion and susceptibility to hepatotoxicity after paracetamol overdose. Open Access Emerg. Med. 2011, 3, 87–96.

[113] Ramachandran, A.; Jaeschke, H. Mechanisms of acetaminophen hepatotoxicity and their translation to the human pathophysiology. J Clin Transl Res. 2017 Feb; 3(Suppl 1): 157–169.
[114] Henderson, C. J.; Wolf, C. R.; Kitteringham, N.; Powell, H.; Otto, D.; Park, B. K. Increased resistance to acetaminophen heptotoxicity in mice lacking glutathione S-transferase Pi. Proc. Natl. Acad. Sci. USA. 2000, 97, 12741-12745.
[115] Stevens, J. F.; Maier, C. S. Acrolein: Sources, metabolism, and biomolecular interactions relevant to human health and disease. Mol. Nutr. Food Res. 2008, 52, 7–25.
[116] Kehrer, J. P.; Biswal, S.S. The molecular effects of acrolein. Toxicol. Sci. 2000, 57, 6-15.
[117] Cai, J.; Bhatnagar, A.; Pierce, W. M. Jr. Protein modification by acrolein: formation and stability of cysteine adducts. Chem. Res. Toxicol. 2009, 22, 708-716.
[118] Esterbauer, H.; Schaur, R. J.; Zollner, H. Chemistry and biochemistry of 4-hydroxynonenal, malonaldehyde and related aldehydes. Free. Rad. Biol. Med. 1991, 11, 81–128.
[119] Berhane, K.; Widersten, M.; Engström, A.; Kozarich, J W.; Mannervik, B. Detoxification of base propenals and other alpha, beta-unsaturated aldehyde products of radical reactions and lipid peroxidation by human glutathione transferase. Proc. Natl. Acad. Sci. USA. 1994, 91, 1480-1484.
[120] Yang, Y.; Yang, Y.; Trent, M. B. He, N.; Lick, S. D.; Zimniak, P.; Awashti, Y. C.; Boor, P. J. Glutathione-S-transferase A4-4 modulates oxidative stress in endothelium: possible role in human atherosclerosis. Atherosclerosis. 2004, 173, 211–221.
[121] Ploemen, J.H. T. M.; Van Ommen, B.; Bogaards, J. J. P.; Van Bladeren, P. J. Ethacrynic acid and its glutathione conjugate as inhibitors of glutathione S-transferases. Xenobiotica. 1993, 23, 913-923.
[122] Ploemen, J. H. T. M.; Van Ommen, B.; Van Bladeren, P. J. Inhibition of rat and human glutathione S-transferase isoenzymes by ethacrynic acid and its glutathione conjugate. Biochem Pharmacol. 1990, 40, 1631–1635.
[123] Ploemen, J. H. T. M.; Van Schanke, A.; Van Ommen, B.; Van Bladeren, P. J. Reversible conjugation of ethacrynic acid with glutathione and human glutathione S-transferase P1–1. Cancer Res. 1994, 54, 915–919.
[124] O'Dwyer, P.J.; LaCreta, F.; Nash, S.; Tinsley, P. W.; Schilder, R.; Clapper, M. L.; Tew, K. D.; Panting, L.; Litwin, S.; Comis, R. L.; Ozols, R. F. Phase I study of thiotepa in combination with the glutathione transferase inhibitor ethacrynic acid. Cancer Res. 1991, 51, 6059 – 6065.

[125] Tirona, R. G.; Pang, K. S. Bimolecular glutathione conjugation kinetics of ethacrynic acid in rat liver: in vitro and perfusion studies. J. Pharmacol. Exp. Ther. 1999, 290, 1230-1241.
[126] van Iersel, M. L. P. S.; van Lipzig, M. M. H.; Rietjens, I. M. C. M.;Vervoort, J.; van Bladeren, P. J. GSTP1-1 stereospecifically catalyzes glutathione conjugation of ethacrynic acid. FEBS Letters. 1998, 441, 153-157.
[127] Rozmer, Z.; Perjési, P. Naturally occurring chalcones and their biological activities. Phytochem. Rev. 2016, 15, 87-120.
[128] Go, M. L.; Wu, X.; Liu, X. L. Chalcones: an update on cytotoxic and chemoprotective properties. Curr. Med. Chem. 2005, 12, 483-499.
[129] Nowakowska, Z. A review of anti-infective and anti-inflammatory chalcones. Eur. J. Med. Chem. 2007, 42, 125-137.
[130] Rahman, M. A. Chalcone: A valuable insight into the recent advances and potential pharmacological activities. Chem. Sci. J. 2011, 29, 1-16.
[131] Aquilano, K.; Baldelli, S.; Ciriolo, M. R.,Glutathione: new roles in redox signaling for an old antioxidant. Front. Pharmacol. 2014, 5, 196.
[132] Dinkova-Kostova, A. T.; Massiah, M. A.; Bozak, R. E.; Hicks, R. J.; Talalay, P. Potency of Michael reaction acceptors as inducers of enzymes that protect against carcinogenesis depends on their reactivity with sulfhydryl groups. Proc. Natl. Acad. Sci. 2001, 98, 3404-3409.
[133] Jin, Y. L.; Jin, X. Y.; Jin, F.; Sohn, D. H.; Kim, H. S. Structure activity relationship studies of anti-inflammatory TMMC derivatives: 4-dimethylamino group on the B ring responsible for lowering the potency. Arch. Pharm. Res. 2008, 31, 1145-1152.
[134] Wang, J.; Wang, S.; Song, D.; Zhao, D.; Sha, Y.; Jiang, Y.; Jing, Y.; Cheng, M. Chalcone derivatives inhibit glutathione S-transferase P1-1 activity: insights into the interaction mode of alpha, beta-unsaturated carbonyl compounds. Chem. Biol. Drug Des. 2009, 73, 511-514.
[135] Kubo, Y.; Armstrong, R. N. Observation of a substituent effect on the stereoselectivity of glutathione S-transferase toward para-substituted 4-phenyl-3-buten-2-ones., Chem. Res. Toxicol. 1989, *2*, 144-145.
[136] Bernardes, A.; D'Oliveira, G. D.C.; Silezin, A.; Kuzma, M.; Molnár, S.; Noda Pérez, C.; Perjési. P. Reagent-induced asymmetric induction in addition reaction of reduced glutathione onto bis-Mannich chalcones. Arch. Pharm. 2018, 351, e1700386.

molecules

MDPI

Article

Reaction of Chalcones with Cellular Thiols. The Effect of the 4-Substitution of Chalcones and Protonation State of the Thiols on the Addition Process. Diastereoselective Thiol Addition

Fatemeh Kenari [1], Szilárd Molnár [1,2] and Pál Perjési [1,*]

[1] Institute of Pharmaceutical Chemistry, University of Pécs, H-7624 Pécs, Hungary; kenari.fatemeh@pte.hu (F.K.); molnar.szilard@pte.hu (S.M.)
[2] Research Institute for Viticulture and Oenology, University of Pécs, H-7624 Pécs, Hungary
* Correspondence: pal.perjesi@gytk.pte.hu; Tel.: +36-72-503-650

Abstract: Several biological effects of chalcones have been reported to be associated with their thiol reactivity. In vivo, the reactions can result in the formation of small-molecule or protein thiol adducts. Both types of reactions can play a role in the biological effects of this class of compounds. Progress of the reaction of 4-methyl- and 4-methoxychalcone with glutathione and *N*-acetylcysteine was studied by the HPLC-UV-VIS method. The reactions were conducted under three different pH conditions. HPLC-MS measurements confirmed the structure of the formed adducts. The chalcones reacted with both thiols under all incubation conditions. The initial rate and composition of the equilibrium mixtures depended on the ratio of the deprotonated form of the thiols. In the reaction of 4-methoxychalcone with N-acetylcysteine under strongly basic conditions, transformation of the kinetic adduct into the thermodynamically more stable one was observed. Addition of S-protonated *N*-acetylcysteine onto the polar double bonds of the chalcones showed different degrees of diastereoselectivity. Both chalcones showed a Michael-type addition reaction with the ionized and non-ionized forms of the investigated thiols. The initial reactivity of the chalcones and the equilibrium composition of the incubates showed a positive correlation with the degree of ionization of the thiols. Conversions showed systematic differences under each set of conditions. The observed differences can hint at the difference in reported biological actions of 4-methyl- and 4-methoxy-substituted chalcones.

Keywords: chalcone; glutathione; cysteine; thiols; Michael addition; diastereoselective addition

Citation: Kenari, F.; Molnár, S.; Perjési, P. Reaction of Chalcones with Cellular Thiols. The Effect of the 4-Substitution of Chalcones and Protonation State of the Thiols on the Addition Process. Diastereoselective Thiol Addition. *Molecules* **2021**, *26*, 4332. https://doi.org/10.3390/molecules26144332

Academic Editor: Federica Belluti

Received: 18 June 2021
Accepted: 14 July 2021
Published: 17 July 2021

1. Introduction

Chalcones (Figure 1) are intermediary compounds of the biosynthetic pathway of a large and widespread group of plant constituents known collectively as flavonoids [1]. Several compounds display in vitro cytotoxic (cell growth inhibitor) activity toward cultured tumor cells among the naturally occurring chalcones and their synthetic analogues. Chalcones are also effective as cell proliferation inhibitors and as antitumor-promoting, anti-inflammatory, and chemopreventive agents [2–5]. Their activity is the result of either covalent or noncovalent interactions [2]. Covalent interactions are mainly based on the Michael acceptor activity of the α,β-unsaturated carbonyl system or the radical-scavenging or reductive potential of the compounds [6–8]. Several biological effects (e.g., NQO1 inducer [9], anti-inflammatory [10], GST P1-1 inhibitory [11]) of chalcones have been associated with their Michael-type reactivity toward protein thiols or reduced glutathione (GSH). It was suggested that the lower GSH depletion potential of chalcones with strong electron donor substituents (e.g., dimethylamino) on the B ring could be the consequence of the lower Michael-type reactivity of the derivatives toward GSH [12]. In contrast, higher reactivity toward GSH and other thiols was parallel with the higher NQO1-inducing potential of the investigated chalcones [13].

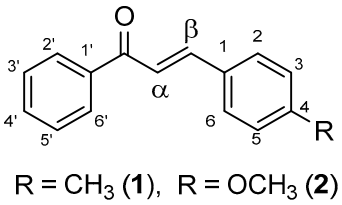

Figure 1. Structure and numbering of the investigated chalcones (**1** and **2**).

In our present study, reactions of two chalcones with different 4-substitutions (4-CH_3 (**1**) and 4-OCH_3 (**2**)) with two cellular thiols (GSH and NAC) were investigated to get information about (a) how the pH of the reaction medium affects the reactivity and stereochemical outcome of the reactions and (b) how the thiol reactivity of the compounds is related to their biological activities. Since thiol reactivity can be the molecular basis of modulation of the function of thiol switches [14] and the biological effects of covalent modifiers [15], the thiol reactivity of different chalcones is of interest in understanding their biological activities. Glutathione is an endogenous thiol, whose thiol reactivity plays an important role in maintaining redox homeostasis and protecting cellular nucleophilic sites of proteins from harmful electrophiles [16]. NAC is an exogenous thiol; however, it is one of the precursors of GSH biosynthesis, possesses mucolytic action, and is used as an antidote in paracetamol intoxication [17]. Considering their different pK_a values [18], the two compounds are also perfect models for reactivity screening of compounds with surface protein thiols with different molecular surroundings [19].

The selected substituents have different electron-donating capacities, which results in different reactivities and biological activities. For example, the tumor promotion inhibitory effect of 4-methyl-4′-hydroxychalcone is about twice as high as that of the 4-methoxy analogue [20]. Comparison of the in vitro cytotoxicity of **1** and **2** toward five different cancer cells showed that the 4-methyl derivative (**1**) is more effective toward most of the tested cell lines [21]. Furthermore, multiple regression analysis showed that cytotoxicity of a series of chalcones toward murine and human cancer cells increases as the Hammett sigma (σ) values of the substituent elevates [22]. In contrast, among the cyclic analogues (n = 5, 6, and 7) of the two chalcones, the methoxy-substituted (**2**) cyclic derivatives showed much higher in vitro cancer cell cytotoxicity than those of **1** [23]. Furthermore, the seven-membered analogues of **1** and **2** showed different in vitro effects on the cell cycle of Jurkat T cells [24].

The Michael reaction refers to the addition of a nucleophile (Michael donor) to an activated α,β-unsaturated carbonyl compound (Michael acceptor), and it is typically base-catalyzed. Among the most commonly studied nucleophiles, one finds hydroxide ions (OH^-), water, and amines; a more limited number of investigations have been reported with thiolate ions (ArS^-, RS^-), oxide ions (ArO^-, RO^-), and cyanide ions (CN^-). The reactions can also be categorized based on the charge of the nucleophilic reactants, which could be (a) negatively charged (e.g., OH^-, RS^-, CN^-) or (b) neutral (e.g., amines, thiols). Both kinds of nucleophiles can be added onto protonated or non-protonated α,β-unsaturated enones. Since the experimental pK_b value of (*E*)-chalcone was reported to be −5.00 [25], only additions onto the non-protonated chalcones were taken into consideration. The general mechanisms of the addition of deprotonated (path A) and neutral (path B) nucleophiles onto non-protonated chalcones are shown in Figure 2.

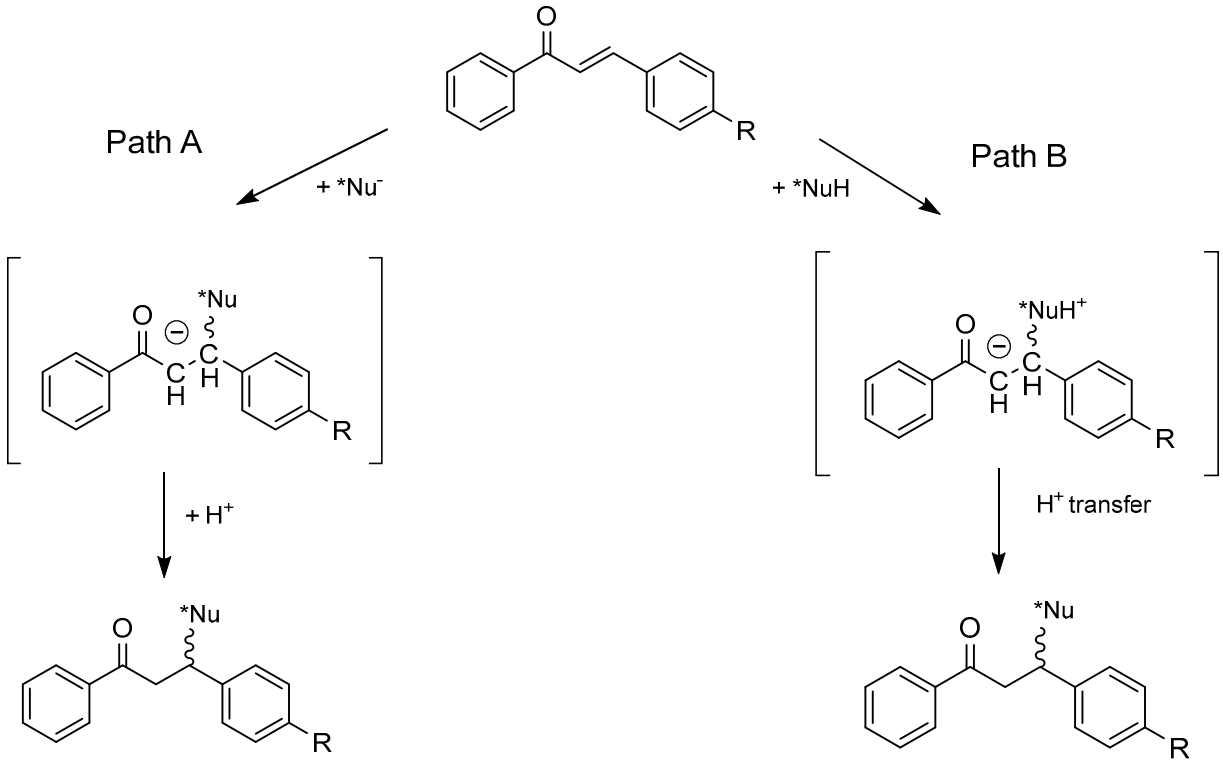

Figure 2. General mechanisms of the addition reaction of nucleophiles onto the activated double bonds of chalcones.

As shown in Figure 2, the primary adduct of the addition reactions either possesses a negative charge (path A) or has a zwitterion structure (path B). The second step of the reactions is an acid–base process, which can occur in an intermolecular or—in the case of the zwitterion intermediates—an intramolecular manner [26].

Previously, we reported the synthesis and reactions of two 4′-hydroxychalcones and their bis-methyleneamino (Mannich) derivatives. It was found that the Mannich derivatives showed significantly increased reactivity [27] and diastereoselectivity [28] in comparison to the respective non-Mannich derivatives when the reactions were conducted under acidic (about pH 3) conditions.

We investigated the reactions under three conditions with different pH: (a) pH 8.0/8.53, (b) pH 6.3/6.8, and (c) pH 3.2/3.7. The first pH values indicate the pH of the aqueous solution of the thiols before starting the incubations. The second pH values indicate the virtual pH of the incubation mixtures, which contained 75.5% *v*/*v* methanol (MeOH). The basic pH was selected because such conditions mimic the GST-catalyzed reactions; the ionization of the GSH thiol moiety increases due to its interaction with the basic imidazole N atom in the active site of the enzyme [29]. The slightly acidic conditions resemble the slightly acidic pH of the cancer cells [30]. The stronger acid conditions were selected to compare the reactivity of the protonated (neutral) and the ionized forms of the thiol functions of the two compounds. The pK_a of the thiol group of GSH and NAC was reported to be 8.83 and 9.52, respectively [18]. Accordingly, the thiol function of both compounds exists exclusively in the protonated (neutral) form under such acidic conditions. The stereoselectivity of the reactions was monitored by comparing the HPLC peak areas of the respective chalcone–GSH and chalcone–NAC adducts.

The reactions are reported to be reversible, accordingly resulting in the formation of an equilibrium mixture. To qualitatively characterize the progress of the addition processes, the composition of the incubation mixtures was analyzed at the 15, 45, 75, 105, 135, 165, 195, 225, 255, 285, and 315 min time points by HPLC-UV-VIS.

2. Results

2.1. Reactions under Basic (pH 8.0/8.5) Conditions

Initially, we investigated the reactions of the two chalcones under basic conditions. Considering the pK_a values of GSH (8.83) and NAC (9.52), about 31.9% of the GSH molecules and 8.7% of the NAC molecules existed under pH 8.5 conditions (the virtual pH of the incubates) in the more reactive thiolate form. By the end of the investigated period (315 min), the initial area of the HPLC peak corresponding to the parent compounds **1** and **2** reduced to 3.7% and 7.9%, respectively (Table 1). While the compounds were incubated with NAC, the respective figures were 5.2% and 9.8% (Table 2). Progress curve changes in the chromatographic peak areas of the starting chalcones (**1** and **2**) as a function of the incubation time of the reactions indicated that the compositions reflect those of the equilibrium in each case (Figures 3 and 4).

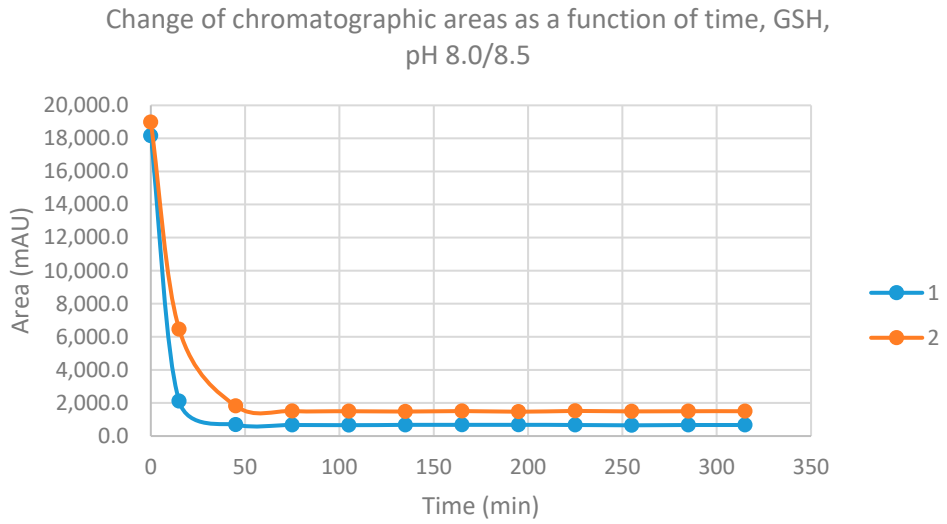

Figure 3. Change in the chromatographic peak area of chalcones **1** and **2** in the chalcone–GSH incubations at pH 8.0/8.5.

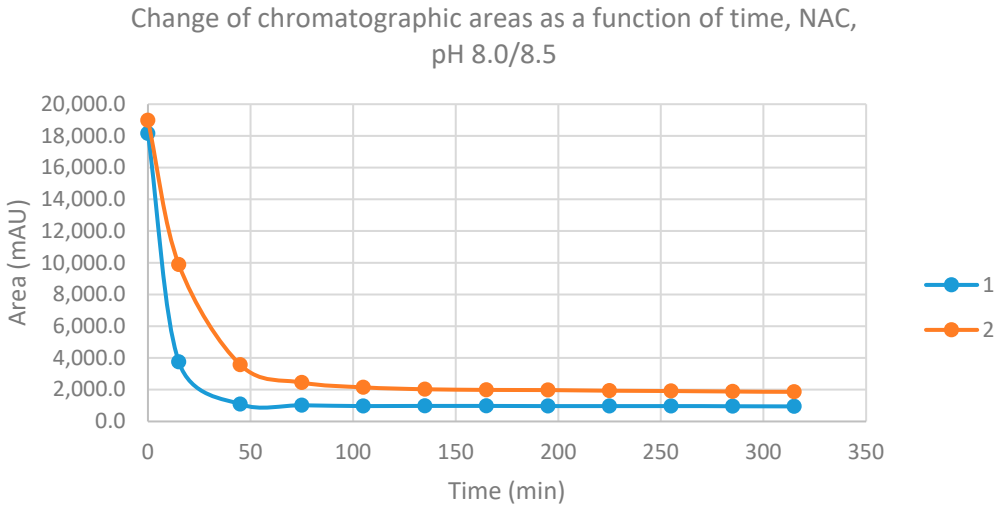

Figure 4. Change in the chromatographic peak area of chalcones **1** and **2** in the chalcone–NAC incubations at pH 8.0/8.5.

As a result of the addition reactions, a new chiral center was formed. Considering the inherent chirality of the two thiols, the formation of two diastereomeric adducts was

expected. However, using our HPLC conditions, the **1**-GSH and **2**-GSH conjugates were not separated (Table 1).

In the case of NAC incubations, the formed **1**-NAC and **2**-NAC adducts were only partially separated. Based on the integration of the two overlapping peaks, the ratio of the two diastereomeric adducts (NAC–**1** and NAC–**2**) showed a different (1.7–1.2 times) excess of the less polar diastereomers (Table 2). The structure of the parent chalcones (**1** and **2**) as well as their GSH and NAC conjugates was verified by HPLC-MS (Table S1 and Figures S10–S15).

Table 1. Retention times (t_R) [1] and integrated peak areas (A) of the investigated chalcones (**1** and **2**) and their GSH adducts [2].

pH [3]	Compound	t_R (*E*)-Chalcone	Area Ratio [4] A_{315}/A_0	t_R (*Z*)-Chalcone	Area (*Z*)-Chalcone	t_R GSH–1	Area GSH–1	t_R GSH–2	Area GSH–2
3.2	1	16.4	0.81	16.2	<100	13.8	4245	N/D [5]	-
3.2	2	15.9	0.96	15.7	<100	11.9	3352	N/D [5]	-
6.3	1	16.3	0.09	16.0	<100	13.2	16,571	N/D [5]	-
6.3	2	15.8	0.21	15.5	<100	11.3	17,160	N/D [5]	-
8	1	16.3	0.04	16.1 [6]	<100	13.3	17,419	N/D [5]	-
8	2	15.7	0.08	15.5	<100	11.0	20,387	N/D [5]	-

[1] Retention times in minutes; [2] data refer to the average of two independent measurements at the 315 min time point; [3] pH value of the aqueous thiol solution; [4] ratio of peak areas measured at 0 and 315 min; [5] not detectable; [6] only detectable at the 15, 45, 75, 135, and 165 min time points.

Table 2. Retention times (tr) [1] and integrated peak areas (A) of the investigated chalcones (**1** and **2**) and their NAC adducts [2].

pH [3]	Compound	t_R (*E*)-Chalcone	Area Ratio [4] A_{315}/A_0	t_R (*Z*)-Chalcone	Area (*Z*)-Chalcone	t_R NAC–1	Area NAC–1	t_R NAC–2	Area NAC–2
3.2	1	16.3	0.89	16.1	<100	15.2	1260	15.3	2173
3.2	2	15.8	0.98	15.5	<100	14.1	1156	14.2	1507
6.3	1	16.3	0.24	16.0	<100	15.1	4906	15.2	6457
6.3	2	15.8	0.47	15.5	<100	14.1	4712	14.2	5422
8	1	16.2	0.05	16.0	<100	15.1	6167	15.2	8875
8	2	15.7	0.10	15.5	<100	14.1	7167	14.2	8975

[1] Retention times in minutes; [2] data refer to the average of two independent measurements at the 315 min time point; [3] pH value of the aqueous thiol solution; [4] ratio of peak areas measured at 0 and 315 min.

The progress curves of the formation of the diastereomeric NAC adducts—based on the integrated HPLC peak areas (AUCs)—are shown in Figures 5 and 6. As shown, the formation of the **1**-NAC diastereomers is increased in the first 45 min and remained the same over the time of incubation. In the case of the **2**-NAC diastereomers, rapid formation of the kinetic product (NAC–**1**) was observed in the first 15 min. After that, however, the NAC–**1** isomer of **2** was transisomerized to the thermodynamic product (NAC–**2**), reaching the equilibrium composition by the 105 min time point (Figures 5 and 6).

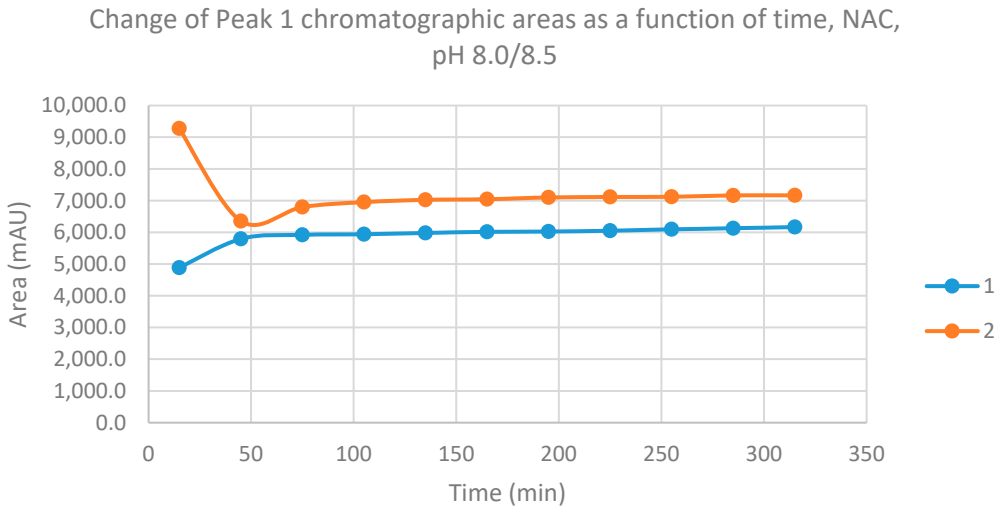

Figure 5. Change in the chromatographic peak area of adduct 1 of chalcones **1** and **2** in the chalcone–NAC incubations at pH 8.0/8.5.

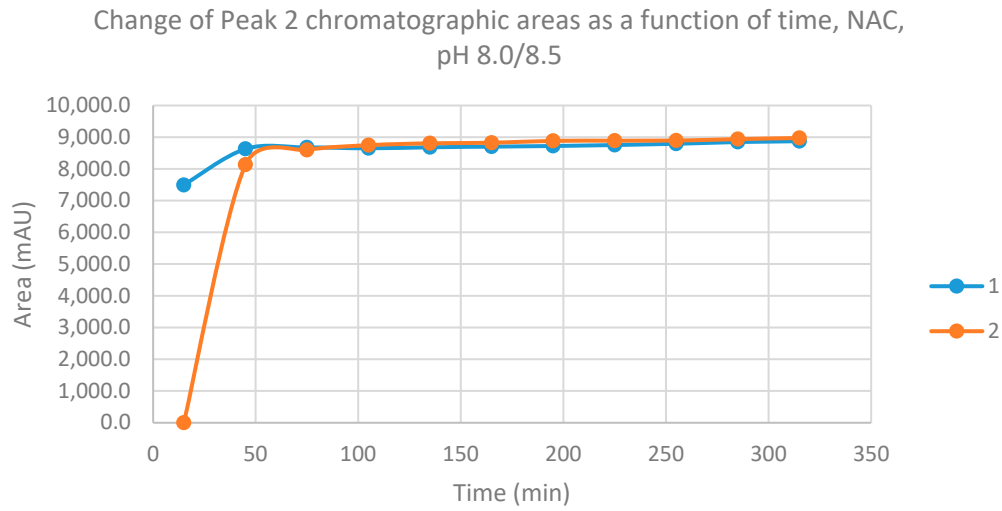

Figure 6. Change in the chromatographic peak area of adduct 2 of chalcones **1** and **2** in the chalcone–NAC incubations at pH 8.0/8.5.

Further to the above data, it is worth mentioning that during the incubations with GSH and NAC, small new peaks appeared in the chromatograms with a somewhat shorter retention time than that of unreacted **1** and **2** (Tables 1 and 2). Based on our previous results [31], the new peaks were supposed to be those of the respective (*Z*) diastereomers. Since such isomerization could not be observed in the incubations performed without the thiols, the formation of the (*Z*) isomer can be considered due to the retro-Michael reaction. To identify the structure of the expected (*Z*) diastereomers, light-initiated isomerization of **1** and **2** was performed. Based on the result of the light-initiated isomerization experiment, the formed compounds were identified as the respective (*Z*) isomers (Figures S16 and S17).

2.2. Reactions under Slightly Acidic (pH 6.3/6.8) Conditions

Reactions under slightly acidic conditions mimic the cellular milieu of cancer cells [30]. Under these experimental conditions (pH 6.8), about 0.9% of GSH and 0.2% of NAC molecules exist in the more reactive thiolate form. The progress of the reactions under such conditions was more restricted than that observed at pH 8.0/8.5. In the GSH incubations, the initial area of the parent compounds **1** and **2** was reduced to 9.4% and 21.4%, respec-

tively, by the end of the investigated period (Table 1). The respective figures for the NAC incubations were 24.4% and 46.8% (Table 2).

Progression curves of the reactions (Figures 7 and 8) indicated that the percentage figures represent compositions close to equilibrium. Similar to the results obtained under pH 8.0/8.5 conditions, the formation of a small amount of (*Z*) isomers was detected in the incubation mixtures.

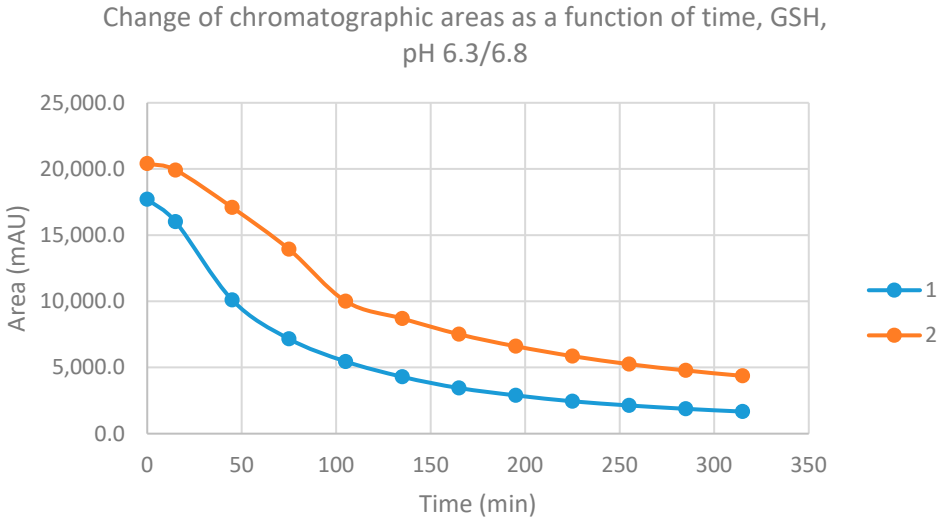

Figure 7. Change in the chromatographic peak area of chalcones **1** and **2** in the chalcone–GSH incubations at pH 6.3/6.8.

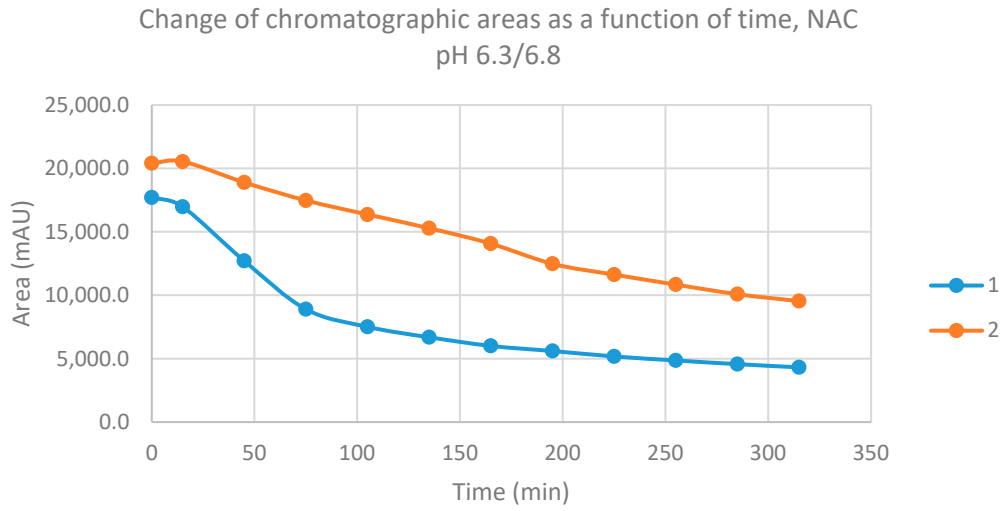

Figure 8. Change in the chromatographic peak area of chalcones **1** and **2** in the chalcone–NAC incubations at pH 6.3/6.8.

Progression curves of the formation of the chalcone–GSH and chalcone–NAC adducts showed two parallel concave curves with finite limits (Figures S1–S4).

2.3. Reactions under Acidic (pH 3.2/3.7) Conditions

Reactions under stronger acidic conditions proceeded to a much lower extent than those under the above two conditions. Under stronger acidic conditions, the thiol function of both GSH and NAC exists exclusively in protonated (neutral) form. Although protonated thiols can act as nucleophilic reagents, their reactivity is much lower than that of their deprotonated (negatively charged) counterparts [32].

Only a small amount of adducts were detected in each case in the chalcone–GSH/NAC incubates (Table 2). The chromatographic peak area values of the (*Z*) isomers were similar to those in the respective incubates at pH 8.0/8.5 and pH 6.3/6.8 (Tables 1 and 2).

Progression curves of the reaction of chalcones with GSH showed a linear downhill shape (Figure S5). A similar linear reduction in the chromatographic peak areas was observed in the NAC incubations (Figure S6).

Over the whole incubation period, the chromatographic peak areas of the chalcone–GSH (Figure S7) and chalcone–NAC diastereomers continuously increased (Figures S8 and S9).

3. Discussion

Our experiments demonstrated that both GSH and NAC react with the investigated chalcones under acidic (pH 3.2/3.7, pH 6.3/6.8) and basic (pH 8.0/8.5) conditions. However, the rate of the initial reactions and the composition of the equilibrium mixtures were affected by the nature of the reactants and the pH of the incubation mixtures.

Analysis of the effect of the 4-substituents under basic (pH 8.0/8.5) or slightly acidic (pH 6.3/6.8) conditions showed 4-methyl-substituted **1** to display higher initial reactivity. ^{13}C NMR shifts, indicating the electron density around the particular nucleus of the *beta*-C atom of **1** (144.9 ppm) and **2** (144.6 ppm), were reported to be similar [33]. The observed difference in the reactivity of chalcones **1** and **2** can be explained by the stability of the thiol adducts. An early work of Humphlett et al. demonstrated that the activity of the α-hydrogen atom of the adduct, the resonance stabilization of the enone formed by cleavage, and the anionic stability of the thiolate ion are the determining factors of the reverse process. The authors found the α-keto and β-phenyl substitutions as determining factors in the effective reverse reactions [34]. Since the 4-methoxy substitution can more effectively increase the electron density on the carbon–carbon double bond, and the formed chalcone is resonance stabilized, the elimination process is more effective in the case of **2** than **1**. Similar conclusions were made by d'Oliveira et al. while investigating a few chalcones and their rigid quinolone analogues [35].

The retro-thia-Michael reactions can result in the formation of the respective (*Z*) isomers as well. Therefore, to obtain authentic reference (*Z*) isomers, the stereochemically homogeneous (*E*) isomers (**1** and **2**) were submitted with light-initiated isomerization, as published before [30]. As a result, HPLC-MS data agreed with the respective (*Z*) isomers (Figures S16 and S17).

Comparison of the pK_a values of GSH (8.83) and NAC (9.52) thiols, and the respective conversions of the starting chalcones (Tables 1 and 2), showed that the higher the pK_a of the thiol, the lower the conversion of the chalcones in the case of both derivatives at each investigated pH. This observation reflects the importance of acidity (K_a) of the thiol group that regulates the relative amount of RS^- concerning RSH, hence the equilibrium.

HPLC analysis of the reactions of **1** and **2** with NAC showed a different (1.7–1.2 times) excess of the less polar diastereomer (Table 2). The observed diastereoselectivity was affected by both the nature of the 4-substituent and the pH. Thus, at each different pH value, it was the methyl-substituted **1** that showed higher diastereoselectivity. In contrast, in the case of both chalcones, diastereoselectivity decreased with the increase in the pH. HPLC-UV-Vis chromatograms of the chalcone **1**-NAC incubations at pH 8.0/8.3, pH 6.3/6.8, and pH 3.2/3.7 (315 min time point) are shown in Figures S18–S20, respectively. The corresponding HPLC-UV-Vis chromatograms of the chalcone **2**-NAC incubations are shown in Figures S21–S23.

These observations give additional indirect support to the formation of a six-membered, hydrogen-bond-stabilized cyclic intermediate in the reactions of chalcones with the protonated form of thiols. The formation of such a cyclic intermediate was suggested earlier in the reaction of GSH with the bis-Mannich derivatives of 4′-hydroxychalcones [27]. According to our previous explanation, the protonated thiol attacks the planar enone moiety from

the *Re*-side, resulting in a six-membered intermediate with a pseudoequatorial position of the bulky aryl ring (Figure 9).

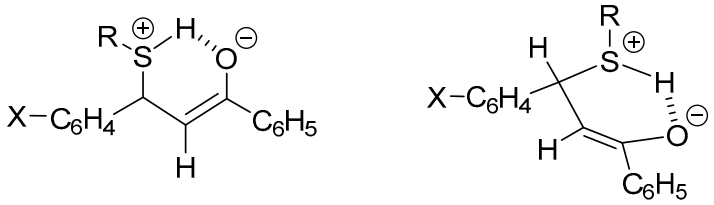

Figure 9. Possible enolate intermediate of the addition of protonated thiols onto chalcones.

Michael-type thiol reactivity of chalcones and related compounds is frequently associated with biological activities [6–11,36]. In contrast, several examples demonstrate that non-covalent interactions of chalcones with cellular macromolecules can play an important role in the biological effects of the compounds [37]. In a QSAR study, Katsori et al. found the clog *P* parameter to play an important part in the QSAR relationships. The authors found the electronic effects are comparatively unimportant in the anticancer effect of the investigated chalcones [38]. Comparison of the spontaneous thiol reactivities of the two chalcones under pH 8.0/8.5 and pH 6.3/6.8 conditions toward GSH and NAC showed some characteristic differences. Conversion of **1** with both GSH and NAC was higher than **2** under all investigated conditions (Tables 1 and 2). The experimental log *P* of **2** and **3** has been reported to be 4.12 and 3.67, respectively [39]. Thus, it is reasonable to suppose that both the thiol reactivity and the lipophilic properties contributed to the reported biological effects of the investigated compounds and their cyclic analogues.

4. Materials and Methods

4.1. Chemicals and Reagents

Chalcones **1** and **2** were synthesized, as reported before [40]. Their purity was tested by TLC and HPLC-UV-VIS. Reduced L-glutathione and *N*-acetyl L-cysteine were obtained from Sigma-Aldrich (Budapest, Hungary). The methanol CHROMASOLV gradient for HPLC was obtained from Honeywell (Hungary). Trifluoroacetic acid HiperSolve CHROMANORM was obtained from VWR (Budapest, Hungary) and formic acid from Fischer Chemicals. Deionized water for use in HPLC and HPLC-MS measurements was purified by Millipore Direct-Q^{TM} at the Institute of Pharmaceutical Chemistry (University of Pécs). Mobile phases used for HPLC measurements were degassed by an ultrasonic water bath before use.

4.2. Preparation of Solutions

To evaluate the reactivity of the investigated chalcones and their analogues with thiols, reduced glutathione (GSH) and *N*-acetylcysteine (NAC) solutions were prepared as follows: Each solution was prepared at three different pH values (3.2, 6.3, and 8.0). The pH was set using 1M NaOH solution. (a) Solutions of GSH and NAC were prepared in water to a final volume of 1.5 cm^3 with a concentration of 2.0 $\times$ 10^{-1} mol·L^{-1} (0.3 mmol thiol). (b) Chalcone solutions were freshly prepared before incubation to a 4.6 cm^3 volume of HPLC-grade methanol with a concentration of 6.5 $\times$ 10^{-3} mol·L^{-1} (0.03 mmol chalcone). (c) The GSH/NAC and chalcone solutions were pre-incubated in a 37 °C water bath for 15 min in the dark. Then, the solutions were mixed, resulting in a mixture of the thiol and the chalcone in a molar ratio of 10:1. The mixture was kept in the dark in a temperature-controlled (37 °C) water bath for a total duration of 315 min. To monitor the reaction by RP-HPLC, samples were taken at time points of 15, 45, 75, 105, 135, 165, 195, 225, 255, 285, and 315 min.

To evaluate the initial (0 min) peak area of chalcones **1** and **2**, 4.6 cm^3 methanolic solution of each was prepared as above (method (b)), and the solutions were diluted with

1.5 mL of aqueous solution with the respective pH before analysis. Before mixing, the solutions were pre-incubated at 37 °C for 30 min.

To compare the products of the previously proven light-initiated *E/Z* isomerization of the parent compounds [26] with those of the non-light (retro-Michael addition)-initiated isomerization, solutions of chalcones **1** and **2** were prepared by method (b), and the solutions were subjected to unscattered laboratory light for 1 week. The solutions were analyzed by HPLC-UV-VIS and HPLC-MS.

4.3. RP-HPLC-UV-VIS Measurements

The measurements were performed on an Agilent 1100 HPLC system coupled with a UV–VIS detector. The wavelength was set at 260 nm. The separation of the components was carried out in a reversed-phase chromatographic system. A Zobrax Eclipse XBD-C8 column (150 mm × 4.6 mm, particle size 5 µm; Agilent Technologies, Waldbronn, Germany) was used. The injection volume was 10 µL. During the time of the measurement, the column oven was set at room temperature (25 °C). Data were recorded and evaluated by the use of Agilent Chem Station (B.03.01). Gradient elution was performed at a flow rate of 1.2 mL/min; the mobile phase consisted of (A) water and 0.1% trifluoroacetic acid and (B) methanol and 0.1% trifluoroacetic acid. The gradient profile was as follows: an isocratic period of 8 min of 40% mobile phase B, followed by a linear increase to 60% in 4 min, a second linear gradient to 90% in 3 min, and a 5 min isocratic period of 90%. The column was then equilibrated to the initial conditions with a 2 min linear gradient to 40%, followed by 3 min of the isocratic period.

4.4. HPLC-MS Measurements

HPLC ESI-MS analyses were performed on an Ultimate 3000 liquid chromatograph (Dionex, Sunnyvale, CA, USA) coupled with a Thermo Q Exactive Focus quadrupole-Orbitrap hybrid mass spectrometer (Thermo Fisher Scientific, Waltham, MA, USA). The scan monitored *m/z* values ranging from 100 to 1000 Da. Data acquisition was carried out using Q Exactive Focus 2.1 and Xcalibur 4.2 software (Thermo Fisher Scientific). Analysis of compounds and adducts was performed in HESI positive and negative ionization modes with the following parameters: spray voltage, 3500 V; vaporizer temperature, 300 °C; capillary temperature, 350 °C; spray and auxiliary gas flows, 30 and 10 arbitrary units, respectively; resolution, 35,000 at 200 *m/z*; and fragmentation, 20 eV.

HPLC separation was performed on an Accucore C18 column (150 mm × 2.1 mm, particle size 2.6 µm), and an Accucore C18 guard column (5 mm × 2.1 mm, particle size 2.6 µm) was also used. The injection volume was 5 µL; the flow rate was set to 0.4 mL/min. Data analysis and evaluations were performed using Xcalibur 4.2 and FreeStyle 1.7 software. A binary gradient of eluents was used, consisting of mobile phases A and B.

The parameters of the gradient in chalcones were (A) water and 0.1% formic acid and (B) methanol and 0.1% formic acid. The gradient elution was as follows: isocratic elution for 1 min to 20% eluent B, continued by a linear gradient to 100% in 9 min, followed by an isocratic plateau for 2 min. Then, the column was equilibrated back to 20% in 0.5 min and continued isocratically for 2.5 min. The sampler was at room temperature, and the column oven was kept at 40 °C.

The parameters of the gradient in the case of adducts were (A) water and 0.1% formic acid and (B) methanol and 0.1% formic acid. The gradient elution was as follows: isocratic elution for 1 min to 10% eluent B, continued by a linear gradient to 95% in 13 min, followed by an isocratic plateau for 3 min. Finally, the column was equilibrated back to 10% in 0.1 min and continued isocratically for 2.9 min. The sampler was at room temperature, and the column oven was kept at 40 °C. The diode array detector was also set at 260 nm wavelength alongside MS analysis.

5. Conclusions

The present work aimed to investigate the thiol reactivity of two 4-substituted chalcone derivatives (**1** and **2**) with different experimental log-*P*-values. HPLC-UV-VIS and HPLC-MS investigations of spontaneous reactions of the two chalcones at three different pH values revealed that the compounds have similar reactivities. Furthermore, comparison of the composition of the equilibrium mixtures revealed the importance of the electronic effect of the 4-substituent on the stability of the enolate intermediates.

HPLC analysis of the incubation mixtures of **1** and **2** with NAC demonstrated different stereochemistry of the addition of the protonated and non-protonated thiol nucleophile onto the enone moiety. The results provided further support for the dominant conformation-derived diastereoselective addition of the protonated thiols onto the chalcones' polar carbon–carbon double bond.

We could not find a direct correlation of the thiol reactivities and the previously published biological (cancer cell cytotoxic) effects of chalcones **1** and **2**. It is reasonable to suppose that both thiol reactivities and lipophilic properties contributed to the reported biological effects of the investigated compounds and their cyclic analogues.

Supplementary Materials: The following are available: Table S1. Mass spectrometry data; Figure S1. Change in the chromatographic peak area of adduct 1 of chalcones **1** and **2** in the chalcone–GSH incubations at pH 8.0/8.5. Figure S2. Change in the chromatographic peak area of adduct 1 of chalcones **1** and **2** in the chalcone–GSH incubations at pH 6.3/6.8. Figure S3. Change in the chromatographic peak area of adduct 1 of chalcones **1** and **2** in the chalcone–NAC incubations at pH 6.3/6.8. Figure S4. Change in the chromatographic peak area of adduct 2 of chalcones **1** and **2** in the chalcone–NAC incubations at pH 6.3/6.8. Figure S5. Change in the chromatographic peak area of chalcones **1** and **2** in the chalcone–GSH incubations at pH 3.2/3.7. Figure S6. Change in the chromatographic peak area of chalcones **1** and **2** in the chalcone–NAC incubations at pH 3.2/3.7. Figure S7. Change in the chromatographic peak area of adduct 1 of chalcones **1** and **2** in the chalcone–GSH incubations at pH 3.2/3.7. Figure S8. Change in the chromatographic peak area of adduct 1 of chalcones **1** and **2** in the chalcone–NAC incubations at pH 3.2/3.7. Figure S9. Change in the chromatographic peak area of adduct 2 of chalcones **1** and **2** in the chalcone–NAC incubations at pH 3.2/3.7. Figure S10. High-resolution, positive-mode HESI MS spectrum of chalcone **1**. Figure S11. High-resolution, positive-mode HESI MS spectrum of chalcone **2**. Figure S12. High-resolution, positive-mode HESI MS spectrum of chalcone **1**–GSH conjugate. Figure S13. High-resolution, negative-mode HESI MS spectrum of chalcone **1**–NAC conjugate. Figure S14. High-resolution, positive-mode HESI MS spectrum of chalcone **2**–GSH conjugate. Figure S15. High-resolution, negative-mode HESI MS spectrum of chalcone **2**–NAC conjugate. Figure S16. HPLC-UV-VIS spectrum of (*E*)(t_R 16.354 min)/(*Z*)(t_r 16.128 min) isomeric mixture of chalcone **1**. Figure S17. HPLC-UV-VIS spectrum of (*E*)(t_R 15.607 min)/(*Z*)(t_r 15.855 min) isomeric mixture of chalcone **2**. Figure S18. HPLC-UV-VIS chromatogram of pH 8.0/8.5 incubation (315 min time point) of chalcone **1** and NAC. Figure S19. HPLC-UV-VIS chromatogram of pH 6.3/6.8 incubation (315 min time point) of chalcone **1** and NAC. Figure S20. HPLC-UV-VIS chromatogram of pH 3.2/3.7 incubation (315 min time point) of chalcone **1** and NAC. Figure S21. HPLC-UV-VIS chromatogram of pH 8.0/8.5 incubation (315 min time point) of chalcone **2** and NAC. Figure S22. HPLC-UV-VIS chromatogram of pH 6.3/6.8 incubation (315 min time point) of chalcone **2** and NAC. Figure S23. HPLC-UV-VIS chromatogram of pH 3.2/3.7 incubation (315 min time point) of chalcone **2** and NAC.

Author Contributions: Conceptualization, P.P.; methodology, P.P., F.K. and S.M.; formal analysis, F.K. and S.M.; writing—original draft preparation, P.P., F.K. and S.M.; writing—review and editing, P.P. All authors have read and agreed to the published version of the manuscript.

Funding: This research was funded by the EFOP Operational Program "Comprehensive Development for Implementing Smart Specialization Strategies" at the University of Pécs (grant no. EFOP-3.6.1-16-2016-00004).

Institutional Review Board Statement: Not applicable.

Informed Consent Statement: Not applicable.

Data Availability Statement: Not applicable.

Conflicts of Interest: The authors declare no conflict of interest.

Sample Availability: Samples of the compounds **1** and **2** are available from the authors.

References

1. Rozmer, Z.; Perjési, P. Naturally occurring chalcones and their biological activities. *Phytochem. Rev.* **2016**, *15*, 87–120. [CrossRef]
2. Gomes, M.N.; Muratov, E.N.; Pereira, M.; Peixoto, J.C.; Rosseto, L.P.; Cravo, P.V.L.; Andrade, C.H.; Neves, B.J. Chalcone derivatives: Promising starting points for drug design. *Molecules* **2017**, *22*, 1210. [CrossRef]
3. Zhou, B. Diverse molecular targets for chalcones with varied bioactivities. *Med. Chem.* **2015**, *5*, 388–404. [CrossRef]
4. Mahapatra, D.K.; Bharti, S.K.; Asati, V. Chalcone derivatives: Anti-inflammatory potential and molecular targets perspectives. *Curr. Top. Med. Chem.* **2017**, *17*, 3146–3169. [CrossRef]
5. Orlikova, B.; Tasdemir, D.; Golais, F.; Dicato, M.; Diederich, M. Dietary chalcones with chemopreventive and chemotherapeutic potential. *Genes Nutr.* **2011**, *6*, 125–147. [CrossRef]
6. Amslinger, S.; Al-Rifai, N.; Winter, K.; Wörmann, K.; Scholz, R.; Baumeister, P.; Wild, M. Reactivity assessment of chalcones by a kinetic thiol assay. *Org. Biomol. Chem.* **2013**, *11*, 549–554. [CrossRef]
7. Al-Rifai, N.; Rücker, H.; Amslinger, S. Opening or closing the lock? when reactivity is the key to biological activity. *Chem. Eur. J.* **2013**, *19*, 15384–15395. [CrossRef]
8. Zhuang, C.; Zhang, W.; Sheng, C.; Zhang, W.; Xing, C.; Miao, Z. Chalcone: A privileged structure in medicinal chemistry. *Chem. Rev.* **2017**, *117*, 7762–7810. [CrossRef]
9. Dinkova-Kostova, A.T.; Holtzclaw, W.D.; Cole, R.N.; Itoh, K.; Wakabayashi, N.; Katoh, Y.; Yamamoto, M.; Talalay, P. Direct Evidence That sulfhydryl groups of keap1 are the sensors regulating induction of phase 2 enzymes that protect against carcinogens and oxidants. *Proc. Natl. Acad. Sci. USA* **2002**, *99*, 11908–11913. [CrossRef]
10. Nasir Abbas Bukhari, S.; Jantan, I.; Jasamai, M. Anti-inflammatory trends of 1, 3-diphenyl-2-propen-1-one derivatives. *Mini Rev. Med. Chem.* **2012**, *13*, 87–94. [CrossRef]
11. Wang, J.; Wang, S.; Song, D.; Zhao, D.; Sha, Y.; Jiang, Y.; Jing, Y.; Cheng, M. Chalcone derivatives inhibit glutathione S-transferase P1-1 activity: Insights into the interaction mode of α, β-unsaturated carbonyl compounds. *Chem. Biol. Drug Des.* **2009**, *73*, 511–514. [CrossRef]
12. Jin, Y.L.; Jin, X.Y.; Jin, F.; Sohn, D.H.; Kim, H.S. Structure activity relationship studies of anti-inflammatory TMMC derivatives: 4-dimethylamino group on the B ring responsible for lowering the potency. *Arch. Pharm. Res.* **2009**, *31*, 1145. [CrossRef]
13. Dinkova-Kostova, A.T.; Massiah, M.A.; Bozak, R.E.; Hicks, R.J.; Talalay, P. Potency of michael reaction acceptors as inducers of enzymes that protect against carcinogenesis depends on their reactivity with sulfhydryl groups. *Proc. Natl. Acad. Sci. USA* **2001**, *98*, 3404–3409. [CrossRef] [PubMed]
14. Groitl, B.; Jakob, U. Thiol-based redox switches. *Biochim. Biophys. Acta* **2014**, *1844*, 1335–1343. [CrossRef] [PubMed]
15. Jackson, P.A.; Widen, J.C.; Harki, D.A.; Brummond, K.M. Covalent modifiers: A chemical perspective on the reactivity of α,β-unsaturated carbonyls with thiols via hetero-michael addition reactions. *J. Med. Chem.* **2017**, *60*, 839–885. [CrossRef] [PubMed]
16. Poole, L.B. The basics of thiols and cysteines in redox biology and chemistry. *Free Radic. Biol. Med.* **2015**, *80*, 148–157. [CrossRef]
17. Samuni, Y.; Goldstein, S.; Dean, O.M.; Berk, M. The chemistry and biological activities of N-acetylcysteine. *Biochim. Biophys. Acta* **2013**, *1830*, 4117–4129. [CrossRef] [PubMed]
18. Aldini, G.; Altomare, A.; Baron, G.; Vistoli, G.; Carini, M.; Borsani, L.; Sergio, F. N-acetylcysteine as an antioxidant and disulphide breaking agent: The reasons why. *Free Radic. Res.* **2018**, *52*, 751–762. [CrossRef]
19. Roos, G.; Foloppe, N.; Messens, J. Understanding the pK(a) of redox cysteines: The key role of hydrogen bonding. *Antioxid. Redox Signal.* **2013**, *18*, 94–127. [CrossRef]
20. Shibata, S. Anti-tumorigenic chalcones. *Stem Cells* **1994**, *12*, 44–52. [CrossRef]
21. Drutovic, D.; Chripkova, M.; Pilatova, M.; Kruzliak, P.; Pal Perjesi, P.; Sarissky, M.; Lupi, M.; Damia, G.; Broggini, M.; Mojzis, J. Benzylidenetetralones, cyclic chalcone analogues, induce cell cycle arrest and apoptosis in HCT116 colorectal cancer cells. *Tumor Biol.* **2014**, *35*, 9967–9975. [CrossRef]
22. Dimmock, J.R.; Elias, D.W.; Beazely, M.A.; Kandepu, N.M. Bioactivities of chalcones. *Curr. Med. Chem.* **1999**, *6*, 1125–1149.
23. Dimmock, J.R.; Kandepu, N.M.; Nazarali, A.J.; Kowalchuk, T.P.; Motaganahalli, N.; Quail, J.W.; Mykytiuk, P.A.; Audette, G.F.; Prasad, L.; Perjési, P.; et al. Conformational and quantitative structure−activity relationship study of cytotoxic 2-arylidenebenzocycloalkanones. *J. Med. Chem.* **1999**, *42*, 1358–1366. [CrossRef]
24. Rozmer, Z.; Berki, T.; Maász, G.; Perjési, P. Different effects of two cyclic chalcone analogues on redox status of jurkat T cells. *Toxicol. In Vitro* **2014**, *28*, 1359–1365. [CrossRef]
25. Noyce, D.S.; Jorgenson, M. Jefraim. Carbonyl reactions. XIX. The basicities of substituted chalcones. *J. Am. Chem. Soc.* **1962**, *84*, 4312–4319. [CrossRef]
26. Bernasconi, C.R. Nucleophilic addition to olefins. Kinetics and mechanism. *Tetrahedron* **1989**, *45*, 4017–4090. [CrossRef]
27. Bernardes, A.; Pérez, C.; Mayer, M.; da Silva, C.; Martins, F.; Perjési, P. Study of reactions of two mannich bases derived of 4′-hydroxychalcones with glutathione by RP-TLC, RP-HPLC and RP-HPLC-ESI-MS analysis. *J. Braz. Chem. Soc.* **2017**, *28*, 1048–1062. [CrossRef]

28. Bernardes, A.; D'Oliveira, G.D.C.; Silezin, A.; Kuzma, M.; Molnár, S.; Noda Pérez, C.; Perjési, P. Reagent-induced asymmetric induction in addition reaction of reduced glutathione onto bis-mannich chalcones. *Arch. Pharm.* **2018**, *351*, 1700386. [CrossRef]
29. Caccuri, A.M.; Antonini, G.; Board, P.G.; Parker, M.W.; Nicotra, M.; Bello, M.L.; Federici, G.; Ricci, G. Proton release on binding of glutathione to alpha, mu and delta class glutathione transferases. *Biochem. J.* **1999**, *344*, 419–425. [CrossRef] [PubMed]
30. Rohani, N.; Hao, L.; Alexis, M.; Joughin, B.; Krismer, K.; Moufarrej, M.; Soltis, A.; Lauffenburger, D.; Yaffe, M.; Burge, C.; et al. Acidification of tumor at stromal boundaries drives transcriptome alterations associated with aggressive phenotypes. *Cancer Res.* **2019**, *79*, 1952–1966. [CrossRef] [PubMed]
31. Perjési, P. (E)-2-benzylidenebenzocyclanones: Part XIII—(E)/(Z)-isomerization of some cyclic chalcone analogues. Effect of ring size on lipophilicity of geometric isomers. *Monatsh. Chem. Chem. Mon.* **2015**, *146*, 1275–1281. [CrossRef]
32. LoPachin, R.M.; Gavin, T. Reactions of electrophiles with nucleophilic thiolate sites: Relevance to pathophysiological mechanisms and remediation. *Free Radic. Res.* **2016**, *50*, 195–205. [CrossRef] [PubMed]
33. Perjési, P.; Linnanto, J.; Kolehmainen, E.; Ősz, E.; Virtanen, E. E-2-benzylidenebenzocycloalkanones. IV. Studies on transmission of substituent effects on ^{13}C NMR chemical shifts of E-2-(X-benzylidene)-1-tetralones, and -benzosuberones. Comparison with the ^{13}C NMR data of chalcones and E-2-(X-benzylidene)-1-indanones. *J. Mol. Struct.* **2005**, *740*, 81–89. [CrossRef]
34. Allen, C.F.H.; Humphlett, W.J. The thermal reversibility of the michael reaction V. The effect of the structure of certain thiol adducts on cleavage. *Can. J. Chem.* **1966**, *44*, 2315–2321. [CrossRef]
35. d'Oliveira, G.D.C.; Custodio, J.M.F.; Moura, A.F.; Napolitano, H.B.; Pérez, C.N.; Moraes, M.O.; Prókai, L.; Perjési, P. Different reactivity to glutathione but similar tumor cell toxicity of chalcones and their quinolinone analogues. *Med. Chem. Res.* **2019**, *28*, 1448–1460. [CrossRef]
36. De Freitas Silva, M.; Pruccoli, L.; Morroni, F.; Sita, G.; Seghetti, F.; Viegas Jr, C.; Tarozzi, A. The keap1/Nrf2-ARE pathway as a pharmacological target for chalcones. *Molecules* **2018**, *23*, 1803. [CrossRef] [PubMed]
37. Kozurkova, M.; Tomeckova, V. Interaction of chalcone derivatives with important biomacromolecules. In *Chalcones and Their Synthetic Analogs*; Perjési, P., Ed.; Nova Science Publisher: New York, NY, USA, 2020; pp. 95–133.
38. Katsori, A.-M.; Hadjipavlou-Litina, D. Chalcones in cancer: Understanding their role in terms of QSAR. *Curr. Med. Chem.* **2009**, *16*, 1062–1081. [CrossRef] [PubMed]
39. Rozmer, Z.; Perjési, P.; Takács-Novák, K. Use of RP-TLC for determination of log P of isomeric chalcones and cyclic chalcone analogues. *JPC Mod. TLC* **2006**, *19*, 124–128. [CrossRef]
40. Perjési, P.; Földesi, A.; Szabó, D. Synthesis of 4,6-diaryl-2,3-dihydro-6H-1,3-thiazine-2-thiones by the reaction of chalcones with dithiocarbamic acid. *Acta Chim. Hung.* **1986**, *122*, 119–125. [CrossRef]

J Pharm Biopharm Res, 2023, 4(2): 326-339
DOI: 10.25082/JPBR.2022.02.004

RESEARCH ARTICLE

(*E*)-2-Benzylidenecyclanones: Part XVII [1]. An LC-MS study of microsomal transformation reactions of (*E*)-2-[(4'-methoxyphenyl)methylene]-benzosuberon -1-one: A cyclic chalcone analog

Fatemeh Kenari[1] **Szilárd Molnár**[2] **Zoltán Pintér**[1] **Sobhan Bitaraf**[1] **Pál Perjési**[1*]

[1] Institute of Pharmaceutical Chemistry, University of Pécs, H-7624, Pécs, Hungary
[2] Research Institute for Viticulture and Oenology, University of Pécs, H-7634, Hungary

Correspondence to: Pál Perjési, Institute of Pharmaceutical Chemistry, University of Pécs, H-7624, Pécs, Hungary; Email: pal.perjesi@gytk.pte.hu

Received: January 18, 2023;
Accepted: March 18, 2023;
Published: March 22, 2023.

Citation: Kenari F, Molnár S, Pintér Z, *et al*. (*E*)-2-Benzylidenecyclanones: Part XVII. An LC-MS study of microsomal transformation reactions of (*E*)-2-[(4'-methoxyphenyl)methylene]-benzosuberon-1-one: A cyclic chalcone analog. *J Pharm Biopharm Res*, 2023, **4**(2): 326-339.
https://doi.org/10.25082/JPBR.2022.02.004

Abstract: Biotransformation of the antiproliferative (*E*)-2-[(4'-methoxyphenyl)methylene]-benzosuberon-1-one (**2c**) was studied using rat liver microsomes. As a result of the CYP-catalyzed transformations, one monooxygenated (**2c+O**) and the demethylated (**2c-CH$_2$**) metabolites were identified by HPLC-MS. (*E*)-2-[(4'-methoxyphenyl)methylene]-benzosuberon-1-ol, the expected product of rat liver microsomal carbonyl reductase, was not found in the incubates. Microsomal GST-catalyzed reaction of the compound resulted in formation of diastereomeric GST-conjugates. Under the present HPLC conditions, the diastereomeric adducts were separated into two chromatographic peaks (**2c-GSH-1** and **2c-GSH-2**).

Keywords: chalcone, benzosuberone, microsome, CYP, chalcone reductase, glutathione, microsomal glutathione transferase

1 Introduction

Chalcones (Figure 1) are intermediary compounds of the biosynthetic pathway of a very large and widespread group of plant constituents known collectively as flavonoids [2]. Among the naturally occurring chalcones and their synthetic analogs, several compounds displayed cytotoxic (cell growth inhibitor) activity toward cultured tumor cells. Chalcones are also effective *in vivo* as cell proliferating inhibitors, antitumor promoting, anti-inflammatory and chemopreventive agents [3–5]. The chalcone structure can be divided into three structural units; the aromatic rings A and B and the propenone linker. Modifying any of them can tune the main feature of interactions of the synthetic chalcones towards the non-covalent or the covalent pathway.

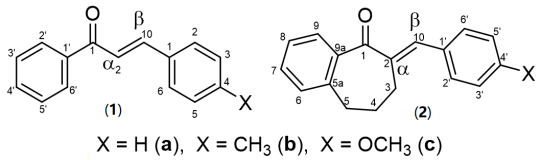

Figure 1 Structure and numbering of 4-X-chalcones (**1**) and (*E*)-2-[(4'methoxyphenyl) methylene]-1-benzosuberones (**2**)

In our previous studies, we have investigated how the substitution of the B-ring and the ring size (n = 0, 5, 6, 7) of some cyclic chalcone analogs affect their cancer cell cytotoxic effect [6–8]. Comparison of the average IC$_{50}$ values of the series, the benzosuberone (n = 7) (**2**) analogs (Figure 1) displayed the most prosperous data against the investigated murine and human tumor cell lines. In particular, the (*E*)-2-[(4-methoxyphenyl)methylene]-1-benzosuberone (**2c**) had the most remarkable cytotoxicity [6, 7].

In consecutive publications, we have performed cell cycle analysis of Jurkat cells exposed to equitoxic doses of **2c** and its methyl-substituted counterpart **2b**. Compound **2c** showed to cause an immediate G1 lift and G2/M arrest, followed by hypoploidity and aneuploidy. Such a remarkable effect of **2b** on the G1 and G2 checkpoints could not be observed [9, 10]. TLC and HPLC analysis showed the compounds to have intrinsic reactivity towards GSH [9, 11]. However, the two compounds had different effects on the thiol status of the cells. Compound **2c** significantly increased the oxidized glutathione (GSSG) level. On the contrary, **2b** increased the GSH level, indicating enhanced cellular antioxidant potency [12].

Although chalcones are a family of compounds with several beneficial biological activities, a limited number of metabolism studies of the compounds can be found in the literature.

Microsomal oxidation of chalcone and *(E)*-4-phenyl-3-buten-2-one, for example, resulted in the formation of aromatic hydroxylated metabolites [13]. In another publication of the research group, microsomal reduction of the carbonyl function of the compound was reported [14]. Incubation of the chemoprevention agent licochalcone A with human liver microsomes also resulted in oxygenated Phase I metabolites [15]. Similar results were obtained while investigating 8-prenylnaringenin [16].

In an earlier publication, we reported intestinal elimination and Phase 2 metabolism of 4'-hydroxy-4-methoxychalcone and its bis-Mannich analog in the rat. HPLC-MS analysis of the perfusates indicated the presence of glucuronide, sulfate, and glutathione conjugates of the parent molecules [17]. To compare GSH reactivity, two bis-Mannich bases of two 4'-hydroxychalcones were synthesized and reacted with GSH under non-cellular conditions. At pH values below 8.0, the two bis-Mannich bases showed higher GSH reactivity than two 4'-hydroxychalcones [18].

Previously demonstrated intrinsic reactivity of **2b** and **2c** towards GSH [9, 11] might play a role in their cancer cell cytotoxic effects. Oxidation of GSH to GSSG or chemical modification of the SH group of the tripeptide causes a change in the redox potential of the GSSG/2GSH system. Previously, a correlation has been found between the cell cycle, the condition of the cell (stressed, apoptotic, etc.), and the GSSG/2GSH ratio. For instance, in cell proliferation (E_{hc} = ˜-240 mV), in cell differentiation (E_{hc} = ˜-200 mV), and in apoptosis (E_{hc} = ˜-170 mV), which can be applicable for a better understanding of oxidative stress [19, 20]. Thus, changes in the GSSG/2GSH ratio are fundamental in controlling signal transduction that supports cell cycle regulation and other cellular processes [21, 22].

To investigate if **2b** and **2c** or their reactive metabolites react with thiols under cellular conditions, microsomal incubation of the compounds in the presence of reduced glutathione (GSH) was performed. The incubations were analyzed for the expected derivatives by HPLC-UV and HPLC-MS methods.

Microsomes are fragments of endoplasmic reticulum and attached ribosomes that are isolated together when homogenized cells are centrifuged. Microsomal enzymes are typically found in the smooth endoplasmic reticulum, primarily in the liver, but also in the kidney, intestinal mucosa, and lung. There are several microsomal enzymes, including flavin monooxygenases (FMO), cytochrome P450s (CYP), NADPH cytochrome c reductase, UDP glucuronyl transferases (UGT), glutathione-S-transferases (GST), epoxide hydrolases, among others. Hence, hepatic microsomes are commonly used to study the metabolic fate of drugs, as the liver is one of the major organs responsible for enzymatic drug elimination [23].

2 Materials and methods

2.1 Chemicals and reagents

(*E*)-2-[(4-methoxyphenyl)methylene]-1-benzosuberone (**2c**) was synthesized as previously published [6]. Its structure was characterized by IR and NMR spectroscopy [24]. The purity and structures of the investigated sample were verified by HPLC-MS (Figure 2 and 3). Male rat pooled liver microsome 10 mg, magnesium chloride, 25mm syringe filters nylon membrane, pore size 0.45 μm, and ß-nicotinamide adenine dinucleotide 2'-phosphate reduced tetrasodium salt hydrate (NADPH) were purchased from Sigma Aldrich (Budapest, Hungary). Alamethicin and reduced L-glutathione were obtained from Cayman Chemicals and ITW reagents. Methanol CHROMASOLV HPLC grade was obtained from Honeywell (Hungary). Trifluoroacetic acid was obtained from VWR (Budapest, Hungary), and formic acid from Fischer Chemicals (Budapest, Hungary). Deionized water for use in HPLC and HPLC-MS measurements was purified by Millipore Direct-QTM at the Institute of Pharmaceutical Chemistry (University of Pécs). Phosphate buffered Saline (PBS) pH 7.4 was prepared freshly on the day of incubation based on the 2014 Cold Spring Harbor Laboratory press method [25]. Mobile phases used for HPLC measurements were degassed by an ultrasonic water bath before use.

2.2 Light-initiated isomerization of 2c

Freshly prepared 6.5 $\times$ 10^{-3} M solution of **2c** in HPLC-grade methanol was subjected to scattered laboratory light for one week. The solution was analyzed by HPLC-UV and HPLC-MS.

2.3 Microsomal incubations

490μL PBS was mixed with 50μL of rat liver microsome (20 mg/mL protein) and 10 μL of alamethicin in methanol (50 μg/mg protein) and was left on ice for 15 minutes for microsomal activation. Then 100μL of NADPH solution (2.0 μmol/mL final concentration) was added, and the solution vortexed to mix well. 25μL of a freshly prepared acetonitrile solution of **2c**

(final concentration 0.25 μmol/mL) and 100μL of $MgCl_2$ solution (final concentration of 5.0 μmol/mL) were added. After each addition, the solution was vortexed. The incubation volume was set to a total of 980 μL by the addition of 205 μL of PBS and left in a 37°C water bath for 3 minutes. Then 20 μL of GSH solution in PBS (final concentration of 5.0 μmol/mL) was added to bring the final volume to 1.0 mL. The mixture was vortex mixed for 10 seconds, taken to a shaking water bath, and kept in it for the incubation period (120 minutes). 150 μL samples were taken at 0, 15, 30, 60, and 90-minute timepoints. (The 0-minute points were considered the time of placement of the incubates into the water bath.) 150 μL ice-cold methanol was used to stop the reaction at each time point. The 300 μL sample was centrifuged at 6000 rpm for 5 min; the supernatant was collected using a syringe and passed through a 0.45μm nylon membrane syringe filter. Control incubation containing all the constituents except the liver microsome was analyzed at 0, 30, 60, and 90-minute time points.

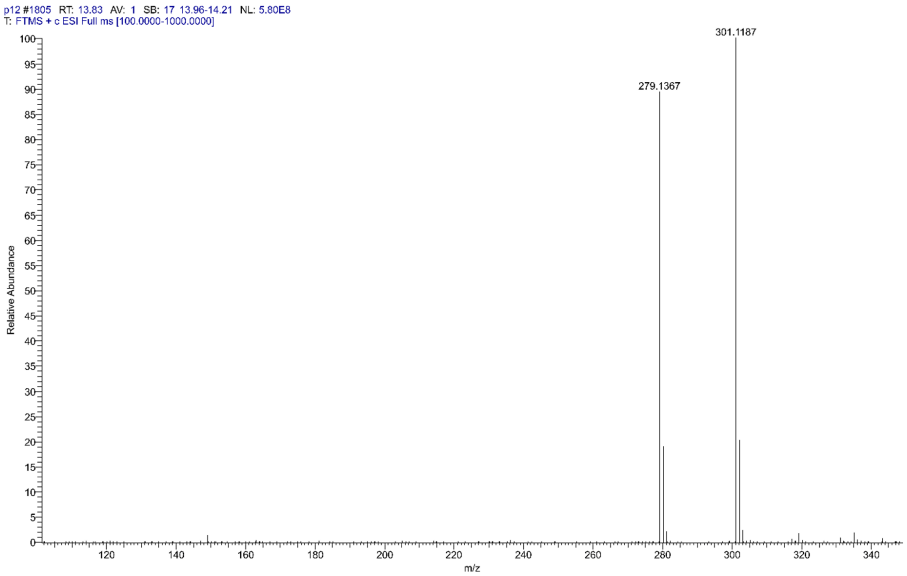

Figure 2 High resolution, positive mode HESI MS spectrum of (*E*)-2-[(4-methoxyphenyl) methylene]-1-benzosuberone (**2c**). (Protonated m/z 279.1367 and Na^+-adduct m/z 301.1187).

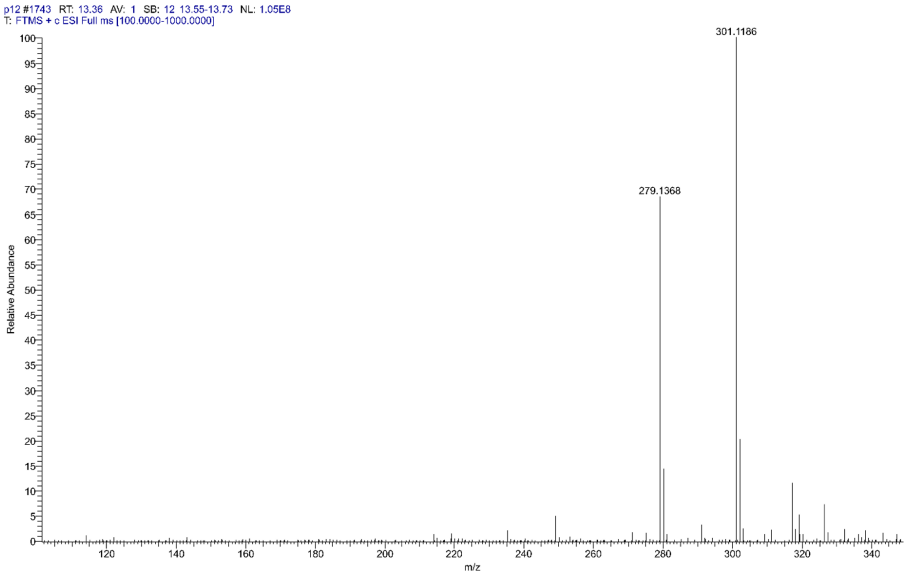

Figure 3 High resolution, positive mode HESI MS spectrum of (*Z*)-2-[(4-methoxyphenyl) methylene]-1-benzosuberone (**2c**). (Protonated m/z 279.1368 and Na^+-adduct m/z 301.1186).

2.4 HPLC-UV-MS measurements

HPLC-UV-ESI-MS analyses were performed on an Ultimate 3000 liquid chromatograph (Dionex, Sunnyvale, CA, USA) coupled with a Thermo Q Exactive Focus quadrupole-Orbitrap hybrid mass spectrometer (Thermo Fisher Scientific, Waltham, MA, USA). The scan monitored *m/z* values ranging from 100 to 1000 Da. Data acquisition was carried out using Q Exactive Focus 2.1 and Xcalibur 4.2 software (Thermo Fisher Scientific). Analysis of compounds and adducts was performed in HESI positive and negative ionization modes with the following parameters: spray voltage, 3500 V; vaporizer temperature, 300 °C; capillary temperature, 350 °C; spray and auxiliary gas flows, 30 and 10 arbitrary units, respectively; resolution, 35,000 at 200 *m/z*.

The parameters of the gradient were (A) water and 0.1% formic acid and (B) methanol and 0.1% formic acid. The gradient elution was as follows: isocratic elution for 1 min to 10% eluent B, continued by a linear gradient to 95% in 13 min, followed by an isocratic plateau for 3 min. Finally, the column was equilibrated to 10% in 0.1 min and continued isocratically for 2.9 min. The sampler was at room temperature, and the column oven was at 40 °C. The diode array detector was also set at 260, 280, 300, and 350 nm wavelength alongside MS analysis.

3 Results and discussion

Cytotoxic (antimitotic, cell growth inhibitor) effects of α,β-unsaturated carbonyl compounds are frequently associated with their expected reactivity with the essential thiol groups in living organisms [3–5, 26, 27]. Such a reaction can alter intracellular redox status (redox signaling), which can modulate events such as DNA synthesis, enzyme activation, selective gene expression, and cell cycle regulation [28, 29]. Several biological effects (e.g., NQO1 inducer [30], anti-inflammatory [31], GST P1-1 inhibitory [32]) of chalcones have been associated with their Michael-type reactivity towards reduced glutathione.

Microsomal incubation of **2c** was performed using alamethicin-activated rat liver microsomes. Alamethicin is a peptide antibiotic that forms voltage-dependent channels in the lipid bilayers by oligomerizing various alamethicin molecules [33]. The effect of alamethicin on the implementation rate for in vitro glucuronidation was previously studied by several authors [34–36]. It was found that alamethicin leads to an increase in metabolite formation. The authors assumed that the alamethicin forms a channel through the microsomal (endoplasmic reticulum) membranes, and the substrates may diffuse more easily into and through it. Accordingly, the formation of Phase 2 metabolites (such as glucuronides) is enhanced. Further studies showed that using alamethicin as an activator does not affect the microsomal CYP activities [37, 38].

In the first three minutes of the experiments, **2c** were incubated with rat liver microsomes in the presence of alamethicin. Since the parent compound does not have hydroxyl substituent, only the oxidation and reduction reactions were expected over this period. Then, GSH was added to the mixtures. From then on, reaction with GSH of the parent compound and its possible oxidative metabolites could also occur. These latter derivatives could be formed in spontaneous or GST-catalyzed reactions.

In earlier work, the non-enzyme-catalyzed reaction of **2c** with GSH was investigated by HPLC-UV. In that reaction, formation of four diastereomeric adducts was expected (Figure 4). Two of them result from a *cis*-, and another two from a *trans*-addition of GSH onto the carbon-carbon double bond. Under the used HPLC conditions, however, only two separated peaks appeared in the chromatograms. The separated peaks were tentatively assigned to the *cis*- and the *trans*-adducts [11].

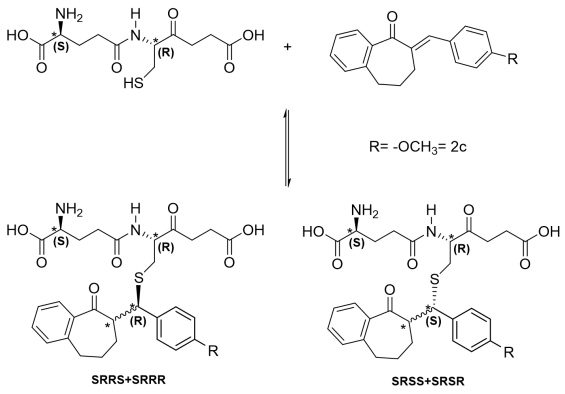

Figure 4 Structure and stereochemistry of the **2c-GSH** adducts

HPLC-MS investigation of the control incubates (without adding microsomes) indicated formation of the expected **2c-GSH** adducts (Table 1). Under the present chromatographic conditions, similar to the previous results, two separated chalcone-GSH peeks appeared in the chromatograms (Figure 5 lower panel). The structure of the **2c-GSH**-adducts (**2c-GSH-1** and **2c-GSH-2**) was verified by positive mode HR-MS (Figure 6 and 7).

Table 1 HPLC-MS peak areas (AUCs) of the **2c** and the **2c-GSH** isomeric peak as a function of incubation time

Sample	Area **2c-GSH**-1	Area **2c-GSH-2**	Area **2c-GSH-1** + **2c-GSH-2**	Area (***Z***)**-2c**	Area (***E***)**-2c**
Microsomal incubation (0 min)	2,210,842	4,293,434	6,504,276	856,426,548	8,297,984,438
Microsomal incubation (30 min)	22,983,588	32,617,903	55,601,491	966,438,207	4,610,557,010
Microsomal incubation (60 min)	22,454,721	29,934,874	52,389,595	524,872,308	2,750,174,832
Microsomal incubation (90 min)	50,714,479	61,666,740	112,381,219	550,348,953	3,815,982,269
Control (0 min)	1,466,946	2,493,046	3,959,992	495,826,994	4,093,677,464
Control (30 min)	1,396,532	1,181,043	2,577,575	138,997,108	1,308,801,409
Control (60 min)	9,585,848	5,960,060	15,545,908	161,346,308	1,305,287,139
Control (90 min)	18,724,489	12,017,553	30,742,042	299,494,818	2,215,039,743

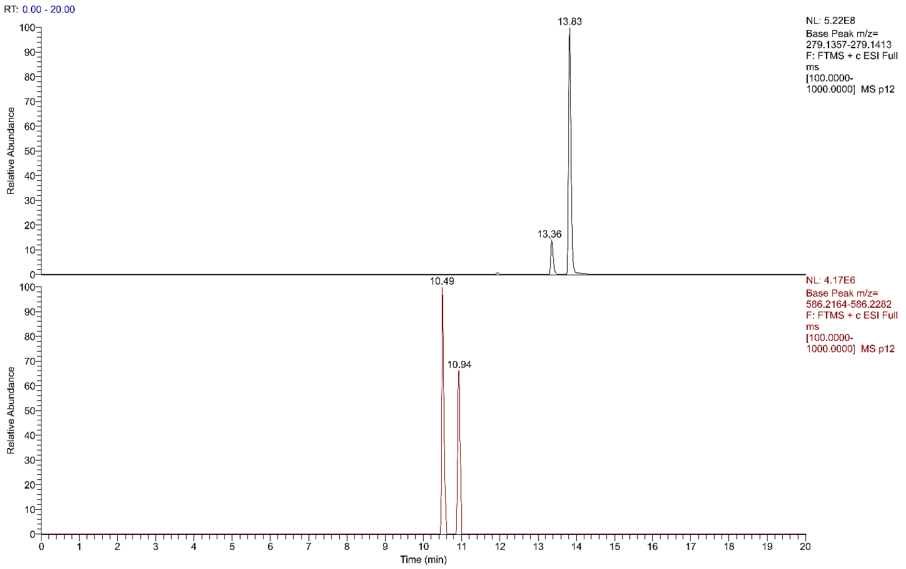

Figure 5 High resolution, positive mode HESI MS chromatogram of (*E*)-2-[(4-methoxyphenyl)methylene]-1-benzosuberone (**2c**) control incubate (90-minute sample). Upper panel: t_r 13.36 min: (*Z*)-2-[(4-methoxyphenyl)methylene]-1-benzo suberone; t_r 13.83 min: (*E*)-2-[(4-methoxyphenyl)methylene]-1-benzosuberone. Lower panel: **2c-GSH-1**: 10.49 min.; **2c-GSH-2**: 10.94 min.

Besides the GSH conjugates, formation of the respected (*Z*)-isomer of the parent **(*E*)-2c** was observed. Since the reaction mixtures were kept in the dark, the formation of the **(*Z*)-2c** can only be explained due to the retro-Michael reaction of the formed adducts [39]. The structure of the **(*E*)-2c** and **(*Z*)-2c** was verified based on the positive mode HR-MS of the isomeric mixture obtained by light isomerization f the pure **(*E*)-2c** (Figure 3).

Similar HPLC-MS analysis of the microsomal incubates also indicated formation of the **(*Z*)-2c** and the diastereomeric **2c-GSH** adducts (Figure 8). The mass spectra of the compounds formed in the microsomal incubations are shown in Figure 9-11. The sum of the AUC of the two diastereomeric **2c-GSH** peaks was higher at each timepoint than in the respective control incubate (Table 1). Although the ionization response factors of the four diastereomers are not known, the significant differences between the AUCs measured in the control and the microsomal incubates strongly support that the alamethicin-activated microsomes accelerate the chalcone-GSH conjugation reaction (Table 1). Since compound **2c** is a relatively lipophilic chalcone analog [40], it could be the substrate of both the microsomal glutathione transferases (MGSTs) [41–44] and the so-called microsome-associated GST enzymes. These latter GST forms are associated with the outer microsomal membranes, and their characteristics resemble those of the cytosolic GSTs [45].

Over the first 60 minutes of the incubation period, the total AUC of **2c-GSH** was only slightly changed (Table 1). However, by the end of the incubation, much higher AUC peak values of

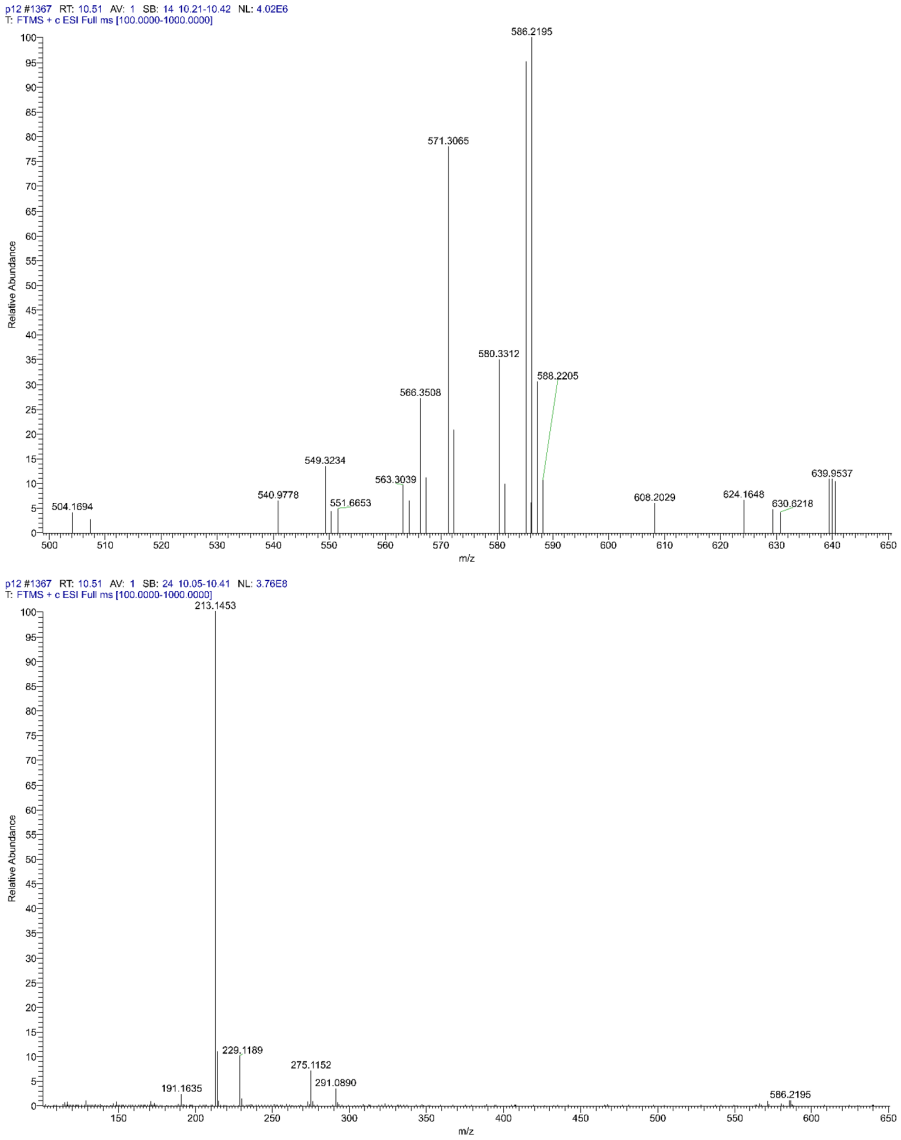

Figure 6 High resolution, positive mode HESI MS spectrum of the **2c-GSH-1** conjugate formed in the 90-minute sample of the control incubate (m/z 586.2195).

the **2c-GSH** conjugates could be observed (Table 2). On longer incubation times, dissolution of **2c** and GSH into the microsomal (ER) membranes can occur. There they can bind to the overlapping hydrophobic and the GSH binding sites of the MSGT enzymes [46]. In parallel, the added GSH can react with the enzyme's Cys49 sensor, resulting in its activation [47]. On activation of the MSGT enzymes, the reaction rate between the **2c** and GSH increased.

Liver microsomes are rich in cytochrome P450 enzymes. CYPs are located in the smooth endoplasmic reticulum membrane of cells. Thus, they can be recovered in microsomal fractions. Microsomal P450 families 1-3 play a major role in the metabolism of the majority of pharmaceuticals and a large number of other lipophilic xenobiotics [48]. CYP enzymes preferentially incorporate one of the oxygen atoms of molecular oxygen at one of the carbon atoms of the target molecule. Accordingly, chalcone **2c** possesses several possible primary sites for CYP-catalyzed oxidation.

In analysis of the total ion MS spectrum of the microsomal incubates, two products were found whose formation can be explained by CYP-catalyzed reactions: an oxygenated **2c (2c+O)** (Figure 12 and 13) and the demethylated derivative (**2c-CH$_2$**) (Figure 14 and 15). The AUC of both peaks increased over the incubation time (Table 2). The exact structure of the formed oxygenated metabolite needs further investigation. Lack of formation of a GSH-adduct of the possible epoxide metabolite, however, it is reasonable to suppose that the formed oxygenated metabolite is a hydroxyl derivative of **2c**. The demethylation reaction of **2c** resulted in the respective 4'-OH derivative (Figure 16).

Earlier studies on the 4'-OH-metabolite (**2c-CH$_2$**) showed the compound to have a pro-

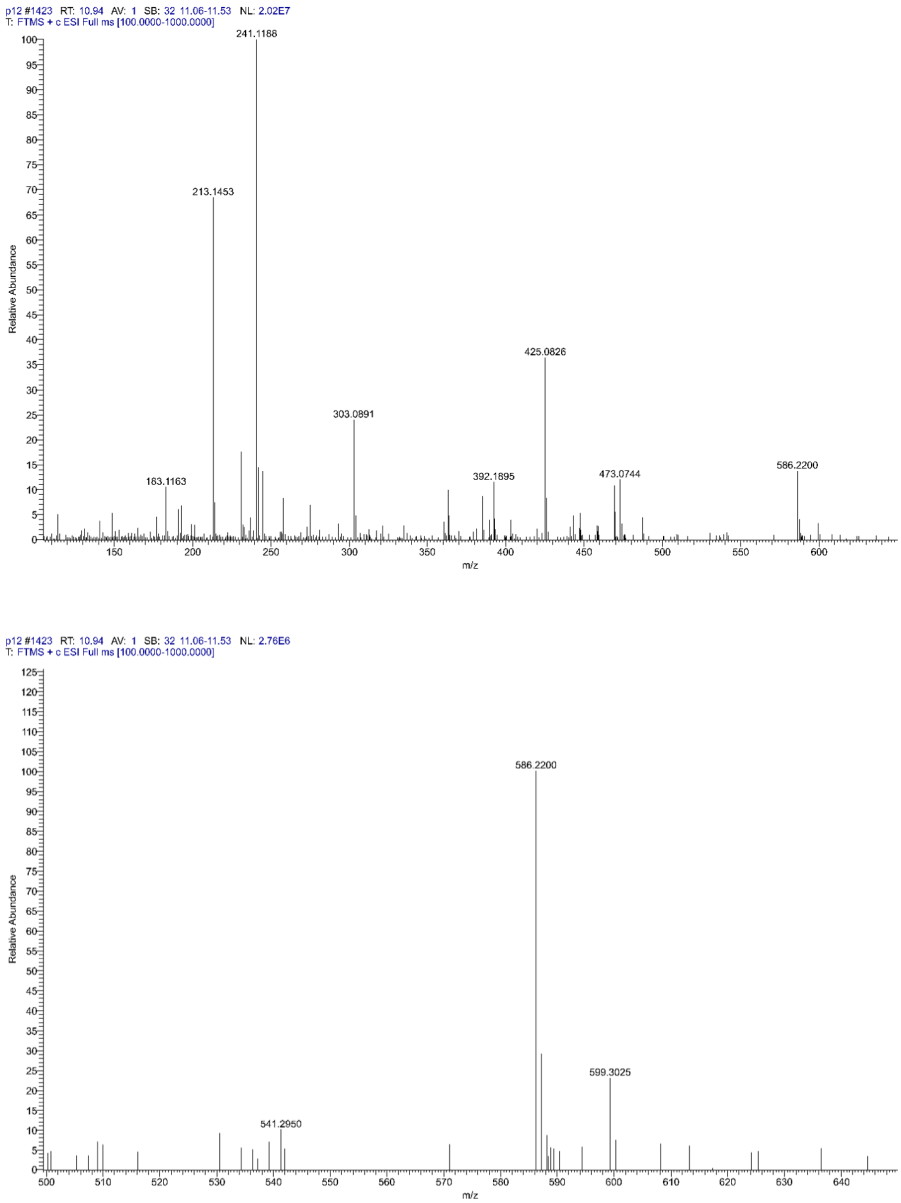

Figure 7 High resolution, positive mode HESI MS spectrum of the **2c-GSH-2** conjugate formed in the 90-minute sample of the control incubate (m/z 586.2200).

nounced effect on the modulation of mitochondrial respiratory functions. Phosphorylation inhibitory effect and/or partial uncoupling of the compound resulted in stimulation of mitochondrial activity and increased formation of ROS [49].

Okamoto *et al.* reported the reduction of (*E*)-4-phenyl-3-buten-2-one (a chalcone analog) by rat microsomal carbonyl reductase. The reduction was stereoselective, yielding *R*-(*E*)-4-phenyl-3-buten-2-ol [14]. Based on this finding, the total ion MS spectrum of the 90-minute microsomal incubate was screened for the presence of the respective reduced form of **2c**. The analysis didn't indicate the presence of a signal of the corresponding alcohol.

4 Conclusions

Microsomal biotransformation of the antiproliferative (*E*)-2-[(4'-methoxyphenyl)methylene]-benzosuberon-1-one (**2c**) showed the compound to be metabolized by the CYP and the GST enzymes. As a result of CYP-catalyzed transformations, one monooxygenated (**2c+O**) and the demethylated (**2c-CH$_2$**) metabolites were identified. Microsomal GST-catalyzed reaction of the compound resulted in formation of diastereomeric GST-conjugates. Under the present HPLC conditions, the compounds were separated into two chromatographic peaks. A noticeable amount of **(*Z*)-2c** was also identified in the incubates. Since the (*Z*)-isomer of the parent compound has a different three-dimensional structure, degree of conjugation, and lipophilicity [50],

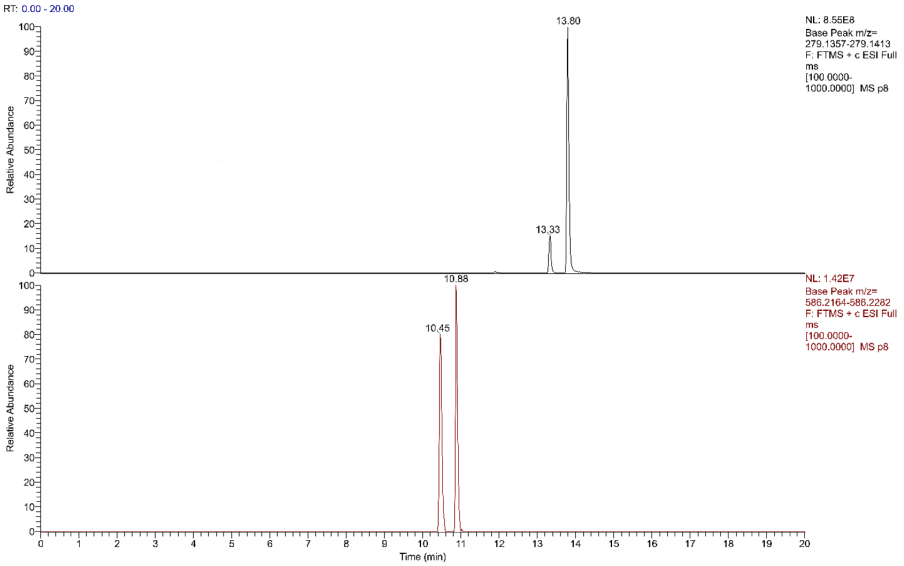

Figure 8 High resolution, positive mode HESI MS chromatogram of (*E*)-2-[(4-methoxyphenyl)methylene]-1-benzosuberone (**2c**) microsomal incubate (90-minute sample). Upper panel: t_r 13.33 min: (*Z*)-2-[(4-methoxyphenyl) methylene]-1-benzosuberone; t_r 13.80 min: (*E*)-2-[(4-methoxyphenyl)methylene]-1-benzosuberone. Lower panel: **2c-GSH-1**: 10.45 min.; **2c-GSH-2**: 10.88 min.

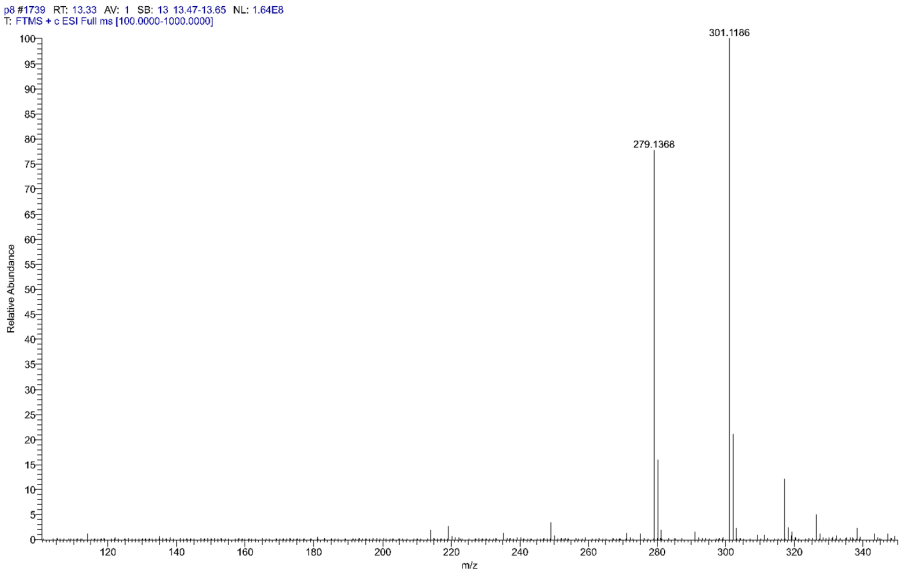

Figure 9 High resolution, positive mode HESI MS spectrum of (*Z*)-2-[(4-methoxyphenyl) methylene]-1-benzosuberone (**2c**) formed in the 90-minute sample of the microsomal incubate. (Protonated m/z 279.1368 and Na^+-adduct m/z 301.1186).

Table 2 HPLC-MS peak areas (AUCs) of the **2c**, the **2c-GSH** isomeric peaks, and that of the oxidative metabolites of **2c** as a function of incubation time.

Compound	t_r (min)	Control (0 min)	Control (90 min)	Microsome (0 min)	Microsome (90 min)
(*E*)-2c	13.8	4,093,677,464	2,215,039,743	8,297,984,438	3,815,982,269
(*Z*)-2c	13.32	495,826,994	299,494,818	856,426,548	550,348,953
2c-GSH-1	10.47	1,466,946	18,724,489	2,210,842	50,714,479
2c-GSH-2	10.86	2,493,046	12,017,553	4,293,434	61,264,226
2c-CH_2	12.25	N/D	N/D	7,206,428	81,441,916
2c+O	11.93	N/D	N/D	11,740,789	44,057,081

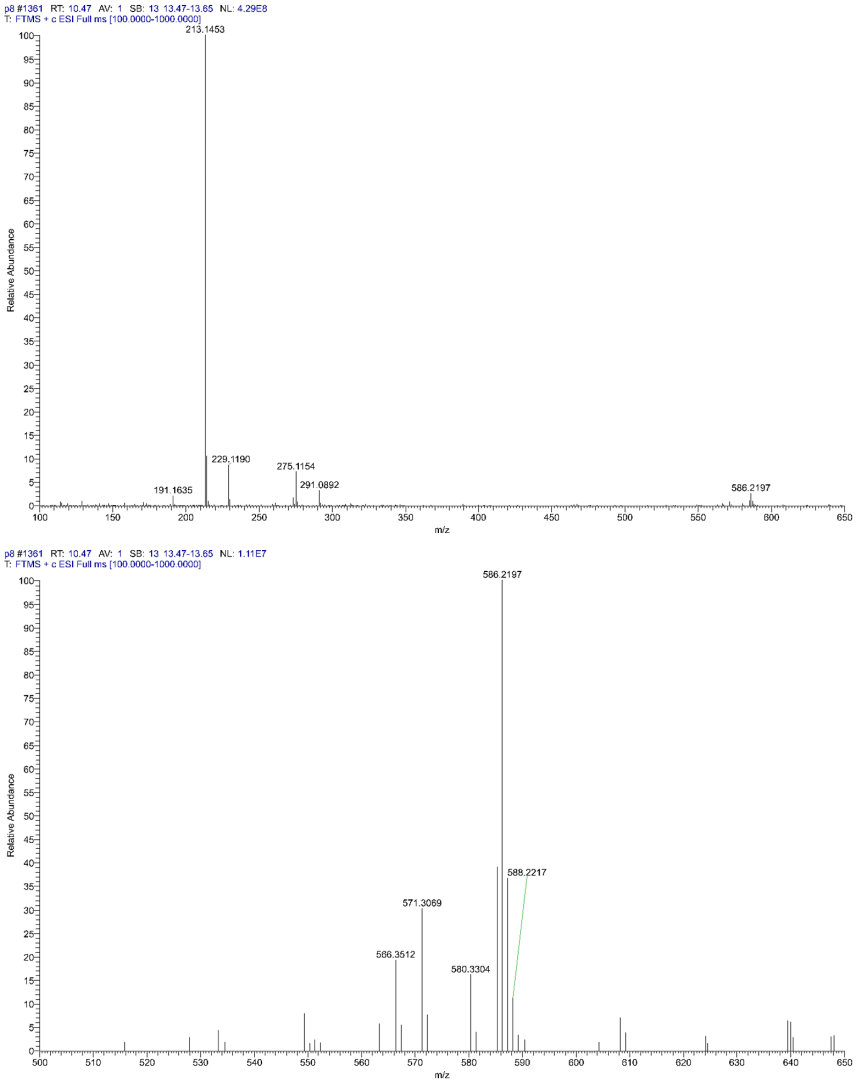

Figure 10 High resolution, positive mode HESI MS spectrum of the **2c-GSH-1** conjugate formed in the 90-minute sample of the microsomal incubate (m/z 586.2197).

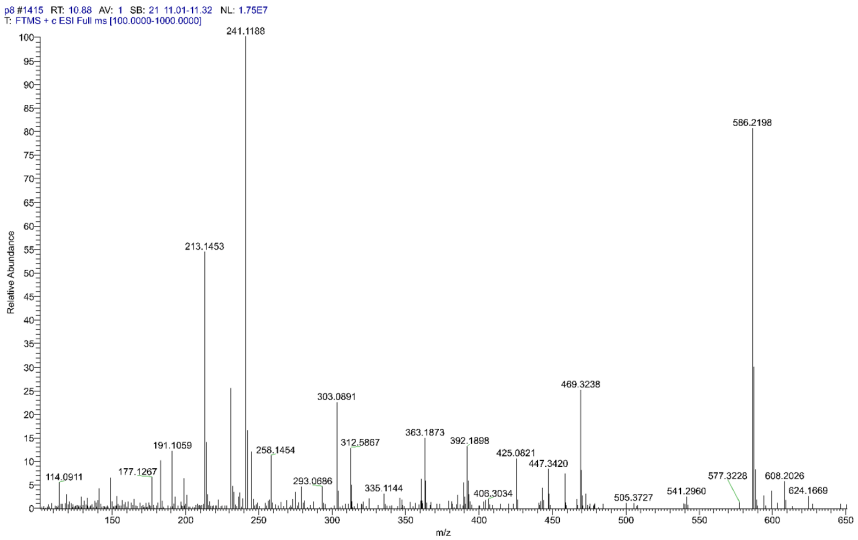

Figure 11 High resolution, positive mode HESI MS spectrum of the **2c-GSH-2** conjugate formed in the 90-minute sample of the microsomal incubate (m/z 586.2198).

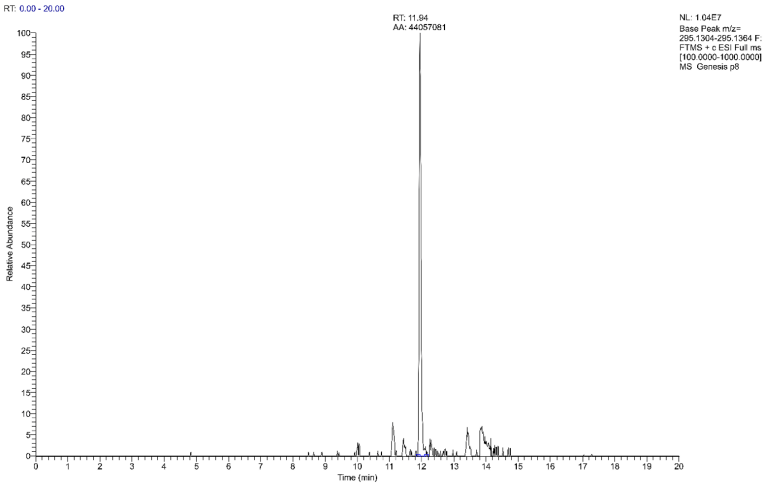

Figure 12 High resolution, positive mode HESI MS chromatogram of the monohydroxylated derivative of (*E*)-2-[(4-methoxyphenyl)methylene]-1-benzosuberone (**2c**) formed in the 90-minute sample of the microsomal incubate. (t_r 11.94 min).

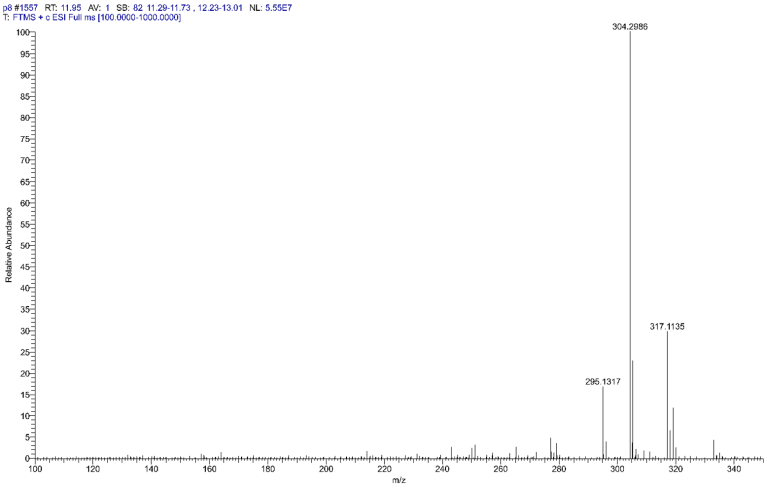

Figure 13 High resolution, positive mode HESI MS spectrum of the monohydroxylated derivative of (*E*)-2-[(4-methoxyphenyl)methylene]-1-benzosuberone (**2c**) formed in the 90-minute sample of the microsomal incubate. (Protonated m/z 295.1317 and Na^+-adduct m/z 317.1135)

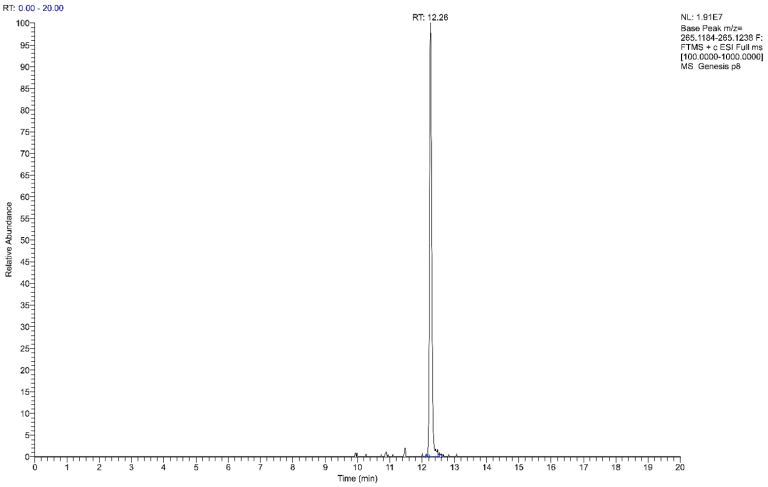

Figure 14 High resolution, positive mode HESI MS chromatogram of the O-demethylated derivative of (*E*)-2-[(4-methoxyphenyl)methylene]-1-benzosuberone (**2c**) formed in the 90-minute sample of the microsomal incubate. (t_r 12.26 min).

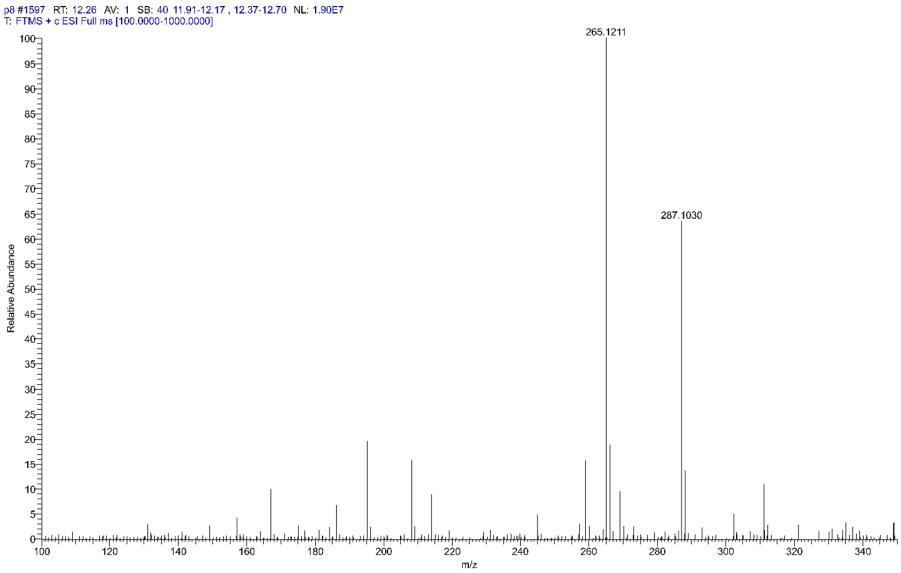

Figure 15 High resolution, positive mode HESI MS spectrum of of the O-demethylated derivative of (*E*)-2-[(4-methoxyphenyl)methylene]-1-benzosuberone (**2c**) formed in the 90-minute sample of the microsomal incubate. (Protonated m/z 265.1213 and Na^+-adduct m/z 287.1030).

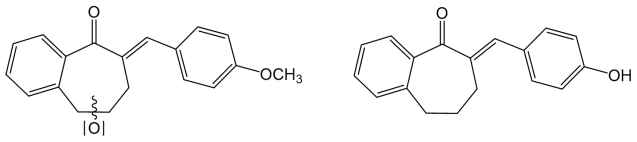

Figure 16 Structures of the products formed in the microsomal oxidation of **2c**

formation of this isomer might be a molecular event that plays a role in the observed biological effects of the compound. Furthermore, the GSH-reactivity of **2c** can also take part in the previously reported apoptotic effect of the compound.

References

[1] Part XVI, Rozmer Z and Perjesi P. (*E*)-2-Benzylidenecyclanones: Part XVI. Study on the interaction of some (*E*)-2-benzyldenebenzosuberone derivatives with serum albumin by UV-Vis method, inhibitory effect on topoisomerase. Journal of Pharmaceutical and Biopharmaceutical Research, 2020, **2**(1):118-125. https://doi.org/10.25082/JPBR.2020.01.003

[2] Rozmer Z and Perjési P. Naturally occurring chalcones and their biological activities. Phytochemistry Reviews, 2016, **15**(1): 87-120. https://doi.org/10.1007/s11101-014-9387-8

[3] Mahapatra DK, Bharti SK and Asati V. Anti-cancer chalcones: Structural and molecular target perspectives. European Journal of Medicinal Chemistry, 2015, **98**: 69-114. https://doi.org/10.1016/j.ejmech.2015.05.004

[4] Zhuang C, Zhang W, Sheng C, *et al*. Chalcone: a privileged structure in medicinal chemistry. Chemical reviews, 2017, **117**(12): 7762-7810. https://doi.org/10.1021/acs.chemrev.7b00020

[5] Gomes MN, Muratov EN, Pereira M, *et al*. Chalcone Derivatives: Promising starting points for drug design. Molecules, 2017, **22**(8): 1210. https://doi.org/10.3390/molecules22081210

[6] Dimmock JR, Kandepu NM, Nazarali AJ, *et al*. Conformational and quantitative structure-activity relationship study of cytotoxic 2-arylidenebenzocycloalkanones. Journal of Medicinal Chemistry, 1999, **42**(8): 1358-1366. https://doi.org/10.1021/jm9806695

[7] Dimmock JR, Zello GA, Oloo EO, *et al*. Correlations between cytotoxicity and topography of some 2-arylidenebenzocycloalkanones determined by X-ray crystallography. Journal of Medicinal Chemistry, 2002, **45**(14): 3103-3111. https://doi.org/10.1021/jm010559p

[8] Perjési P, Das U, De Clercq E, *et al*. Design, synthesis and antiproliferative activity of some 3-benzylidene-2,3-dihydro-1-benzopyran-4-ones which display selective toxicity for malignant cells. European Journal of Medicinal Chemistry, 2007, **43**(4): 839-845. https://doi.org/10.1016/j.ejmech.2007.06.017

[9] Rozmer Z, Berki T and Perjési P. Different effects of two cyclic chalcone analogues on cell cycle of Jurkat T cells. Toxicology in Vitro, 2006, **20**(8): 1354-1362. https://doi.org/10.1016/j.tiv.2006.05.006

[10] Pilatova M, Varinska L, Perjesi P, *et al*. In vitro antiproliferative and antiangiogenic effects of synthetic chalcone analogues. Toxicology in Vitro, 2010, **24**(5): 1347-1355. https://doi.org/10.1016/j.tiv.2010.04.013

[11] Perjési P, Maász G, Reisch R, *et al*. (*E*)-2-Benzylidenebenzocyclanones: Part VII. Investigation of the conjugation reaction of two cytotoxic cyclic chalcone analogues with glutathione: an HPLC–MS study. Monatshefte für Chemie, 2012, **143**(8): 1107-1114. https://doi.org/10.1007/s00706-012-0768-7

[12] Rozmer Z, Berki T, Maász G, *et al*. Different effects of two cyclic chalcone analogues on redox status of Jurkat T cells. Toxicology in Vitro, 2014, **28**(8):1359-1365. https://doi.org/10.1016/j.tiv.2014.06.006

[13] Kohno Y, Kitamura S, Sanoh S, *et al*. Metabolism of the α,β-unsaturated ketones, chalcone and trans -4-phenyl-3-buten-2-one, by rat liver microsomes and estrogenic activity of the metabolites. Drug Metabolism and Disposition, 2005, **33**(8): 1115-1123. https://doi.org/10.1124/dmd.104.002634

[14] Okamoto Y, Kitamura S, Takeshita M, *et al*. Microsomal carbonyl reductase responsible for reduction of 4-phenyl-3-buten-2-one in rats. IUBMB Life, 1999, 48(5): 543-547. https://doi.org/10.1080/713803550

[15] Huang L, Nikolic D and van Breemen RB. Hepatic metabolism of licochalcone A, a potential chemopreventive chalcone from licorice (Glycyrrhiza inflata), determined using liquid chromatography-tandem mass spectrometry. Analytical and Bioanalytical Chemistry, 2017, **409**(30): 6937-6948. https://doi.org/10.1007/s00216-017-0642-x

[16] Nikolic D, Li Y, Chadwick LR, *et al*. Metabolism of 8-prenylnaringenin, a potent phytoestrogen from hops (Humulus lupulus), by human liver microsomes. Drug metabolism and disposition, 2004, **32**(2): 272-279. https://doi.org/10.1124/dmd.32.2.272

[17] Bernardes A, Kuzma M, Almási A, *et al*. HPLC and HPLC-MS analysis of intestinal elimination and phase 2 metabolism of 4'-hydroxy-4-methoxychalcone and its bis-Mannich analog in the rat. The Open Medicinal Chemistry Journal, 2022, **16**(1): e187410452208110. https://doi.org/10.2174/18741045-v16-e2208110

[18] Bernardes A, Pérez CN, Mayer M, *et al*. Study of reactions of two Mannich bases derived of 4'-hydroxychalcones with glutathione by RP-TLC, RP-HPLC and RP-HPLC-ESI-MS analysis. Journal of the Brazilian Chemical Society, 2017, **28**: 1048-1062. https://doi.org/10.21577/0103-5053.20160260

[19] Jones DP. Redox potential of GSH/GSSG couple: Assay and biological significance. In: Methods in Enzymology (Internet). Elsevier, 2002, 93-112. https://doi.org/10.1016/s0076-6879(02)48630-2

[20] Aw TY. Cellular Redox: A Modulator of Intestinal Epithelial Cell Proliferation. Physiology, 2003, **18**(5): 201-204. https://doi.org/10.1152/nips.01448.2003

[21] Schafer FQ and Buettner GR. Redox environment of the cell as viewed through the redox state of the glutathione disulfide/glutathione couple. Free Radical Biology and Medicine, 2001, **30**(11): 1191-1212. https://doi.org/10.1016/s0891-5849(01)00480-4

[22] Perjési P. Glutathione: biosynthesis, functions and biological implications. Nova Science Publishers, New York, 2019. ISBN 978-1-53614-740-7.

[23] Hill JR. In vitro drug metabolism using liver microsomes. Current Protocols in Pharmacology, 2004. https://doi.org/10.1002/0471141755.ph0708s23

[24] Perjési P, Nusser T, Tarczay Gy, *et al*. *E*-2-Benzylidenebenzocycloalkanones. Stereostructure and NMR spectroscopic investigation. Journal of Molecular Structure, 1999, **479**(1): 13-19. https://doi.org/10.1016/S0022-2860(98)00805-9

[25] Phosphate-Buffered Saline (PBS; 0.1 M, pH 7.4). Cold Spring Harbor Protocols, 2014, **2014**(12): pdb.rec085126. https://doi.org/10.1101/pdb.rec085126

[26] Karthikeyan C, Narayana Moorthy NSH, Ramasamy S, *et al*. Advances in Chalcones with Anticancer Activities. Physical Review A, 2014, **10**(1): 97-115. https://doi.org/10.2174/1574892809666140819153902

[27] Constantinescu T and Mihis AG. Two Important Anticancer Mechanisms of Natural and Synthetic Chalcones. International Journal of Molecular Sciences, 2022, **23**(19): 11595. https://doi.org/10.3390/ijms231911595

[28] Powis G, Gasdaska JR and Baker A. Redox signaling and the control of cell growth and death. Advances in pharmacology, 1996, **38**: 329-359. https://doi.org/10.1016/s1054-3589(08)60990-4

[29] Vašková J, Kočan L, Vaško L, *et al*. Glutathione-Related Enzymes and Proteins: A Review. Molecules, 2023, **28**(3): 1447.
https://doi.org/10.3390/molecules28031447

[30] Dinkova-Kostova AT, Massiah MA, Bozak RE, *et al*. Potency of Michael reaction acceptors as inducers of enzymes that protect against carcinogenesis depends on their reactivity with sulfhydryl groups. Proceedings of the National Academy of Sciences, 2001, **98**(6):3 404-309.
https://doi.org/10.1073/pnas.051632198

[31] Jin YL, Jin XY, Jin F, *et al*. Structure activity relationship studies of anti-inflammatory TMMC derivatives: 4-Dimethylamino group on the B ring responsible for lowering the potency. Archives of Pharmacal Research 2009, **31**(9): 1145.
https://doi.org/10.1007/s12272-001-1281-7

[32] Wang J, Wang S, Song D, *et al*. Chalcone Derivatives Inhibit Glutathione S-Transferase P1-1 Activity: Insights into the Interaction Mode of α,β-Unsaturated Carbonyl Compounds. Chemical biology & drug design, 2009, **73**(5): 511-514.
https://doi.org/10.1111/j.1747-0285.2009.00807.x

[33] Leitgeb B, Szekeres A, Manczinger L, *et al*. The history of alamethicin: a review of the most extensively studied peptaibol. Chemistry & biodiversity, 2007, **4**(6): 1027-1051.
https://doi.org/10.1002/cbdv.200790095

[34] Fisher MB, Campanale K, Ackermann BL, *et al*. In vitro glucuronidation using human liver microsomes and the pore-forming peptide alamethicin. Drug metabolism and disposition, 2000, **28**(5): 560-566.

[35] Kumar S, Samuel K, Subramanian R, *et al*. Extrapolation of diclofenac clearance from in vitro microsomal metabolism data: role of acyl glucuronidation and sequential oxidative metabolism of the acyl glucuronide. Journal of Pharmacology and Experimental Therapeutics, 2002, **303**(3): 969-978.
https://doi.org/10.1124/jpet.102.038992

[36] Walsky RL, Bauman JN, Bourcier K, *et al*. Optimized assays for human UDP-glucuronosyltransferase (UGT) activities: altered alamethicin concentration and utility to screen for UGT inhibitors. Drug Metabolism and Disposition, 2012, **40**(5): 1051-1065.
https://doi.org/10.1124/dmd.111.043117

[37] Boase S and Miners JO. In vitro–in vivo correlations for drugs eliminated by glucuronidation: investigations with the model substrate zidovudine. British Journal of Clinical Pharmacology, 2002, **54**(5): 493-503.
https://doi.org/10.1046/j.1365-2125.2002.01669.x

[38] Yan Z and Caldwell GW. Metabolic assessment in liver microsomes by co-activating cytochrome P450s and UDP-glycosyltransferases. European Journal of Drug Metabolism and Pharmacokinetics, 2003, **28**(3): 223-232.
https://doi.org/10.1007/BF03190489

[39] Berne D, Ladmiral V, Leclerc E, *et al*. Thia-Michael reaction: The route to promising covalent adaptable networks. Polymers, 2022, **14**(20): 4457.
https://doi.org/10.3390/polym14204457

[40] Rozmer Z, Perjési P and Takács-Novák K. Application of RP-TLC for logP determination of isomeric chalcones and cyclic chalcone analogues. Journal of Planar Chromatography — Modern TLC, 2006, **19**: 124-128.
https://doi.org/10.1556/jpc.19.2006.2.7

[41] Lundqvist G, Yücel-Lindberg T and Morgenstern R. The oligomeric structure of rat liver microsomal glutathione transferase studied by chemical cross-linking. Biochimica et Biophysica Acta (BBA)-Protein Structure and Molecular Enzymology, 1992, **1159**(1): 103-108.
https://doi.org/10.1016/0167-4838(92)90081-n

[42] Jakobsson PJ, Mancini JA, Riendeau D, *et al*. Identification and characterization of a novel microsomal enzyme with glutathione-dependent transferase and peroxidase activities. Journal of Biological Chemistry, 1997, **272**(36): 22934-22939.
https://doi.org/10.1074/jbc.272.36.22934

[43] Jakobsson PJ, Morgenstern R, Mancini J, *et al*. Common structural features of MAPEG—a widespread superfamily of membrane associated proteins with highly divergent functions in eicosanoid and glutathione metabolism. Protein Science, 1999, **8**(3): 689-692.
https://doi.org/10.1110/ps.8.3.689

[44] Weinander R, Ekström L, Andersson C, *et al*. Structural and Functional Aspects of Rat Microsomal Glutathione Transferase. Journal of Biological Chemistry, 1997, **272**(14): 8871-8877.
https://doi.org/10.1074/jbc.272.14.8871

[45] Morgenstern R, Guthenberg C, Mannervik B, *et al*. The amount and nature of glutathione transferases in rat liver microsomes determined by immunochemical methods. FEBS letters, 1983, **160**(1-2): 264-268.
https://doi.org/10.1016/0014-5793(83)80979-x

[46] Busenlehner LS, Ålander J, Jegerscöhld C, *et al*. Location of substrate binding sites within the integral membrane protein microsomal glutathione transferase-1. Biochemistry 2007, **46**(10): 2812-2822.
https://doi.org/10.1021/bi6023385

[47] Morgenstern R, Depierre JW and Ernster L. Activation of microsomal glutathione S-transferase activity by sulfhydryl reagents. Biochemical and Biophysical Research Communications, 1979, **87**(3): 657-663.
https://doi.org/10.1016/0006-291x(79)92009-6

[48] Parkinson A, Ogilvie BW, Buckley DB, *et al*. Biotransformation of Xenobiotics. In "Casarett and Doull's Toxicology: The Basic Science of Poisons (Editor: C. D. Klassen). 9th edition. McGraw Hill, 2019.

[49] Guzy J, Vasková-Kubalkova J, Rozmer Z, *et al*. Activation of oxidative stress response by hydroxyl substituted chalcones and cyclic chalcone analogues in mitochondria. FEBS Letters, 2010, **584**: 567-570.
https://doi.org/10.1016/j.febslet.2009.11.098

[50] Perjési P. (E)-2-benzylidenebenzocyclanones: Part XIII. Light-induced in solution (E)/(Z) isomerization of some cyclic chalcone analogues. Effect of ring size on lipophilicity of geometric isomers. Monatshefte der Chemie, 2015, **146**(8): 1275-1281.
https://doi.org/10.1007/s00706-015-1463-2

International Journal of
Molecular Sciences

MDPI

Article

(*E*)-2-Benzylidenecyclanones: Part XVIII Study the Possible Link between Glutathione Reactivity and Cancer Cell Cytotoxic Effects of Some Cyclic Chalcone Analogs A Comparison of the Reactivity of the Open-Chain and the Seven-Membered Homologs

Fatemeh Kenari [1], Szilárd Molnár [1,2], Igor D. Borges [3], Hamilton B. Napolitano [3] and Pál Perjési [1,3,*]

[1] Institute of Pharmaceutical Chemistry, University of Pécs, H-7624 Pécs, Hungary; kenari.fatemeh@pte.hu (F.K.); molnar.szilard@pte.hu (S.M.)
[2] Research Institute for Viticulture and Oenology, University of Pécs, H-7634 Pécs, Hungary
[3] Grupo de Química Teórica e Estrutural de Anápolis, Universidade Estadual de Goiás, Anápolis 75070-290, GO, Brazil; i.dalarmelino@gmail.com (I.D.B.); hamilton@ueg.br (H.B.N.)
* Correspondence: pal.perjesi@gytk.pte.hu; Tel.: +36-72-503-650

Abstract: Non-enzymatic thiol addition into the α,β-unsaturated carbonyl system is associated with several biological effects. In vivo, the reactions can form small-molecule thiol (e.g., glutathione) or protein thiol adducts. The reaction of two synthetic (4′-methyl- and 4′-methoxy substituted) cyclic chalcone analogs with reduced glutathione (GSH) and *N*-acetylcysteine (NAC) was studied by (high-pressure liquid chromatography-ultraviolet spectroscopy) HPLC-UV method. The selected compounds displayed in vitro cancer cell cytotoxicity (IC_{50}) of different orders of magnitude. The structure of the formed adducts was confirmed by (high-pressure liquid chromatography-mass spectrometry) HPLC-MS. The incubations were performed under three different pH conditions (pH 3.2/3.7, 6.3/6.8, and 8.0/7.4). The chalcones intrinsically reacted with both thiols under all incubation conditions. The initial rates and compositions of the final mixtures depended on the substitution and the pH. The frontier molecular orbitals and the Fukui function were carried out to investigate the effects on open-chain and seven-membered cyclic analogs. Furthermore, machine learning protocols were used to provide more insights into physicochemical properties and to support the different thiol-reactivity. HPLC analysis indicated diastereoselectivity of the reactions. The observed reactivities do not directly relate to the different in vitro cancer cell cytotoxicity of the compounds.

Keywords: chalcone; glutathione; cysteine; thiols; Michael addition; diastereoselective addition

Citation: Kenari, F.; Molnár, S.; Borges, I.D.; Napolitano, H.B.; Perjési, P. (*E*)-2-Benzylidenecyclanones: Part XVIII Study the Possible Link between Glutathione Reactivity and Cancer Cell Cytotoxic Effects of Some Cyclic Chalcone Analogs A Comparison of the Reactivity of the Open-Chain and the Seven-Membered Homologs. *Int. J. Mol. Sci.* **2023**, *24*, 8557. https://doi.org/10.3390/ijms24108557

Academic Editor: Malcolm D´Souza

Received: 14 April 2023
Revised: 1 May 2023
Accepted: 5 May 2023
Published: 10 May 2023

1. Introduction

Chalcones (**I**) are natural products, the biosynthetic precursors of flavonoids, a large family of plant phenolic secondary metabolites [1,2]. Because of the wide range of beneficial biological actions of the natural chalcones, several analogs have been synthesized and—among others—tested for their antioxidant, antimicrobial, antiprotozoal, antiulcer, antihistaminic, antidiabetic, anti-inflammatory, anticancer and neuroprotective activities [3–6]. The molecular mechanisms of the published biological/pharmacological effects can be associated with their (a) non-covalent interactions with biological macromolecules and (b) covalent modification of preferably the soft nucleophilic thiol function(s) of amino acids, peptides, and proteins [7–9].

The chalcone structure can be divided into three different structural units: the aromatic rings A and B and the propenone linker (Figure 1). Modifying any of them can tune the main feature of interactions of the synthetic chalcones towards the non-covalent or the covalent pathway. In our previous studies, we have investigated how the substitution of the

B-ring and modifying the ring size (n = 5–7) of cyclic chalcone analogs can affect the cancer cell cytotoxic effect of more than one hundred twenty derivatives [10–12]. While comparing the average IC_{50} values of the series, the benzosuberone (**II**) analogs proved to be the most effective against P388, L1210, Molt 4/C8, and CEM cells, as well as a panel of human tumor cell lines. In particular, the (*E*)-2-(4-methoxyphenylmethylene)-1-benzosuberone (**II c**) had the most remarkable cytotoxicity, when all five screens were considered [10,11].

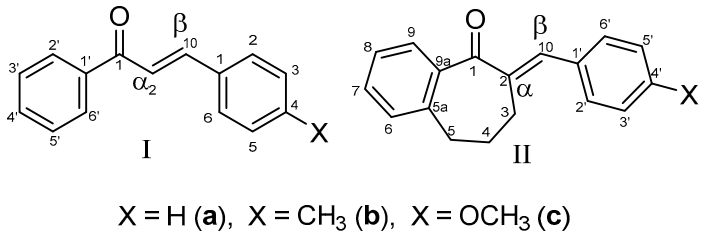

Figure 1. Structure and numbering of 4-X-chalcones (**I**) and (*E*)-2-(4′-X-phenylmethylene-1-benzosuberones (**II**).

In consecutive publications, we have performed cell cycle analysis of Jurkat cells exposed to **IIc** and its methyl-substituted analogue **IIb**. It was demonstrated that equitoxic doses of the two cyclic chalcone analogs have different effects on the cell cycle progression of the investigated Jurkat cells. Compound **IIc** showed to cause an immediate G1 lift and G2/M arrest, followed by hypoploidity and aneuploidy. Such a remarkable effect of **IIb** on the G1 and G2 checkpoints could not be observed [13,14]. Thin layer chromatographic (TLC) and high-pressure liquid chromatographic (HPLC) analysis showed the compounds to react with reduced glutathione (GSH) under basic conditions [13,15]. However, the two compounds had different effects on the thiol status of the Jurkat cells [16].

Glutathione is ubiquitous in mammalian cells ranging in 1–10 mM concentrations [17]. Under physiological conditions, more than 98% of total glutathione occurs in reduced form [18,19]. The reduced glutathione (GSH)/oxidized glutathione (GSSG) (GSH/GSSG) redox system has a vital role in maintaining the (a) environment of the intracellular redox system, (b) the antioxidant defense system, and (c) the cellular signaling processes [20]. Furthermore, it is one of the endogenous substances involved in the metabolism of endogenous (e.g., estrogens, leukotrienes, prostaglandins) and exogenous compounds (e.g., drugs, non-energy-producing xenobiotics) [21].

Covalent bond formation of GSH with electrophilic species affects the half-cell reduction potential of the GSSG/2GSH redox system. The GSH/GSSG ratio is a critical mechanism for cell survival; in fact, it is known that it varies in association with proliferation, differentiation, and apoptosis [22,23]. In our earlier publication [24], we reported on the thiol reactivity of two open-chain chalcones (**Ib** and **Ic**) with different cancer cell cytotoxicities [25]. We could not find a direct correlation of the thiol reactivities and the previously published biological (cancer cell cytotoxic) effects of the two chalcones. Continuing the previous studies on the molecular mechanism of the cancer cell cytotoxic and cell cycle modulating effects of **IIb** and **IIc**, we report on a comparative HPLC study on their intrinsic reactivity towards GSH and N-acetylcysteine (NAC). Compound **IIc** showed IC_{50} values towards the most investigated cancer cell lines close to two magnitudes lower than the 4-methyl analog **IIb** (Table 1). Thus, the differences in the reactivities could reflect the differences in their previously published biological activities.

Similar to the previous publication [24], the reactions were studied under three conditions with different pH: (a) pH 8.0/7.4, (b) pH 6.3/6.8, and (c) pH 3.2/3.7. The first pH values indicate the pH of the aqueous solution of the thiols before starting the incubations; the second pH values indicate the virtual pH of the incubation mixtures, containing 75.5% *v/v* methanol (MeOH). The basic pH was selected to mimic the conditions of the GST-catalyzed reactions; the ionization of the GSH thiol-moiety is increased due to its interaction with the basic imidazole N-atom in the active site of the enzyme [26]. The pH

6.3 was selected to mimic the slightly acidic pH of cancerous cells [27], while a strongly acidic condition (pH 3.2) was chosen to compare how the thiol function of the compounds reacts in its protonated and ionized forms. GSH and NAC have reported pKa values of 8.83 and 9.52, respectively. Accordingly, the thiol function of both compounds exists exclusively in the protonated (neutral) form under the pH 3.2/3.7 conditions [28].

Table 1. IC_{50} (μM) data of selected *E*-2-(4′-*X*-benzylidene)-1-benzosuberones (**II**) [10].

Compound	P388	L1210	Molt 4/C8	CEM	Human Tumor Cells
IIa	12.7	106.0	42.7	28.9	18.6
IIb	11.8	25.0	21.3	11.4	11.2
IIc	1.6	0.34	0.47	0.35	0.27

The thiol additions to enones are reported to be reversible, resulting in an equilibrium mixture's formation. To qualitatively characterize the progress of the reactions, the composition of the incubation mixtures was analyzed at the 15, 45, 75, 105, 135, 165, 195, 225, 255, 285, and 315 min timepoints by HPLC-UV. Furthermore, density functional theory (DFT) calculations and machine learning (ML) protocols were used to analyze the stability and regioselectivity of chalcone analogs on a structural basis. In the analyses, methanethiol (**CH_3SH**) and its deprotonated form (**CH_3S^-**) were used as model thiols.

2. Results

2.1. Reactions under Slightly Basic (pH 8.0/7.4) Conditions

Initially, we investigated the reactions of **IIb** and **IIc** under basic conditions. Considering the pKa values of GSH (8.83) and NAC (9.52), about 3.6% of the GSH and 0.75% of the NAC molecules are under pH 7.4 conditions. The reaction with GSH (Figure 2) and NAC (Figure 3) of both cyclic chalcones have intrinsic reactivity with the investigated thiols. By the end of the incubation period (315 min) with GSH, the initial area of the HPLC peak corresponding to the parent compounds **IIb** and **IIc** reduced by 43.5% and 26.3 %, respectively (Table 2). While the compounds were incubated with NAC, the respective figures were 7.9% and 7.6% (Table 3). Changes in the chromatographic peak areas of the starting chalcones as a function of the incubation time indicated that the compositions reflect the equilibrium only in the case of the NAC incubation (Figure 3). The overlayed HPLC-UV chromatograms obtained by analysis of the **IIb** with GSH and NAC (Figures S1 and S2), and **IIc** with GSH and NAC (Figures S3 and S4) at the different timepoints are shown on Figures S1–S4.

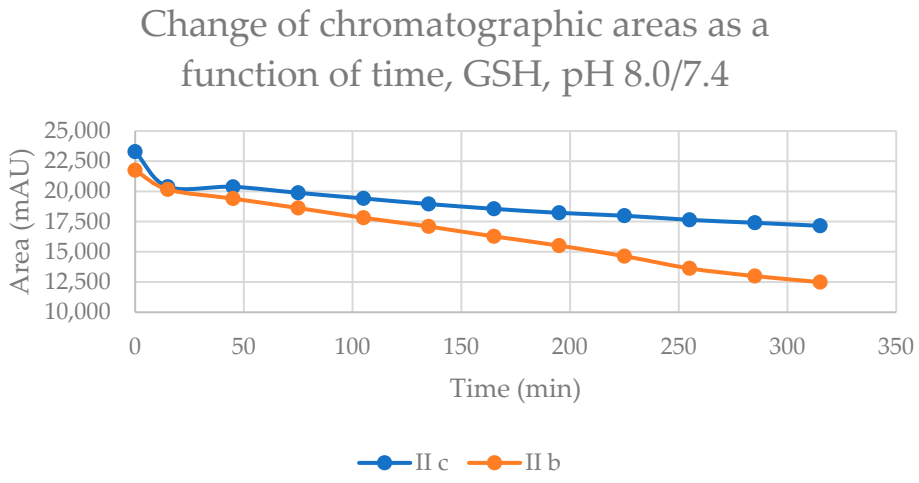

Figure 2. Change in the chromatographic peak area of chalcones **IIb** and **IIc** in the chalcone–GSH incubations at pH 8.0/7.4.

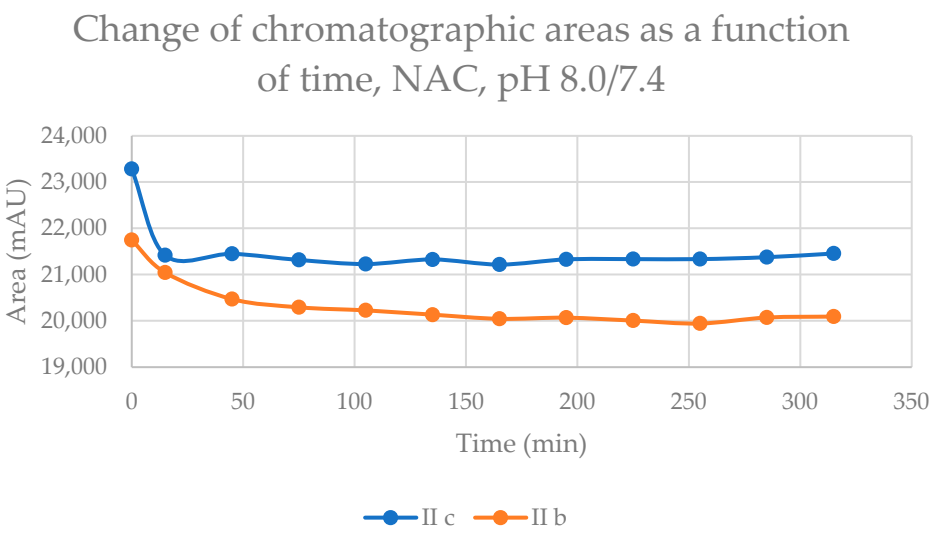

Figure 3. Change in the chromatographic peak area of chalcones **IIb** and **IIc** in the chalcone–NAC incubations at pH 8.0/7.4.

Table 2. Retention times (t_R) [1] and integrated peak areas (A) of the investigated cyclic chalcone analogs (**IIb** and **IIc**) and their GSH adducts [2].

pH [3]	Compound	t_R (*E*)-Chalcone	Area Ratio [4] A_{315}/A_0	t_R (*Z*)-Chalcone	Area (*Z*)-Chalcone	t_R GSH–1	Area GSH–1	t_R GSH–2	Area GSH–2
3.2	**IIb**	17.1	0.89	16.8	55.1	14.8 [5]	74.9	15.2 [5]	111.5
3.2	**IIc**	16.6	0.95	16.3	136.1	ND [5]	-	ND [5]	-
6.3	**IIb**	17.0	0.84	16.7	446.6	14.6	297.2	15.1	331.8
6.3	**IIc**	16.9	0.91	16.7	513.4	14.2	233.6	14.8	256.4
8.0	**IIb**	17.4	0.57	17.1	302.8	15.0	2847.0	15.4	3216.3
8.0	**IIc**	16.8	0.74	16.5	412.0	13.9	2584.9	14.6	2785.0

[1] Retention times in minutes; [2] data refer to the average of two independent measurements at the 315 min time point; [3] pH value of the aqueous thiol solution; [4] ratios of peak areas measured at 0 and 315 min; [5] not detectable.

Table 3. Retention times (t_r) [1] and integrated peak areas (A) of the investigated cyclic chalcone analogs (**IIb** and **IIc**) and their NAC adducts [2].

pH [3]	Compound	t_R (*E*)-Chalcone	Area Ratio [4] A_{315}/A_0	t_R (*Z*)-Chalcone	Area (*Z*)-Chalcone	t_R NAC–1	Area NAC–1	t_R NAC–2	Area NAC–2
3.2	**IIb**	17.1	0.76	16.8	124.1	N/D [5]	-	N/D [5]	-
3.2	**IIc**	16.6	0.88	16.3	126.9	N/D [5]	-	N/D [5]	-
6.3	**IIb**	17.5	0.93	17.2	118.9	16.3	60.0	16.5	513.9
6.3	**IIc**	16.7	0.91	16.4	184.5	15.3	61.8	15.6	392.1
8.0	**IIb**	17.5	0.92	17.2	467.5	16.3	477.7	16.5	913.4
8.0	**IIc**	17.0	0.92	16.8	541.9	15.7	347.5	15.9	624.2

[1] Retention times in minutes; [2] data refer to the average of two independent measurements at the 315 min time point; [3] pH value of the aqueous thiol solution; [4] ratios of peak areas measured at 0 and 315 min, [5] not detectable.

As a result of the addition reactions, two new chiral centers are formed. Considering the inherent chirality of the two thiols, the formation of four diastereomeric adducts was expected. However, only two separate peaks could be detected under the present chromatographic conditions. The analysis showed a slight excess of the less polar diastereomers in both cases. The structure of the parent chalcones and their GSH and NAC conjugates were verified by HPLC-MS (Figures S5–S10). The exact mass of **IIb**, **IIc**, and the **IIb-GSH**, **IIb-NAC**, **IIc-GSH** and **IIc-NAC** adducts are summarized in Table S1.

The time course of increase in the two separated peaks, GSH-1 (Figure 4) and GSH-2 (Figure 5), and NAC-1 (Figure 6) and NAC-2 (Figure 7) showed some characteristic differences. In the case of the GSH adducts of **IIb** and **IIc**, the peak areas almost linearly increased over time. The progression curves of formation of the adducts, however, showed somewhat different slopes, especially from the 105 min timepoint (Figures 4 and 5). In the

case of the NAC-adducts, the progression curves deviate from linearity. The curvatures of the concave curves are different from the 75 min timepoint (Figures 6 and 7) By the end of the incubation period (315 min), the ratio of the two peaks of the GSH incubations remained close to unity (1.13 and 1.08 for **IIb** and **IIc**, respectively). In the case of the NAC incubations, the respective ratios were 1.91 and 1.80 (Tables 2 and 3). The formation of (*Z*)-chalcones could be detected in all four incubations. In the case of the NAC incubations, the area of the (*Z*)-peaks is comparable with those of the chalcone–NAC adducts (Tables 2 and 3).

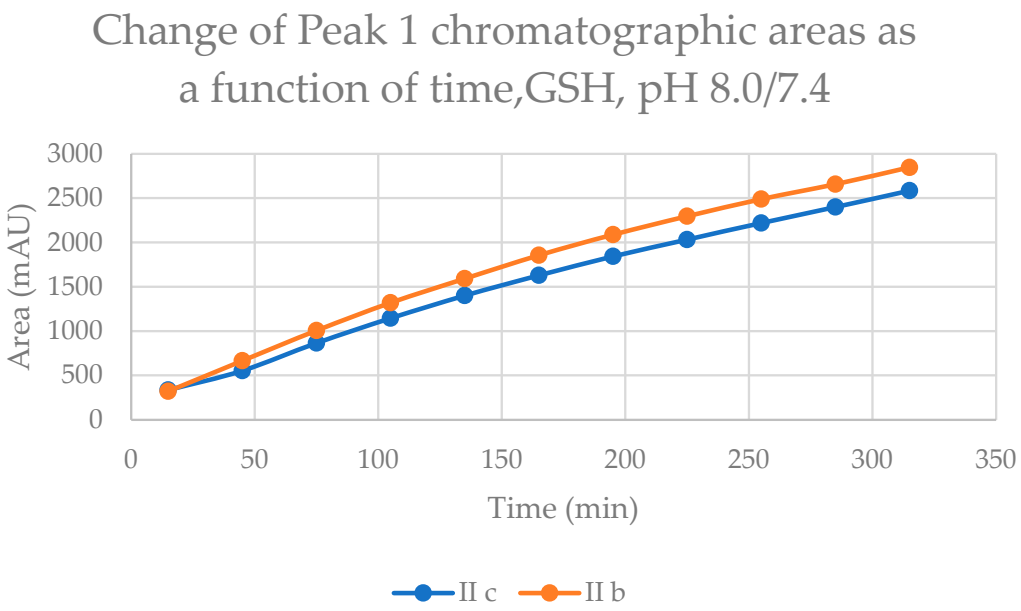

Figure 4. Change in the chromatographic peak area of adduct 1 of **IIb** and **IIc** in the chalcone–GSH incubations at pH 8.0/7.4.

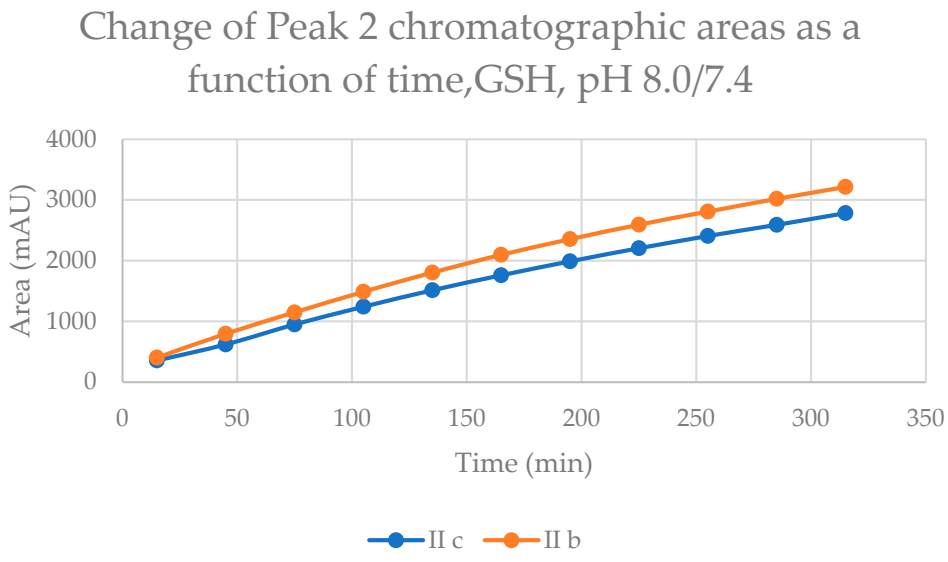

Figure 5. Change in the chromatographic peak area of adduct 2 of **IIb** and **IIc** in the chalcone–GSH incubations at pH 8.0/7.4.

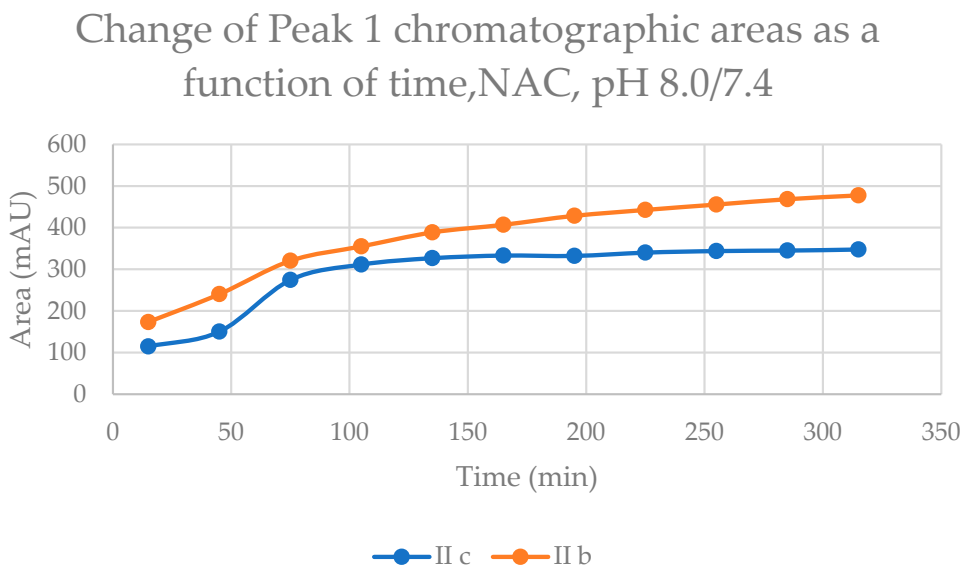

Figure 6. Change in the chromatographic peak area of adduct 1 of **IIb** and **IIc** in the chalcone–NAC incubations at pH 8.0/7.4.

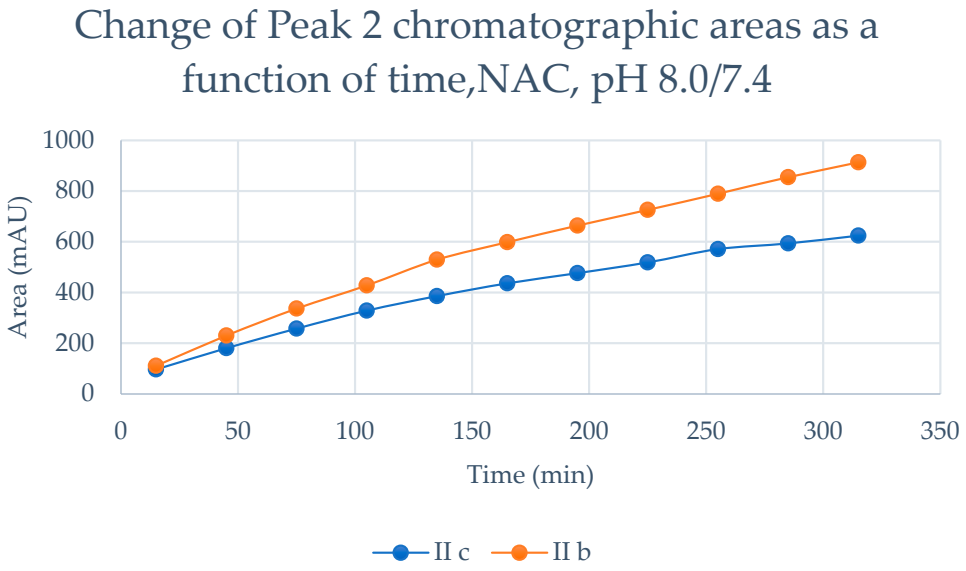

Figure 7. Change in the chromatographic peak area of adduct 2 of **IIb** and **IIc** in the chalcone–NAC incubations at pH 8.0/7.4.

2.2. Reaction under Slightly Acidic (pH 6.3/6.8) Conditions

The reaction of the cyclic chalcones with the two thiols under slightly acidic conditions (virtual pH 6.8) mimics the cellular milieu of the cancer cells [27]. Under such conditions, about 0.9% of the GSH molecules and 0.2% of the NAC molecules exist in the more reactive thiolate form. The change in the concentration (chromatographic peak areas) of the starting chalcones **IIb** and **IIc** shows parallelism in both reactions (Figures 8 and 9). By the end of the incubation period (315 min) with GSH, the initial area of the HPLC peak of **IIa** and **IIb** was reduced by 16.1% and 9.1%, respectively. While the compounds were incubated with NAC, the respective figures were 8.9% and 7.1%. These latter figures are very close to those obtained under slightly basic conditions (Tables 2 and 3).

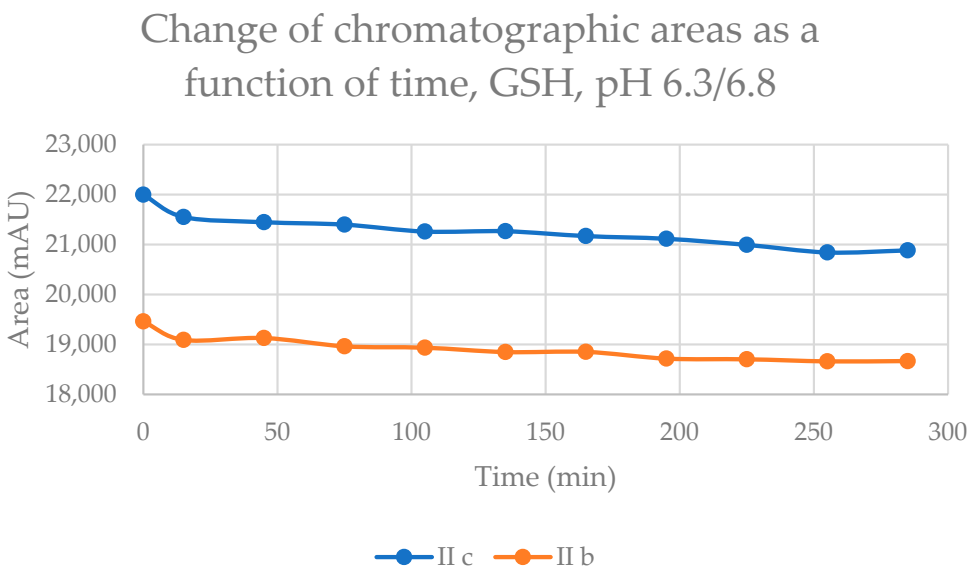

Figure 8. Change in the chromatographic peak area of chalcones **IIb** and **IIc** in the chalcone–GSH incubations at pH 6.3/6.8.

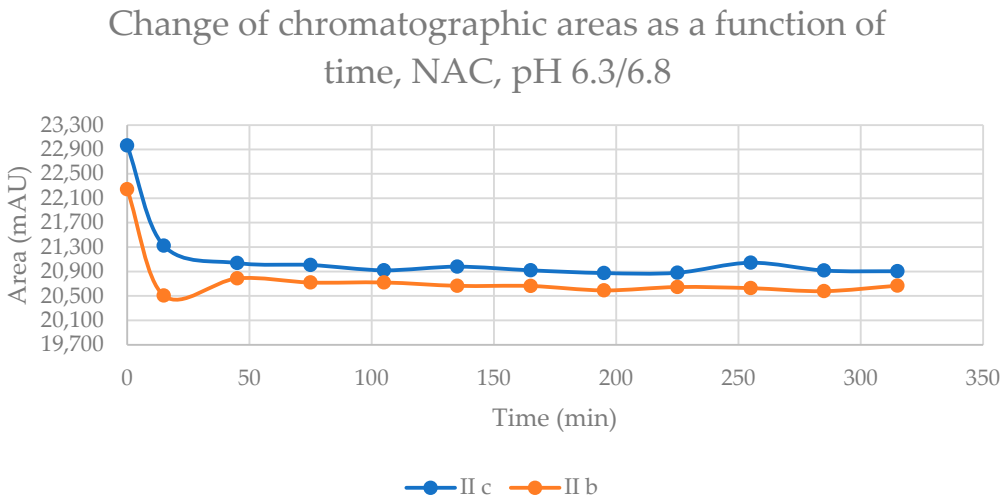

Figure 9. Change in the chromatographic peak area of chalcones **IIb** and **IIc** in the chalcone–NAC incubations at pH 6.3/6.8.

In the GSH incubations, the separated HPLC peak areas of the **IIb-GSH** and **IIc-GSH** diastereomers increased as closely parallel over time (Figures S11 and S12). At the end of the incubation period, the ratio of the area of two separated peaks of the chalcone–GSH adducts is close to unity (1.12 and 1.10 for **IIb** and **IIc**, respectively) (Table 4). A similar tendency could be observed for the NAC-2 peak (peak with the higher retention time) area of **IIb** and **IIc** (Figure S14). At the same time, the chromatographic peak area of the NAC-1 peak of **IIc** remained practically unchanged, but that of **IIb** slightly increased (Figure S13). As a result, the ratio of the NAC-2/NAC-1 areas at the 315 timepoint was 8.57 and 6.34 for **IIb** and **IIc**, respectively (Table 4). In all four incubations, the peak areas of the (*Z*)-chalcones are comparable to those of the formed adducts (Table 4). Since the only source of the (Z) isomers under the experimental conditions is the retro-Michael reactions, it is reasonable to presume that the observed diastereomeric distributions do not reflect the results of the kinetics-controlled reactions.

Table 4. HPLC-UV areas of the (*Z*) isomers and the diastereomeric NAC-1 and NAC-2 peaks in the NAC-incubation of **IIb** and **IIc** under slightly acidic (pH 6.3/6.7) conditions.

Compound	Time (Minute)	Area Z-Chalcone	Area NAC-1	Area NAC-2	Ratio Area NAC-2/NAC-1
IIb	75	91.8	35.3	224.1	6.3
	165	107.2	52.7	349.7	6.6
	255	114.9	56.8	448.3	7.9
	315	118.9	60.0	513.9	8.6
IIc	75	136.5	54.0	148.9	2.8
	165	159.4	59.5	249.3	4.2
	255	175.3	58.4	333.2	5.7
	315	184.5	61.8	392.1	6.3

2.3. Reaction under Acid (pH 3.2/3.7) Conditions

Under stronger acidic conditions, the thiol function of both GSH and NAC exists exclusively in protonated (neutral) form. Although the protonated thiols can act as nucleophilic reagents, their reactivity is much lower than that of their deprotonated (negatively charged) counterparts [29]. In the chalcone–GSH incubations, progression curves of the reactions (reduction in the initial area of the chalcones) showed a very slight downhill linear shape (Figure S15). At the end of the incubations, the initial values of the peak areas of **IIb** and **IIc** were reduced by 10.6% and 5.3%, respectively. At the same time, a linear increase in the peak area of the **IIb-GSH** adducts (peak 1 and peak 2) could be observed (Figures S16 and S17). The peaks corresponding to the respective **IIc-GSH** adducts could not be detected. The ratio of the **IIb-GSH** isomeric peaks (315 min timepoint) was 1.48. The areas of the respective (*Z*) isomers were much lower than in the pH 8.0 and pH 6.3 incubations (Table 2).

In the chalcone–NAC incubations, the reduction in the initial area of the chalcones showed a very slight downhill linear shape with somewhat different slopes (Figure S18). The initial peak area of **IIb** and **IIc** was reduced by 23.7% and 12.1% by the 315 min timepoint (Table 3). However, no **II-NAC** peaks could be identified. HPLV-UV analysis of the incubates showed the formation of several small peaks that were more polar than the parent **IIb** and **IIc**. HPLC-MS investigations indicated the expected adduct formation, but it was impossible to identify them in the HPLC-UV chromatograms (Figures S19 and S20). In both incubations, the formation of the (*Z*) isomers could be seen (Table 3).

2.4. Molecular Modeling Analysis

Table 5 shows the calculated values for molecular properties of **Ia**, **IIa**, methanethiol (**CH_3SH**), and deprotonated methanethiol (**CH_3S^-**). The highest occupied molecular orbital energy (E_{HOMO}) reflects the ability of a molecule to donate electrons, the lowest unoccupied molecular orbital energy (E_{LUMO}) demonstrates the ability to accept electrons (see Figure 10), and the gap energies ($\Delta E_{LUMO\text{-}HOMO}$) are related to the chemical stability of molecules.

Table 5. Reactivity indices were obtained for **Ia**, **IIa**, **CH_3SH**, and **CH_3S^-** at the M06-2X/6-311++G(d,p) level of theory.

Descriptors	Ia kcal.mol^{-1}	IIa kcal.mol^{-1}	CH_3SH kcal.mol^{-1}	CH_3S^- kcal.mol^{-1}
E_{HOMO}	−183.24	−180.38	−183.240	−173.453
E_{LUMO}	−35.98	−28.44	−2.979	77.998
$\Delta E_{HOMO\text{-}LUMO}$	147.27	151.94	180.261	251.451
Chemical Potential (η)	−109.608	−104.405	−93.109	−47.728
Chemical Hardness (μ)	147.264	151.930	180.261	251.451
Electrophilicity Index (ω)	40.791	35.873	24.047	4.530

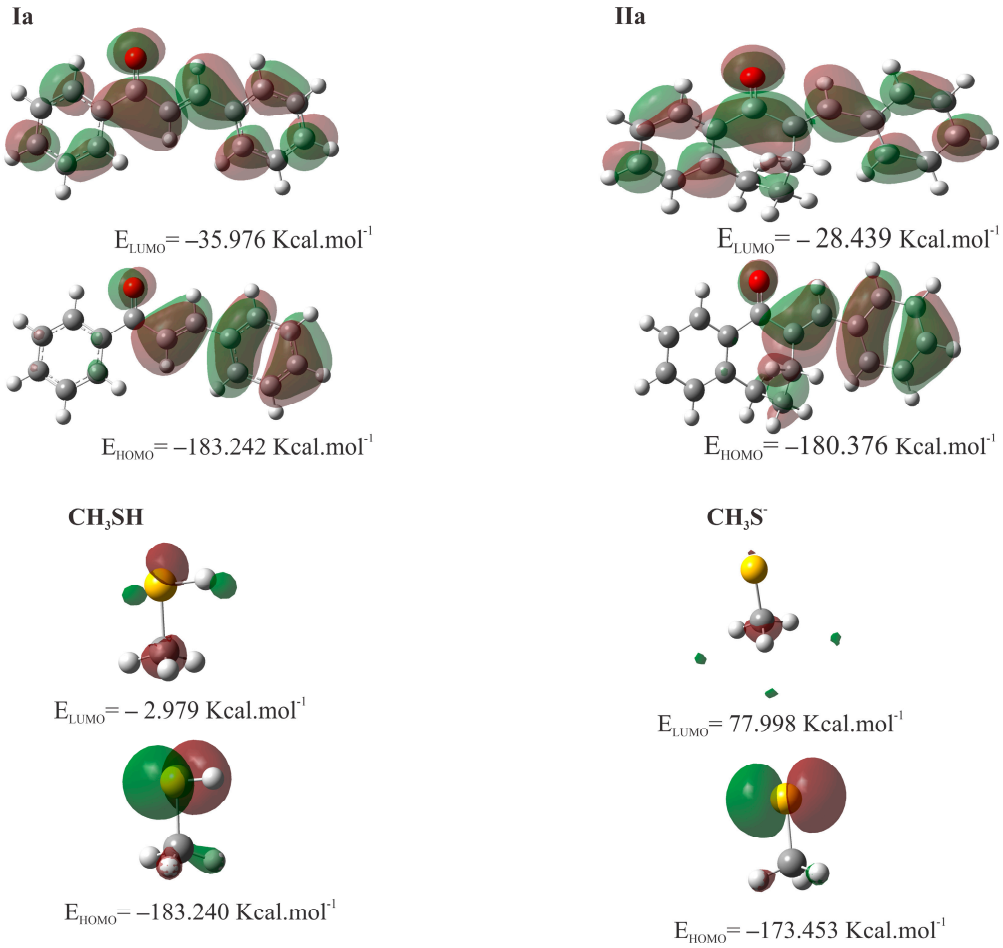

Figure 10. HOMO and LUMO plots for **Ia**, **IIa** $\mathbf{CH_3SH}$, and $\mathbf{CH_3S^-}$ calculated at the M06-2X/6-311++G (d,p) level of theory.

The chemical potential, chemical hardness, and electrophilicity are defined as ($\mu = \left(\frac{\partial E}{\partial N}\right)_v$), ($\eta = \frac{1}{2}\left(\frac{\partial^2 E}{\partial N^2}\right)_v$), and ($\omega = \frac{\mu^2}{2\eta}$), respectively. η indicates the resistance of the molecule to alter its electronic density distribution and is higher for **IIa**. On the other hand, μ indicates the change in free energy when electrons are added or removed from the molecule. At the same time, ω is a measure of a molecule's tendency to act as an electrophile. The value of ω increased for **Ia**, and μ decreased when compared to **IIa**.

Figure 11 shows the isosurfaces of the Fukui function (obtained from electron density) for the molecules **Ia**, **IIa**, and $\mathbf{CH_3SH}$, with a focus on atoms that can undergo nucleophilic attack (). The positive and negative regions of the Fukui function are represented by the green and blue isosurfaces, respectively.

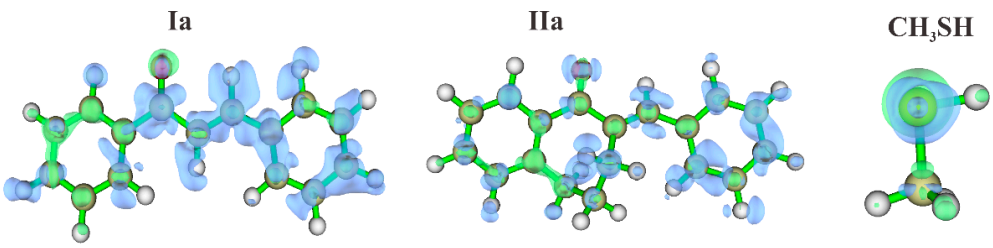

Figure 11. Isosurfaces of the Fukui Function, calculated at a proper value of 0.08 for the molecules **Ia**, **IIa**, $\mathbf{CH_3SH}$, and $\mathbf{CH_3S^-}$.

In order to depict the distribution of electric charge on the molecular surface, a molecular electrostatic potential (MEP) map was generated (Figure 12). The red spots on the MEP surface represent the electron-rich sites and are susceptible to electrophilic attack. In contrast, the blue spots represent the electron-depleted regions and are sites susceptible to nucleophilic attack. For $\mathbf{CH_3S^-}$, the MEP is reddish due to the −1 negative charge resulting from deprotonation.

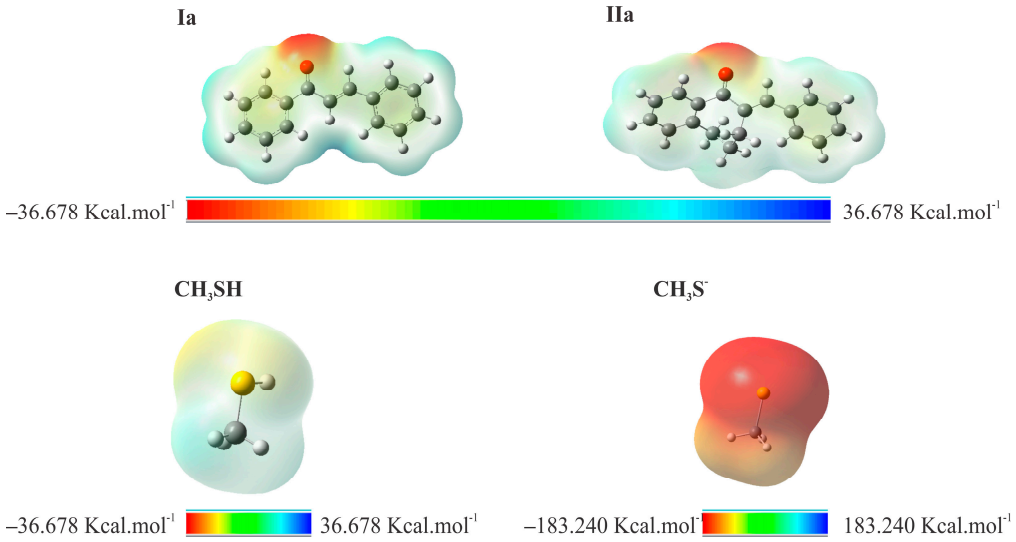

Figure 12. MEP surface contour of the total SCF electronic density for molecules **Ia**, **IIa**, $\mathbf{CH_3SH}$, and $\mathbf{CH_3S^-}$ at the M06-2X/6-311++G (d,p) level of theory.

The k_{OH} rate constants were calculated for chalcone compounds, and the results indicate that the compounds with the highest k_{OH} values point to greater reactivity. The order of reactivity potential was observed as $\mathbf{CH_3SH}$ (9.15×10^9 M^{-1} s^{-1}) **Ia** (9.01×10^9 M^{-1} s^{-1}) > **IIa** (7.85×10^9 M^{-1} s^{-1}) > $\mathbf{CH_3S^-}$ (5.48×10^9 M^{-1} s^{-1}).

3. Discussion

Our experiment showed that both cyclic chalcone analogs (**IIb** and **IIc**) have intrinsic reactivity with GSH and NAC under all three experimental conditions. The results strengthen the results of our previous studies obtained by TLC analysis of similar incubations with GSH of the two compounds [13]. Considering the pKa values of GSH (8.83) and NAC (9.52) thiols, it can be seen that the fraction of the stronger nucleophile thiolate form of GSH is higher than that of NAC under each experimental condition. Under the slightly basic conditions (pH 8.0/7.4), the rate of reduction in the HPLC peak area of the starting chalcones showed a linear decrease. Since the area is based on the absorbance (logarithmic function of the concentration) of the compounds, the reactions follow pseudo-first-order kinetics. In the case of both thiols, relatively high amounts of (*Z*)-chalcone isomers could be detected in the incubations (Tables 2 and 3). Since the reaction mixtures were incubated in the dark, the corresponding retro-Michael reactions are the only source of the (*Z*)-isomer formations. Accordingly, the progression curves of the incubations (Figures 2 and 3) reflect the disappearance of the starting compounds due to the net change in the reversible reactions. Similar levels of the respective (*Z*)-isomers could be detected in the incubations performed under slightly acidic (pH 6.3/6.7) conditions (Tables 2 and 3). On the contrary, the reactions of the respective open-chain chalcones (**Ib** and **Ic**) performed under identical conditions did not result in a detectable level of (*Z*)-isomers in the GSH or the NAC incubations [24].

The results obtained in the pH 6.3/6.7 incubations are similar to those of the pH 8.0/7.4 ones (Tables 2 and 3). Under such conditions, however, the composition of both incubations represents the equilibrium mixtures. Similar to the pH 8.0/7.4 incubations, the conversion of **IIb** is somewhat higher in the case of both thiols. The observation further strengthens the

previously suggested view that the different reactivities can be (at least partly) the result of the different stability of the thiol adducts [24,30]. Similar to the results obtained under identical conditions with the respective open-chain chalcones (**I**), the 4-methyl-substituted derivative (**IIb**) forms the more stable adducts.

Comparing the compositions of the 315 min incubation mixtures of the two series (**I** and **II**), it can be seen that the conversions of the 4-CH_3- and 4-OCH_3-substituted chalcones (**Ib** and **Ic**) are much higher than those of the **IIb** and **IIc** (Table 6). ^{13}C NMR shifts, indicating the electron density around the particular nucleus, of the β-carbon atom of **IIb** (138.0 ppm) and **IIc** (137.7 ppm), were reported to be similar. A similar slight (0.3 ppm) difference was observed in the case of the respective open-chain chalcones **Ib** and **Ic** [31]. Since the nature of thiols and the aromatic substituents are the same, the ring structure can explain the observed differences in reactivities of the two series.

Table 6. Percent reduction in initial chalcone HPLC-UV peaks in the 315 min GSH and NAC incubation mixtures of the series **I** and **II**.

Compound	pH	Reagent Thiol	Reduction in Initial Peak Area at the 315 min Timepoint (%)	Reagent Thiol	Reduction in Initial Peak Area at the 315 min Timepoint (%)
Ib	8.0/7.4	GSH	96.3 *	NAC	94.8 *
IIb	8.0/7.4	GSH	43.5	NAC	7.6
Ic	8.0/7.4	GSH	92.1 *	NAC	90.2 *
IIc	8.0/7.4	GSH	26.3	NAC	7.9
Ib	6.3/6.7	GSH	90.6 *	NAC	75.6 *
IIb	6.3/6.7	GSH	16.1	NAC	7.1
Ic	6.3/6.7	GSH	78.3 *	NAC	53.3 *
IIc	6.3/6.7	GSH	9.1	NAC	9.0
Ib	3.2/3.7	GSH	19.3 *	NAC	10.9 *
IIb	3.2/3.7	GSH	10.6	NAC	23.7
Ic	3.2/3.7	GSH	4.2 *	NAC	1.5 *
IIc	3.2/3.7	GSH	5.3	NAC	12.1

* Calculated on the bases of data published in [24].

Amslinger et al. investigated the thiol reactivity of chalcones with various substituents in their α-position. The kinetics of thiol reactivities of the derivatives were correlated with some of their biological effects directly connected to their Michael acceptor ability [32,33]. For example, α-methyl substitution of 2′,3,4,4′-tetramethoxychalcone (TMC) decreased, α-cyano substitution substantially increased the thiol reactivity of the nonsubstituted TMC [34]. Based on these earlier observations, it is reasonable to suppose that the reduced reactivity of the benzosuberone derivatives **IIb** and **IIc** is the consequence of added effects of the α-alkyl substitution and the conformational strain caused by the cyclic structure of the starting enone and the reaction intermediate. Further research is needed to characterize the electronic and stereochemical effects of the ring numerically.

As a result of the addition reactions, the formation of four diastereomeric adducts is possible. Because of the inherent chirality of GSH and NAC, two *cis* adducts and two *trans* adducts are expected to be formed. Earlier, Armstrong et al. reported on the stereochemistry of the GSTM 4-4-catalyzed reaction of GSH and the open-chain chalcone analog (*E*)-(4′-X-phenyl)-3-butene-2-ones (PBO). In the reactions, a higher amount of the more polar adducts were formed [35]. Based on the results of HPLC separation of the diastereomeric pairs of the PBO-GSH [35] and the **I**-GSH [24] adducts, we can presume that the two separated peaks formed in the present reactions correspond to the diastereomeric *cis* and *trans* adducts.

The ratio of the area of the two separated peaks in the GSH incubates (315 min time-point) was close to the unity for **IIb** and **IIc** under both pH 8.0/7.4 and 6.3/6.8 conditions (Table 2). Similar to our previous results, higher peak areas of the least polar adducts were observed in each case. On the contrary, HPLC analysis of the reactions of **IIb** and **IIc** with NAC showed different (1.8–8.57 times) excess of the least polar diastereomer (Table 3). Similar to the previous results obtained with the open-chain chalcones (**Ib** and **Ic**) [24], the

observed diastereoselectivity was affected by the nature of the 4-substituent and the pH. Thus, the methyl–substituted **IIb** showed higher diastereoselectivity at both pH values. Diastereoselectivity was increased as the pH was reduced (Table 3). It is worth mentioning, however, that the observed diastereoselectivities do not reflect the diastereoselectivity of the addition reactions. Under both conditions (pH 8.0/7.4 and 6.3/6.8), the peak areas of the (*Z*)-isomers and the adducts are comparable (Table 3). Since the retro-Michael reaction is the only source of formation of the (*Z*)-isomers, the observed ratios reflect the actual balance of the kinetic and thermodynamic controls.

Under the acid conditions (pH 3.2/3.7), the formation of the respective conjugates is exclusively due to the nucleophilic addition of the protonated thiol forms onto the polarized carbon-carbon double bounds. In comparison of the respective compositions of the GSH incubates with those of the previously reported (open chain) chalcones (**Ib** and **Ic**) [24], the derivatives with the same substituent showed similar GSH reactivities (Table 2). However, different results were obtained in the case of the reactions with NAC. The 315min percent conversion (reduction in the initial peak area) was found to be higher for **IIb** (23.7%) and **IIc** (12.1%) than those of the corresponding open-chain chalcones **Ib** and **Ic** (10.9% and 1.5%, respectively (Table 6). However, no **II-NAC** adducts could be identified in the HPLC-UV chromatograms. Instead, several small, unidentified peaks appeared (Figures S19 and S20). HPLC-MS analysis could identify the expected conjugates. The structural characterization of the other products is out of the scope of the present work.

To obtain physicochemical properties insights into different reactivities of chalcones (**I**) [24] and their seven-membered cyclic analogs (**II**), HOMO and LUMO molecular orbital energy and some electrophilic reactivity parameters of **Ia**, **IIa**, and as model thiols **CH_3SH** and **CH_3S^-** were calculated (Table 5). According to the Hard and Soft, Acids and Bases (HSAB) theory [36], nucleophilic-electrophilic reactions occur preferably between electrophiles and nucleophiles of similar hardness or softness. In the case of the α,ß-unsaturated ketone, the carbonyl oxygen atom withdraws electrons from the C_2=C_{10} bond—generating an electron deficiency at C_{10}—the most likely site to receive nucleophilic attacks. In methanethiol, the electrophilic attacks can occur at the sulfur atom. In compounds **Ia** and **IIa**, the carbonyl O has a high negative charge density, indicating its Lewis base behavior. On the other hand, regions of lower charge density, which appear in blue, indicate the Lewis acid behavior of the molecules.

The LUMO energy showed that **Ia** (−35.98 kcal/mol) is more acidic than **IIa** (−28.44 kcal/mol. The HOMO energy of **CH_3SH** is (−183.240 kcal/mol). It increases to (−173.453 kcal/mol) in the deprotonated form (**CH_3S^-**) indicating its higher nucleophilic reactivity. These characters are also reflected by all of the other determined parameters (Table 5). Therefore, molecular orbital calculations provided data to support the experimental findings. The equilibrium (close-to-equilibrium) compositions of **Ib** and **Ic** show a higher product ratio than the cyclic chalcone analog **IIb** and **IIc**.

4. Materials and Methods

4.1. Chemicals and Reagents

Chalcones **IIb** and **IIc** were synthesized as previously published [10]. Their structures were characterized by IR and NMR spectroscopy [37]. The purity and structures of the investigated samples were verified by TLC, melting point, and HPLC-MS (Figures S5 and S6). Reduced L-glutathione, N-acetyl l-cysteine, HPLC, and MS-grade methanol solvent were obtained from Sigma-Aldrich (Budapest, Hungary). Trifluoroacetic acid HiperSolve CHROMANORM and formic acid were obtained from VWR (Budapest, Hungary) and Fischer Scientific (Budapest, Hungary), respectively. Deionized water for use in HPLC and HPLC-MS measurements was purified by Millipore Direct-Q^{TM} (Merck Life Science, Budapest, Hungary), at the Institute of Pharmaceutical Chemistry (University of Pécs, Pécs, Hungary). Mobile phases used for HPLC measurements were degassed by an ultrasonic water bath before use.

4.2. Preparation of Solutions

The thiol solutions (reduced glutathione (GSH) and *N*-acetylcysteine (NAC)) preparation were as follows: 2.0×10^{-1} mol·L^{-1} (0.3 mmol) of the respective thiol was dissolved in water, and the pH was set to either 3.2, 6.3, or 8.0 using 1M NaOH solution to a final volume of 1.5 mL (solution-1). The chalcone solution consisted of 6.5×10^{-3} mol·L^{-1} (0.03 mmol) chalcone analog dissolved in 4.6 mL HPLC-grade methanol (solution-2). Solution-1 and solution-2 were mixed to give a final volume of 6.1 mL. The molar ratio of thiol to chalcone in the mixture was 10:1. The mixture was kept in the dark, 37 °C water bath for 315 min. The first sample was taken at 15 min, and onward samples were taken at every 30 min time points (11 samples in total).

To evaluate the initial (0 min) peak area of chalcones **IIa** and **IIb**, solution-2 was prepared without any change, while solution-1 was prepared without the thiol component. Before mixing, the solutions were pre-incubated at 37 °C for 30 min to mimic the incubation conditions. To compare the products of the previously proven light-initiated *E/Z* isomerization of the parent compounds [27] with those of the non-light (retro-Michael addition)-initiated isomerization, solution-2 of the respective chalcones were prepared and exposed to the unscattered laboratory light for 1 week. The solutions were analyzed by HPLC-UV-VIS and HPLC-MS. (Figures S21 and S22).

4.3. RP-HPLC-UV-VIS Measurements

UV–VIS detector coupled Agilent 1100 HPLC system analyzed the samples at 260 nm wavelength. The separation system was a reversed-phase chromatographic system, and the column Zorbax Eclipse XBD-C8 (150 mm × 4.6 mm, particle size 5 µm; Agilent Technologies, Waldbronn, Germany) was used. The oven temperature was set to 25 °C to avoid room temperature fluctuations. The injection volume was 10 µL. At a 1.2 mL/min flow rate, gradient elution was performed by (A) water and 0.1% trifluoroacetic acid and (B) methanol and 0.1% trifluoroacetic acid. The elution profile consisted of 8 min of 40% isocratically, an increase to 60% B in 4 min, and a further linear increase of eluent B to 90% in 3 min. The elution gradient remained constant for a 5 min period. Then it was linearly decreased to the initial 40% in 2 min, followed by a 3 min constant of 40% of eluent B for equilibration of the column.

4.4. HPLC-MS Measurements

HPLC ESI-MS analyses were performed on an Ultimate 3000 liquid chromatograph (Dionex, Sunnyvale, CA, USA) coupled with a Thermo Q Exactive Focus quadrupole-Orbitrap hybrid mass spectrometer (Thermo Fisher Scientific, Waltham, MA, USA). The scan monitored *m/z* values ranging from 100 to 1000 Da. Data acquisition was carried out using Q Exactive Focus 2.1 and Xcalibur 4.2 software (Thermo Fisher Scientific). Analysis of compounds and adducts was performed in HESI positive and negative ionization modes with the following parameters: spray voltage, 3500 V; vaporizer temperature, 300 °C; capillary temperature, 350 °C; spray and auxiliary gas flows, 30 and 10 arbitrary units, respectively; resolution, 35,000 at 200 *m/z*; and fragmentation, 20 eV.

HPLC separation was performed on an Accucore C18 column (150 mm × 2.1 mm, particle size 2.6 µm), and an Accucore C18 guard column (5 mm × 2.1 mm, particle size 2.6 µm) was also used. The injection volume was 5 µL; the flow rate was 0.4 mL/min. Data analysis and evaluations were performed using Xcalibur 4.2 and FreeStyle 1.7 software. A binary gradient of eluents was used, consisting of mobile phases A and B.

The gradient parameters in chalcones were (A) water and 0.1% formic acid and (B) methanol and 0.1% formic acid. The gradient elution was as follows: isocratic elution for 1 min to 20% eluent B, continued by a linear gradient to 100% in 9 min, followed by an isocratic plateau for 2 min. Then, the column was equilibrated back to 20% in 0.5 min and continued isocratically for 2.5 min. The sampler was at room temperature and the column oven was at 40 °C.

The parameters of the gradient in the case of adducts were (A) water and 0.1% formic acid and (B) methanol and 0.1% formic acid. The gradient elution was as follows: isocratic elution for 1 min to 10% eluent B, continued by a linear gradient to 95% in 13 min, followed by an isocratic plateau for 3 min. Finally, the column was equilibrated to 10% in 0.1 min and continued isocratically for 2.9 min. The sampler was at room temperature, and the column oven was at 40 °C. The diode array detector was also set at 260 nm wavelength alongside MS analysis.

4.5. Molecular Modeling Analysis

The structures **Ia**, **IIa**, **CH_3SH**, and **CH_3S^-** were constructed using the Gaussview 6.0 software. Theoretical calculations were performed by DFT [38,39], implemented in the G16 [40] software package. The molecules were optimized using the hybrid exchange and correlation functional with long-range correction, M06-2X [41], combined with the basis set 6-311++G(d,p) in the gas phase. Frontier molecular orbitals (FMO) [42] were obtained. Molecular electrostatic potential maps contributed to the global electrophilicity analysis through their electronic isodensity surfaces. MEP [43] maps provide a visual representation of the electrostatic potential on the surface of a molecule, which can reveal regions of high and low electron density. The electrostatic potential V(**r**) [44] at point **r** is defined as.

$$V(\mathbf{r}) = \sum_{\alpha} \frac{Z_A}{|r_\alpha - r_A|} - \int \frac{\rho(r)}{r_\alpha - r} dr \quad (1)$$

where Z_A is the charge of nuclei a at point $\mathbf{r}a$ and $\boldsymbol{\rho}(\mathbf{r})$ is the charge density at point **r**. The local electrophilicity of the molecules was determined by the Fukui function [45,46], and then it was possible to predict the molecular site selectivity.

$$f(\mathbf{r}) = \left[\frac{\partial \rho(\mathbf{r})}{\partial N}\right]_v \quad (2)$$

where N is the number of electrons in the system, and the constant term v in the partial derivative is external potential. Multiwfn 3.6 program [47] was used to calculate the Fukui. In addition, the *py*SiRC [48], a machine-learning computational platform, was used to simulate oxidation reactions facilitated by free-radical compounds. To imitate the oxidation impact induced by a radical attack, the hydroxyl radical (OH) was chosen as the archetype system of degradation reactions. The reaction rate constant of the oxidative attack caused by the hydroxyl radical on chalcones compounds was predicted using the XGBoost ML algorithm and the MACCS fingerprint was employed as a structural descriptor.

5. Conclusions

The present work investigated the instantaneous GSH- and NAC-reactivity of two cyclic chalcones analogs (**IIb** and **IIc**) with different cancer cell cytotoxicities. The reactivity of the two compounds was investigated under three different acid-base conditions. The progress of the reactions, disappearance of the parent compounds, and appearance of the thiol-conjugates were monitored by the HPLC-UV method. Comparison of the reactivities of **IIb** and **IIc** with those of the respective open-chain chalcones showed the cyclic analogs to be less reactive under each investigated conditions. In both series, the 4-CH_3 substituted derivatives displayed higher reactivities. The substituent effect could be rationalized by the higher electron-donating power of the 4-OCH_3 substituent. The alkyl substitution of the α-carbon atom and the cyclic structure can explain the lower reactivities of **IIb** and **IIc** compared to the open-chain counterparts (**Ib** and **Ic**). The theoretical calculations of orbital energies and electrophilic reactivity parameters provided evidence that supports the experimental findings—the open chalcone exhibits higher electronegativity and reactivity than its cyclic counterpart.

Cytotoxicity and cell cycle modulating effects of **IIb** and **IIc** showed characteristic differences. The present results do not indicate a direct correlation with the cancer cell

cytotoxicity of the two derivatives, which are of two orders of magnitude different against most of the investigated cell lines. The anticancer potential of chalcones is correlated with their ability to act on various molecular targets such as ABCG2, tubulin, activated nuclear B cell growth (NF-κB), vascular endothelial growth factor (VEGF), tyrosine kinase receptor (EGFR), mesenchymal-epithelial transition factor (MET), 5-α reductase, ACP-reductase, histone deacetylase, p53, CDC25B (protein tyrosine phosphatase), retinoic acid receptors, estrogenic topoisomerase receptors and MDM2 [9]. Considering the present and our previous results [10–16], it is reasonable to suppose that the molecular basis of the different biological effects of **IIb** and **IIc** is related to the non-covalent interactions of the compounds [49].

Supplementary Materials: The supporting information can be downloaded at: https://www.mdpi.com/article/10.3390/ijms24108557/s1.

Author Contributions: F.K.: Writing initial draft, writing review, investigation, data curation; S.M.: Writing-review, investigation, data curation; I.D.B.: Writing initial draft, writing review, investigation, data curation, H.B.N.: Conceptualization, writing initial draft, writing review and editing; P.P.: Project administration, conceptualization, writing initial draft, writing-review, and editing. All authors have read and agreed to the published version of the manuscript.

Funding: This study was supported by the European Union and co-financed by the European Social Fund (EFOP-3.6.1.-16-2016-00004). The financial support is highly appreciated. The authors are grateful to Conselho Nacional de Desenvolvimento Científico e Tecnológico (CNPq) and Fundação de Amparo à Pesquisa de Goiás (FAPEG). Theoretical calculations were performed in the High-Performance Computing Center of the Universidade Estadual de Goiás.

Institutional Review Board Statement: Not applicable.

Informed Consent Statement: Not applicable.

Data Availability Statement: Not applicable.

Conflicts of Interest: The authors declare no conflict of interest.

Sample Availability: Samples of the compounds **I** and **II** are available from the authors.

References

1. Kenari, F.; Molnár, S.; Pintér, Z.; Bitaraf, S.; Perjési, P. (E)-2-Benzylidenecyclanones: Part XVII. An LC-MS Study of Microsomal Transformation Reactions of (E)-2-[(4′-Methoxyphenyl)Methylene]-Benzosuberon-1-One: A Cyclic Chalcone Analog. *J. Pharm. Biopharm. Res.* **2023**, *4*, 326–339. [CrossRef]
2. Rozmer, Z.; Perjési, P. Naturally Occurring Chalcones and Their Biological Activities. *Phytochem. Rev.* **2016**, *15*, 87–120. [CrossRef]
3. Sahu, N.K.; Balbhadra, S.S.; Choudhary, J.; Kohli, V.D. Exploring Pharmacological Significance of Chalcone Scaffold: A Review. *Curr. Med. Chem.* **2012**, *19*, 209–225. [CrossRef]
4. Singh, P.; Anand, A.; Kumar, V. Recent Developments in Biological Activities of Chalcones: A Mini Review. *Eur. J. Med. Chem.* **2014**, *85*, 758–777. [CrossRef]
5. Zhou, B. Diverse Molecular Targets for Chalcones with Varied Bioactivities. *Med. Chem.* **2015**, *5*, 388–404. [CrossRef] [PubMed]
6. Zhuang, C.; Zhang, W.; Sheng, C.; Zhang, W.; Xing, C.; Miao, Z. Chalcone: A Privileged Structure in Medicinal Chemistry. *Chem. Rev.* **2017**, *117*, 7762–7810. [CrossRef] [PubMed]
7. Karthikeyan, C.; Narayana Moorthy, N.S.H.; Ramasamy, S.; Vanam, U.; Manivannan, E.; Karunagaran, D.; Trivedi, P. Advances in Chalcones with Anticancer Activities. *Recent Pat. Anti-Cancer Drug Discov.* **2014**, *10*, 97–115. [CrossRef]
8. Gomes, M.; Muratov, E.; Pereira, M.; Peixoto, J.; Rosseto, L.; Cravo, P.; Andrade, C.; Neves, B. Chalcone Derivatives: Promising Starting Points for Drug Design. *Molecules* **2017**, *22*, 1210. [CrossRef]
9. Constantinescu, T.; Mihis, A.G. Two Important Anticancer Mechanisms of Natural and Synthetic Chalcones. *Int. J. Mol. Sci.* **2022**, *23*, 11595. [CrossRef]
10. Dimmock, J.R.; Kandepu, N.M.; Nazarali, A.J.; Kowalchuk, T.P.; Motaganahalli, N.; Quail, J.W.; Mykytiuk, P.A.; Audette, G.F.; Prasad, L.; Perjési, P.; et al. Conformational and Quantitative Structure−Activity Relationship Study of Cytotoxic 2-Arylidenebenzocycloalkanones. *J. Med. Chem.* **1999**, *42*, 1358–1366. [CrossRef]
11. Dimmock, J.R.; Zello, G.A.; Oloo, E.O.; Quail, J.W.; Kraatz, H.-B.; Perjési, P.; Aradi, F.; Takács-Novák, K.; Allen, T.M.; Santos, C.L.; et al. Correlations between Cytotoxicity and Topography of Some 2-Arylidenebenzocycloalkanones Determined by X-Ray Crystallography. *J. Med. Chem.* **2002**, *45*, 3103–3111. [CrossRef] [PubMed]

12. Perjési, P.; Das, U.; De Clercq, E.; Balzarini, J.; Kawase, M.; Sakagami, H.; Stables, J.P.; Lorand, T.; Rozmer, Z.; Dimmock, J.R. Design, Synthesis and Antiproliferative Activity of Some 3-Benzylidene-2,3-Dihydro-1-Benzopyran-4-Ones Which Display Selective Toxicity for Malignant Cells. *Eur. J. Med. Chem.* **2008**, *43*, 839–845. [CrossRef] [PubMed]
13. Rozmer, Z.; Berki, T.; Perjési, P. Different Effects of Two Cyclic Chalcone Analogues on Cell Cycle of Jurkat T Cells. *Toxicol. In Vitro* **2006**, *20*, 1354–1362. [CrossRef]
14. Pilatova, M.; Varinska, L.; Perjesi, P.; Sarissky, M.; Mirossay, L.; Solar, P.; Ostro, A.; Mojzis, J. In Vitro Antiproliferative and Antiangiogenic Effects of Synthetic Chalcone Analogues. *Toxicol. In Vitro* **2010**, *24*, 1347–1355. [CrossRef]
15. Perjési, P.; Maász, G.; Reisch, R.; Benkő, A. (E)-2-Benzylidenebenzocyclanones: Part VII. Investigation of the Conjugation Reaction of Two Cytotoxic Cyclic Chalcone Analogues with Glutathione: An HPLC–MS Study. *Mon. Für Chem. Chem. Mon.* **2012**, *143*, 1107–1114. [CrossRef]
16. Rozmer, Z.; Berki, T.; Maász, G.; Perjési, P. Different Effects of Two Cyclic Chalcone Analogues on Redox Status of Jurkat T Cells. *Toxicol. In Vitro* **2014**, *28*, 1359–1365. [CrossRef]
17. Lu, S.C. Glutathione Synthesis. *Biochim. Biophys. Acta (BBA) Gen. Subj.* **2013**, *1830*, 3143–3153. [CrossRef]
18. Ballatori, N.; Krance, S.M.; Notenboom, S.; Shi, S.; Tieu, K.; Hammond, C.L. Glutathione Dysregulation and the Etiology and Progression of Human Diseases. *Biol. Chem.* **2009**, *390*, 191–214. [CrossRef] [PubMed]
19. Forman, H.J.; Zhang, H.; Rinna, A. Glutathione: Overview of Its Protective Roles, Measurement, and Biosynthesis. *Mol. Asp. Med.* **2009**, *30*, 1–12. [CrossRef] [PubMed]
20. Jones, D.P. Redox Potential of GSH/GSSG Couple: Assay and Biological Significance. In *Methods in Enzymology*; Elsevier: Amsterdam, The Netherlands, 2002; Volume 348, pp. 93–112. ISBN 978-0-12-182251-4.
21. Dickinson, D.A.; Forman, H.J. Cellular Glutathione and Thiols Metabolism. *Biochem. Pharmacol.* **2002**, *64*, 1019–1026. [CrossRef] [PubMed]
22. Moran, L.; Gutteridge, J.; Quinlan, G. Thiols in Cellular Redox Signalling and Control. *Curr. Med. Chem.* **2001**, *8*, 763–772. [CrossRef] [PubMed]
23. Aw, T.Y. Cellular Redox: A Modulator of Intestinal Epithelial Cell Proliferation. *Physiology* **2003**, *18*, 201–204. [CrossRef] [PubMed]
24. Kenari, F.; Molnár, S.; Perjési, P. Reaction of Chalcones with Cellular Thiols. The Effect of the 4-Substitution of Chalcones and Protonation State of the Thiols on the Addition Process. Diastereoselective Thiol Addition. *Molecules* **2021**, *26*, 4332. [CrossRef] [PubMed]
25. Drutovic, D.; Chripkova, M.; Pilatova, M.; Kruzliak, P.; Perjesi, P.; Sarissky, M.; Lupi, M.; Damia, G.; Broggini, M.; Mojzis, J. Benzylidenetetralones, Cyclic Chalcone Analogues, Induce Cell Cycle Arrest and Apoptosis in HCT116 Colorectal Cancer Cells. *Tumor Biol.* **2014**, *35*, 9967–9975. [CrossRef] [PubMed]
26. Caccuri, A.M.; Antonini, G.; Board, P.G.; Parker, M.W.; Nicotra, M.; Bello, M.L.; Federici, G.; Ricci, G. Proton Release on Binding of Glutathione to Alpha, Mu and Delta Class Glutathione Transferases. *Biochem. J.* **1999**, *344*, 419–425. [CrossRef]
27. Rohani, N.; Hao, L.; Alexis, M.S.; Joughin, B.A.; Krismer, K.; Moufarrej, M.N.; Soltis, A.R.; Lauffenburger, D.A.; Yaffe, M.B.; Burge, C.B.; et al. Acidification of Tumor at Stromal Boundaries Drives Transcriptome Alterations Associated with Aggressive Phenotypes. *Cancer Res.* **2019**, *79*, 1952–1966. [CrossRef]
28. Aldini, G.; Altomare, A.; Baron, G.; Vistoli, G.; Carini, M.; Borsani, L.; Sergio, F. N-Acetylcysteine as an Antioxidant and Disulphide Breaking Agent: The Reasons Why. *Free Radic. Res.* **2018**, *52*, 751–762. [CrossRef]
29. LoPachin, R.M.; Gavin, T. Reactions of Electrophiles with Nucleophilic Thiolate Sites: Relevance to Pathophysiological Mechanisms and Remediation. *Free Radic. Res.* **2016**, *50*, 195–205. [CrossRef]
30. d'Oliveira, G.D.C.; Custodio, J.M.F.; Moura, A.F.; Napolitano, H.B.; Pérez, C.N.; Moraes, M.O.; Prókai, L.; Perjési, P. Different Reactivity to Glutathione but Similar Tumor Celltoxicity of Chalcones and Their Quinolinone Analogues. *Med. Chem. Res.* **2019**, *28*, 1448–1460. [CrossRef]
31. Perjési, P.; Linnanto, J.; Kolehmainen, E.; Ősz, E.; Virtanen, E. E-2-Benzylidenebenzocycloalkanones. IV. Studies on Transmission of Substituent Effects on 13C NMR Chemical Shifts of E-2-(X-Benzylidene)-1-Tetralones, and -Benzosuberones. Comparison with the 13C NMR Data of Chalcones and E-2-(X-Benzylidene)-1-Indanones. *J. Mol. Struct.* **2005**, *740*, 81–89. [CrossRef]
32. Amslinger, S. The Tunable Functionality of α,β-Unsaturated Carbonyl Compounds Enables Their Differential Application in Biological Systems. *Chemmedchem* **2010**, *5*, 351–356. [CrossRef] [PubMed]
33. Amslinger, S.; Al-Rifai, N.; Winter, K.; Wörmann, K.; Scholz, R.; Baumeister, P.; Wild, M. Reactivity Assessment of Chalcones by a Kinetic Thiol Assay. *Org. Biomol. Chem.* **2013**, *11*, 549–554. [CrossRef] [PubMed]
34. Al-Rifai, N.; Rücker, H.; Amslinger, S. Opening or Closing the Lock? When Reactivity Is the Key to Biological Activity. *Chem. Eur. J.* **2013**, *19*, 15384–15395. [CrossRef] [PubMed]
35. Armstrong, R.N. Glutathione S-Transferases: Reaction Mechanism, Structure, and Function. *Chem. Res. Toxicol.* **1991**, *4*, 131–140. [CrossRef]
36. LoPachin, R.M.; Gavin, T.; DeCaprio, A.; Barber, D.S. Application of the Hard and Soft, Acids and Bases (HSAB) Theory to Toxicant–Target Interactions. *Chem. Res. Toxicol.* **2012**, *25*, 239–251. [CrossRef]
37. Perjési, P.; Nusser, T.; Tarczay, G.; Sohár, P. E-2-Benzylidenebenzocycloalkanones. Stereostructure and NMR Spectroscopic Investigation. *J. Mol. Struct.* **1999**, *479*, 13–19. [CrossRef]
38. Hohenberg, P.; Kohn, W. Inhomogeneous Electron Gas. *Phys. Rev.* **1964**, *136*, B864. [CrossRef]
39. Kohn, W.; Sham, L.J. Self-Consistent Equations Including Exchange and Correlation Effects. *Phys. Rev.* **1965**, *140*, A1133. [CrossRef]

40. Frisch, M.; Trucks, G.; Schlegel, H.; Scuseria, G.; Robb, M.; Cheeseman, J.; Scalmani, G.; Barone, V.; Petersson, G.; Nakatsuji, H. *Gaussian 16 Revision C. 01. 2016*; Gaussian Inc.: Wallingford, CT, USA, 2016; Volume 421.
41. Zhao, Y.; Truhlar, D.G. The M06 Suite of Density Functionals for Main Group Thermochemistry, Thermochemical Kinetics, Non-covalent Interactions, Excited States, and Transition Elements: Two New Functionals and Systematic Testing of Four M06-Class Functionals and 12 Other Functionals. *Theor. Chem. Acc.* **2008**, *120*, 215–241.
42. Zhang, G.; Musgrave, C.B. Comparison of DFT Methods for Molecular Orbital Eigenvalue Calculations. *J. Phys. Chem. A* **2007**, *111*, 1554–1561. [CrossRef]
43. Weiner, P.K.; Langridge, R.; Blaney, J.M.; Schaefer, R.; Kollman, P.A. Electrostatic Potential Molecular Surfaces. *Proc. Natl. Acad. Sci. USA* **1982**, *79*, 3754–3758. [CrossRef] [PubMed]
44. Naray-Szabo, G.; Ferenczy, G.G. Molecular Electrostatics. *Chem. Rev.* **1995**, *95*, 829–847. [CrossRef]
45. Fukui, K. The Role of Frontier Orbitals in Chemical Reactions (Nobel Lecture). *Angew. Chem. Int. Ed. Engl.* **1982**, *21*, 801–809. [CrossRef]
46. Fukui, K. Role of Frontier Orbitals in Chemical Reactions. *Science* **1982**, *218*, 747–754. [CrossRef]
47. Lu, T.; Chen, F. Multiwfn: A Multifunctional Wavefunction Analyzer. *J. Comput. Chem.* **2012**, *33*, 580–592. [CrossRef] [PubMed]
48. Sanches-Neto, F.O.; Dias-Silva, J.R.; Keng Queiroz Junior, L.H.; Carvalho-Silva, V.H. "*Py* SiRC": Machine Learning Combined with Molecular Fingerprints to Predict the Reaction Rate Constant of the Radical-Based Oxidation Processes of Aqueous Organic Contaminants. *Environ. Sci. Technol.* **2021**, *55*, 12437–12448. [CrossRef]
49. Kozurkova, M.; Tomeckova, V.V. Interaction of Chalcone Derivatives with Important Biomacromolecules. In *Chalcones and Their Synthetic Analogs*; Nova Science Publisher: New York, NY, USA, 2020; pp. 95–133. ISBN 978-1-5361-8709-0.